Analytic progress in open string field theory

by

Michael Stefan Kiermaier

Submitted to the Department of Physics
in partial fulfillment of the requirements for the degree of

Doctor of Philosophy

at the

MASSACHUSETTS INSTITUTE OF TECHNOLOGY

June 2009

Author .....
Department of Physics
May 20, 2009

Certified by..... .....
Barton Zwiebach
Professor of Physics
Thesis Supervisor

Accepted by..... .....
Thomas J. Greytak
Lester Wolfe Professor of Physics, Associate Department Head for Education

Analytic progress in open string field theory

by

Michael Stefan Kiermaier

Submitted to the Department of Physics
on May 20, 2009, in partial fulfillment of the
requirements for the degree of
Doctor of Philosophy

Abstract

Open string field theory provides an action functional for open string fields, and it is thus a manifestly off-shell formulation of open string theory. The solutions to the equation of motion of open string field theory are expected to describe consistent classical open string backgrounds. In this thesis, I present a number of analytic results in bosonic open string field theory. Firstly, I present analytic solutions to the equation of motion that describe an exactly marginal deformation of the chosen open string background. A prominent example in this class is the rolling-tachyon solution, which describes the decay of an unstable D-brane. Furthermore, I demonstrate that the Riemann surface geometry of string perturbation theory can be radically simplified using propagators of Schnabl gauge instead of Siegel gauge. In principle, this simplification allows the analytic computation of arbitrary off-shell one-loop open string amplitudes. Finally, I show that this simplicity of Schnabl gauge one-loop Riemann surfaces can be combined with the knowledge of analytic solutions to construct an analytically computable string field theory boundary state. For all known solutions, this boundary state precisely coincides with the BCFT boundary state of the open string background that the solution is expected to describe. This construction thus confirms the physical interpretation of known analytic solutions and thus provides a nice consistency check on open string field theory.

Thesis Supervisor: Barton Zwiebach
Title: Professor of Physics

Acknowledgments

I would like to thank Barton Zwiebach and Dan Freedman for their patient advising, exceptional support, and countless stimulating discussions during my time at MIT. Their advice over the past years will be invaluable for my future in academia and beyond. I thank Barton for his patience during my initial steps into research, and Dan for his patience during the fifty-mile bike ride!

I thank Yuji Okawa for taking the risk of collaborating with me at an early stage when my knowledge and research experience was still very limited. I thank Henriette Elvang for her patient and pedagogic explanations that tremendously helped me to to get started on a completely different field of research. Working with Yuji and Henriette was both an honor and a pleasure, and I am looking forward to our future work!

I also thank Stephen Naculich, Leonardo Rastelli, and Ashoke Sen for very enjoyable first collaborations, and I hope there will be many more to come!

I want to thank Gita for her invaluable support over the past years, for her help to get through sometimes stressful and difficult stages of my graduate career. You found the right balance between encouragement and distraction from physics!

I want to thank Mark for being a true friend here in Cambridge, for discussions on physics, life, and beyond. I am looking forward to crashing NYC parties with you in the future! I also want to thank Murad, Martin, Frank, Frodo, and Peter for making the trip across the Atlantic to visit Cambridge. In a new environment, there is nothing more valuable than the visit of an old friend!

I also want to thank my parents for their support and council with all the decisions that I made over the last years, and for all the wonderful trips back home that allowed me to "recharge" for future challenges!

Finally, I want to thank "Mom" Holly Kroncke for a wonderful exchange year in the US that was a formative experience and, among many other things, sparked my interest in MIT. A decade later, that dream actually became true!

Contents

Chapter 1

Introduction

The action principle has traditionally been a central concept for the formulation of theories in physics. In many theories, from mechanics to the standard model of elementary particle physics, an action function (or functional) is used to determine the equations of motion for the degrees of freedom in the theory and to calculate quantum effects through the path integral formalism. Applying the action principle to string fields, however, turns out to pose enormous challenges. While the action of bosonic open string field theory [1] and the action of bosonic closed string field theory [2] have been known for many years, the equations of motion derived from them are notoriously hard to solve. In 2005, nearly two decades after the initial formulation of the theory, Schnabl found the first analytic solution of open string field theory. It describes the "tachyon vacuum", *i.e.* a classical open string background with no D-branes present. A new gauge choice, the so-called Schnabl gauge, provided the simplification that made an analytic solution to the equation of motion possible.

Since Schnabl's discovery of an analytic solution, there has been remarkable progress in the analytic understanding of open string field theory [3–41]. The discussion of some of these advances is the main focus of this thesis. We will limit ourselves to bosonic open string field theory, which is an ideal toy model for the more physically relevant open superstring field theory. In fact, almost all results presented in the following chapters have since been generalized to open superstring field theory in a straight-forward manner. Before discussing the details of the new analytic results, however, we will motivate and explain bosonic open string field theory in the remainder of this chapter.

1.1 From string theory to string field theory

The traditional formulation of string theory is a perturbative description of strings propagating in a fixed classical background. The choice of background amounts to the choice of a two-dimensional "world-sheet" conformal field theory (CFT). The choice of a closed string background, which for example includes the choice of a spacetime geometry, is reflected in the bulk action of the CFT. We

also need to choose an open string background by specifying, for example, a classical configuration of D-branes. This choice is reflected in the boundary conditions on the world-sheet, which is equivalent to the choice of a boundary conformal field theory (BCFT). Backgrounds are consistent if the world-sheet theory is indeed conformal.

Once a choice of background has been made, the spectrum of the corresponding world-sheet CFT reflects the possible excitations of a classical string propagating in the chosen background. Different excitation modes are interpreted as distinct spacetime particle species. More precisely, each cohomology class of the BRST operator Q of the CFT represents a distinct particle. The state space of the CFT is a Fock space and can be built from the CFT vacuum $|0\rangle$ by acting with appropriate creation operators. Unlike in quantum field theory, however, acting with several creation operators does not correspond to the creation of several spacetime particles. Instead, this corresponds to creating a *different* spacetime particle associated with a more highly excited and therefore more massive string.

In bosonic string theory formulated around a flat spacetime background, the only matter fields of the world-sheet CFT are the spacetime coordinates X^μ. Denoting the coordinates on the two-dimensional world-sheet by τ and σ, field configurations $X^\mu(\tau,\sigma)$ correspond to embeddings of the world-sheet in spacetime. These configurations thus describe the propagation of a classical string. A consistent Lorentz-invariant quantization of the CFT requires $D = 26$ spacetime dimensions, *i.e.* $\mu = 0, \ldots 25$. The critical dimension for the superstring is lower ($D = 10$), but the number of spacetime dimensions will not play a crucial role in the following. The world-sheet theory has a gauge invariance, which corresponds to reparametrization of the string world-sheet. This gauge symmetry reflects the redundancy in parameterizing the embedding of the two-dimensional world-sheet in spacetime. BRST quantization of the world-sheet theory introduces the ghost field c and the antighost field b of conformal dimensions minus one and two, respectively.

A Dp-brane is a (p+1)-dimensional extended membrane-like object to which open strings attach. If we include a flat D-brane in our choice of a classical background, we obtain a CFT whose state space contains open string excitations. For example a photon of momentum p with polarization ϵ in bosonic open string theory is represented by the state[1]

$$\Psi = \epsilon_\mu \alpha^\mu_{-1} c_1 |k\rangle \,. \qquad \text{with} \quad |k\rangle = e^{ik\,X}|0\rangle \,. \tag{1 1.1}$$

Here α^μ_{-1} is an oscillator of the primary operator ∂X^μ of conformal dimension one, $|0\rangle$ is the SL(2,R) invariant vacuum of the CFT which carries ghost number zero. Finally, c_1 is an oscillator of the ghost field c, so that Ψ carries total ghost number one.

An interesting feature of bosonic open string theory is the existence of a tachyon in its spectrum. Indeed, the state[2]

$$\Psi = c_1|k\rangle \,, \quad \text{with} \quad k^2 = -m^2 = \frac{1}{\alpha'} \,, \tag{1.1.2}$$

[1]Here, and in the following, we use the flat metric $\eta_{\mu\nu}$ with signature $(-,+,+,\ldots,+)$ to raise, lower, and contract Lorentz indices.

[2]The dimensionful parameter α' sets the scale of string theory. It is related to the *string length* ℓ_s through $\ell_s = \sqrt{\alpha'}$.

is on-shell, but it has negative m^2 and is thus a *tachyon.* A tachyon signals an instability in the theory. In field theory, a tachyon arises if we quantize the action around an unstable background, *i.e.* around a classical solution that is not a local minimum of the action. This property of bosonic open string theory was originally interpreted as a signal for its inconsistency, and it led to the subsequent discovery of superstring theory in which many backgrounds permit a tachyon-free quantization. As we will see, however, the tachyon has a clear physical interpretation and bosonic string theory is the ideal testing ground to study instabilities which can in fact also occur in certain backgrounds of superstring theory.

The world-sheet CFT formulation of string theory allows us to perturbatively probe string theory in the vicinity of a chosen background. For example, we can use it to compute scattering amplitudes in this background. Non-perturbative properties of string theory, however, are much harder to obtain in this formulation. Some non-perturbative insights into string theory were obtained from strong-weak dualities, *i.e.* dual descriptions of the theory that become valid when some parameter in the original formulation becomes large. One of the most prominent example of such a duality is the AdS/CFT correspondence, which describes closed superstring theory in an $\mathrm{AdS}_5 \times \mathrm{S}^5$ spacetime geometry in terms of a dual four-dimensional conformal field theory,[3] namely $\mathcal{N} = 4$ super Yang-Mills theory. The gauge theory description becomes weakly coupled precisely when the supergravity description of the string theory breaks down. This happens when the string scale ℓ_s becomes comparable to the characteristic length of the spacetime geometry.

The intricate web of string theory dualities that was developed relies on (an overwhelming amount of) consistency checks, and there is no unified framework or underlying description from which these dualities can be derived. For example, the AdS/CFT correspondence is limited to closed string backgrounds in asymptotically AdS spacetime geometries. Furthermore, evidence for its validity comes for example from the study of symmetries and the study of operators which are protected under the renormalization group flow, rather than from a rigorous derivation from an underlying description.

One of the main motivations and long-term goals for string field theory is to provide such a unified description for string theory. The idea is to develop and study a field theory for the string field Ψ, *i.e.* an action functional $S(\Psi)$. In the current formulations of string field theory, the string field Ψ "lives" in the state space $\mathcal{H}$ of the CFT associated with a chosen background.[4] The classical solutions to the free (quadratic) part $S_0(\Psi)$ of the action $S(\Psi)$ correspond to the perturbative particle excitations of string theory in that background. Non-trivial classical solutions to the full action $S(\Psi)$, on the other hand, are expected describe a different classical background of string theory, distinct from the background the theory is formulated around.

[3] This CFT "lives" on the boundary of the $\mathrm{AdS}_5 \times \mathrm{S}^5$ spacetime, and is not to be confused with the two-dimensional world-sheet CFT.

[4] Because of the ghost fields, the state space of the CFT does not have a positive definite inner product and is thus not a Hilbert space, contrary to what the symbol $\mathcal{H}$ may suggest.

1.2 Sen's conjectures

The tachyonic mode in an open string spectrum signals an instability in the chosen D-brane background. In bosonic string theory, for example, D-branes do not carry any conserved charges and are therefore not protected from decay. The tachyonic mode is the perturbative instability that triggers this decay. The endpoint of the decay, however, is not accessible in perturbation theory. Based on this insight, Ashoke Sen conjectured three properties of open string field theory formulated around such an unstable D-brane background [42]:

1. There should be a classical solution Ψ of open string field theory which describes the endpoint of the decay, *i.e.* the endpoint of *tachyon condensation*. This *tachyon vacuum* solution thus describes a background in which the original D-brane is absent. In particular, the energy of this solution should be precisely $-\mathcal{T}V$, where $\mathcal{T}$ and V are, respectively, the tension and the volume of the original D-brane.

2. As open strings only exist in the presence of D-branes, no perturbative open string excitations should exist around the new background described by Ψ. This then translates into the statement that the cohomology of the BRST operator associated with the vacuum solution is trivial.

3. Starting from bosonic open string field theory formulated around an unstable Dp-brane, lower dimensional D-branes should arise as *solitonic lump* solutions of this theory. These are the endpoints of a tachyon condensation in which the tachyon does not condense homogenously in space, but instead forms a spatial "lump". If there are q spatial dimensions extended along the lump ($q < p$), the solution should be interpreted as a Dq-brane configuration.

Immediately after Sen conjectured these properties, a host of numerical evidence was collected that supplied quantitative support to these conjectures. The first conjecture was since proven analytically by Schnabl [43], who constructed an exact tachyon vacuum solution for Witten's cubic open string field theory.[5] In the following section, we will discuss the basic algebraic ingredients of cubic open string field theory.

1.3 Witten's cubic open string field theory

A candidate for the free (*i.e.* quadratic) part $S_0(\Psi)$ of the open string field action $S(\Psi)$ is easy to construct. Recall that this part of the action must give rise to an equation of motion whose solutions correspond to the physical particle states associated with the chosen background. As mentioned above, physical states live in the cohomology of the BRST operator Q, *i.e.* they satisfy

$$Q\Psi = 0\,, \tag{1.3.1}$$

[5] A formal proof for the second conjecture was also given in [7], where Schnabl and Ellwood argued that the cohomology of the BRST operator around the vacuum solution is trivial.

and Ψ is physically equivalent to Ψ' if

$$\Psi' = \Psi + Q\chi \tag{1.3.2}$$

for some state χ of ghost number zero. Here, and in the following, we assume that the string field Ψ has ghost number one and is thus Grassmann-odd. The equation of motion (1.3.1) arises from the simple action

$$S_0(\Psi) \propto \langle \Psi, Q\Psi \rangle \tag{1.3.3}$$

where $\langle \cdot, \cdot \rangle$ denotes the BPZ inner product of the CFT. For two states $|A\rangle$, $|B\rangle$, it is defined as

$$\langle A, B \rangle \equiv \mathrm{bpz}(|A\rangle)|B\rangle = \langle A|B\rangle \,. \tag{1.3.4}$$

The BPZ inner product is bilinear.

The equivalence relation (1.3.2) arises from the gauge symmetry of the action (1.3.3):

$$\Psi \to \Psi + \delta_\chi \Psi \quad \text{with} \quad \delta_\chi \Psi = Q\chi \,. \tag{1.3.5}$$

To check gauge invariance, we note that the operator Q is nilpotent,

$$Q^2 = 0 \,, \tag{1.3.6}$$

and odd under BPZ conjugation,

$$\langle A, QB \rangle = -(-)^A \langle QA, B \rangle \,. \tag{1.3.7}$$

Here $(-)^A$ is -1 if A is Grassmann-odd, and $+1$ otherwise. The invariance of $S_0(\Psi)$ under the gauge transformation (1.3.5) now immediately follows from (1.3.6) and (1.3.7).

The challenge now is to construct a consistent interacting theory. For bosonic open strings, this problem has a (deceptively simple) solution, which was constructed by Witten in 1985 [1]. His action for the fully interacting theory only contains a cubic interaction term, and takes the Chern-Simons-like form

$$\boxed{S(\Psi) = -\frac{1}{g_o^2}\left[\frac{1}{2}\int \Psi * Q\Psi + \frac{1}{3}\int \Psi * \Psi * \Psi\right].} \tag{1.3.8}$$

Here g_o is the open string coupling constant, and we have introduced the algebraic structures of star multiplication $*$ and integration $\int$:

$$* : \ \mathcal{H} \otimes \mathcal{H} \to \mathcal{H} \,, \qquad \int : \ \mathcal{H} \to \mathbb{C} \,. \tag{1.3.9}$$

The form (1.3.8) of the action is convenient to study classical solutions because it implies the simple equation of motion

$$\boxed{Q\Psi + \Psi * \Psi = 0 \,.} \tag{1.3.10}$$

However, the quadratic term in (1.3.8) leads to kinetic terms for the component fields which are not canonically normalized due to overall multiplication by $1/g_o^2$. To obtain a form that is suitable for (quantum) perturbation theory, we can redefine $\Psi \to g_o \Psi$, which places the coupling g_o in its canonical place in front of the cubic interaction term.

Comparing (1.3.8) to (1.3.3) , we see that it is consistent to define

$$\int A * B \equiv \langle A, B \rangle \,. \tag{1.3.11}$$

We will postpone a concrete conformal field theory implementation of $*$ and $\int$ to the next section, and will limit ourselves to their algebraic properties for now. In Witten's axiomatic approach to string field theory, the algebraic objects Q, $*$, and $\int$ satisfy the following properties:

- The (linear) operator $Q: \mathcal{H} \to \mathcal{H}$ is nilpotent ($Q^2 = 0$).
- Q is a total derivative with respect to the (linear) integration $\int$:

$$\int QA = 0 \qquad \text{for any} \quad A \in \mathcal{H} \,. \tag{1.3.12}$$

- Q is a derivation with respect to the (bilinear) star multiplication $*$:

$$Q(A * B) = (QA) * B + (-)^A A * (QB) \qquad \text{for any} \quad A, B \in \mathcal{H} \,. \tag{1.3.13}$$

- The integration $\int$ satisfies the cyclicity property

$$\int A * B = (-)^{AB} \int B * A \qquad \text{for any} \quad A, B \in \mathcal{H} \,, \tag{1.3.14}$$

  where $(-)^{AB}$ is -1 if both A and B are Grassmann-odd, and $+1$ otherwise.

- Associativity

$$(A * B) * C = A * (B * C) \qquad \text{for any} \quad A, B, C \in \mathcal{H} \,. \tag{1.3.15}$$

The action (1.3.8) has the gauge invariance

$$\Psi \to \Psi + \delta_\chi \Psi \quad \text{with} \quad \delta_\chi \Psi = Q\chi + \Psi * \chi - \chi * \Psi \,, \tag{1.3.16}$$

where the gauge parameter χ is infinitesimal and carries ghost number zero. This is the natural generalization of the gauge transformation (1.3.5) of the free theory. The gauge invariance (1.3.16) is easily checked using the above axioms:

$$\begin{aligned}
(-g_o^2)\, \delta_\chi S(\Psi) &= \frac{1}{2} \int \Big[\Psi * Q(\delta_\chi \Psi) + (\delta_\chi \Psi) * Q\Psi \Big] \\
&\quad + \frac{1}{3} \int \Big[(\delta_\chi \Psi) * \Psi * \Psi + \Psi * (\delta_\chi \Psi) * \Psi + \Psi * \Psi * (\delta_\chi \Psi) \Big] \\
&= \int \Psi * Q(\delta_\chi \Psi) + \int (\delta_\chi \Psi) * \Psi * \Psi \\
&= \int \Psi * Q(\Psi * \chi - \chi * \Psi) + \int (Q\chi + \Psi * \chi - \chi * \Psi) * \Psi * \Psi \\
&= \int Q\big(\chi * \Psi * \Psi\big) = 0 \,.
\end{aligned} \tag{1.3.17}$$

The finite form of the gauge transformation (1.3.16) is

$$\boxed{\Psi \to U^{-1} * \Psi * U + U^{-1} * (QU)\,.} \tag{1.3.18}$$

Here the gauge transformation U is a string field of ghost number zero, and U^{-1} is understood as the inverse of U with respect to the star product:

$$U * U^{-1} = U^{-1} * U = 1\,, \tag{1.3.19}$$

where 1 denotes the identity sting field:

$$A * 1 = 1 * A = A\,, \qquad \text{for any} \quad A \in \mathcal{H}\,. \tag{1.3.20}$$

We can make contact with the infinitesimal gauge transformation (1.3.16) by setting

$$U \equiv \exp(\chi)\,, \quad U^{-1} \equiv \exp(-\chi)\,. \tag{1.3.21}$$

Here the exponentiation of a string field is defined as a series expansion using the star multiplication:

$$\exp\chi = 1 + \chi + \frac{1}{2!}\,\chi * \chi + \frac{1}{3!}\,\chi * \chi * \chi + \ldots\,. \tag{1.3.22}$$

Now that we have explored the algebraic structure of cubic string field theory, we turn to the concrete implementation of this structure in conformal field theory.

1.4 Surface states, star products, and the algebra of wedge states

Above, we already introduced the CFT implementation of the derivation Q - it acts on open string states simply as the BRST operator that arises in the quantization of the world-sheet theory. The CFT implementation of the operations $*$ and $\int$ is most naturally explained for *surface states*.

A surface state $|\Sigma\rangle$ is a CFT state that is specified in terms of a Riemann surface Σ. See Figure 1-1a. The Riemann surface has a *puncture*, *i.e.* a marked point P on its boundary. Furthermore, the Riemann surface carries a *coordinate patch* that is specified by a map f_Σ from the upper half unit disk to a neighborhood of the point P. The real axis is mapped to the boundary of Σ. Denoting the coordinate on the upper half disk by ξ, we thus have

$$f_\Sigma :\ \xi \to \Sigma\,, \qquad f_\Sigma(0) = P\,, \qquad f_\Sigma(\xi) \in \partial\Sigma \quad \text{for} \quad \xi \in \mathbb{R}\,. \tag{1.4.1}$$

To completely specify the state $|\Sigma\rangle$, it is sufficient to specify its inner product $\langle\phi|\Sigma\rangle$ with any state $|\phi\rangle$. Recall that, by the state-operator-correspondence, a state $|\phi\rangle$ can be associated with an operator ϕ. The desired inner products that specify $|\Sigma\rangle$ are then given by

$$\langle\phi|\Sigma\rangle = \langle\phi\,,\,\Sigma\rangle \equiv \big\langle f_\Sigma \circ \phi(0)\big\rangle_\Sigma\,, \tag{1.4.2}$$

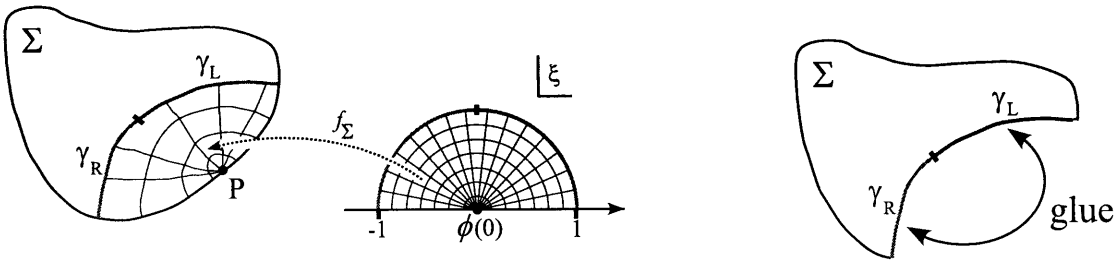

(a) (b)

Figure 1-1: (a) Illustration of a surface state $|\Sigma\rangle$, defined on the Riemann surface Σ with a local coordinate patch around the puncture P. (b) Illustration of $\int \Sigma$, which computes the path integral over the surface with disk topology that arises from the indicated gluing of the coordinate line.

where $\langle [\ldots] \rangle_\Sigma$ denotes the path integral over the Riemann surface Σ, with operator insertions $[\ldots]$ on Σ. Furthermore, $f_\Sigma \circ \phi(0)$ denotes the conformal mapping of the operator $\phi(0)$ from the ξ coordinate to the Riemann surface Σ using f_Σ.

More generally, we will also consider *dressed surface states*. These are surface states $|\Sigma(\mathcal{O})\rangle$ whose Riemann surface Σ is dressed with additional operator insertions $\mathcal{O}$. We require that all operators in $\mathcal{O}$ lie outside the coordinate patch, *i.e.* outside of the image of the upper half disk under f_Σ. A dressed surface state is then completely specified by the inner products

$$\big\langle \phi\,,\, \Sigma(\mathcal{O}) \big\rangle \equiv \big\langle\, f_\Sigma \circ \phi(0)\; \mathcal{O} \,\big\rangle_\Sigma\,. \tag{1.4.3}$$

For string field theory, the midpoint of the coordinate line of a surface state, *i.e.* the point $f_\Sigma(i)$, plays a prominent role. It is natural to split the coordinate line along the midpoint into two parameterized curves γ_L and γ_R:

$$\gamma_L(\theta) = f_\Sigma(e^{\imath\theta})\,, \qquad \gamma_R(\theta) = f_\Sigma(e^{i(\pi-\theta)})\,, \qquad \text{with } \; 0 \le \theta \le \frac{\pi}{2}\,. \tag{1.4.4}$$

See Figure 1-1a. To define the integral over a (dressed) surface state $|\Sigma(\mathcal{O})\rangle$, *i.e.* $\int \Sigma(\mathcal{O})$, we first remove the coordinate patch from the surface Σ, and then glue the parameterized curve $\gamma_L(\theta)$ to $\gamma_R(\theta)$. The resulting surface has the topology of a disk, with operator insertions $\mathcal{O}$. Then $\int \Sigma(\mathcal{O})$ is simply defined as the path integral over this surface. See Figure 1-1b.

The definition of the star product $\Sigma_A * \Sigma_B$ of two (possibly dressed) surface states Σ_A and Σ_B is now straightforward. We remove the coordinate patches from both surface states, and glue the curve $\gamma_R^A(\theta)$ to $\gamma_L^B(\theta)$. The resulting surface still contains two "unglued" curves $\gamma_L^A(\theta)$ and $\gamma_R^B(\theta)$. We use these curves to insert a new coordinate patch. See Figure 1-2. We have thus obtained a surface with disk topology, and a new coordinate patch whose coordinate line consists of γ_L^A and γ_R^B. We use the resulting surface state as our definition of $\Sigma_A * \Sigma_B$. Notice, that the star product of two surface states turned out to be again a surface state.

We have now defined $\int$ and $*$, but the Riemann surfaces resulting from these operations are in general very complicated, and it will then not be simple to compute CFT correlators of operators

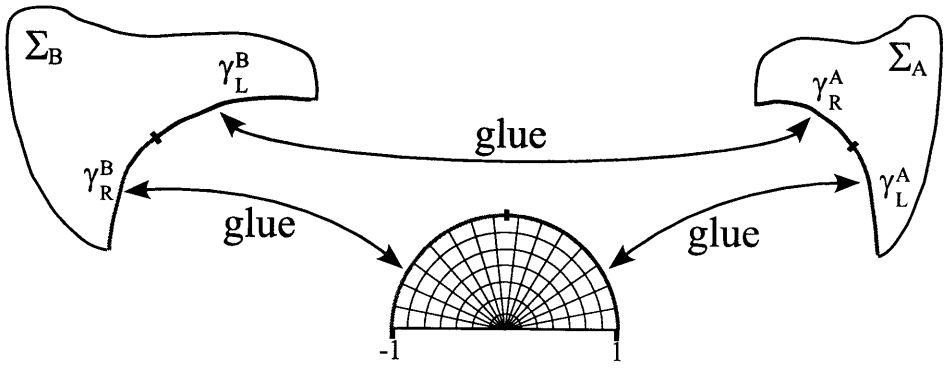

Figure 1-2: Illustration of the star product $\Sigma_A * \Sigma_B$ of two surface states.

on these surfaces. We may therefore ask whether there is a frame in which these operations are natural and calculable. Such a frame indeed exists. It is the *sliver frame*. The sliver frame can be represented in the upper half plane z ($\Re(z) \geq 0$) with the coordinate patch defined through

$$f(\xi) = \frac{2}{\pi} \arctan \xi \,. \tag{1.4.5}$$

Note that the puncture P now sits at the origin in the z frame, and that γ_L and γ_R, *i.e.* the left and right half of the coordinate line, are vertical lines at $\Re(z) = \pm\frac{1}{2}$. The midpoint $f(i)$ has moved off to infinity.

A natural class of surface states that can be defined in the sliver frame are the *wedge states* [44]. We first define the wedge surface $\mathcal{W}_\alpha$ as the Riemann surface that arises in the sliver frame z from the identification $z \sim z+\alpha+1$. In the following, we will represent $\mathcal{W}_\alpha$ in the region $-\frac{1}{2} \leq \Re(z) \leq \frac{1}{2}+\alpha$, with the vertical boundaries $\Re(z) = -\frac{1}{2}$ and $\Re(z) = \frac{1}{2} + \alpha$ identified. Note that the coordinate patch defined through $f(\xi)$ is a vertical strip of unit width on $\mathcal{W}_\alpha$. The remainder of $\mathcal{W}_\alpha$ is a strip of width α. We now define wedge states W_α of width α as the surface state associated with $\mathcal{W}_\alpha$:

$$\langle \phi \,, W_\alpha \rangle \equiv \langle f \circ \phi(0) \rangle_{\mathcal{W}_\alpha} \,. \tag{1.4.6}$$

See Figure 1-3a.

Star multiplication of wedge states is simple - gluing two strips of width α and β to each other with the prescription above results in a strip of width $\alpha + \beta$. Wedge states thus satisfy the simple algebra

$$W_\alpha * W_\beta = W_{\alpha+\beta} \,. \tag{1.4.7}$$

The wedge states of width zero, one, and infinity are of particular importance. Indeed, the wedge of vanishing width is a surface state representation of the identity string field:

$$W_0 = 1 \,. \tag{1.4.8}$$

The wedge of unit width is nothing but the SL(2,R)-invariant vacuum:

$$W_1 = |0\rangle \,. \tag{1.4.9}$$

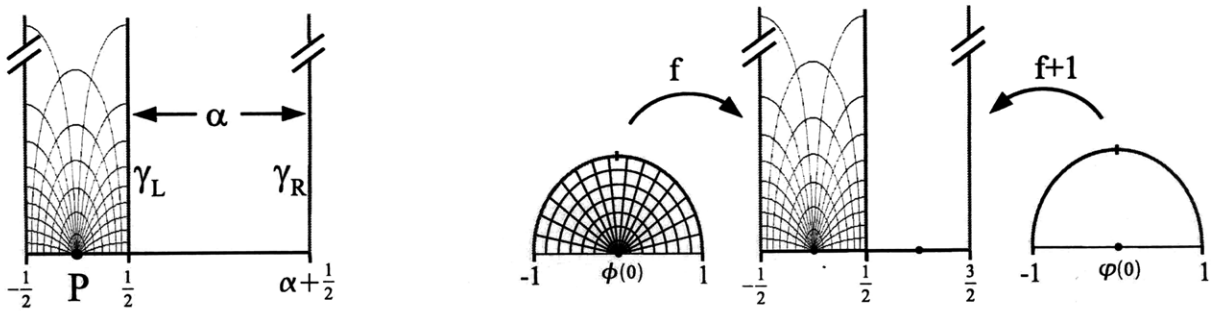

(a) (b)

Figure 1-3: (a) Illustration of a wedge state W_α of width α in the sliver frame. (b) Illustration of a Fock space state $|\varphi\rangle$, represented as a dressed wedge state of unit width. The path integral over the displayed surface computes the BPZ inner product $\langle \phi\,,\, \varphi \rangle$.

Finally, the wedge of infinite width is also a well-defined state in the CFT. It is the *sliver state.* The sliver state is a *projector*, *i.e.* it squares to itself:

$$W_\infty \equiv \lim_{\alpha\to\infty} W_\alpha\,, \qquad W_\infty * W_\infty = W_\infty\,. \tag{1.4.10}$$

We will be particularly interested in dressed wedge states, *i.e.* wedge states W_α that carry additional operator insertions $\mathcal{O}$ in the sliver frame:

$$\big\langle \phi\,,\, W_\alpha(\mathcal{O})\big\rangle \equiv \big\langle f\circ\phi(0)\;\mathcal{O}\,\big\rangle_{\mathcal{W}_\alpha}\,. \tag{1.4.11}$$

For example, any Fock state space $|\varphi\rangle$ associated with an operator φ is a dressed surface state of unit width. We simply map the operator φ from the origin of the upper half unit disk to the point $z = 1$:

$$\big\langle \phi\,,\, \varphi\big\rangle \equiv \big\langle f\circ\phi(0)\;\;(f{+}1)\circ\varphi(0)\,\big\rangle_{\mathcal{W}_1}\,. \tag{1.4.12}$$

See Figure 1-3b. To see that this is the correct prescription to compute the BPZ inner product of two Fock space states ϕ and φ, notice that the maps f and $f+1$ that we used precisely fill the entire wedge surface $\mathcal{W}_1$. This prescription thus simply glues the boundaries of the upper half disks on which ϕ and φ are defined to each other, as expected for the BPZ inner product. One particular example of the wedge representation of a Fock space state was already given above. In fact, the vacuum $|0\rangle$ defined in (1.4.9) is simply the Fock space state associated with the identity operator $\varphi = \mathbf{1}$.

Star multiplication of dressed wedge states is also simple. When we perform the gluing, we only have to be careful to translate the operator insertions to the correct position on the combined strip $\mathcal{W}_{\alpha+\beta}$. Defining the shift map $s_\alpha(z) = z + \alpha$, we have

$$\big\langle \phi\,,\, W_\alpha(\mathcal{O}) * W_\beta(\tilde{\mathcal{O}})\big\rangle \equiv \big\langle f\circ\phi(0)\;\mathcal{O}\;s_\alpha\circ\tilde{\mathcal{O}}\,\big\rangle_{\mathcal{W}_{\alpha+\beta}}\,. \tag{1.4.13}$$

Here $s_\alpha\circ\tilde{\mathcal{O}}$ simply shifts all operators contained in $\tilde{\mathcal{O}}$ by a distance α to the right so that they are correctly placed on the combined wedge of width $\alpha+\beta$.

We have now assembled the basic ingredients necessary for our upcoming discussion of the recent analytic progress in string field theory.

1.5 The outline of this thesis

This thesis will present the results of references [13,21,33,38]. These papers contain various analytical advances in bosonic open string field theory that have been made since Schnabl's discovery of the tachyon vacuum solution. Many of these results have since been translated to open superstring field theory (see, for example, [14, 15, 17, 20, 23]).

In chapter 2, we present the first analytic solution of open string field theory that describes exactly marginal deformations [12, 13]. Whenever a chosen classical open string background is part of a continuously connected one-parameter family of consistent open string backgrounds, the corresponding boundary conformal field theory (BCFT) contains an *exactly marginal operator* V. This operator V is a conformal primary operator of dimension one, and it describes the infinitesimal deformation of the chosen background within the family of backgrounds. For such an exactly marginal deformation, we then expect a one-parameter family of solutions to open string field theory. The solutions describe the other backgrounds to which the chosen background is continuously connected. The solutions presented in chapter 2 satisfy the Schnabl gauge condition and describe *regular* marginal deformations. The deformation associated with an operator V is called regular, if operator products of V with itself do not contain any singularities. An interesting regular marginal deformation is the *rolling-tachyon* solution.[6] It describes the dynamical process of tachyon condensation in which an unstable D-brane starts condensing in the far past and has completely decayed into the vacuum in the far future. We study the rolling-tachyon solution in particular detail, and find that the time evolution of the tachyon field exhibits a wildly oscillating behavior. This behavior is surprising, as one might naively expect a smooth relaxation of the tachyon field to the minimum of its potential. In fact, Sen computed the time evolution of the pressure of the rolling tachyon using the BCFT boundary state, and found a smooth decay of the pressure to zero. We will reconcile these seemingly contradictory results in chapter 5, as explained below.

In chapter 3, we present a different solution of open string field theory that also describes marginal deformations [21]. This solution has the advantage that it is valid for *any* exactly marginal deformation. In particular, it is valid even if operator products of the marginal operator V with itself are singular. Furthermore, the solution is constructed directly from the BCFT operators which implement a change of boundary conditions along a segment of the world-sheet boundary. It thus represents a first step towards a map between consistent conformal boundary conditions (the space of BCFT's), and the space of classical solutions in open string field theory. A simple examples of an exactly marginal deformation whose operator V has singular operator products is the translation of the chosen D-brane background along a spatial direction. A physically more interesting example is the deformation from a Dp-brane to a periodic array of D$(p-1)$-branes. For

[6] This solution is sometimes also called the *half S-brane* solution.

this deformation to be exactly marginal, the periodicity of the D-branes must be a multiple of the critical radius R_c. In this case, the final array of branes has the same energy as the initial D-brane. A general solution for lower dimensional branes, *i.e.* the lump solution conjectured by Sen, remains an interesting open challenge of open string field theory.

The sliver frame, which plays an important role in our construction of solutions in chapters 2 and 3, also has other surprising applications. In chapter 4, we use a sliver frame analysis to show that string perturbation theory in Schnabl gauge leads to a much simpler Riemann surface geometry of tree and one-loop diagrams than in the conventional Siegel gauge or other linear b-gauges [33,45,46]. This is surprising because naively Siegel gauge seems to be the simplest possible gauge for string perturbation theory. In fact, using a Schwinger parametrization for the Siegel gauge propagators, we can build the Riemann surface associated with an amplitude simply by gluing together rectangular strips of width π. The length of the strips are given by the Schwinger parameters. Furthermore, each external state of the amplitude supplies a semi-infinite strip to the Riemann surface. Unfortunately, the assembled Riemann surface is complicated. With few exceptions, it is then impossible to conformally map the surface to a simpler region (such as the disk or the annulus) on which CFT correlators can be computed. Therefore, off-shell amplitude computations in Siegel gauge are prohibitively complicated. In chapter 4, we demonstrate that the computation in Schnabl gauge simplifies significantly. In fact, the moduli of Riemann surfaces can be exactly determined as functions of the Schnabl-gauge Schwinger parameters. In particular, the Riemann surfaces associated with tree and one-loop amplitudes can be analytically mapped to the disk and the annulus, respectively. This in principle allows the computation of arbitrary off-shell tree and one-loop amplitudes in Schnabl gauge.[7]

Finally, in chapter 5, we present a first step towards constructing the BCFT associated with solutions of open string field theory. An important object of every BCFT is its boundary state $|B\rangle$, which encodes all closed-string one-point functions on a disk. Using the simplicity of one-loop Riemann surfaces in Schnabl gauge [33], we construct an analytically calculable "string field theory boundary state" [38]. The construction is motivated by the open string field theory one-loop annulus diagram. The diagram is computed in the background of a classical solution. Surprisingly, we precisely recover the BCFT boundary state from the known wedge-based analytic solutions of open string field theory. This result is surprising, because string field theory boundary states in general only agree *on-shell* with the BCFT boundary state, *i.e.* they agree when contracted with on-shell closed string states. The precise equivalence of boundary states that we find in the computation is thus much stronger than the expected equivalence "up to BRST-exact terms". In particular, this construction is valid for the rolling tachyon solution mentioned above. We thus recover Sen's result of a smoothly decaying pressure, which is encoded in the BCFT boundary state, from the corresponding analytic solution of open string field theory, which exhibits wildly oscillating component fields. This construction of an important BCFT object from string field theory solutions thus confirms the physical interpretation of known analytic solutions and provides a nice check for the consistency of open string field theory as a whole.

[7] We note however, that a proof of the consistency of Schnabl gauge remains an interesting open question.

The recent success of analytic methods for open string field theory has led to exciting progress in the field. However, many interesting open questions remain. While analytic solutions for some classical open string backgrounds were successfully constructed, a systematic prescription for the construction of solutions for a given boundary conformal field theory is still lacking. In particular, Sen's conjectured solitonic lump solution, which describes a lower-dimensional D-brane in the background of a higher dimensional D-brane, has not yet been found. The opposite map, from open string field theory solutions to the space of boundary conformal field theories, has been partially established with the construction of the BCFT boundary state from known analytic solutions, but a deep understanding why this construction succeeded is still lacking.

Analytic progress in string field theory has so far been limited to open strings. It would be interesting to see whether the newly gained insights can be also be used to probe closed string physics. Closed string field theory is a manifestly non-polynomial string field theory, and its current formulation is intimately tied to the use of Siegel gauge. Overcoming these obstacles, for example by finding a new, more flexible formulation of closed string field theory would be an exciting first step. Alternatively, closed string physics may also be accessible within the framework of open string field theory. In fact, the AdS/CFT correspondence suggests that theories of open strings secretely contain a dual closed string description. It would be interesting to see how these non-perturbative degrees of freedom emerge within the framework of string field theory.

Chapter 2

Marginal deformations in Schnabl gauge

2.1 Introduction

In this chapter we describe Schnabl gauge analytic solutions of open string field theory (OSFT) corresponding to exactly marginal deformations of the boundary conformal field theory. We closely follow the approach in [13]. Previous work on exactly marginal deformations in OSFT [47] was based on solving the level-truncated equations of motion in Siegel gauge. The level-truncated string field was determined as a function of the vacuum expectation value of the exactly marginal mode fixed to an arbitrary finite value. Level truncation lifts the flat direction, but it was seen that as the level is increased the flat direction is recovered with better and better accuracy. Instead, our approach is to expand the solution as $\Psi_\lambda = \sum_{n=1}^{\infty} \lambda^n \Psi^{(n)}$, where λ parameterizes the exact flat direction. We solve the equation of motion recursively to find an analytic expression for $\Psi^{(n)}$. Our results are exact in that we are solving the full OSFT equation of motion, but they are perturbative in λ; by contrast, the results of [47] are approximate since the equation of motion has been level-truncated, but they are non-perturbative in the deformation parameter.

The perturbative approach of this chapter has certainly been attempted earlier using the Siegel gauge. Analytic work, however, is out of the question because in the Siegel gauge the Riemann surfaces associated with $\Psi^{(n)}$, with $n > 2$, are very complicated. The new insight that makes the problem tractable is to use, as in [43], the remarkable properties of wedge states with insertions [44, 48, 49].

In this chapter, the matter vertex operator V that generates the deformation is assumed to have regular operator products with itself. In this case, the equation of motion can be systematically solved in the Schnabl gauge. The solution takes a strikingly compact form given in the CFT language by (2.3.3), and its geometric picture is presented in Figure 1. The solution $\Psi^{(n)}$ is made of a wedge state with n insertions of cV on its boundary. The relative separations of the boundary insertions are specified by $n-1$ moduli $\{t_i\}$, with $0 \leq t_i \leq 1$, which are to be integrated over.

Each modulus is accompanied by an antighost line integral $\mathcal{B}$. The explicit evaluation of $\Psi^{(n)}$ in the level expansion is straightforward for a specific choice of V.

We apply this general result to the operator $V = e^{\frac{1}{\sqrt{\alpha'}}X^0}$ [50–56]. This deformation describes a time-dependent tachyon solution that starts at the perturbative vacuum in the infinite past and (if $\lambda < 0$) begins to roll towards the non-perturbative vacuum. The parameter λ can be rescaled by a shift of the origin of time, so the solutions are physically equivalent. The time-dependent tachyon field takes the form

$$T(x^0) = \lambda\, e^{\frac{1}{\sqrt{\alpha'}}x^0} + \sum_{n=2}^{\infty} \lambda^n\, \beta_n\, e^{\frac{1}{\sqrt{\alpha'}}nx^0}\,. \tag{2.1.1}$$

We derive a closed-form integral expression for the coefficients β_n and evaluate them numerically. We find that the coefficients decay so rapidly as n increases that it is plausible that the solution is absolutely convergent for any value of x^0. Our exact result confirms the surprising oscillatory behavior found in the p-adic model [52] and in level-truncation studies of OSFT [52,56]. The tachyon (2.1.1) overshoots the non-perturbative vacuum and oscillates with ever-growing amplitude. It has been argued that a field redefinition to the variables of boundary SFT would map this oscillating tachyon to a tachyon field monotonically relaxing to the non-perturbative vacuum [56]. It would be very interesting to calculate the pressure of this exact solution and check whether it tends to zero in the infinite future, as would be expected from Sen's analysis of tachyon matter [57, 58]. We will address this question in chapter 5.

2.2 The action of B/L

2.2.1 Solving the equation of motion in the Schnabl gauge

For any matter primary field V of dimension one, the state $\Psi^{(1)}$ corresponding to the operator $cV(0)$ is BRST closed:

$$Q_B\Psi^{(1)} = 0\,. \tag{2.2.1}$$

In the context of string field theory, this implies that the linearized equation of motion of string field theory is satisfied. When the marginal deformation associated with V is *exactly* marginal, we expect that a solution of the form

$$\Psi_\lambda = \sum_{n=1}^{\infty} \lambda^n\, \Psi^{(n)}\,, \tag{2.2.2}$$

where λ is a parameter, solves the nonlinear equation of motion

$$Q_B\Psi_\lambda + \Psi_\lambda * \Psi_\lambda = 0\,. \tag{2.2.3}$$

The equation that determines $\Psi^{(n)}$ for $n > 1$ is

$$Q_B\Psi^{(n)} = \Phi^{(n)} \quad \text{with} \quad \Phi^{(n)} = -\sum_{k=1}^{n-1} \Psi^{(n-k)} * \Psi^{(k)}\,. \tag{2.2.4}$$

For this equation to be consistent, $\Phi^{(n)}$ must be BRST closed. This is easily shown using the equations of motion at lower orders. For example,

$$Q_B\Phi^{(2)} = -Q_B\left(\Psi^{(1)} * \Psi^{(1)}\right) = -Q_B\Psi^{(1)} * \Psi^{(1)} + \Psi^{(1)} * Q_B\Psi^{(1)} = 0 \tag{2.2.5}$$

when $Q_B\Psi^{(1)} = 0$. It is crucial that $\Phi^{(n)}$ be BRST *exact* for all $n > 1$, or else we would encounter an obstruction in solving the equations of motion. No such obstruction is expected to arise if the matter operator V is exactly marginal, so we can determine $\Psi^{(n)}$ recursively by solving $Q_B\Psi^{(n)} = \Phi^{(n)}$. This procedure is ambiguous as we can add any BRST-closed term to $\Psi^{(n)}$, so we need to choose some prescription. A traditional choice would be to work in Siegel gauge. The solution $\Psi^{(n)}$ is then given by acting with b_0/L_0 on $\Phi^{(n)}$. In practice this is cumbersome since the combination of star products and operators b_0/L_0 in the Schwinger representation generates complicated Riemann surfaces in the CFT formulation.

Inspired by Schnabl's success in finding an analytic solution for tachyon condensation, it is natural to look for a solution Ψ_λ in the Schnabl gauge:

$$B\Psi_\lambda = 0\,. \tag{2.2.6}$$

Our notation is the same as in [3, 6, 9]. In particular the operators B and L are the zero modes of the antighost and of the energy-momentum tensor T, respectively, in the conformal frame of the sliver,[1]

$$B \equiv \oint \frac{d\xi}{2\pi i}\,\frac{f(\xi)}{f'(\xi)}\,b(\xi)\,, \quad L \equiv \oint \frac{d\xi}{2\pi i}\,\frac{f(\xi)}{f'(\xi)}\,T(\xi)\,, \quad f(\xi) \equiv \frac{2}{\pi}\arctan(\xi)\,. \tag{2.2.7}$$

We define $L^\pm \equiv L \pm L^\star$ and $B^\pm \equiv B \pm B^\star$, where the superscript $\star$ indicates BPZ conjugation, and we denote with subscripts L and R the left and right parts, respectively, of these operators. Formally, a solution of (2.2.4) obeying (2.2.6) can be constructed as follows:

$$\Psi^{(n)} = \frac{B}{L}\Phi^{(n)}\,. \tag{2.2.8}$$

This can also be written as

$$\Psi^{(n)} = \int_0^\infty dT\, Be^{-TL}\,\Phi^{(n)}\,, \tag{2.2.9}$$

if the action of e^{-TL} on $\Phi^{(n)}$ vanishes in the limit $T \to \infty$. It turns out that the action of B/L on $\Phi^{(n)}$ is not always well defined. As was discussed in detail in section 4 of [13], if the matter primary field V has a singular OPE with itself, the formal solution breaks down and the required modification necessarily violates the gauge condition (2.2.6). On the other hand, if operator products of the matter primary field are regular, the formal solution is well defined, as we will confirm later. In the rest of this section, we study the expression (2.2.9) for $n = 2$ in detail.

[1] Using reparameterizations, as in [9], it should be straightforward to generalize the discussion to general projectors. In this chapter we restrict ourselves to the simplest case of the sliver.

2.2.2 Algebraic preliminaries

We prepare for our work by reviewing and deriving some useful algebraic identities. For further details and conventions the reader can refer to [6, 9].

An important role will be played by the operator $L - L_L^+$ and the antighost analog $B - B_L^+$. These operators are derivations of the star algebra. This is seen by writing the first one, for example, as a sum of two familiar derivations in the following way:

$$L - L_L^+ = \frac{1}{2}L^- + \frac{1}{2}(L_R^+ + L_L^+) - L_L^+ = \frac{1}{2}L^- + \frac{1}{2}(L_R^+ - L_L^+) = \frac{1}{2}(L^- + K)\,. \tag{2.2.10}$$

We therefore have

$$(L - L_L^+)\,(\phi_1 * \phi_2) = (L - L_L^+)\,\phi_1 * \phi_2 + \phi_1 * (L - L_L^+)\phi_2\,. \tag{2.2.11}$$

Noting that $L_L^+\,(\phi_1 * \phi_2) = L_L^+\,\phi_1 * \phi_2$, we find

$$L(\phi_1 * \phi_2) = L\phi_1 * \phi_2 + \phi_1 * (L - L_L^+)\,\phi_2\,, \tag{2.2.12}$$

$$B(\phi_1 * \phi_2) = B\phi_1 * \phi_2 + (-1)^{\phi_1}\phi_1 * (B - B_L^+)\phi_2\,. \tag{2.2.13}$$

Here and in what follows. a string field in the exponent of -1 denotes its Grassmann property: it is 0 mod 2 for a Grassmann-even string field and 1 mod 2 for a Grassmann-odd string field. From (2.2.12) and (2.2.13) we immediately deduce formulas for products of multiple string fields. For B, for example, we have

$$B(\phi_1 * \phi_2 * \ldots \phi_n) = (B\phi_1) * \ldots * \phi_n + \sum_{m=2}^{n}(-1)^{\sum_{k=1}^{m-1}\phi_k}\,\phi_1 * \ldots * (B - B_L^+)\phi_m * \ldots * \phi_n\,. \tag{2.2.14}$$

Exponentiation of (2.2.12) gives

$$e^{-TL}(\phi_1 * \phi_2) = e^{-TL}\phi_1 * e^{-T(L - L_L^+)}\phi_2\,. \tag{2.2.15}$$

From the familiar commutators

$$[L, L^+] = L^+\,, \quad [B, L^+] = B^+\,, \tag{2.2.16}$$

we deduce

$$[L, L_L^+] = L_L^+\,, \quad [B, L_L^+] = B_L^+\,. \tag{2.2.17}$$

See section 2 of [6] for a careful analysis of this type of manipulations. We will need to reorder exponentials of the derivation $L - L_L^+$. We claim that

$$e^{-T(L - L_L^+)} = e^{(1 - e^{-T})L_L^+}\,e^{-TL}\,. \tag{2.2.18}$$

The above is a particular case of the Baker-Campbell-Hausdorff formula for a two-dimensional Lie algebra with generators x and y and commutation relation $[x, y] = y$. In the adjoint representation we can write

$$x = \begin{pmatrix} 0 & 1 \\ 0 & 1 \end{pmatrix}\,, \quad y = \begin{pmatrix} -1 & 1 \\ -1 & 1 \end{pmatrix}\,. \tag{2.2.19}$$

It follows that as two-by-two matrices, $x^2 = x$, $xy = y$, $yx = 0$, and $y^2 = 0$. One then verifies that

$$e^{\alpha x+\beta y} = e^{\frac{\beta}{\alpha}(e^{\alpha}-1)y}\, e^{\alpha x} \quad \text{when} \quad [x,y] = y\,. \tag{2.2.20}$$

With $\alpha = -\beta = -T$, $x = L$, and $y = L_L^+$, (2.2.20) reproduces (2.2.18).

2.2.3 The action of B/L and its geometric interpretation

We are now ready to solve the equation for $\Psi^{(2)}$. The state $\Psi^{(1)}$ satisfies

$$Q_B\Psi^{(1)} = 0\,, \qquad B\Psi^{(1)} = 0\,, \qquad L\Psi^{(1)} = 0\,. \tag{2.2.21}$$

We will use correlators in the sliver frame to represent states made of wedge states and operator insertions. The state $\Psi^{(1)}$ can be described as follows:

$$\langle\, \phi, \Psi^{(1)} \,\rangle = \langle\, f\circ\phi(0)\, cV(1) \,\rangle_{\mathcal{W}_1}\,. \tag{2.2.22}$$

Note that cV is a primary field of dimension zero so that there is no associated conformal factor. Here and in what follows we use ϕ to denote a generic state in the Fock space and $\phi(0)$ to denote its corresponding operator. The surface $\mathcal{W}_\alpha$ is the one associated with the wedge state W_α in the sliver conformal frame. We use the doubling trick in calculating correlators. We define the oriented straight lines $V_\alpha^\pm$ by

$$\begin{aligned} &V_\alpha^\pm = \Big\{\, z \,\Big|\, \mathrm{Re}(z) = \pm\frac{1}{2}(1+\alpha) \,\Big\}\,, \\ &\text{orientation}\,:\, \pm\frac{1}{2}(1+\alpha) - i\,\infty \to \pm\frac{1}{2}(1+\alpha) + i\,\infty\,. \end{aligned} \tag{2.2.23}$$

The surface $\mathcal{W}_\alpha$ can be represented as the region between V_0^- and $V_{2\alpha}^+$, where V_0^- and $V_{2\alpha}^+$ are identified by translation.

A formal solution to the equation $Q_B\Psi^{(2)} = -\Psi^{(1)} * \Psi^{(1)}$ is

$$\Psi^{(2)} = -\int_0^\infty dT\, Be^{-TL}\big[\,\Psi^{(1)} * \Psi^{(1)}\big]\,. \tag{2.2.24}$$

By construction, $B\Psi^{(2)} = 0$. Using the identities (2.2.15) and (2.2.13), we have

$$\Psi^{(2)} = -\int_0^\infty dT\, \Big[\, B\, e^{-TL}\,\Psi^{(1)} * e^{-T(L-L_L^+)}\,\Psi^{(1)} - e^{-TL}\,\Psi^{(1)} * (B - B_L^+)\, e^{-T(L-L_L^+)}\,\Psi^{(1)} \Big]\,. \tag{2.2.25}$$

Because of the properties of $\Psi^{(1)}$ in (2.2.21), the first term vanishes and the second reduces to

$$\Psi^{(2)} = \int_0^\infty dT\, \Psi^{(1)} * (B - B_L^+)\, e^{-T(L-L_L^+)}\,\Psi^{(1)}\,. \tag{2.2.26}$$

We further use the identity (2.2.18) together with $L\Psi^{(1)} = 0$ to find

$$\Psi^{(2)} = \int_0^\infty dT\, \Psi^{(1)} * (B - B_L^+)\, e^{(1-e^{-T})L_L^+}\,\Psi^{(1)}\,. \tag{2.2.27}$$

It follows from $[B, L_L^+] = B_L^+$ that $[B, g(L_L^+)] = B_L^+ g'(L_L^+)$ for any analytic function g. Using this formula with $B\Psi^{(1)} = 0$, we find

$$\Psi^{(2)} = -\int_0^\infty dT\, e^{-T}\, \Psi^{(1)} * e^{(1-e^{-T})L_L^+}\, B_L^+ \Psi^{(1)}\,. \tag{2.2.28}$$

Using the change of variables $t = e^{-T}$, we obtain the following final expression of $\Psi^{(2)}$:

$$\Psi^{(2)} = \int_0^1 dt\, \Psi^{(1)} * e^{-(t-1)L_L^+}\, (-B_L^+)\, \Psi^{(1)}\,. \tag{2.2.29}$$

There is a simple geometric picture for $\Psi^{(2)}$. Let us represent $\langle\, \phi, \Psi^{(2)}\,\rangle$ in the CFT formulation. The exponential action of L_L^+ on a generic string field A can be written as

$$e^{-\alpha L_L^+} A = e^{-\alpha L_L^+}(\mathcal{I} * A) = e^{-\alpha L_L^+}\mathcal{I} * A = W_\alpha * A\,. \tag{2.2.30}$$

Here we have recalled the familiar expression of the wedge state $W_\alpha = e^{-\frac{\alpha}{2}L^+}\mathcal{I} = e^{-\alpha L_L^+}\mathcal{I}$ [43], where $\mathcal{I}$ is the identity string field. We thus learn that $e^{-\alpha L_L^+}$ with $\alpha > 0$ creates a semi-infinite strip with a width of α in the sliver frame, while $e^{-\alpha L_L^+}$ with $\alpha < 0$ deletes a semi-infinite strip with a width of $|\alpha|$. The inner product $\langle\, \phi, \Psi^{(2)}\,\rangle$ is thus represented by a correlator on $\mathcal{W}_{2-|t-1|} = \mathcal{W}_{1+t}$. In other words, the integrand in (2.2.29) is made of the wedge state W_{1+t} with operator insertions. The state ϕ is represented by the region between V_0^- and V_0^+ with the operator insertion $f \circ \phi(0)$ at the origin. The left factor of $\Psi^{(1)}$ in (2.2.29) can be represented by the region between V_0^+ and V_2^+ with an insertion of cV at $z = 1$. For $t = 1$ the right factor of $\Psi^{(1)}$ can be represented by the region between V_2^+ and V_4^+ with an insertion of cV at $z = 2$. For $0 < t < 1$, the region is shifted to the one between $V_{2-2|t-1|}^+ = V_{2t}^+$ and $V_{4-2|t-1|}^+ = V_{2+2t}^+$, and the insertion of cV is at $z = 2 - |t-1| = 1 + t$. Finally, the operator $(-B_L^+)$ is represented by an insertion of $\mathcal{B}$ [9] defined by

$$\mathcal{B} = \int \frac{dz}{2\pi i}\, b(z)\,, \tag{2.2.31}$$

where the contour of the integral can be taken to be $-V_\alpha^+$ with $1 < \alpha < 1 + 2t$. We thus have

$$\langle\, \phi, \Psi^{(2)}\,\rangle = \int_0^1 dt\, \langle\, f \circ \phi(0)\, cV(1)\, \mathcal{B}\, cV(1+t)\,\rangle_{\mathcal{W}_{1+t}}\,. \tag{2.2.32}$$

As $t \to 0$ the pair of cV's collide, and at $t = 1$ they attain the maximum separation.

The state $\Psi^{(2)}$ should formally solve the equation of motion by construction. Let us examine the BRST transformation of $\Psi^{(2)}$ more carefully based on the expression (2.2.32). The BRST operator in $\langle\, \phi, Q_B\Psi\,\rangle$ can be represented as an integral of the BRST current on $V_{2(1+t)}^+ - V_0^+$:[2]

$$\langle\, \phi, Q_B\Psi^{(2)}\,\rangle = \int_0^1 dt \left\langle\, f \circ \phi(0) \int_{-V_0^+ + V_{2(1+t)}^+} \frac{dz}{2\pi i}\, j_B(z)\; cV(1)\, \mathcal{B}\, cV(1+t) \right\rangle_{\mathcal{W}_{1+t}}\,, \tag{2.2.33}$$

[2]To derive this we first use the relation $\langle\, \phi, Q_B\Psi^{(2)}\,\rangle = -(-1)^\phi\, \langle\, Q_B\phi, \Psi^{(2)}\,\rangle$, where Q_B on the right-hand side is an integral of the BRST current j_B over a contour that encircles the origin counterclockwise, with the operator j_B placed to the left of $f \circ \phi(0)$ in the correlator. Using the identification of the surface $\mathcal{W}_{1+t}$, the contour can be deformed to $-V_{2(1+t)}^+ + V_0^+$. In the correlator, we move the BRST current from the left of $f \circ \phi(0)$ to the right of it. This cancels $(-1)^\phi$, and the additional minus sign is canceled by reversing the orientation of the contour.

where j_B is the BRST current. Since cV is BRST closed, the only nontrivial action of the BRST operator is to change the insertion of the antighost to that of the energy-momentum tensor:

$$\langle \phi, Q_B \Psi^{(2)} \rangle = -\int_0^1 dt \, \langle f \circ \phi(0) \, cV(1) \, \mathcal{L} \, cV(1+t) \rangle_{\mathcal{W}_{1+t}} , \tag{2.2.34}$$

where

$$\mathcal{L} = \int \frac{dz}{2\pi i} T(z) , \tag{2.2.35}$$

and the contour of the integral can be taken to be $-V_\alpha^+$ with $1 < \alpha < 1 + 2t$. The minus sign on the right-hand side of (2.2.34) is from anticommuting the BRST current with the left cV. Since $\partial_t \, e^{-tL_L^+} = -L_L^+ \, e^{-tL_L^+}$ and $-L_L^+$ corresponds to $\mathcal{L}$ in the correlator, an insertion of $\mathcal{L}$ is equivalent to taking a derivative with respect to t [3]. We thus find

$$\langle \phi, Q_B \Psi^{(2)} \rangle = -\int_0^1 dt \, \frac{\partial}{\partial t} \langle f \circ \phi(0) \, cV(1) \, cV(1+t) \rangle_{\mathcal{W}_{1+t}} . \tag{2.2.36}$$

The surface term from $t = 1$ gives $-\Psi^{(1)} * \Psi^{(1)}$. The equation of motion is therefore satisfied if the surface term from $t = 0$ vanishes. The surface term from $t = 0$ vanishes if

$$\lim_{t \to 0} cV(0) \, cV(t) = 0 . \tag{2.2.37}$$

Therefore, $\Psi^{(2)}$ defined by (2.2.32) does solve the equation $Q_B \Psi^{(2)} + \Psi^{(1)} * \Psi^{(1)} = 0$ when V satisfies (2.2.37). Since $\Psi^{(1)} * \Psi^{(1)}$ is a finite state, the equation guarantees that $Q_B \Psi^{(2)}$ is also finite. However, it is still possible that $\Psi^{(2)}$ has a divergent term which is BRST closed. The ghost part of $\Psi^{(2)}$ is finite since it is given by an integral of ψ_t over t from $t = 0$ to $t = 1$, where ψ_n is the key ingredient in the tachyon vacuum solution [43]:

$$\langle \phi, \psi_n \rangle = \langle f \circ \phi(0) \, c(1) \, \mathcal{B} \, c(1+n) \rangle_{\mathcal{W}_{1+n}} , \tag{2.2.38}$$

and the contour of the integral for $\mathcal{B}$ can be taken to be $-V_\alpha$ with $1 < \alpha < 2n + 1$. When the operator product of V with itself is regular, the condition (2.2.37) is satisfied and $\Psi^{(2)}$ itself is finite. Note that $V(0) \, V(t)$ in the limit $t \to 0$ can be finite or can be vanishing. We construct $\Psi^{(n)}$ for marginal operators with regular operator products in the next section. When the operator product of V with itself is singular, the formal solution $\Psi^{(2)}$ is not well defined. We postpone the discussion of marginal solutions with singular operator products to chapter 3.

2.3 Solutions for marginal operators with regular operator products

In the previous section we constructed a well-defined solution to the equation $Q_B \Psi^{(2)} + \Psi^{(1)} * \Psi^{(1)} = 0$ when V has a regular operator product. In this section we generalize it to $\Psi^{(n)}$ for any n. We then present the solution that corresponds to the decay of an unstable D-brane in §2.3.2.

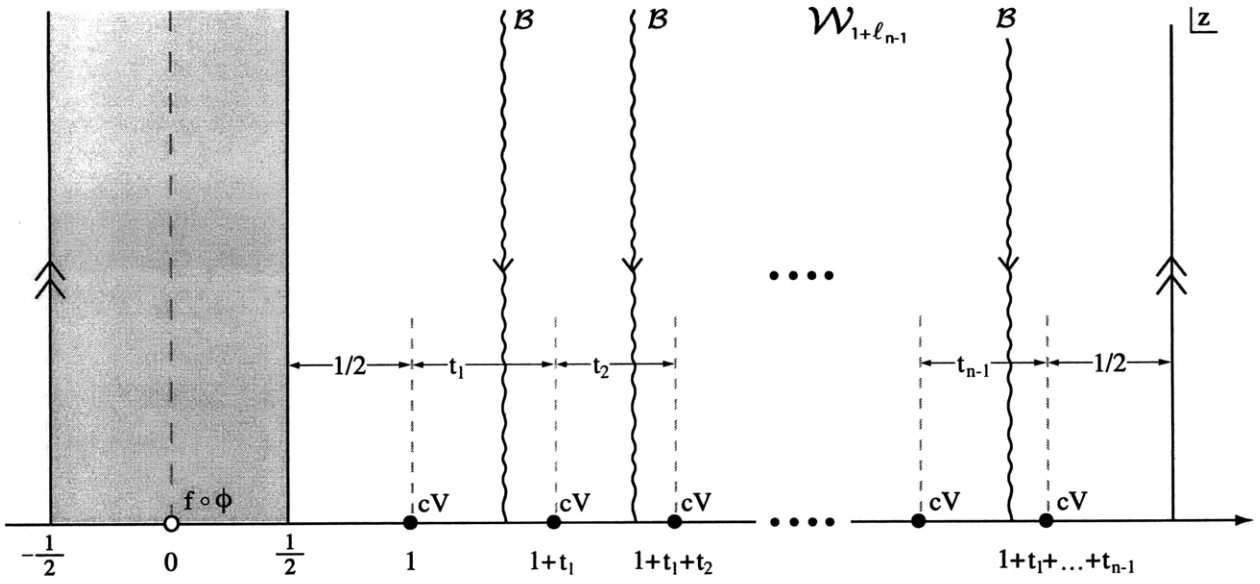

Figure 2-1: The surface $\mathcal{W}_{1+\ell_{n-1}}$ with the operator insertions used to construct the solution $\Psi^{(n)}$ given in (2.3.3). The parameters $t_1, t_2, \ldots, t_{n-1}$ must all be integrated from zero to one. The leftmost and rightmost vertical lines with double arrows are identified.

2.3.1 Solution

Once we understand how $\Psi^{(2)}$ in the form of (2.2.32) satisfies the equation of motion, it is easy to construct $\Psi^{(n)}$ satisfying $Q_B\Psi^{(n)} = \Phi^{(n)}$. It is given by

$$\begin{aligned}\langle\, \phi, \Psi^{(n)} \,\rangle = \int_0^1 dt_1 \int_0^1 dt_2 \ldots \int_0^1 dt_{n-1} \,\langle\, f\circ\phi(0)\, cV(1)\, \mathcal{B}\, cV(1+t_1)\, \mathcal{B}\, cV(1+t_1+t_2)\, \ldots \\ \times \mathcal{B}\, cV(1+t_1+t_2+\ldots+t_{n-1}) \,\rangle_{\mathcal{W}_{1+t_1+t_2+\ldots+t_{n-1}}} .\end{aligned} \tag{2.3.1}$$

Introducing the length parameters

$$\ell_i \equiv \sum_{k=1}^{i} t_k \,, \tag{2.3.2}$$

the solution can be written more compactly as

$$\boxed{\langle\, \phi, \Psi^{(n)} \,\rangle = \int_0^1 dt_1 \int_0^1 dt_2 \ldots \int_0^1 dt_{n-1} \left\langle\, f\circ\phi(0)\, cV(1) \prod_{i=1}^{n-1} \Big[\, \mathcal{B}\, cV(1+\ell_i) \,\Big] \,\right\rangle_{\mathcal{W}_{1+\ell_{n-1}}} .} \tag{2.3.3}$$

See Figure 2-1. The solution obeys the Schnabl gauge condition. It is remarkably simple contrasted with the expression one would obtain in Siegel gauge.

Let us now prove that the equation of motion is satisfied for (2.3.3). It is straightforward to generalize the calculation of $\langle\, \phi, Q_B\Psi^{(2)} \,\rangle$ in the previous section to that of $\langle\, \phi, Q_B\Psi^{(n)} \,\rangle$. The BRST operator in $\langle\, \phi, Q_B\Psi^{(n)} \,\rangle$ can be represented as an integral of the BRST current on $V^+_{2(1+\ell_{n-1})} - V^+_0$.

Since cV is BRST closed, the BRST operator acts only on the insertions of $\mathcal{B}$'s:

$$\begin{aligned}\langle\, \phi, Q_B \Psi^{(n)} \,\rangle = & -\sum_{j=1}^{n-1} \int_0^1 dt_1 \int_0^1 dt_2 \ldots \int_0^1 dt_{n-1} \Big\langle\, f \circ \phi(0)\, cV(1) \prod_{i=1}^{j-1} \Big[\, \mathcal{B}\, cV(1+\ell_i) \,\Big] \\ & \times \mathcal{L}\, cV(1+\ell_j) \prod_{k=j+1}^{n-1} \Big[\, \mathcal{B}\, cV(1+\ell_k) \,\Big] \,\Big\rangle_{\mathcal{W}_{1+\ell_{n-1}}} .\end{aligned} \tag{2.3.4}$$

An insertion of $\mathcal{L}$ between $cV(1+\ell_{j-1})$ and $cV(1+\ell_j)$ corresponds to taking a derivative with respect to t_j. When operator products of V are regular, we have

$$\begin{aligned}\langle\, \phi, Q_B \Psi^{(n)} \,\rangle = & -\sum_{j=1}^{n-1} \int_0^1 dt_1 \int_0^1 dt_2 \ldots \int_0^1 dt_{n-1}\, \partial_{t_j} \Big\langle\, f \circ \phi(0)\, cV(1) \prod_{i=1}^{j-1} \Big[\, \mathcal{B}\, cV(1+\ell_i) \,\Big] \\ & \times cV(1+\ell_j) \prod_{k=j+1}^{n-1} \Big[\, \mathcal{B}\, cV(1+\ell_k) \,\Big] \,\Big\rangle_{\mathcal{W}_{1+\ell_{n-1}}} \\ = & -\sum_{j=1}^{n-1} \int_0^1 dt_1 \int_0^1 dt_2 \ldots \int_0^1 dt_{j-1} \int_0^1 dt_{j+1} \ldots \int_0^1 dt_{n-1} \Big\langle\, f \circ \phi(0)\, cV(1) \\ & \times \prod_{i=1}^{j-1} \Big[\, \mathcal{B}\, cV(1+\ell_i) \,\Big]\, cV(1+\ell_j) \prod_{k=j+1}^{n-1} \Big[\, \mathcal{B}\, cV(1+\ell_k) \,\Big] \,\Big\rangle_{\mathcal{W}_{1+\ell_{n-1}}} \Big|_{t_j=1} \\ = & -\sum_{j=1}^{n-1} \langle\, \phi, \Psi^{(j)} * \Psi^{(n-j)} \,\rangle .\end{aligned} \tag{2.3.5}$$

The equation of motion is thus satisfied.[3]

We can also derive this expression of $\Psi^{(n)}$ by acting with B/L on $\Phi^{(n)}$. It is in fact interesting to see how the region of the integrals over $t_1, t_2, \ldots, t_{n-1}$ is reproduced. Let us demonstrate it taking the case of $\Psi^{(3)}$ as an example. Using the Schwinger representation of B/L, the expression (2.2.26) for $\Psi^{(2)}$, and the identities (2.2.15) and (2.2.14), we have

$$\begin{aligned}\Psi^{(3)} &= -\int_0^\infty dT_2\, B\, e^{-T_2 L} \left[\, \Psi^{(1)} * \Psi^{(2)} + \Psi^{(2)} * \Psi^{(1)} \,\right] \\ &= -\int_0^\infty dT_2 \int_0^\infty dT_1\, B\, e^{-T_2 L} \left[\, \Psi^{(1)} * \Psi^{(1)} * (B - B_L^+)\, e^{-T_1 (L - L_L^+)}\, \Psi^{(1)} \right. \\ &\qquad \left. + \Psi^{(1)} * (B - B_L^+)\, e^{-T_1 (L - L_L^+)}\, \Psi^{(1)} * \Psi^{(1)} \,\right] \\ &= \int_0^\infty dT_1 \int_0^\infty dT_2 \left[\, \Psi^{(1)} * (B - B_L^+)\, e^{-T_2 (L - L_L^+)}\, \Psi^{(1)} * (B - B_L^+)\, e^{-(T_1+T_2)(L - L_L^+)}\, \Psi^{(1)} \right. \\ &\qquad \left. + \Psi^{(1)} * (B - B_L^+)\, e^{-(T_1+T_2)(L - L_L^+)}\, \Psi^{(1)} * (B - B_L^+)\, e^{-T_2 (L - L_L^+)}\, \Psi^{(1)} \,\right] .\end{aligned} \tag{2.3.6}$$

By changing variables as $\tau_1 = T_2$ and $\tau_2 = T_1 + T_2$ for the first term and as $\tau_2 = T_2$ and $\tau_1 = T_1 + T_2$ for the second term, the two terms combine into

$$\Psi^{(3)} = \int_0^\infty d\tau_1 \int_0^\infty d\tau_2\, \Psi^{(1)} * (B - B_L^+)\, e^{-\tau_1 (L - L_L^+)}\, \Psi^{(1)} * (B - B_L^+)\, e^{-\tau_2 (L - L_L^+)}\, \Psi^{(1)} . \tag{2.3.7}$$

[3] We assume that operator products of more than two V's are also regular in order for the surface term from $t_j = 0$ to vanish.

The same manipulations we performed with $\Psi^{(2)}$ give

$$\Psi^{(3)} = \int_0^1 dt_1 \int_0^1 dt_2\, \Psi^{(1)} * e^{-(t_1-1)L_L^+}(-B_L^+)\, \Psi^{(1)} * e^{-(t_2-1)L_L^+}(-B_L^+)\, \Psi^{(1)} \tag{2.3.8}$$

and the following expression in the CFT formulation:

$$\langle\, \phi, \Psi^{(3)} \,\rangle = \int_0^1 dt_1 \int_0^1 dt_2\, \langle\, f\circ\phi(0)\, cV(1)\, \mathcal{B}\, cV(1+t_1)\, \mathcal{B}\, cV(1+t_1+t_2) \,\rangle_{\mathcal{W}_{1+t_1+t_2}} \tag{2.3.9}$$

in agreement with (2.3.3). It is not difficult to use induction to prove that for all n (2.3.3) follows from the action of B/L on $\Phi^{(n)}$.

We conclude the subsection by writing other forms of the solution that are suitable for explicit calculations. We represent the surface $\mathcal{W}_\alpha$ as the region between V_2^- and $V_{2(\alpha-1)}^+$. The operator $cV(1+\ell_{n-1})$ in (2.3.3) is then mapped to $cV(-1)$. We further transform $\langle\, \phi, \Psi^{(n+1)} \,\rangle$ in the following way:

$$\begin{aligned}
\langle\, \phi, \Psi^{(n+1)} \,\rangle &= \int_0^1 dt_1 \ldots \int_0^1 dt_n \Big\langle cV(-1)\, f\circ\phi(0)\, cV(1) \prod_{i=1}^{n-1} \Big[\mathcal{B}\, cV(1+\ell_i)\Big]\mathcal{B} \Big\rangle_{\mathcal{W}_{1+\ell_n}} \\
&= \int_0^1 dt_1 \ldots \int_0^1 dt_n \Big\langle cV(-1)\, f\circ\phi(0)\, cV(1) \prod_{i=1}^{n-1} \Big[V(1+\ell_i)\Big]\mathcal{B} \Big\rangle_{\mathcal{W}_{1+\ell_n}} \\
&= -\int_0^1 dt_1 \ldots \int_0^1 dt_n \frac{1}{2+\ell_n} \\
&\qquad \times \Big\langle \int_{V_{2\ell_n}^+ - V_2^-} \frac{dz}{2\pi i}\, z\, b(z) \Big[cV(-1)\, f\circ\phi(0)\, cV(1)\Big] \prod_{i=1}^{n-1} \Big[V(1+\ell_i)\Big] \Big\rangle_{\mathcal{W}_{1+\ell_n}} .
\end{aligned} \tag{2.3.10}$$

First we recursively used the relation $\mathcal{B}\, c(z)\, \mathcal{B} = \mathcal{B}$, which follows from $\{\, \mathcal{B},\, c(z)\,\} = 1$ and $\mathcal{B}^2 = 0$. In the last step, we used the identity

$$\int_{V_{2(\alpha-1)}^+ - V_2^-} \frac{dz}{2\pi i}\, z\, b(z) = (\alpha+1) \int_{V_{2(\alpha-1)}^+} \frac{dz}{2\pi i}\, b(z) \quad \text{on} \quad \mathcal{W}_\alpha\,. \tag{2.3.11}$$

This follows from

$$\int_{V_2^-} \frac{dz_-}{2\pi i}\, z_-\, b(z_-) = \int_{V_{2(\alpha-1)}^+} \frac{dz_+}{2\pi i} \Big\{\, z_+ - (\alpha+1)\,\Big\}\, b(z_+) \quad \text{on} \quad \mathcal{W}_\alpha\,, \tag{2.3.12}$$

where the coordinate z_- for V_2^- and the coordinate z_+ for $V_{2(\alpha-1)}^+$ are identified by $z_+ = z_- + \alpha + 1$. The contour $V_{2\ell_n}^+ - V_2^-$ can be deformed to encircle $cV(-1)$, $f\circ\phi(0)$, and $cV(1)$, and we obtain

$$\begin{aligned}
\langle\, \phi, \Psi^{(n+1)} \,\rangle = \int_0^1 dt_1 \ldots \int_0^1 dt_n \frac{1}{2+\ell_n} \Big\langle\, \Big\{ & V(-1)\, f\circ\phi(0)\, cV(1) + cV(-1)\, f\circ\phi(0)\, V(1) \\
& + cV(-1) \Big[\oint \frac{dz}{2\pi i}\, z\, b(z)\, f\circ\phi(0) \Big]\, cV(1) \Big\} \prod_{i=1}^{n-1} V(1+\ell_i) \Big\rangle_{\mathcal{W}_{1+\ell_n}} ,
\end{aligned} \tag{2.3.13}$$

where the contour in the last line encircles the origin counterclockwise.

When $\phi(0)$ factorizes into a matter part $\phi_m(0)$ and a ghost part $\phi_g(0)$, we can use the matter-ghost factorization of the correlator to give an alternative form of (2.3.3):

$$\begin{aligned}\langle\, \phi, \Psi^{(n)} \,\rangle = \int_0^1 dt_1 \int_0^1 dt_2 \ldots \int_0^1 dt_{n-1} \Big\langle\, f \circ \phi_m(0) \prod_{i=0}^{n-1} V(1+\ell_i) \,\Big\rangle_{\mathcal{W}_{1+\ell_{n-1}},\, m} \\ \times \Big\langle\, f \circ \phi_g(0)\, c(1)\, \mathcal{B}\, c(1+\ell_{n-1}) \,\Big\rangle_{\mathcal{W}_{1+\ell_{n-1}},\, g}\,,\end{aligned} \tag{2.3.14}$$

where $\ell_0 \equiv 0$ and we denoted matter and ghost correlators by subscripts m and g, respectively. The ghost correlator in the above expression is $\langle\, \phi_g, \psi_{\ell_{n-1}} \,\rangle$ in (2.2.38). The algorithm for its calculation has been developed in [9, 43].

2.3.2 Rolling tachyon marginal deformation to all orders

We can now apply the general solution (2.3.13) to the special case of a marginal deformation corresponding to a rolling tachyon. For this purpose we pick the operator

$$V(z,\bar{z}) = e^{\frac{1}{\sqrt{\alpha'}} X^0(z,\bar{z})} \tag{2.3.15}$$

restricted to the boundary $z = \bar{z} = y$ of the upper-half plane $\mathbb{H}$, where we write it as[4]

$$V(y) = e^{\frac{1}{\sqrt{\alpha'}} X^0(y)}\,, \qquad X^0(y) \equiv X^0(y,y)\,. \tag{2.3.16}$$

The operator $e^{ik\cdot X(y)}$ has dimension $\alpha' k^2$ and we can write

$$V(y) = e^{ik\cdot X(y)} \quad \text{with} \quad k^\mu = \frac{i}{\sqrt{\alpha'}}(1,\vec{0}\,) \;\to\; \alpha' k^2 = 1\,, \tag{2.3.17}$$

showing that V is a matter primary field of dimension one. We also have

$$V(y)V(0) \sim |y|^2 V(0)^2\,, \tag{2.3.18}$$

and the matter operator satisfies the requisite regularity condition.

We will also use exponential operators of X^0 with different exponents. We thus record the following transformation law and ordering results:

$$f \circ e^{\frac{1}{\sqrt{\alpha'}} n X^0(y)} = \Big|\frac{df}{dy}\Big|^{n^2} e^{\frac{1}{\sqrt{\alpha'}} n X^0(f(y))}\,, \tag{2.3.19}$$

[4]We use the signature $(-,+,+,\ldots,+)$. For a point $z = \bar{z} = y$ on the boundary of $\mathbb{H}$ we write $X^\mu(y) \equiv X^\mu(y,y)$. The singular part of $X^\mu(y)X^\nu(y')$ is given by $-2\alpha'\eta^{\mu\nu}\ln|y-y'|$, and the mode expansion for a Neumann coordinate reads $i\partial_y X^\mu(y) = \sqrt{2\alpha'}\sum_m \frac{\alpha_m^\mu}{y^{m+1}}$. The basic correlator is $\langle e^{ik\,X(y)} e^{ik'\,X(y')}\rangle = (2\pi)^D \delta^{(D)}(k+k')|y-y'|^{2\alpha' k\cdot k'}$, where D is the spacetime dimension. The operator $e^{ik\,X(y)}$ has dimension $\alpha' k^2$ and transforms as $f \circ e^{ik\,X(y)} = |\frac{df}{dy}|^{\alpha' k^2} e^{ik\,X(f(y))}$. We do not use the doubling trick for the matter sector in §2.3.2. In these subsections, $\partial X^\mu \equiv \partial_z X^\mu + \partial_{\bar{z}} X^\mu$ when μ is a direction along the D-brane and $\partial X^\mu \equiv \partial_z X^\mu - \partial_{\bar{z}} X^\mu$ when μ is a direction transverse to the D-brane.

$$e^{\frac{1}{\sqrt{\alpha'}}mX^0(y)}e^{\frac{1}{\sqrt{\alpha'}}nX^0(y')} = |y-y'|^{2mn} : e^{\frac{1}{\sqrt{\alpha'}}mX^0(y)}e^{\frac{1}{\sqrt{\alpha'}}nX^0(y')} : . \tag{2.3.20}$$

Physically, deformation by cV represents a rolling tachyon solution in which the state of the system at time $x^0 = -\infty$ is the perturbative vacuum. We set $\Psi^{(1)}$ to be

$$\Psi^{(1)} = e^{\frac{1}{\sqrt{\alpha'}}X^0(0)}\, c_1|0\rangle \tag{2.3.21}$$

and calculate $\Psi^{(n)}$ with $n \geq 2$ which, by momentum conservation, must take the form

$$\Psi^{(n)} = e^{\frac{1}{\sqrt{\alpha'}}nX^0(0)}\Big[\beta_n\, c_1|0\rangle + \dots\Big], \quad n \geq 2\,. \tag{2.3.22}$$

In the above we have separated out the tachyon component, and higher-level fields are indicated by dots. The profile of the tachyon field T is determined by the coefficients β_n that we aim to calculate:

$$T(x^0) = \lambda\, e^{\frac{1}{\sqrt{\alpha'}}x^0} + \sum_{n=2}^{\infty}\beta_n\,\lambda^n e^{\frac{1}{\sqrt{\alpha'}}nx^0}\,. \tag{2.3.23}$$

Since the solution (for every component field) depends on λ and x^0 only through the combination $\lambda e^{\frac{1}{\sqrt{\alpha'}}x^0}$, a scaling of λ can be absorbed by a shift of x^0. We can therefore focus on the case $\lambda = \mp 1$. The sign of λ makes a physical difference. In our conventions the tachyon vacuum lies at some $T < 0$, so $\lambda = -1$ corresponds to the tachyon rolling in the direction of the tachyon vacuum, which we are mostly interested in. For $\lambda = +1$ the tachyon begins to roll towards the unbounded region of the potential. After setting $\lambda = \mp 1$, we write

$$T(x^0) = \mp\, e^{\frac{1}{\sqrt{\alpha'}}x^0} + \sum_{n=2}^{\infty}(\mp 1)^n\beta_n\, e^{\frac{1}{\sqrt{\alpha'}}nx^0}\,. \tag{2.3.24}$$

In order to extract the coefficients β_n from the solution we introduce test states ϕ_n and their BPZ duals:

$$|\phi_n\rangle = e^{-\frac{1}{\sqrt{\alpha'}}nX^0(0)}\, c_0c_1|0\rangle\,, \qquad \langle\phi_n| = \lim_{y\to\infty}\langle 0|c_{-1}c_0e^{-\frac{1}{\sqrt{\alpha'}}nX^0(y)}\,\frac{1}{|y|^{2n^2}}\,. \tag{2.3.25}$$

The state ϕ_n has dimension n^2-1. Using (2.3.22) we find

$$\langle\phi_n, \Psi^{(n)}\rangle = \langle\phi_n|\Psi^{(n)}\rangle = \beta_n\cdot(\mathrm{vol})\,, \qquad \mathrm{vol} = (2\pi)^D\delta^{(D)}(0)\,. \tag{2.3.26}$$

The spacetime volume (vol) always factors out, so we will simply use vol$=1$ in the following. We now use (2.3.13) to write $\beta_{n+1} = \langle\phi_{n+1}, \Psi^{(n+1)}\rangle$ as

$$\begin{aligned}\beta_{n+1} = \int_0^1 dt_1\dots\int_0^1 dt_n\,\frac{1}{2+\ell_n}\Big\langle\ \Big\{ & e^{\frac{1}{\sqrt{\alpha'}}X^0(-1)}\, f\circ(\partial c)ce^{-\frac{1}{\sqrt{\alpha'}}(n+1)X^0}(0)\, ce^{\frac{1}{\sqrt{\alpha'}}X^0}(1) \\ & + ce^{\frac{1}{\sqrt{\alpha'}}X^0}(-1)\, f\circ(\partial c)ce^{-\frac{1}{\sqrt{\alpha'}}(n+1)X^0}(0)\, e^{\frac{1}{\sqrt{\alpha'}}X^0(1)} \\ & + ce^{\frac{1}{\sqrt{\alpha'}}X^0}(-1)\, f\circ ce^{-\frac{1}{\sqrt{\alpha'}}(n+1)X^0}(0)\, ce^{\frac{1}{\sqrt{\alpha'}}X^0}(1)\Big\}\prod_{i=1}^{n-1}e^{\frac{1}{\sqrt{\alpha'}}X^0(1+\ell_i)}\Big\rangle_{\mathcal{W}_{1+\ell_n}}\,.\end{aligned} \tag{2.3.27}$$

In the last term, due to the simple structure of ϕ_{n+1}, the antighost line integral acts as b_0 and simply removes the c_0 part of the state. We must now evaluate the correlator on the right-hand side.

This calculation requires the map from the surface $\mathcal{W}_{1+\ell_n}$ to the upper-half plane. We recall that the surface $\mathcal{W}_0$ of unit width can be mapped to the upper-half plane by the function

$$g(z) = \frac{1}{2}\tan(\pi z)\,. \tag{2.3.28}$$

Due to the periodicity $g(z+1) = g(z)$, this map works independent of the position of the surface $\mathcal{W}_0$ in the direction of the real axis. Consequently, we merely need to rescale $\mathcal{W}_{1+\ell_n}$ to $\mathcal{W}_0$ by $z \to \frac{z}{2+\ell_n}$ and then map it to the upper-half plane by $g(z)$. The overall conformal transformation on the test states is therefore the map h given by

$$h(\xi) \equiv g\Big(\frac{1}{2+\ell_n}\,f(\xi)\Big)\,. \tag{2.3.29}$$

All other vertex operators are mapped with $g\big(\frac{1}{2+\ell_n}\,z\big)$. It is therefore natural to define

$$g_i \equiv g\Big(\frac{1+\ell_i}{2+\ell_n}\Big)\,, \qquad g_i' \equiv g'\Big(\frac{1+\ell_i}{2+\ell_n}\Big)\,, \quad i = 0,1,\ldots,n\,, \quad \ell_0 \equiv 0\,. \tag{2.3.30}$$

With these abbreviations, the correlator on the upper-half plane reads

$$\begin{aligned}\beta_{n+1} = \int d^n t\,\frac{h'(0)^{(n+1)^2-1}}{2+\ell_n}\Big\langle \Big\{ \frac{g_0'}{2+\ell_n}\Big(& e^{\frac{1}{\sqrt{\alpha'}}X^0(-g_0)}\,(\partial c)c e^{-\frac{1}{\sqrt{\alpha'}}(n+1)X^0}(0)\,c e^{\frac{1}{\sqrt{\alpha'}}X^0}(g_0) \\ & + c e^{\frac{1}{\sqrt{\alpha'}}X^0}(-g_0)\,(\partial c)c e^{-\frac{1}{\sqrt{\alpha'}}(n+1)X^0}(0)\,e^{\frac{1}{\sqrt{\alpha'}}X^0(g_0)}\Big) \\ & + c e^{\frac{1}{\sqrt{\alpha'}}X^0}(-g_0)\,c e^{-\frac{1}{\sqrt{\alpha'}}(n+1)X^0}(0)\,c e^{\frac{1}{\sqrt{\alpha'}}X^0}(g_0)\Big\} \prod_{i=1}^{n-1}\frac{g_i'}{2+\ell_n}e^{\frac{1}{\sqrt{\alpha'}}X^0(g_i)}\Big\rangle_{\mathbb{H}}\,,\end{aligned} \tag{2.3.31}$$

where $h'(0) = \frac{1}{2+\ell_n}$ and we have defined $\int d^n t \equiv \int_0^1 dt_1 \ldots \int_0^1 dt_n$. We can now factor this into matter and ghost correlators:

$$\begin{aligned}\beta_{n+1} = \int d^n t\,(2+\ell_n)^{-(n+1)^2}\Big\langle e^{\frac{1}{\sqrt{\alpha'}}X^0(-g_0)}\,e^{-\frac{1}{\sqrt{\alpha'}}(n+1)X^0(0)}\,e^{\frac{1}{\sqrt{\alpha'}}X^0(g_0)}\prod_{i=1}^{n-1}\frac{g_i'}{2+\ell_n}e^{\frac{1}{\sqrt{\alpha'}}X^0(g_i)}\Big\rangle_m \\ \times\Big\langle \frac{g_0'}{2+\ell_n}\Big((\partial c)c(0)\,c(g_0) + c(-g_0)\,(\partial c)c(0)\Big) + c(-g_0)\,c(0)\,c(g_0)\Big\rangle_g\,.\end{aligned} \tag{2.3.32}$$

The ghost correlator can be evaluated using $\big\langle c(-z)c(0)c(z)\big\rangle_g = -2z^3$ and $\big\langle \partial c\,c(0)\,c(z)\big\rangle_g = z^2$. Using also $-g_0 = g_n$ and $g_0' = g_n'$, we find

$$\beta_{n+1} = 2\int d^n t\,(2+\ell_n)^{-n(n+3)}\Big(\frac{g_0'}{2+\ell_n} - g_0\Big)\frac{g_0^2}{g_0'^2}\prod_{i=0}^{n}\Big[g_i'\Big]\Big\langle\, e^{-\frac{1}{\sqrt{\alpha'}}(n+1)X^0(0)}\prod_{i=0}^{n}e^{\frac{1}{\sqrt{\alpha'}}X(g_i)}\,\Big\rangle_m\,. \tag{2.3.33}$$

Evaluating the matter correlator, we obtain our final result for the coefficients of the rolling tachyon solution:

$$\boxed{\beta_{n+1} = 2\int d^n t\,(2+\ell_n)^{-n(n+3)}\Big(\frac{g_0'}{2+\ell_n} - g_0\Big)\frac{g_0^2}{g_0'^2}\Big[\prod_{i=0}^{n}\frac{g_i'}{g_i^{2(n+1)}}\Big]\prod_{0\le i<j\le n}(g_i-g_j)^2.} \tag{2.3.34}$$

Another way to derive (2.3.34) is to use (2.3.14). The ghost correlator, which gives the tachyon coefficient of ψ_{ℓ_n}, has been calculated in [9,43]:

$$\begin{aligned}\langle\, f\circ(\partial c)c(0)\,c(1)\,\mathcal{B}\,c(1+\ell_n)\,\rangle_{\mathcal{W}_{1+\ell_n},g} &= \frac{2+\ell_n}{\pi}\left[1-\frac{2+\ell_n}{2\pi}\sin\frac{2\pi}{2+\ell_n}\right]\sin^2\frac{\pi}{2+\ell_n}\\ &= 2\,(2+\ell_n)\,\frac{g_0^2}{g_0'}\left(1-\frac{(2+\ell_n)\,g_0}{g_0'}\right).\end{aligned} \tag{2.3.35}$$

The calculation of the matter correlator is straightforward:

$$\begin{aligned}&\Big\langle f\circ e^{-\frac{1}{\sqrt{\alpha'}}(n+1)X^0(0)}\prod_{i=0}^{n}e^{\frac{1}{\sqrt{\alpha'}}X^0(1+\ell_i)}\Big\rangle_{\mathcal{W}_{1+\ell_n},m}\\ &=\Big(\frac{2}{\pi}\Big)^{(n+1)^2}\Big[\prod_{i=0}^{n}\frac{(2+\ell_n)^{-2(n+1)}}{\pi^{-2(n+1)}}\sin^{-2(n+1)}\frac{\pi(1+\ell_i)}{2+\ell_n}\Big]\prod_{0\le i<j\le n}\frac{(2+\ell_n)^2}{\pi^2}\sin^2\frac{\pi(\ell_i-\ell_j)}{2+\ell_n}\\ &=(2+\ell_n)^{-(n+1)(n+2)}\Big[\prod_{i=0}^{n}\frac{g_i'}{g_i^{2(n+1)}}\Big]\prod_{0\le i<j\le n}(g_i-g_j)^2.\end{aligned} \tag{2.3.36}$$

It is easy to see that (2.3.34) is reproduced.

The integrand in (2.3.34) is manifestly positive since $g'(z)>0$ and $\frac{g_0'}{2+\ell_n}-g_0>0$. It follows that all β_{n+1} coefficients are positive. For $n=1$ we find

$$\beta_2 = 8\int_0^1 dt\,\frac{\frac{g_0'}{2+t}-g_0}{(2+t)^4 g_0^4} = 8\int_0^1 dt\left(\frac{2\cot\big(\frac{\pi}{2+t}\big)}{2+t}\right)^4\Big(\frac{\pi}{2(2+t)\cos^2\big(\frac{\pi}{2+t}\big)}-\frac{1}{2}\tan\Big(\frac{\pi}{2+t}\Big)\Big). \tag{2.3.37}$$

Surprisingly, analytic evaluation of the integral is possible using *Mathematica*:

$$\beta_2 = \frac{64}{243\sqrt{3}}. \tag{2.3.38}$$

This coefficient is the same as that of the Siegel-gauge solution [56]. For $n=2$ the final integral can be evaluated numerically:

$$\beta_3 = 8\int_0^1 dt_1\int_0^1 dt_2\,\frac{\Big(\frac{g_0'}{2+t_1+t_2}-g_0\Big)g_1'\big(g_0^2-g_1^2\big)^2}{(2+t_1+t_2)^{10}g_0^8 g_1^6} \simeq 2.14766\cdot 10^{-3}. \tag{2.3.39}$$

The results for the first few β_n are summarized in Table 2.1. The resulting tachyon profile (2.3.24) takes the form

$$\begin{aligned}T(x^0) = \mp e^{\frac{1}{\sqrt{\alpha'}}x^0} &+ 0.15206\;e^{\frac{1}{\sqrt{\alpha'}}2x^0} \mp 2.148\cdot 10^{-3}\,e^{\frac{1}{\sqrt{\alpha'}}3x^0}\\ &+ 2.619\cdot 10^{-6}\,e^{\frac{1}{\sqrt{\alpha'}}4x^0} \mp 2.791\cdot 10^{-10}\,e^{\frac{1}{\sqrt{\alpha'}}5x^0}\\ &+ 2.801\cdot 10^{-15}\,e^{\frac{1}{\sqrt{\alpha'}}6x^0} \mp 2.729\cdot 10^{-21}\,e^{\frac{1}{\sqrt{\alpha'}}7x^0} + \ldots\end{aligned} \tag{2.3.40}$$

n	β_n
2	$\frac{64}{243\sqrt{3}} \approx 0.152059$
3	$2.14766 \cdot 10^{-3}$
4	$2.61925 \cdot 10^{-6}$
5	$2.79123 \cdot 10^{-10}$
6	$2.80109 \cdot 10^{-15}$
7	$2.72865 \cdot 10^{-21}$

Table 2.1: Numerical values of the rolling tachyon profile coefficients.

The top sign gives us the physical solution: the tachyon rolls towards the tachyon vacuum, overshoots it, and then begins to develop larger and larger oscillations. The coefficients in the solution decrease so rapidly that the series seems to be absolutely convergent for any value of $\frac{x^0}{\sqrt{\alpha'}}$. Indeed, the n-th term T_n in the above series appears to take the form

$$|T_n| \sim 2.7 \cdot 10^{-\frac{1}{2}n(n-1)} e^{\frac{1}{\sqrt{\alpha'}} n x^0} . \tag{2.3.41}$$

One then finds that the ratio of consecutive coefficients is

$$\left|\frac{T_{n+1}}{T_n}\right| \sim 10^{-n} e^{\frac{1}{\sqrt{\alpha'}} x^0} \simeq e^{-2.303\, n} e^{\frac{1}{\sqrt{\alpha'}} x^0} . \tag{2.3.42}$$

For any value of $\frac{x^0}{\sqrt{\alpha'}}$ the ratio becomes smaller than one for sufficiently large n, suggesting absolute convergence. It would be useful to do analytic estimates of β_n using (2.3.34) to confirm the above speculation.

It is interesting to compare the results with those of the p-adic model [52]. The relevant solution is discussed in §4.2.2 of that paper and has the same qualitative behavior as the solution presented here: the tachyon rolls towards the minimum, overshoots it, and then develops ever-growing oscillations. The solution is of the form

$$\phi(t) = 1 - \sum_{n=1}^{\infty} a_n e^{\sqrt{2}nt} , \quad a_1 = 1 . \tag{2.3.43}$$

The coefficients a_n can be calculated exactly with a simple recursion and fall off very rapidly, but an analytic expression for their large n behavior is not known. A fit of the values of a_n for $n = 3, \ldots, 13$ gives $\ln a_n \simeq -0.1625 + 1.506\, n - 1.389\, n^2$. (A fit with an n^3 term returns a very small coefficient for this term.) The fit implies that the ratio of two consecutive terms in the solution is

$$\left|\frac{a_{n+1}}{a_n}\right| e^{\sqrt{2}t} \sim e^{-2.778\, n + 0.117} e^{\sqrt{2}t} \simeq 1.125 \cdot 16^{-n} e^{\sqrt{2}t} . \tag{2.3.44}$$

This result suggests that the p-adic rolling solution is also absolutely convergent.

A low-level solution of the string theory rolling tachyon in Siegel gauge was also obtained in [52], where significant similarities with the p-adic solution were noted. The higher-level Siegel gauge analysis of the rolling tachyon in [56] confirmed the earlier analysis and added much confidence to the validity of the oscillatory solution. We believe that the exact analytic solution presented here has settled the issue convincingly.

It remains to construct solution for marginal deformations associated with operators V whose OPE with itself is singular. Such a solution unfortunately cannot be constructed in Schnabl gauge, as was argued in [13]. Instead, we will take a different approach in the next chapter to construct solutions associated with general marginal operators.

Chapter 3

A general framework for marginal deformations

3.1 Introduction

In this chapter, we present a procedure to construct a solution satisfying the reality condition in open bosonic string field theory for any exactly marginal deformation in any boundary conformal field theory (BCFT) when properly renormalized operator products of the marginal operator are given [21]. The analytic solution in chapter 2 was constructed using unintegrated vertex operators and b-ghost insertions. We now follow a different strategy and use integrated vertex operators, which are closely related to finite deformations in BCFT. We assume several properties of the properly renormalized operator products of the marginal operator, which we believe are satisfied for any exactly marginal deformation in any BCFT. Since the identification of a set of assumptions which are sufficient for the construction of a solution is one of the main points of this chapter, we will explain these assumptions in detail in the following. We will then present our solutions.

3.1.1 Assumptions

For any exactly marginal deformation in a given BCFT, we have a family of consistent boundary conditions labeled by the deformation parameter which we denote by λ. Consider the BCFT on the upper-half plane and suppose that we change boundary conditions on a segment of the boundary between a and b. Since the new boundary condition is also conformal, an integral of the BRST current along a contour vanishes if both end points of the contour lie inside the region between a and b. By $C(t_f, t_i)$ we denote a contour in the upper-half plane which starts from the point t_i on the real axis and ends on t_f on the real axis, and we use $C(t_f, t_i)$ with $t_f < t_i$ in what follows. We have

$$\int_{C(t_f,t_i)} \Big[\frac{dz}{2\pi i} j_B(z) - \frac{d\bar{z}}{2\pi i} \tilde{j}_B(\bar{z}) \Big] = 0 \quad \text{when} \quad a < t_f < t_i < b\,, \tag{3.1.1}$$

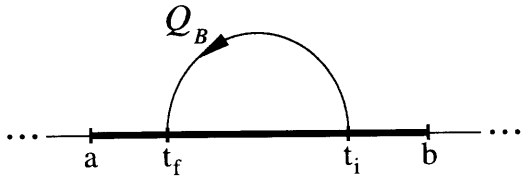

Figure 3-1: Illustration of (3.1.1). The bold line indicates a change of boundary conditions on the segment between a and b. The integral of the BRST current in (3.1.1) vanishes when $a < t_f < t_i < b$.

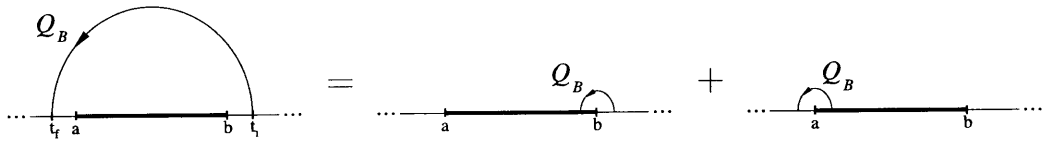

Figure 3-2: Illustration of (3.1.2). When $t_f < a < b < t_i$, the integral of the BRST current on the left-hand side decomposes into a sum of two integrals localized at the end points a and b of the segment.

where $j_B(z)$ and $\tilde{j}_B(\bar{z})$ are the holomorphic and antiholomorphic components of the BRST current, respectively. See figure 3-1. This identity holds inside any correlation function of the deformed CFT as long as no operators are inserted between the contour $C(t_f, t_i)$ and the real axis. When $t_f < a < b < t_i$, there are contributions from the points a and b where the boundary condition changes:

$$\begin{aligned}&\int_{C(t_f,t_i)}\Big[\frac{dz}{2\pi i}\,j_B(z)-\frac{d\bar{z}}{2\pi i}\,\tilde{j}_B(\bar{z})\Big]\\&=\int_{C(b)}\Big[\frac{dz}{2\pi i}\,j_B(z)-\frac{d\bar{z}}{2\pi i}\,\tilde{j}_B(\bar{z})\Big]+\int_{C(a)}\Big[\frac{dz}{2\pi i}\,j_B(z)-\frac{d\bar{z}}{2\pi i}\,\tilde{j}_B(\bar{z})\Big]\,,\end{aligned}\tag{3.1.2}$$

where we have defined the infinitesimal contour $C(t)$ around any point t by

$$C(t) \;=\; \lim_{\epsilon\to 0} C(t-\epsilon, t+\epsilon)\,. \tag{3.1.3}$$

See figure 3-2. The nonvanishing contributions in (3.1.2) can be thought of as the BRST transformations of the boundary-condition changing operators. We also have

$$\begin{aligned}&\int_{C(t_f,t_i)}\Big[\frac{dz}{2\pi i}\,j_B(z)-\frac{d\bar{z}}{2\pi i}\,\tilde{j}_B(\bar{z})\Big]\int_{C(a)}\Big[\frac{dz}{2\pi i}\,j_B(z)-\frac{d\bar{z}}{2\pi i}\,\tilde{j}_B(\bar{z})\Big]\\&=-\int_{C(a)}\Big[\frac{dz}{2\pi i}\,j_B(z)-\frac{d\bar{z}}{2\pi i}\,\tilde{j}_B(\bar{z})\Big]\int_{C(b)}\Big[\frac{dz}{2\pi i}\,j_B(z)-\frac{d\bar{z}}{2\pi i}\,\tilde{j}_B(\bar{z})\Big]\,,\end{aligned}\tag{3.1.4}$$

where again $t_f < a < b < t_i$, as shown in figure 3-3.

The BCFT with a different boundary condition on a segment between a and b discussed above can also be described in the BCFT with the original boundary condition on the whole real axis by

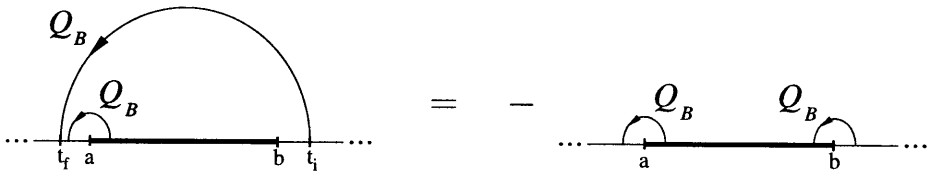

Figure 3-3: Illustration of (3.1.4). With the presence of the BRST integral localized at a, the integral of the BRST current along $C(t_f, t_i)$ on the left-hand side localizes only at the other end point b because of the nilpotency of the BRST transformation.

inserting an exponential of the marginal operator $V(t)$ integrated over the segment between a and b,

$$\exp\left[\lambda \int_a^b dt\, V(t)\right] = 1 + \lambda \int_a^b dt\, V(t) + \frac{\lambda^2}{2!} \int_a^b dt_1 \int_a^b dt_2\, V(t_1)\, V(t_2) + \ldots , \tag{3.1.5}$$

into the correlation function. When operator products of the marginal operator are singular, we need to renormalize the operator (3.1.5) properly to make it well defined, and we denote the renormalized operator by

$$[\, e^{\lambda V(a,b)} \,]_r , \tag{3.1.6}$$

where

$$V(a,b) \equiv \int_a^b dt\, V(t) . \tag{3.1.7}$$

Then the equations (3.1.2) and (3.1.4) can be translated into the following assumptions on the operator $[\, e^{\lambda V(a,b)} \,]_r$.

1. *The BRST transformation of the operator* $[\, e^{\lambda V(a,b)} \,]_r$ *takes the following form:*

$$Q_B \cdot [\, e^{\lambda V(a,b)} \,]_r = [\, e^{\lambda V(a,b)}\, O_R(b) \,]_r - [\, O_L(a)\, e^{\lambda V(a,b)} \,]_r , \tag{I}$$

where $O_L(a)$ *and* $O_R(b)$ *are some local operators at* a *and* b*, respectively.*

2. *The BRST transformation of the operator* $[\, O_L(a)\, e^{\lambda V(a,b)} \,]_r$ *is given by*

$$Q_B \cdot [\, O_L(a)\, e^{\lambda V(a,b)} \,]_r = -\, [\, O_L(a)\, e^{\lambda V(a,b)}\, O_R(b) \,]_r . \tag{II}$$

These are our first two assumptions. They are illustrated in figures 3-4 and 3-5.

We can also introduce different boundary conditions on different segments on the boundary by inserting

$$[\prod_{i=1}^{n} e^{\lambda_i V(a_i, a_{i+1})} \,]_r \tag{3.1.8}$$

with $a_i < a_{i+1}$ for $i = 1, 2, \ldots, n$ into the correlation function. We make the following two assumptions on this operator.

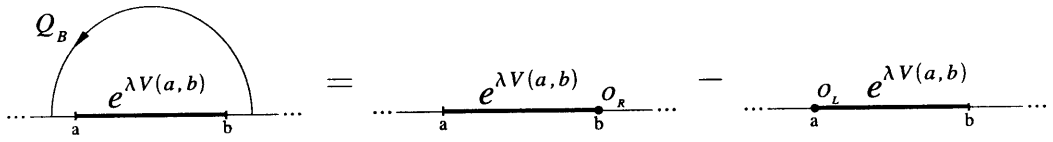

Figure 3-4: Illustration of the assumption (I). The BRST transformation on the operator $[\,e^{\lambda V(a,b)}\,]_r$ generates local operators $O_L(a)$ and $O_R(b)$ at the end points of the segment. Compare this figure with figure 3-2.

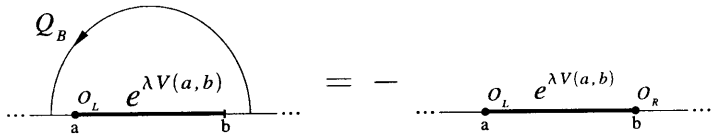

Figure 3-5: Illustration of the assumption (II). The BRST transformation on the operator $[\,O_L(a)\,e^{\lambda V(a,b)}\,]_r$ generates the local operator $O_R(b)$. Compare this figure with figure 3-3.

3. Replacement. When $\lambda_{j+1} = \lambda_j$, the product $e^{\lambda_j V(a_j,a_{j+1})}\,e^{\lambda_{j+1} V(a_{j+1},a_{j+2})}$ inside the operator (3.1.8) can be replaced by $e^{\lambda_j V(a_j,a_{j+2})}$:

$$[\ldots e^{\lambda_j V(a_j,a_{j+1})}\,e^{\lambda_j V(a_{j+1},a_{j+2})}\ldots]_r = [\ldots e^{\lambda_j V(a_j,a_{j+2})}\ldots]_r\,. \tag{III}$$

4. Factorization. When λ_j vanishes, the renormalized product (3.1.8) factorizes as follows:

$$[\ldots e^{\lambda_{j-1} V(a_{j-1},a_j)}\,e^{\lambda_{j+1} V(a_{j+1},a_{j+2})}\ldots]_r = [\ldots e^{\lambda_{j-1} V(a_{j-1},a_j)}]_r\,[e^{\lambda_{j+1} V(a_{j+1},a_{j+2})}\ldots]_r\,. \tag{IV}$$

We also assume that (III) and (IV) hold when $O_L(a_1)$, $O_R(a_{n+1})$, or both of them are inserted in (3.1.8).

A change of boundary conditions on a segment between a and b is local and independent of other regions of the Riemann surface where the BCFT is defined. Thus the operator $[\,e^{\lambda V(a,b)}\,]_r$ should be independent of the global shape of the Riemann surface. However, renormalization schemes such as the standard normal ordering can depend on the global shape of the surface through the propagator, and normal ordered products of nonlocal operators generically do depend on the surface. We consider boundary conformal field theory defined on a family of semi-infinite cylinders $\mathcal{W}_n$ obtained from the upper-half plane of z by the identification $z \sim z+n+1$ and make the following assumption.

5. Locality. The operators $[\,e^{\lambda V(a,b)}\,]_r$ and $[\,O_L(a)\,e^{\lambda V(a,b)}\,]_r$ defined on $\mathcal{W}_n$ coincide with those defined on $\mathcal{W}_m$ with $m > n$:

$$\begin{aligned} [\,e^{\lambda V(a,b)}\,]_r \text{ on } \mathcal{W}_n &= [\,e^{\lambda V(a,b)}\,]_r \text{ on } \mathcal{W}_m\,, \\ [\,O_L(a)\,e^{\lambda V(a,b)}\,]_r \text{ on } \mathcal{W}_n &= [\,O_L(a)\,e^{\lambda V(a,b)}\,]_r \text{ on } \mathcal{W}_m\,. \end{aligned} \tag{V}$$

Finally, $e^{\lambda V(a,b)}$ is classically invariant under the reflection where $V(t)$ is replaced by $V(a+b-t)$, and we assume that $[\,e^{\lambda V(a,b)}\,]_r$ preserves this symmetry.

6. Reflection. The operator $[\,e^{\lambda V(a,b)}\,]_r$ *is invariant under the reflection where* $V(t)$ *is replaced by* $V(a+b-t)$:

$$\left[\exp\left(\lambda\int_a^b dt\, V(a+b-t)\right)\right]_r = \left[\exp\left(\lambda\int_a^b dt\, V(t)\right)\right]_r . \tag{VI}$$

3.1.2 Solutions

We believe that all of these assumptions are satisfied for any exactly marginal deformation in any BCFT if the composite operators are properly renormalized. When the operator $[\,e^{\lambda V(a,b)}\,]_r$ expanded in λ as

$$[\,e^{\lambda V(a,b)}\,]_r = \sum_{n=0}^{\infty}\lambda^n\,[\,V^{(n)}(a,b)\,]_r\,, \tag{3.1.9}$$

where

$$[\,V^{(n)}(a,b)\,]_r \equiv \frac{1}{n!}\,[\,(V(a,b))^n\,]_r \quad \text{for} \quad n\geq 1 \quad \text{and} \quad [\,V^{(0)}(a,b)\,]_r \equiv 1 \tag{3.1.10}$$

is given, we claim that solutions to the equation of motion can be constructed in the following way.

We first define a state U by

$$U \equiv 1 + \sum_{n=1}^{\infty}\lambda^n\, U^{(n)}\,, \tag{3.1.11}$$

where

$$\langle\,\phi\,,\,U^{(n)}\,\rangle = \langle\, f\circ\phi(0)\;[\,V^{(n)}(1,n)\,]_r\,\rangle_{\mathcal{W}_n}\,. \tag{3.1.12}$$

Here and in what follows we denote a generic state in the Fock space by ϕ and its corresponding operator in the state-operator mapping by $\phi(0)$. As above, the conformal transformation $f(\xi)$ is given by

$$f(\xi) = \frac{2}{\pi}\arctan\xi\,, \tag{3.1.13}$$

and we represent the wedge surface $\mathcal{W}_n$ in the region $-1/2 \leq \mathrm{Re}\, z \leq 1/2+n$ of the upper-half plane of z.

If the assumption (I) is satisfied, the BRST transformation of the operator $[\,V^{(n)}(a,b)\,]_r$ takes the form

$$Q_B\cdot[\,V^{(n)}(a,b)\,]_r = \sum_{r=1}^{n}[\,V^{(n-r)}(a,b)\,O_R^{(r)}(b)\,]_r - \sum_{l=1}^{n}[\,O_L^{(l)}(a)\,V^{(n-l)}(a,b)\,]_r\,, \tag{3.1.14}$$

where the local operators O_L and O_R are expanded as follows:

$$O_L = \sum_{n=1}^{\infty}\lambda^n\,O_L^{(n)}\,, \qquad O_R = \sum_{n=1}^{\infty}\lambda^n\,O_R^{(n)}\,. \tag{3.1.15}$$

Thus the BRST transformation of U can be split into two pieces:

$$Q_B U = A_R - A_L \tag{3.1.16}$$

with

$$A_L \equiv \sum_{n=1}^{\infty} \lambda^n A_L^{(n)}\,, \qquad A_R \equiv \sum_{n=1}^{\infty} \lambda^n A_R^{(n)}\,, \tag{3.1.17}$$

where

$$\begin{aligned} \langle\, \phi\,, A_L^{(n)} \,\rangle &= \sum_{l=1}^{n} \langle\, f \circ \phi(0)\, [\, O_L^{(l)}(1)\, V^{(n-l)}(1,n)\,]_r \,\rangle_{\mathcal{W}_n}\,, \\ \langle\, \phi\,, A_R^{(n)} \,\rangle &= \sum_{r=1}^{n} \langle\, f \circ \phi(0)\, [\, V^{(n-r)}(1,n)\, O_R^{(r)}(n)\,]_r \,\rangle_{\mathcal{W}_n}\,. \end{aligned} \tag{3.1.18}$$

We then define Ψ_L and Ψ_R by

$$\Psi_L \equiv A_L * U^{-1}\,, \qquad \Psi_R \equiv U^{-1} * A_R\,, \tag{3.1.19}$$

where U^{-1} is well defined perturbatively in λ because $U = 1 + \mathcal{O}(\lambda)$. We show that Ψ_L and Ψ_R satisfy the equation of motion,

$$Q_B \Psi_L + \Psi_L * \Psi_L = 0\,, \qquad Q_B \Psi_R + \Psi_R * \Psi_R = 0\,, \tag{3.1.20}$$

though they do not satisfy the reality condition on the string field. They are related by the gauge transformation generated by U:

$$\Psi_R \;=\; U^{-1} * \Psi_L * U + U^{-1} * Q_B U\,. \tag{3.1.21}$$

A solution Ψ satisfying the reality condition is obtained from Ψ_L or Ψ_R by gauge transformations as follows:

$$\begin{aligned} \Psi &= \frac{1}{\sqrt{U}} * \Psi_L * \sqrt{U} + \frac{1}{\sqrt{U}} * Q_B \sqrt{U} \\ &= \sqrt{U} * \Psi_R * \frac{1}{\sqrt{U}} + \sqrt{U} * Q_B \frac{1}{\sqrt{U}} \\ &= \frac{1}{2} \left[\frac{1}{\sqrt{U}} * \Psi_L * \sqrt{U} + \sqrt{U} * \Psi_R * \frac{1}{\sqrt{U}} + \frac{1}{\sqrt{U}} * Q_B \sqrt{U} - Q_B \sqrt{U} * \frac{1}{\sqrt{U}} \right], \end{aligned} \tag{3.1.22}$$

where $\sqrt{U}$ and $1/\sqrt{U}$ are defined perturbatively in λ. The three expressions are equivalent because of the relation (3.1.21). This solution is the main result of this chapter. In section 3.4, we present a class of singular marginal deformations for which $[\, e^{\lambda V(a,b)}\,]_r$ satisfying all the assumptions can be constructed explicitly. This class of marginal deformations includes the deformations of flat D-branes in flat backgrounds by constant massless modes of the gauge field and of the scalar fields on the D-branes, the cosine potential for a space-like coordinate, and the hyperbolic cosine potential for the time-like coordinate.

The operators $O_R^{(1)}$ and $O_L^{(1)}$ are

$$O_R^{(1)} = O_L^{(1)} = cV \tag{3.1.23}$$

for any marginal deformation. This follows only from the fact that the marginal operator is a primary field of dimension one. When operator products of the marginal operator are regular, there are no higher-order terms and thus $O_R = O_L = \lambda cV$. For any exactly marginal deformation where the singular part of the operator product of the marginal operator with itself is

$$V(t)\,V(0) \sim \frac{1}{t^2}\,, \tag{3.1.24}$$

the operators $O_L^{(2)}$ and $O_R^{(2)}$ are

$$O_R^{(2)} = -\,O_L^{(2)} = \frac{1}{2}\,\partial c\,. \tag{3.1.25}$$

For the class of marginal deformations to be considered in section 3.4, there are no higher-order terms and the exact expressions of O_R and O_L are

$$O_R = \lambda cV + \frac{\lambda^2}{2}\,\partial c\,, \qquad O_L = \lambda cV - \frac{\lambda^2}{2}\,\partial c\,. \tag{3.1.26}$$

3.1.3 The organization of this chapter

In section 3.2 we first revisit the problem of constructing solutions for marginal deformations with regular operator products. In section 3.2.1 we construct a solution Ψ_L to the string field theory equation of motion using integrated vertex operators without b-ghost insertions. The solution Ψ_L, however, does not satisfy the reality condition on the string field. In § 3.2.2 we construct a gauge transformation which connects Ψ_L and its conjugate solution Ψ_R, and then we generate a real solution Ψ using the gauge transformation. During the construction of this gauge transformation, we find an important identity. It leads us to discover a class of states U_α, which generalize the wedge states W_α in a deformed background. We study the properties of U_α in § 3.2.3.

In the process of constructing the gauge transformation that connects Ψ_L and Ψ_R, we also find another expression of the solution Ψ_L. We study the new form of Ψ_L in § 3.3.1 and prove that it satisfies the equation of motion using the properties of U_α. The new form of Ψ_L can be generalized to marginal deformations with singular operator products. In § 3.3.2 we construct Ψ_L for the singular case using the operator $[\,e^{\lambda V(a,b)}\,]_r$, and we prove in § 3.3.3 that it satisfies the equation of motion under the assumptions stated in § 3.1.1. We then generate a real solution Ψ for the singular case in § 3.3.4 by an appropriate gauge transformation as in the regular case in § 3.2.2.

In section 3.4, we present a class of singular marginal deformations for which the operator $[\,e^{\lambda V(a,b)}\,]_r$ satisfying the assumptions stated in § 3.1.1 can be constructed explicitly. We give several examples of marginal operators included in this class in § 3.4.2. For the details of the construction of $[\,e^{\lambda V(a,b)}\,]_r$, however, we refer the reader to section 4 of [21].

In section 3.5 we discuss string field theory around the deformed background and demonstrate that it can be elegantly formulated in terms of a new set of algebraic structures by defining a

deformed star product, deformed inner product, and deformed BRST operator. In section 3.6 we discuss the results of this chapter.

3.2 Marginal deformations with regular operator products

3.2.1 Solutions using integrated vertex operators

When we calculate n-point scattering amplitudes for open bosonic strings on the disk, we use three *unintegrated* vertex operators and $n-3$ *integrated* vertex operators. The unintegrated vertex operator takes the form cV, where c is the c ghost and V is a matter primary field of dimension one. The unintegrated vertex operator is invariant under the BRST transformation:

$$Q_B \cdot cV(t) \equiv \int_{C(t)} \Big[\frac{dz}{2\pi i} j_B(z) - \frac{d\bar{z}}{2\pi i} \tilde{j}_B(\bar{z}) \Big] cV(t) = 0 \,. \tag{3.2.1}$$

The integrated vertex operator is an integral of V on the boundary. The BRST transformation of V is a total derivative,

$$Q_B \cdot V(t) = \partial_t \left[cV(t) \right], \tag{3.2.2}$$

and thus the integrated vertex operator is invariant under the BRST transformation up to nonvanishing terms from the boundaries of the integral region:

$$Q_B \cdot V(a,b) = Q_B \cdot \int_a^b dt\, V(t) = \int_a^b dt\, \partial_t \left[cV(t) \right] = cV(b) - cV(a) \,. \tag{3.2.3}$$

The vertex operator V generates a marginal deformation of the BCFT. When the deformation is exactly marginal, we expect a corresponding solution Ψ to the equation of motion of open string field theory [1]:

$$Q_B \Psi + \Psi * \Psi = 0 \,. \tag{3.2.4}$$

In chapter 2, we constructed analytic solutions for marginal deformations in open bosonic string field theory to all orders in the deformation parameter λ when operator products $V(t_1)\, V(t_2) \ldots V(t_n)$ of the marginal operator are regular. These solutions take the form of an expansion in λ,

$$\Psi = \sum_{n=1}^{\infty} \lambda^n \, \Psi^{(n)} \,, \tag{3.2.5}$$

and the equation of motion for $\Psi^{(n)}$ is

$$Q_B \Psi^{(n)} = - \sum_{\imath=1}^{n-1} \Psi^{(n-\imath)} * \Psi^{(\imath)} \,. \tag{3.2.6}$$

In the solution constructed in chapter 2, $\Psi^{(n)}$ is made of n unintegrated vertex operators and $n-1$ b-ghost insertions. In this section, we construct $\Psi^{(n)}$ using one unintegrated and $n-1$ integrated vertex operators when operator products of the marginal operator are regular.

We choose the first term $\Psi^{(1)}$ of the solution to be

$$\langle \phi, \Psi^{(1)} \rangle = \langle f \circ \phi(0)\, cV(1) \rangle_{\mathcal{W}_1} . \tag{3.2.7}$$

This satisfies the linearized equation of motion. The starting point of our construction is the observation that $\Psi_L^{(2)}$ made of one unintegrated vertex operator and one integrated vertex operator given by

$$\langle \phi\,, \Psi_L^{(2)} \rangle = \langle f \circ \phi(0)\, cV(1)\, V(1,2) \rangle_{\mathcal{W}_2} = \int_1^2 dt\, \langle f \circ \phi(0)\, cV(1)\, V(t) \rangle_{\mathcal{W}_2} \tag{3.2.8}$$

solves the equation of motion $Q_B \Psi_L^{(2)} = -\Psi^{(1)} * \Psi^{(1)}$. This can be shown as follows:

$$\begin{aligned} \langle \phi\,, Q_B\, \Psi_L^{(2)} \rangle &= -\int_1^2 dt\, \langle f \circ \phi(0)\, cV(1)\, \partial_t [\, cV(t)\,] \rangle_{\mathcal{W}_2} \\ &= -\langle f \circ \phi(0)\, cV(1)\, cV(2) \rangle_{\mathcal{W}_2} \\ &= -\langle \phi\,, \Psi^{(1)} * \Psi^{(1)} \rangle\,, \end{aligned} \tag{3.2.9}$$

where we have used the formulas (3.2.1) and (3.2.3), and

$$\lim_{t_2 \to t_1} cV(t_1)\, cV(t_2) = 0\,, \tag{3.2.10}$$

which follows from the condition that the operator product $V(t_1)\, V(t_2)$ is regular in the limit $t_2 \to t_1$.

Let us next construct a solution to $\mathcal{O}(\lambda^3)$. We look for $\Psi_L^{(3)}$ which satisfies

$$Q_B\, \Psi_L^{(3)} = -\Psi^{(1)} * \Psi_L^{(2)} - \Psi_L^{(2)} * \Psi^{(1)}. \tag{3.2.11}$$

The right-hand side is given by

$$\begin{aligned} -\langle \phi\,, \Psi^{(1)} * \Psi_L^{(2)} + \Psi_L^{(2)} * \Psi^{(1)} \rangle = &-\langle f \circ \phi(0)\, cV(1)\, cV(2)\, V(2,3) \rangle_{\mathcal{W}_3} \\ &-\langle f \circ \phi(0)\, cV(1)\, V(1,2)\, cV(3) \rangle_{\mathcal{W}_3}\,. \end{aligned} \tag{3.2.12}$$

First consider the state $\Psi_{L1}^{(3)}$ defined by

$$\langle \phi\,, \Psi_{L1}^{(3)} \rangle = \langle f \circ \phi(0)\, cV(1)\, V(1,2)\, V(2,3) \rangle_{\mathcal{W}_3}\,. \tag{3.2.13}$$

The BRST transformation of $\Psi_{L1}^{(3)}$ is

$$\begin{aligned} \langle \phi\,, Q_B\, \Psi_{L1}^{(3)} \rangle = &-\langle f \circ \phi(0)\, cV(1)\, cV(2)\, V(2,3) \rangle_{\mathcal{W}_3} \\ &-\langle f \circ \phi(0)\, cV(1)\, V(1,2)\, cV(3) \rangle_{\mathcal{W}_3} \\ &+\langle f \circ \phi(0)\, cV(1)\, V(1,2)\, cV(2) \rangle_{\mathcal{W}_3}\,. \end{aligned} \tag{3.2.14}$$

The first two terms precisely give $-\Psi^{(1)} * \Psi_L^{(2)} - \Psi_L^{(2)} * \Psi^{(1)}$. To cancel the last term, consider $\Psi_{L2}^{(3)}$ defined by

$$\langle \phi\,, \Psi_{L2}^{(3)} \rangle = \frac{1}{2} \langle f \circ \phi(0)\, cV(1)\, (V(1,2))^2 \rangle_{\mathcal{W}_3}\,. \tag{3.2.15}$$

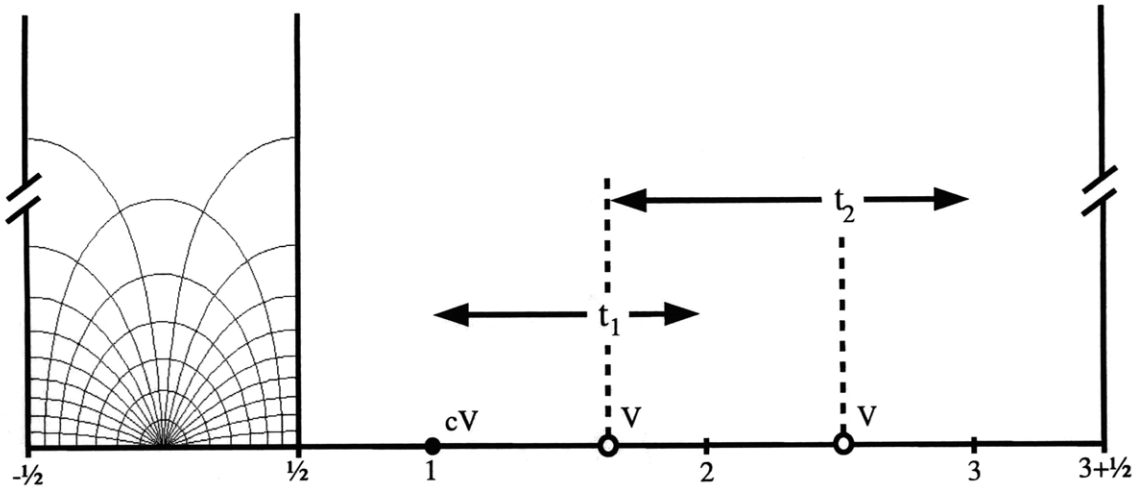

Figure 3-6: Illustration of $\Psi_L^{(3)}$. The solid dot represents the cV insertion, and the circles represent the two V insertions. The left V is integrated from 1 to 2, and the right V is integrated from the position of the left V to 3.

Using the formula

$$Q_B \cdot (V(a,b))^n = n\,[\,(V(a,b))^{n-1}\,cV(b) - cV(a)\,(V(a,b))^{n-1}\,], \tag{3.2.16}$$

which holds for marginal operators with regular operator products, the BRST transformation of $\Psi_{L2}^{(3)}$ can be calculated as follows:

$$\langle\,\phi\,, Q_B\,\Psi_{L2}^{(3)}\,\rangle = -\,\langle\,f\circ\phi(0)\,cV(1)\,V(1,2)\,cV(2)\,\rangle_{\mathcal{W}_3}\,. \tag{3.2.17}$$

This cancels the last term on the right-hand side of (3.2.14). Therefore, $\Psi_L^{(3)}$ can be constructed by adding $\Psi_{L2}^{(3)}$ to $\Psi_{L1}^{(3)}$:

$$\begin{aligned}\langle\,\phi\,,\Psi_L^{(3)}\,\rangle &= \langle\,\phi\,,\Psi_{L1}^{(3)}+\Psi_{L2}^{(3)}\,\rangle \\ &= \langle\,f\circ\phi(0)\,cV(1)\,V(1,2)\,V(2,3)\,\rangle_{\mathcal{W}_3} + \frac{1}{2}\,\langle\,f\circ\phi(0)\,cV(1)\,\,(V(1,2))^2\,\rangle_{\mathcal{W}_3}\,.\end{aligned} \tag{3.2.18}$$

To generalize this solution to higher orders, it turns out to be crucial to rewrite $\Psi_L^{(3)}$ in a different form. Using a path-ordered expression for $\Psi_{L2}^{(3)}$, $\Psi_L^{(3)}$ can also be written as

$$\begin{aligned}\langle\,\phi\,,\Psi_L^{(3)}\,\rangle &= \int_1^2 dt_1 \int_2^3 dt_2\,\langle\,f\circ\phi(0)\,cV(1)\,V(t_1)\,V(t_2)\,\rangle_{\mathcal{W}_3} \\ &\quad + \int_1^2 dt_1 \int_{t_1}^2 dt_2\,\langle\,f\circ\phi(0)\,cV(1)\,V(t_1)\,V(t_2)\,\rangle_{\mathcal{W}_3} \\ &= \int_1^2 dt_1 \int_{t_1}^3 dt_2\,\langle\,f\circ\phi(0)\,cV(1)\,V(t_1)\,V(t_2)\,\rangle_{\mathcal{W}_3}\,.\end{aligned} \tag{3.2.19}$$

See figure 3-6. It is instructive to see how $\Psi_L^{(3)}$ in this form satisfies the equation of motion. The

BRST transformation of $\Psi_L^{(3)}$ is given by

$$\begin{aligned}\langle\,\phi\,,Q_B\Psi_L^{(3)}\,\rangle = &-\int_1^2 dt_1\int_{t_1}^3 dt_2\,\langle\,f\circ\phi(0)\,cV(1)\,\partial_{t_1}\,[\,cV(t_1)\,]\,V(t_2)\,\rangle_{\mathcal{W}_3}\\ &-\int_1^2 dt_1\int_{t_1}^3 dt_2\,\langle\,f\circ\phi(0)\,cV(1)\,V(t_1)\,\partial_{t_2}\,[\,cV(t_2)\,]\,\rangle_{\mathcal{W}_3}\,.\end{aligned}\tag{3.2.20}$$

The integral region of t_2 depends on t_1. The first line on the right-hand side of (3.2.20) can be calculated as follows:

$$\begin{aligned}&-\int_1^2 dt_1\int_{t_1}^3 dt_2\,\langle\,f\circ\phi(0)\,cV(1)\,\partial_{t_1}\,[\,cV(t_1)\,]\,V(t_2)\,\rangle_{\mathcal{W}_3}\\ &=-\int_1^2 dt_1\,\partial_{t_1}\Big[\int_{t_1}^3 dt_2\,\langle\,f\circ\phi(0)\,cV(1)\,cV(t_1)\,V(t_2)\Big]\,\rangle_{\mathcal{W}_3}-\int_1^2 dt_1\,\langle\,f\circ\phi(0)\,cV(1)\,cV^2(t_1)\,\rangle_{\mathcal{W}_3}\\ &=-\int_2^3 dt_2\,\langle\,f\circ\phi(0)\,cV(1)\,cV(2)\,V(t_2)\,\rangle_{\mathcal{W}_3}-\int_1^2 dt_1\,\langle\,f\circ\phi(0)\,cV(1)\,cV^2(t_1)\,\rangle_{\mathcal{W}_3}\\ &=-\langle\,\phi\,,\Psi^{(1)}*\Psi_L^{(2)}\,\rangle-\int_1^2 dt_1\,\langle\,f\circ\phi(0)\,cV(1)\,cV^2(t_1)\,\rangle_{\mathcal{W}_3}\,.\end{aligned}\tag{3.2.21}$$

The calculation of the second line on the right-hand side of (3.2.20) is straightforward:

$$\begin{aligned}&-\int_1^2 dt_1\int_{t_1}^3 dt_2\,\langle\,f\circ\phi(0)\,cV(1)\,V(t_1)\,\partial_{t_2}\,[\,cV(t_2)\,]\,\rangle_{\mathcal{W}_3}\\ &=-\int_1^2 dt_1\,\langle\,f\circ\phi(0)\,cV(1)\,V(t_1)\,cV(3)\,\rangle_{\mathcal{W}_3}+\int_1^2 dt_1\,\langle\,f\circ\phi(0)\,cV(1)\,cV^2(t_1)\,\rangle_{\mathcal{W}_3}\\ &=-\langle\,\phi\,,\Psi_L^{(2)}*\Psi^{(1)}\,\rangle+\int_1^2 dt_1\,\langle\,f\circ\phi(0)\,cV(1)\,cV^2(t_1)\,\rangle_{\mathcal{W}_3}\,.\end{aligned}\tag{3.2.22}$$

Note that the two terms with cV^2, which arise from collisions of cV and V, cancel each other. We have thus reconfirmed that the equation of motion at $\mathcal{O}(\lambda^3)$ is satisfied.

This form of $\Psi_L^{(3)}$ can be generalized to $\Psi_L^{(n)}$ for any n as follows:

$$\begin{aligned}\langle\,\phi\,,\Psi_L^{(n)}\,\rangle &= \Big\langle\,f\circ\phi(0)\;cV(1)\int_1^2 dt_1\int_{t_1}^3 dt_2\int_{t_2}^4 dt_3\,\ldots\int_{t_{n-2}}^n dt_{n-1}\,V(t_1)\,V(t_2)\,V(t_3)\,\ldots\,V(t_{n-1})\Big\rangle_{\mathcal{W}_n}\\ &=\Big\langle\,f\circ\phi(0)\;cV(1)\prod_{j=1}^{n-1}\int_{t_{j-1}}^{j+1} dt_j\,V(t_j)\,\Big\rangle_{\mathcal{W}_n}\qquad\text{with}\quad t_0\equiv 1\,.\end{aligned}\tag{3.2.23}$$

See figure 3-7. It is straightforward to show that $\Psi_L^{(n)}$ satisfies the equation of motion:

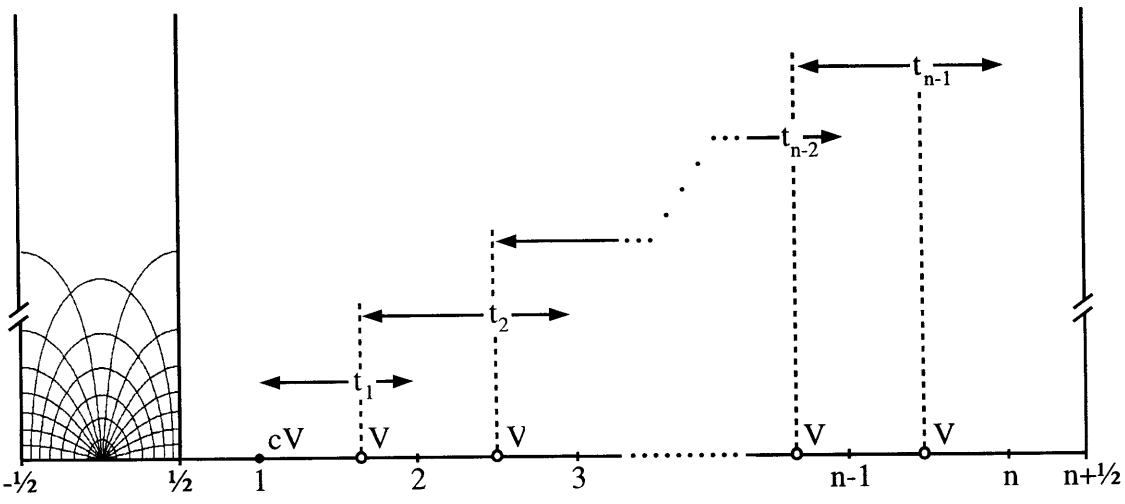

Figure 3-7: Illustration of $\Psi_L^{(n)}$. The solid dot represents the cV insertion, and the circles represent the V insertions. The integration region of t_j is from t_{j-1} to $j+1$.

$$
\begin{aligned}
&\langle\, \phi\,, Q_B \Psi_L^{(n)} \,\rangle \\
&= -\sum_{i=1}^{n-1} \Big\langle\, f\circ\phi(0)\, cV(1) \prod_{j=1}^{i-1} \int_{t_{j-1}}^{j+1} dt_j V(t_j) \int_{t_{i-1}}^{i+1} dt_i\, \partial_{t_i}\,[\,cV(t_i)\,] \prod_{k=i+1}^{n-1} \int_{t_{k-1}}^{k+1} dt_k V(t_k) \,\Big\rangle_{\mathcal{W}_n} \\
&= -\sum_{i=1}^{n-1} \Big\langle\, f\circ\phi(0)\, cV(1) \prod_{j=1}^{i-1} \int_{t_{j-1}}^{j+1} dt_j V(t_j)\; cV(i+1) \int_{i+1}^{i+2} dt_{i+1} \ldots \int_{t_{n-2}}^{n} dt_{n-1}\, V(t_{i+1}) \ldots V(t_k) \,\Big\rangle_{\mathcal{W}_n} \\
&\quad + \sum_{i=2}^{n-1} \Big\langle\, f\circ\phi(0)\, cV(1) \prod_{j=1}^{i-1} \int_{t_{j-1}}^{j+1} dt_j V(t_j)\; cV(t_{i-1}) \int_{t_{i-1}}^{i+2} dt_{i+1} \ldots \int_{t_{n-2}}^{n} dt_{n-1}\, V(t_{i+1}) \ldots V(t_k) \,\Big\rangle_{\mathcal{W}_n} \\
&\quad + \sum_{i=1}^{n-2} \Big\langle\, f\circ\phi(0)\, cV(1) \prod_{j=1}^{i-1} \int_{t_{j-1}}^{j+1} dt_j V(t_j) \int_{t_{i-1}}^{i+1} dt_i\, cV(t_i)\, \partial_{t_i} \Big[\prod_{k=i+1}^{n-1} \int_{t_{k-1}}^{k+1} dt_k V(t_k) \Big] \,\Big\rangle_{\mathcal{W}_n} .
\end{aligned}
\tag{3.2.24}
$$

By carrying out the differentiation in the last line, we find that the last line precisely cancels the second line on the right-hand side. The remaining first line on the right-hand side is a sum of $-\Psi^{(i)} * \Psi^{(n-i)}$ over i. We have thus shown

$$
\langle\, \phi\,,\, Q_B \Psi_L^{(n)} \,\rangle = -\sum_{i=1}^{n-1} \langle\, \phi\,,\, \Psi^{(i)} * \Psi^{(n-i)} \,\rangle\,. \tag{3.2.25}
$$

It is convenient to introduce the following notation:

$$
\begin{aligned}
V_L^{(n)}(1, n+1) &\equiv \int_1^2 dt_1 \int_{t_1}^3 dt_2 \int_{t_2}^4 dt_3 \ldots \int_{t_{n-1}}^{n+1} dt_n\, V(t_1)\, V(t_2) \ldots V(t_n) \quad \text{for} \quad n \geq 1\,, \\
V_L^{(0)}(1,1) &\equiv 1\,.
\end{aligned}
\tag{3.2.26}
$$

The superscript (n) indicates the number of operators and $(1, n+1)$ indicates the region where operators are inserted, although this notation is slightly redundant because the number of operators

and the length of the region are correlated for $V_L^{(n)}(1, n+1)$. The solution $\Psi_L^{(n)}$ can now be compactly written as

$$\langle \phi, \Psi_L^{(n)} \rangle = \langle f \circ \phi(0)\ cV(1)\ V_L^{(n-1)}(1,n) \rangle_{\mathcal{W}_n} . \tag{3.2.27}$$

The state Ψ_L defined by

$$\Psi_L = \sum_{n=1}^{\infty} \lambda^n \Psi_L^{(n)} \tag{3.2.28}$$

thus solves the equation of motion to all orders in λ.

3.2.2 Solutions satisfying the reality condition

The solution Ψ_L constructed in the previous subsection satisfies the equation of motion, but it does not satisfy the reality condition on the string field. In this subsection, we construct a solution satisfying the reality condition from Ψ_L.

The reality condition

The string field Ψ must have a definite parity under the combination of the Hermitean conjugation (hc) and the inverse BPZ conjugation (bpz^{-1}) to guarantee that the string field theory action is real [59]. We define the conjugate $A^\ddagger$ of a string field A by

$$A^\ddagger \equiv \mathrm{bpz}^{-1} \circ \mathrm{hc}\,(A) . \tag{3.2.29}$$

With this definition, the following relations hold:

$$(Q_B A)^\ddagger = -(-1)^A Q_B A^\ddagger , \tag{3.2.30}$$

$$(A * B)^\ddagger = B^\ddagger * A^\ddagger . \tag{3.2.31}$$

Here and in what follows a string field in the exponent of (-1) denotes its Grassmann property: it is 0 mod 2 for a Grassmann-even state and 1 mod 2 for a Grassmann-odd state. Since the string field Ψ is Grassmann odd, it must be *even* under the conjugation $\Psi^\ddagger = \Psi$ in order that $Q_B\Psi$ and $\Psi * \Psi$ have the same parity. We will say that a string field of ghost number one is *real* when it is even under the conjugation.

The class of states we use in constructing solutions for marginal deformations are made of wedge states with insertions of cV and V. Let us consider the conjugate of a state in this class. The wedge state W_α [44] is even under the conjugation $W_\alpha^\ddagger = W_\alpha$ because it is constructed from the $SL(2,R)$-invariant vacuum $|0\rangle$ satisfying $|0\rangle^\ddagger = |0\rangle$ by acting with BPZ-even Virasoro generators $L_{-2}, L_{-4}, \ldots$. The first term $\Psi^{(1)}$ in the solution must be even $(\Psi^{(1)})^\ddagger = \Psi^{(1)}$, as we discussed above. Therefore, the conjugate of $W_\alpha * \Psi^{(1)} * W_\beta$ is $W_\beta * \Psi^{(1)} * W_\alpha$. This means that the operator $cV(t)$ on $\mathcal{W}_n$ is mapped to $cV(n+1-t)$ under the conjugation:

$$cV(t) \longrightarrow cV(n+1-t) \quad \text{on} \quad \mathcal{W}_n . \tag{3.2.32}$$

Its derivative $\partial_t [\, cV(t)\,]$ at $t = a$ is then mapped to $-\partial_t [\, cV(t)\,]$ at $t = n+1-a$. Since $\partial_t [\, cV(t)\,]$ is the BRST transformation of $V(t)$, this means that $Q_B \cdot V(a)$ is mapped to $-Q_B \cdot V(n+1-a)$ on $\mathcal{W}_n$. It then follows from (3.2.30) that $V(t)$ is mapped under the conjugation as follows:

$$V(t) \;\longrightarrow\; V(n+1-t) \quad \text{on} \quad \mathcal{W}_n\,. \tag{3.2.33}$$

It is straightforward to generalize the argument to the case with multiple operator insertions. The conjugate of the state made of the wedge state W_n with $cV(t_1), V(t_2), V(t_3), \ldots, V(t_m)$ is therefore the state made of W_n with $V(n+1-t_m), V(n+1-t_{m-1}), \ldots, V(n+1-t_2), cV(n+1-t_1)$.

The state $\Psi_L^{(n)}$ with $n \geq 2$ does not satisfy the reality condition. Indeed, the operator $V_L^{(n-1)}(1,n)$ defined in (3.2.26) is mapped as

$$\begin{aligned}
&\int_1^2 dt_1 \int_{t_1}^3 dt_2 \int_{t_2}^4 dt_3 \,\ldots \int_{t_{n-2}}^n dt_{n-1}\, V(t_1)\, V(t_2)\, \ldots\, V(t_{n-1}) \\
&\qquad\longrightarrow\; \int_1^2 dt_1 \int_{t_1}^3 dt_2 \int_{t_2}^4 dt_3 \,\ldots \int_{t_{n-2}}^n dt_{n-1}\, V(n+1-t_{n-1})\, V(n+1-t_{n-2})\, \ldots\, V(n+1-t_1) \\
&\qquad\quad = \int_{n-1}^n dt_1' \int_{n-2}^{t_1'} dt_2' \int_{n-3}^{t_2'} dt_3' \ldots \int_1^{t_{n-2}'} dt_{n-1}'\, V(t_{n-1}')\, V(t_{n-2}') \ldots V(t_1')
\end{aligned} \tag{3.2.34}$$

under the conjugation, where $t_i' = n+1-t_i$. We denote the conjugate of $\Psi_L^{(n)}$ by $\Psi_R^{(n)}$. It is given by

$$\langle\, \phi\,, \Psi_R^{(n)}\,\rangle = \langle\, \phi\,, (\Psi_L^{(n)})^\ddagger\,\rangle = \langle\, f\circ\phi(0)\;\, V_R^{(n-1)}(1,n)\; cV(n)\,\rangle_{\mathcal{W}_n}\,, \tag{3.2.35}$$

where we defined

$$\begin{aligned}
V_R^{(n)}(1,n+1) &\equiv \int_n^{n+1} dt_1 \int_{n-1}^{t_1} dt_2 \int_{n-2}^{t_2} dt_3 \ldots \int_1^{t_{n-1}} dt_n\, V(t_n)\, V(t_{n-1}) \ldots V(t_1) \quad \text{for} \quad n \geq 1\,, \\
V_R^{(0)}(1,1) &\equiv 1\,.
\end{aligned} \tag{3.2.36}$$

If Ψ satisfies the equation of motion, its conjugate $\Psi^\ddagger$ also satisfies the equation of motion because

$$Q_B\Psi^\ddagger + \Psi^\ddagger * \Psi^\ddagger = (Q_B\Psi + \Psi * \Psi)^\ddagger = 0\,. \tag{3.2.37}$$

Therefore, Ψ_R defined by

$$\Psi_R = \sum_{n=1}^{\infty} \lambda^n\, \Psi_R^{(n)} \tag{3.2.38}$$

satisfies the equation of motion.

Gauge transformation

We have found two solutions Ψ_L and Ψ_R, and we expect that they are related by a gauge transformation generated by some gauge parameter U:

$$\Psi_R \;=\; U^{-1} * \Psi_L * U + U^{-1} * Q_B U\,. \tag{3.2.39}$$

For a physical gauge transformation which relates two string fields satisfying the reality condition, the gauge parameter U must satisfy the unitarity relation $U^\ddagger = U^{-1}$. As we will see later, the gauge parameter U that relates Ψ_L and Ψ_R is even under the conjugation: $U^\ddagger = U$. The component fields of Ψ_L and Ψ_R which do not satisfy the reality condition are thus related through the component fields of U which also violate the reality condition on the gauge parameter.

Let us now construct U which relates Ψ_L and Ψ_R. It is convenient to rewrite the equation (3.2.39) as follows:

$$Q_B U \;=\; U * \Psi_R \;-\; \Psi_L * U\,. \tag{3.2.40}$$

We can expand U as

$$U = \sum_{n=0}^{\infty} \lambda^n\, U^{(n)} \quad \text{with} \quad U^{(0)} = 1\,, \tag{3.2.41}$$

and we solve the equation perturbatively in λ. We can choose

$$U^{(1)} = 0 \tag{3.2.42}$$

because $\Psi_L^{(1)} = \Psi_R^{(1)}$ and therefore $Q_B U^{(1)} = 0$. The equation for $U^{(2)}$ is

$$\langle\, \phi, Q_B\, U^{(2)} \,\rangle = \langle\, \phi, \Psi_R^{(2)} \,\rangle - \langle\, \phi, \Psi_L^{(2)} \,\rangle = \langle\, f \circ \phi(0)\, [\, V(1,2)\, cV(2) - cV(1)\, V(1,2)\,]\,\rangle_{\mathcal{W}_2}\,. \tag{3.2.43}$$

This can be easily solved using the formula (3.2.16), and a solution is

$$\langle\, \phi, U^{(2)} \,\rangle = \frac{1}{2}\, \langle\, f \circ \phi(0)\; (V(1,2))^2 \,\rangle_{\mathcal{W}_2}\,. \tag{3.2.44}$$

We can construct $U^{(n)}$ at higher orders recursively in this way. However, we can infer $U^{(n)}$ from the structure of (3.2.40). If we assume that U can be written without using c ghosts, the only c ghost is inserted at $t = n$ in the $\mathcal{O}(\lambda^n)$ term of $\langle\, \phi, U * \Psi_R \,\rangle$ when represented on $\mathcal{W}_n$ and at $t = 1$ on $\mathcal{W}_n$ in the $\mathcal{O}(\lambda^n)$ term of $\langle\, \phi, \Psi_L * U \,\rangle$. This motivates us to make the following ansatz:

$$\langle\, \phi, U^{(n)} \,\rangle \propto \langle\, f \circ \phi(0)\, V^{(n)}(1,n) \,\rangle_{\mathcal{W}_n}\,, \tag{3.2.45}$$

where

$$V^{(n)}(a,b) \equiv \frac{1}{n!}\, (V(a,b))^n \qquad \text{for} \qquad n \geq 1\,, \qquad V^{(0)}(a,b) \equiv 1\,. \tag{3.2.46}$$

We in fact show that the gauge transformation U in (3.2.39) is given by

$$\langle\, \phi\,, U^{(n)} \,\rangle = \langle\, f \circ \phi(0)\; V^{(n)}(1,n) \,\rangle_{\mathcal{W}_n}\,. \tag{3.2.47}$$

See figure 3-8. The BRST transformation of $U^{(n)}$ given in (3.2.47) is

$$\langle\, \phi, Q_B U^{(n)} \,\rangle = \Big\langle\, f \circ \phi(0)\;\; \big(V^{(n-1)}(1,n)\, cV(n) \;-\; cV(1)\, V^{(n-1)}(1,n)\big) \,\Big\rangle_{\mathcal{W}_n}\,, \tag{3.2.48}$$

where we used (3.2.16). For the special case of $n = 1$, the terms on the right-hand side cancel, which is consistent because $U^{(1)} = 0$. The $\mathcal{O}(\lambda^n)$ term of $U * \Psi_R \;-\; \Psi_L * U$ in (3.2.40) is given by

$$\begin{aligned} &\sum_{m=1}^{n} \langle\, f \circ \phi(0)\;\; V^{(n-m)}(1, n-m)\, V_R^{(m-1)}(n-m+1, n)\, cV(n) \,\rangle_{\mathcal{W}_n} \\ &- \sum_{m=1}^{n} \langle\, f \circ \phi(0)\;\; cV(1)\, V_L^{(m-1)}(1,m)\, V^{(n-m)}(m+1, n) \,\rangle_{\mathcal{W}_n}\,. \end{aligned} \tag{3.2.49}$$

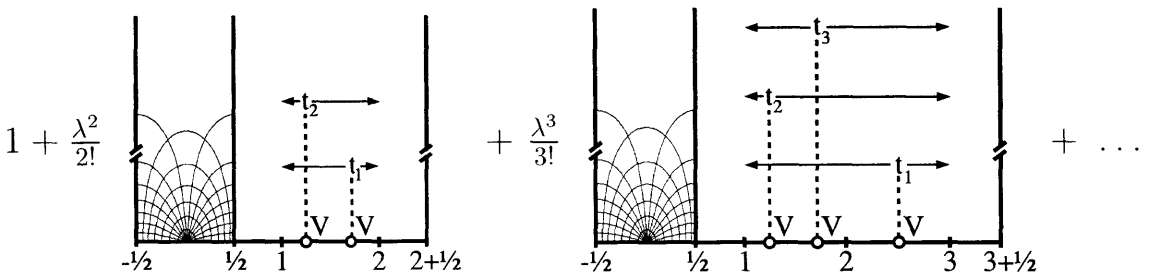

Figure 3-8: Illustration of the expansion $U = 1 + \lambda^2 U^{(2)} + \lambda^3 U^{(3)} + \mathcal{O}(\lambda^4)$.

The proof of (3.2.40) for U given in (3.2.47) thus reduces to showing that

$$\langle f \circ \phi(0)\ cV(1)\, V^{(n-1)}(1,n) \rangle_{\mathcal{W}_n} = \sum_{m=1}^{n} \langle f \circ \phi(0)\ cV(1)\, V_L^{(m-1)}(1,m)\, V^{(n-m)}(m+1,n) \rangle_{\mathcal{W}_n} \tag{3.2.50}$$

and

$$\langle f \circ \phi(0)\ V^{(n-1)}(1,n)\, cV(n) \rangle_{\mathcal{W}_n} = \sum_{m=1}^{n} \langle f \circ \phi(0)\ V^{(n-m)}(1,n-m)\, V_R^{(m-1)}(n-m+1,n)\, cV(n) \rangle_{\mathcal{W}_n} . \tag{3.2.51}$$

Since the second equation follows from the first one by the conjugation, it is sufficient to show (3.2.50). The operator $V^{(n-1)}(1,n)$ on the left-hand side can be written in a path-ordered form as follows:

$$V^{(n-1)}(1,n) = \int_1^n dt_1 \int_{t_1}^n dt_2 \ldots \int_{t_{n-2}}^n dt_{n-1}\, V(t_1) \ldots V(t_{n-1}) . \tag{3.2.52}$$

We now decompose the integration region $1 \le t_1 \le t_2 \le \ldots \le t_{n-1} \le n$ in the following way:

$$\begin{aligned}
&t_1 \ge 2 , \\
&t_1 \le 2 , t_2 \ge 3 , \\
&t_1 \le 2 , t_2 \le 3 , t_3 \ge 4 , \\
&\qquad \vdots \\
&t_1 \le 2 , t_2 \le 3 , \ldots , t_{m-1} \le m , t_m \ge m+1 , \\
&\qquad \vdots \\
&t_1 \le 2 , t_2 \le 3 , t_3 \le 4 , \ldots\ldots\ldots , t_{n-2} \le n-1 , t_{n-1} \ge n , \\
&t_1 \le 2 , t_2 \le 3 , t_3 \le 4 , \ldots\ldots\ldots , t_{n-2} \le n-1 , t_{n-1} \le n .
\end{aligned} \tag{3.2.53}$$

This decomposition of the integration region precisely matches the right-hand side of (3.2.50). For example, the fourth line of (3.2.53) corresponds to the integration region for the product of the operators $V_L^{(m-1)}(1,m)\, V^{(n-m)}(m+1,n)$. Furthermore, the fifth line vanishes because of the vanishing integration range $n \le t_{n-1} \le n$. This is consistent with the right-hand side of (3.2.50) because $V^{(1)}(n,n) = 0$. The last line is nonvanishing and corresponds to $V_L^{(n-1)}(1,n)\, V^{(0)}(n+$

$1,n) = V_L^{(n-1)}(1,n)$, where we used $V^{(0)}(a,b) \equiv 1$. We conclude that

$$V^{(n-1)}(1,n) = \sum_{m=1}^{n} V_L^{(m-1)}(1,m)\, V^{(n-m)}(m+1,n)\,, \tag{3.2.54}$$

and we have thus shown (3.2.50). This completes the proof that U is the gauge transformation that relates Ψ_L and Ψ_R.

Construction of a real solution

The state U takes the form

$$U = 1 + \sum_{n=2}^{\infty} \lambda^n\, U^{(n)}\,, \tag{3.2.55}$$

and $U^{(n)}$ is even under the conjugation: $(U^{(n)})^\ddagger = U^{(n)}$. If a state X is even under the conjugation, then $\ln(1+X)$ defined by

$$\ln(1+X) \equiv \sum_{n=1}^{\infty} \frac{(-1)^{n+1}}{n}\, \underbrace{X * X * \ldots * X}_{n} \tag{3.2.56}$$

is also even. If a state Y is even, then $\exp(a\,Y)$ with real a defined by

$$\exp(a\,Y) \equiv 1 + \sum_{n=1}^{\infty} \frac{a^n}{n!}\, \underbrace{Y * Y * \ldots * Y}_{n} \tag{3.2.57}$$

is also even. Therefore, $(1+X)^{-1}$, $\sqrt{1+X}$ and $1/\sqrt{1+X}$ defined by

$$\begin{aligned} (1+X)^{-1} &\equiv \exp\left[-\ln(1+X)\right] = 1 + \sum_{n=1}^{\infty} (-1)^n\, \underbrace{X * X * \ldots * X}_{n}\,, \\ \sqrt{1+X} &\equiv \exp\left[\frac{1}{2}\ln(1+X)\right]\,, \qquad \frac{1}{\sqrt{1+X}} \equiv \exp\left[-\frac{1}{2}\ln(1+X)\right] \end{aligned} \tag{3.2.58}$$

are all even if $X^\ddagger = X$. We define U^{-1}, $\sqrt{U}$, and $1/\sqrt{U}$ in this way, which are well defined to all orders in λ and are even under the conjugation.

We can now construct a real solution Ψ from Ψ_L as follows:

$$\begin{aligned} \Psi &\equiv \frac{1}{\sqrt{U}} * \Psi_L * \sqrt{U} + \frac{1}{\sqrt{U}} * Q_B\sqrt{U} \\ &= \sqrt{U} * \Psi_R * \frac{1}{\sqrt{U}} + \sqrt{U} * Q_B \frac{1}{\sqrt{U}} \\ &= \frac{1}{2}\left[\frac{1}{\sqrt{U}} * \Psi_L * \sqrt{U} + \sqrt{U} * \Psi_R * \frac{1}{\sqrt{U}} + \frac{1}{\sqrt{U}} * Q_B\sqrt{U} - Q_B\sqrt{U} * \frac{1}{\sqrt{U}}\right]. \end{aligned} \tag{3.2.59}$$

The second expression is obtained from the first one using $Q_B U = U*\Psi_R - \Psi_L * U$, and Ψ manifestly satisfies the reality condition in the third expression because of the relations $\Psi_L^\ddagger = \Psi_R$, $(\sqrt{U}\,)^\ddagger = \sqrt{U}$, $(1/\sqrt{U}\,)^\ddagger = 1/\sqrt{U}$, and $(Q_B\sqrt{U}\,)^\ddagger = -\,Q_B\sqrt{U}$. The state Ψ also satisfies the equation of motion because it is obtained from the solution Ψ_L by the gauge transformation generated by $\sqrt{U}$.

We have successfully constructed real analytic solutions for marginal deformations with regular operator products. To summarize, our solution takes the form

$$\Psi = \frac{1}{\sqrt{U}} * \Psi_L * \sqrt{U} + \frac{1}{\sqrt{U}} * Q_B \sqrt{U}\,, \tag{3.2.60}$$

where Ψ_L and U are defined by

$$\begin{aligned}
\Psi_L &= \sum_{n=1}^{\infty} \lambda^n \Psi_L^{(n)}\,, \\
\langle \phi\,, \Psi_L^{(n)} \rangle &= \langle f\circ\phi(0)\; cV(1)\; V_L^{(n-1)}(1,n) \rangle_{\mathcal{W}_n} \\
&= \int_1^2 dt_1 \int_{t_1}^3 dt_2 \,\ldots \int_{t_{n-2}}^n dt_{n-1} \,\langle f\circ\phi(0)\; cV(1)\; V(t_1)\,V(t_2)\,\ldots\,V(t_{n-1}) \rangle_{\mathcal{W}_n}\,, \\
U &= 1 + \sum_{n=2}^{\infty} \lambda^n U^{(n)}\,, \\
\langle \phi\,, U^{(n)} \rangle &= \langle f\circ\phi(0)\, V^{(n)}(1,n) \rangle_{\mathcal{W}_n} \\
&= \frac{1}{n!} \int_1^n dt_1 \int_1^n dt_2 \ldots \int_1^n dt_n \,\langle f\circ\phi(0)\, V(t_1)\, V(t_2)\,\ldots V(t_n) \rangle_{\mathcal{W}_n}\,.
\end{aligned} \tag{3.2.61}$$

3.2.3 Generalization of wedge states

In the previous subsection, we found the identity (3.2.54). It is simply a consequence of the decomposition of the integral region (3.2.53). The identity (3.2.54) can be generalized in the following way. We define $V_{L,\alpha}^{(n)}(1,n+\alpha)$ for $\alpha \geq 0$ by

$$\begin{aligned}
V_{L,\alpha}^{(n)}(1,n+\alpha) &\equiv \int_1^{1+\alpha} dt_1 \int_{t_1}^{2+\alpha} dt_2 \int_{t_2}^{3+\alpha} dt_3 \,\ldots \int_{t_{n-1}}^{n+\alpha} dt_n\, V(t_1)\, V(t_2)\,\ldots\, V(t_n) \quad \text{for} \quad n \geq 1\,, \\
V_{L,\alpha}^{(0)}(1,\alpha) &\equiv 1\,.
\end{aligned} \tag{3.2.62}$$

This reduces to $V_L^{(n)}(1,n+1)$ defined in (3.2.26) when $\alpha = 1$. We then find that

$$V^{(n)}(1,n+\alpha+\beta) \;=\; \sum_{m=0}^{n} V_{L,\alpha}^{(m)}(1,m+\alpha)\, V^{(n-m)}(m+\alpha+1,n+\alpha+\beta) \tag{3.2.63}$$

for any non-negative real numbers α and β. This identity reduces to (3.2.54) when $\alpha = 1$, $\beta = 0$. This generalized identity can be shown, as before, by decomposing the path-ordered integration

region $1 \le t_1 \le t_2 \le \ldots \le t_n \le n+\alpha+\beta$ of $V^{(n)}(1, n+\alpha+\beta)$ in the following way:

$$
\begin{aligned}
& t_1 \ge 1+\alpha\,, \\
& t_1 \le 1+\alpha\,,\ t_2 \ge 2+\alpha\,, \\
& t_1 \le 1+\alpha\,,\ t_2 \le 2+\alpha\,,\ t_3 \ge 3+\alpha\,, \\
& \qquad \vdots \\
& t_1 \le 1+\alpha\,,\ t_2 \le 2+\alpha\,,\ \ldots\,,\ t_m \le m+\alpha\,,\ t_{m+1} \ge m+1+\alpha\,, \\
& \qquad \vdots \\
& t_1 \le 1+\alpha\,,\ t_2 \le 2+\alpha\,,\ t_3 \le 3+\alpha\,,\ \ldots\ldots\ldots\,,\ t_{n-1} \le n-1+\alpha\,,\ t_n \ge n+\alpha\,, \\
& t_1 \le 1+\alpha\,,\ t_2 \le 2+\alpha\,,\ t_3 \le 3+\alpha\,,\ \ldots\ldots\ldots\,,\ t_{n-1} \le n-1+\alpha\,,\ t_n \le n+\alpha\,.
\end{aligned}
\tag{3.2.64}
$$

This identity can be promoted to a relation of string fields. We define U_α and $U_{L,\alpha}$ with $\alpha \ge 0$ by

$$
U_\alpha \equiv \sum_{n=0}^{\infty} \lambda^n\, U_\alpha^{(n)}\,, \qquad U_{L,\alpha} \equiv \sum_{n=0}^{\infty} \lambda^n\, U_{L,\alpha}^{(n)}\,, \tag{3.2.65}
$$

where

$$
\begin{aligned}
&\langle\, \phi\,, U_\alpha^{(n)} \,\rangle = \langle\, f\circ\phi(0)\ V^{(n)}(1, n+\alpha)\,\rangle_{\mathcal{W}_{n+\alpha}} \quad \text{for} \quad n+\alpha > 0\,, \qquad U_0^{(0)} = 1\,, \\
&\langle\, \phi\,, U_{L,\alpha}^{(n)} \,\rangle = \langle\, f\circ\phi(0)\ V_{L,\alpha}^{(n)}(1, n+\alpha)\,\rangle_{\mathcal{W}_{n+\alpha}} \quad \text{for} \quad n+\alpha > 0\,, \qquad U_{L,0}^{(0)} = 1\,.
\end{aligned}
\tag{3.2.66}
$$

The gauge parameter U in the previous subsection is thus

$$
U = U_0\,, \tag{3.2.67}
$$

and the solution Ψ_L in (3.2.27) is $U_{L,1}$ with an extra insertion of $\lambda\, cV(1)$. It then follows from (3.2.63) that

$$
U_{\alpha+\beta} = U_{L,\alpha} * U_\beta\,. \tag{3.2.68}
$$

When $\beta = 0$, we have

$$
U_\alpha = U_{L,\alpha} * U\,, \tag{3.2.69}
$$

where we have used $U_0 = U$. As we discussed in the previous subsection, the inverse of U is well defined to all orders in λ. We thus find that

$$
U_{L,\alpha} = U_\alpha * U^{-1}\,. \tag{3.2.70}
$$

It follows from this and (3.2.68) that

$$
U_{\alpha+\beta} = U_\alpha * U^{-1} * U_\beta\,. \tag{3.2.71}
$$

The state U_α is $W_\alpha + \mathcal{O}(\lambda)$ for $\alpha > 0$, where W_α is the well-known wedge state defined by

$$
\langle\, \phi\,, W_\alpha \,\rangle = \langle\, f\circ\phi(0)\,\rangle_{\mathcal{W}_\alpha}\,. \tag{3.2.72}
$$

The relation (3.2.71) for positive α and β thus reduces to the famous relation $W_{\alpha+\beta} = W_\alpha * W_\beta$ when $\lambda = 0$, and the state U_α can be thought of as a generalization of the wedge state W_α. When α is a positive integer, U_α can be written in terms of U_1 and U^{-1}:

$$\begin{aligned} U_2 &= U_1 * U^{-1} * U_1 \,, \\ U_3 &= U_1 * U^{-1} * U_1 * U^{-1} * U_1 \,, \\ U_4 &= U_1 * U^{-1} * U_1 * U^{-1} * U_1 * U^{-1} * U_1 \,, \\ &\vdots \end{aligned} \tag{3.2.73}$$

This structure indicates a modification of the star product for finite λ defined by

$$A \star B \equiv A * U^{-1} * B \,, \tag{3.2.74}$$

and the relation (3.2.71) can be written as

$$U_{\alpha+\beta} = U_\alpha \star U_\beta \,. \tag{3.2.75}$$

On a technical level, the relation (3.2.71) will play an important role in the next section for the construction of solutions associated with general marginal deformations. On a more conceptual level, we will see in section 3.5 that the modified star product (3.2.74) naturally appears in the string field theory action expanded around a deformed background.

3.3 Marginal deformations with singular operator products

3.3.1 Another form of the solution with regular operator products

In the process of constructing a real solution from Ψ_L in the previous section, we proved that

$$Q_B U = U * \Psi_R - \Psi_L * U \,. \tag{3.3.1}$$

As we have seen in (3.2.48), the BRST transformation of U can be decomposed into two pieces:

$$Q_B U = A_R - A_L \,, \tag{3.3.2}$$

where A_L and A_R are given by

$$\begin{aligned} \langle \phi \,, A_L \rangle &= \sum_{n=1}^{\infty} \lambda^n \, \langle \, f \circ \phi(0) \, cV(1) \, V^{(n-1)}(1,n) \, \rangle_{\mathcal{W}_n} \,, \\ \langle \phi \,, A_R \rangle &= \sum_{n=1}^{\infty} \lambda^n \, \langle \, f \circ \phi(0) \, V^{(n-1)}(1,n) \, cV(n) \, \rangle_{\mathcal{W}_n} \,. \end{aligned} \tag{3.3.3}$$

See figure 3-9. At $\mathcal{O}(\lambda^n)$ with $n \geq 2$, A_L and A_R account for the term with $cV(1)$ and the term with $cV(n)$ in $Q_B U^{(n)}$, respectively. At $\mathcal{O}(\lambda)$, $Q_B U$ vanishes because $U^{(1)} = 0$, but we have chosen A_L and A_R at $\mathcal{O}(\lambda)$ to be $\lambda \, \Psi^{(1)}$ for later convenience.

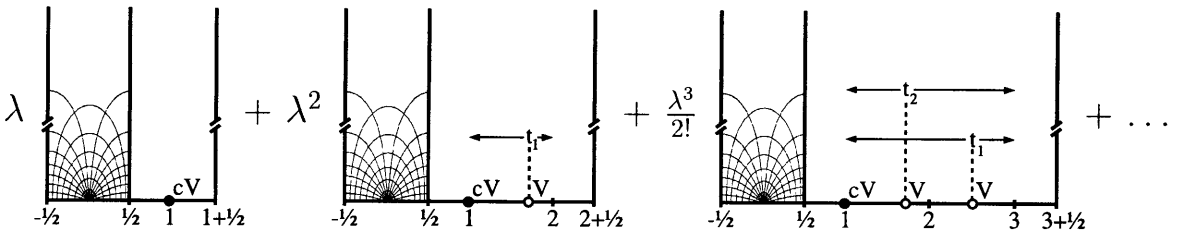

Figure 3-9: Illustration of the expansion $A_L = \lambda\, A_L^{(1)} + \lambda^2\, A_L^{(2)} + \lambda^3\, A_L^{(3)} + \mathcal{O}(\lambda^4)$.

In the proof of (3.3.1), we have actually shown that

$$A_L = \Psi_L * U\,, \qquad A_R = U * \Psi_R\,. \tag{3.3.4}$$

As we discussed in the previous section, the inverse of U is well defined to all orders in λ. We thus obtain new expressions for Ψ_L and Ψ_R:

$$\Psi_L = A_L * U^{-1}\,, \qquad \Psi_R = U^{-1} * A_R\,. \tag{3.3.5}$$

We have shown that Ψ_L with $\Psi_L^{(n)}$ in the form of (3.2.27) satisfies the equation of motion. Let us now see how Ψ_L in the new form satisfies the equation of motion. The BRST transformation of Ψ_L can be calculated as follows:

$$\begin{aligned} Q_B\Psi_L &= Q_B\,(A_L * U^{-1}) \\ &= (Q_B A_L) * U^{-1} + A_L * U^{-1} * (Q_B U) * U^{-1} \\ &= (Q_B A_L) * U^{-1} + A_L * U^{-1} * (A_R - A_L) * U^{-1} \\ &= (Q_B A_L + A_L * U^{-1} * A_R) * U^{-1} - A_L * U^{-1} * A_L * U^{-1} \\ &= (Q_B A_L + A_L * U^{-1} * A_R) * U^{-1} - \Psi_L * \Psi_L\,. \end{aligned} \tag{3.3.6}$$

Therefore, the equation of motion is satisfied if

$$-\,Q_B A_L = A_L * U^{-1} * A_R\,. \tag{3.3.7}$$

The left-hand side of the equation can be calculated as follows:

$$-\,\langle\,\phi\,, Q_B A_L\,\rangle = \sum_{n=2}^{\infty} \lambda^n\,\langle\, f\circ\phi(0)\, cV(1)\, V^{(n-2)}(1,n)\, cV(n)\,\rangle_{\mathcal{W}_n}\,. \tag{3.3.8}$$

Let us next consider the structure of the state $A_L * U^{-1} * A_R$ on the right-hand side of (3.3.7). The $\mathcal{O}(\lambda^n)$ terms of A_L and A_R are made of the wedge state W_n with operator insertions. The inverse U^{-1} can be written as a linear combination of string products made of $\lambda^n\, U^{(n)}$, and their $\mathcal{O}(\lambda^n)$ terms are again made of the wedge state W_n with operator insertions. It thus follows that all of the $\mathcal{O}(\lambda^n)$ terms of $A_L * U^{-1} * A_R$ are made of W_n with operator insertions. This is consistent with the structure of (3.3.8). Furthermore, the insertions of $\lambda\, cV$ on the surface $\mathcal{W}_n$ are always $\lambda\, cV(1)$ and $\lambda\, cV(n)$, which is again consistent with the structure of (3.3.8). Finally, let us consider the

structure of integrated vertex operators. The state $-Q_B A_L$ takes the form of the state U_2 defined in (3.2.65) with insertions of λcV. Similarly, A_L and A_R take the form of U_1 with an insertion of λcV. The equation (3.3.7) thus follows from (3.2.71) with $\alpha = \beta = 1$:

$$U_2 = U_1 * U^{-1} * U_1 \,. \tag{3.3.9}$$

We conclude that Ψ_L of the form given in (3.3.5) satisfies the equation of motion.

3.3.2 Generalization to the case with singular operator products

The form $\Psi_L = A_L * U^{-1}$ for the solution can be generalized to the case where operator products of the marginal operator are singular. As we discussed in the introduction, we denote the properly renormalized operator implementing the change of the boundary condition between the points a and b by $[\, e^{\lambda V(a,b)} \,]_r$, which is given in the form of an expansion in λ:

$$[\, e^{\lambda V(a,b)} \,]_r = \sum_{n=0}^{\infty} \frac{\lambda^n}{n!} [\, (V(a,b))^n \,]_r \,, = \sum_{n=0}^{\infty} \lambda^n [\, V^{(n)}(a,b) \,]_r \,. \tag{3.3.10}$$

We define U in the general case by

$$U \equiv \sum_{n=0}^{\infty} \lambda^n U^{(n)} \,, \tag{3.3.11}$$

where

$$\langle\, \phi \,, U^{(n)} \,\rangle = \langle\, f \circ \phi(0) \, [\, V^{(n)}(1,n) \,]_r \,\rangle_{\mathcal{W}_n} \,. \tag{3.3.12}$$

As we discussed in the introduction, we assume that the BRST transformation of $[\, e^{\lambda V(a,b)} \,]_r$ for any exactly marginal deformation takes the form

$$Q_B \cdot [\, e^{\lambda V(a,b)} \,]_r = [\, e^{\lambda V(a,b)} \, O_R(b) \,]_r - [\, O_L(a) \, e^{\lambda V(a,b)} \,]_r \,, \tag{3.3.13}$$

where O_L and O_R are λ-dependent, Grassmann-odd local operators. The operators O_L and O_R are closely related and mapped to each other under the conjugation discussed in § 3.2.2 when the reflection assumption (VI) is satisfied. We will discuss the relation between O_L and O_R in more detail in § 3.3.4, but it is relevant only when generating a real solution from Ψ_L and we do not need to assume any relation between O_L and O_R in the construction of the solution Ψ_L. In the case of marginal deformations with regular operator products, we see from (3.2.16) that

$$Q_B \cdot e^{\lambda V(a,b)} = \lambda \left(e^{\lambda V(a,b)} \, cV(b) - cV(a) \, e^{\lambda V(a,b)} \right) \tag{3.3.14}$$

and identify

$$O_L^{regular} = O_R^{regular} = \lambda cV \,. \tag{3.3.15}$$

In the case of marginal deformations with singular operator products, there can be corrections to O_L and O_R, which are determined from the BRST transformation of $[\, V^{(n)}(a,b) \,]_r$ in the form

$$Q_B \cdot [\, V^{(n)}(a,b) \,]_r = \sum_{r=1}^{n} [\, V^{(n-r)}(a,b) \, O_R^{(r)}(b) \,]_r - \sum_{l=1}^{n} [\, O_L^{(l)}(a) \, V^{(n-l)}(a,b) \,]_r \,, \tag{3.3.16}$$

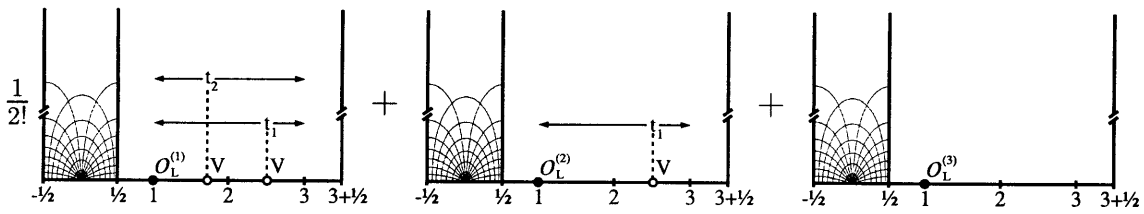

Figure 3-10: Illustration of $A_L^{(3)}$.

where O_L and O_R are expanded as follows:

$$O_L = \sum_{n=1}^{\infty} \lambda^n O_L^{(n)}, \qquad O_R = \sum_{n=1}^{\infty} \lambda^n O_R^{(n)}. \tag{3.3.17}$$

The operators $O_L^{(1)}$ and $O_R^{(1)}$ are determined from the BRST transformation of $[\,V^{(1)}(a,b)\,]_r$. Since $[\,V^{(1)}(a,b)\,]_r$ does not require any renormalization, we find

$$Q_B \cdot [\,V^{(1)}(a,b)\,]_r = Q_B \cdot V(a,b) = cV(b) - cV(a) \tag{3.3.18}$$

for any dimension-one primary field V. Thus the operators $O_L^{(1)}$ and $O_R^{(1)}$ are determined to be

$$O_L^{(1)} = O_R^{(1)} = cV \tag{3.3.19}$$

for any marginal deformation. Similarly, the operators $O_L^{(n)}$ and $O_R^{(n)}$ with $n \geq 2$ are determined from the BRST transformation of $[\,V^{(n)}(a,b)\,]_r$ with $n \geq 2$, but we do not need any specific information on these operators in the construction of solutions. The BRST transformation of U is then given by

$$Q_B U = A_R - A_L, \tag{3.3.20}$$

where

$$A_L \equiv \sum_{n=1}^{\infty} \lambda^n A_L^{(n)}, \qquad A_R \equiv \sum_{n=1}^{\infty} \lambda^n A_R^{(n)}, \tag{3.3.21}$$

with

$$\begin{aligned} \langle\, \phi\,, A_L^{(n)} \,\rangle &= \sum_{l=1}^{n} \langle\, f \circ \phi(0)\, [\, O_L^{(l)}(1)\, V^{(n-l)}(1,n)\,]_r \,\rangle_{\mathcal{W}_n}, \\ \langle\, \phi\,, A_R^{(n)} \,\rangle &= \sum_{r=1}^{n} \langle\, f \circ \phi(0)\, [\, V^{(n-r)}(1,n)\, O_R^{(r)}(n)\,]_r \,\rangle_{\mathcal{W}_n}. \end{aligned} \tag{3.3.22}$$

See figure 3-10. We have defined $A_L^{(1)}$ and $A_R^{(1)}$ to be $\Psi^{(1)}$ as in the regular case.

We now *define* Ψ_L by

$$\Psi_L \equiv A_L * U^{-1}, \tag{3.3.23}$$

and we conclude from the calculation (3.3.6), where we only used the relation $Q_B U = A_R - A_L$, that Ψ_L satisfies the equation of motion if

$$-Q_B A_L = A_L * U^{-1} * A_R. \tag{3.3.24}$$

So far we have only used the assumption (I) on the BRST transformation of $[\,e^{\lambda V(a,b)}\,]_r$. We show in the next subsection that the equation (3.3.24) holds when the assumptions (II)–(V) stated in the introduction are satisfied.

3.3.3 Proof that the equation of motion is satisfied

Let us first examine the left-hand side of (3.3.24). From the assumption (II) on the BRST transformation of $[\,O_L(a)\,e^{\lambda V(a,b)}\,]_r$, it is given by

$$-\,\langle\,\phi\,,Q_B A_L^{(n)}\,\rangle = \sum_{l+r\le n}\langle\,f\circ\phi(0)\,[\,O_L^{(l)}(1)\,V^{(n-l-r)}(1,n)\,O_R^{(r)}(n)\,]_r\,\rangle_{\mathcal{W}_n}\,. \tag{3.3.25}$$

If we define U_α for $\alpha \ge 0$ in the singular case by

$$U_\alpha \equiv \sum_{n=0}^{\infty}\lambda^n\,U_\alpha^{(n)} \tag{3.3.26}$$

with

$$\langle\,\phi\,,U_\alpha^{(n)}\,\rangle = \langle\,f\circ\phi(0)\;[\,V^{(n)}(1,n+\alpha)\,]_r\,\rangle_{\mathcal{W}_{n+\alpha}} \quad \text{for} \quad n+\alpha>0\,, \qquad U_0^{(0)}\equiv 1\,, \tag{3.3.27}$$

then $-\,Q_B A_L$ can be constructed from U_{l+r} by inserting $\lambda^l\,O_L^{(l)}$ and $\lambda^r\,O_R^{(r)}$ and by summing over l and r. We schematically write the state in the following way:

$$-\,Q_B A_L \sim \sum_{l,r}\Big(\,U_{l+r}\ \text{with}\ \lambda^l\,O_L^{(l)}\ \text{and}\ \lambda^r\,O_R^{(r)}\,\Big)\,. \tag{3.3.28}$$

The state A_L on the right-hand side of (3.3.24) can be constructed from U_l by inserting $\lambda^l\,O_L^{(l)}$ and by summing over l. Similarly, the state A_R can be constructed from U_r by inserting $\lambda^r\,O_R^{(r)}$ and by summing over r. Therefore, the state $A_L * U^{-1} * A_R$ can be schematically expressed as follows:

$$\begin{aligned} A_L * U^{-1} * A_R &\sim \sum_{l}\Big(\,U_l\ \text{with}\ \lambda^l\,O_L^{(l)}\,\Big) * U^{-1} * \sum_{r}\Big(\,U_r\ \text{with}\ \lambda^r\,O_R^{(r)}\,\Big) \\ &\sim \sum_{l,r}\Big(\,U_l * U^{-1} * U_r\ \text{with}\ \lambda^l\,O_L^{(l)}\ \text{and}\ \lambda^r\,O_R^{(r)}\,\Big)\,. \end{aligned} \tag{3.3.29}$$

The equation $-\,Q_B A_L = A_L * U^{-1} * A_R$ thus follows if the relation

$$U_{l+r} \;=\; U_l * U^{-1} * U_r \tag{3.3.30}$$

with additional operator insertions of $O_L^{(l)}$ and $O_R^{(r)}$ holds for the singular case.

Motivated by this observation, we first show that the relation $U_{l+r} = U_l * U^{-1} * U_r$ holds for the singular case if the assumptions of replacement (III), factorization (IV), and locality (V) are satisfied. It is then straightforward to generalize the proof by taking into account the insertions of $O_L^{(l)}$ and $O_R^{(r)}$ and show the equation (3.3.24).

We now demonstrate how the equation (3.3.30) holds using a concrete example and then explain how the proof generalizes. Let us consider the equation $U_2 = U_1 * U^{-1} * U_1$ at $\mathcal{O}(\lambda^2)$. Since $U^{-1} = 1 - \lambda^2 U^{(2)} + \mathcal{O}(\lambda^3)$, it can be written as follows:

$$U_2^{(2)} = U_1^{(0)} * U_1^{(2)} + U_1^{(1)} * U_1^{(1)} + U_1^{(2)} * U_1^{(0)} - U_1^{(0)} * U^{(2)} * U_1^{(0)} \,. \tag{3.3.31}$$

All the terms are made of the wedge state W_4 with operator insertions. In the regular case, the equation was a consequence of the following relation of the operator insertions on $\mathcal{W}_4$:

$$(V(1,4))^2 = (V(2,4))^2 + 2\,V(1,2)\,V(3,4) + (V(1,3))^2 - (V(2,3))^2 \,. \tag{3.3.32}$$

In the singular case, we need to show

$$[\,(V(1,4))^2\,]_r = [\,(V(2,4))^2\,]_r + 2\,[\,V(1,2)\,]_r\,[\,V(3,4)\,]_r + [\,(V(1,3))^2\,]_r - [\,(V(2,3))^2\,]_r \,. \tag{3.3.33}$$

Note that we have implicitly used the locality assumption (V). The operators $[\,(V(2,4))^2\,]_r$ and $[\,(V(1,3))^2\,]_r$ on the right-hand side were originally defined on $\mathcal{W}_3$ and $[\,(V(2,3))^2\,]_r$ was defined on $\mathcal{W}_2$. They are now inserted on $\mathcal{W}_4$ in the same forms because of the assumption (V). We next use the factorization assumption (IV) of the following form:

$$[\,e^{\lambda_1 V(1,2)}\,e^{\lambda_2 V(3,4)}\,]_r = [\,e^{\lambda_1 V(1,2)}\,]_r\,[\,e^{\lambda_2 V(3,4)}\,]_r \,. \tag{3.3.34}$$

This relation at $\mathcal{O}(\lambda_1\,\lambda_2)$ is

$$[\,V(1,2)\,V(3,4)\,]_r = [\,V(1,2)\,]_r\,[\,V(3,4)\,]_r \,. \tag{3.3.35}$$

Thus the right-hand side of (3.3.33) can be written as

$$\begin{aligned} &[\,(V(2,4))^2\,]_r + 2\,[\,V(1,2)\,]_r\,[\,V(3,4)\,]_r + [\,(V(1,3))^2\,]_r - [\,(V(2,3))^2\,]_r \\ &= [\,(V(2,4))^2\,]_r + 2\,[\,V(1,2)\,V(3,4)\,]_r + [\,(V(1,3))^2\,]_r - [\,(V(2,3))^2\,]_r \,. \end{aligned} \tag{3.3.36}$$

We then use the assumption (III) of replacement in the final step. It follows from the assumption (III) that

$$[\,e^{\lambda V(a,c)}\,]_r = [\,e^{\lambda V(a,b)}\,e^{\lambda V(b,c)}\,]_r \tag{3.3.37}$$

for $a < b < c$. At $\mathcal{O}(\lambda^2)$, we obtain the following formula:

$$[\,(V(a,c))^2\,]_r = [\,(V(a,b))^2\,]_r + 2\,[\,V(a,b)\,V(b,c)\,]_r + [\,(V(b,c))^2\,]_r \,. \tag{3.3.38}$$

We thus find

$$\begin{aligned} [\,(V(2,4))^2\,]_r &= [\,(\,V(2,3) + V(3,4)\,)^2\,]_r \\ &= [\,(V(2,3))^2\,]_r + 2\,[\,V(2,3)\,V(3,4)\,]_r + [\,(V(3,4))^2\,]_r \,, \\ [\,(V(1,3))^2\,]_r &= [\,(\,V(1,2) + V(2,3)\,)^2\,]_r \\ &= [\,(V(1,2))^2\,]_r + 2\,[\,V(1,2)\,V(2,3)\,]_r + [\,(V(2,3))^2\,]_r \,. \end{aligned} \tag{3.3.39}$$

For the operator $[\,(V(1,4))^2\,]_r$ on the left-hand side of (3.3.33), we use the formula (3.3.38) recursively and obtain

$$\begin{aligned}[\,(V(1,4))^2\,]_r &= [\,(\,V(1,2)+V(2,3)+V(3,4)\,)^2\,]_r \\ &= [\,(V(1,2))^2\,]_r + [\,(V(2,3))^2\,]_r + [\,(V(3,4))^2\,]_r \\ &\quad + 2\,[\,V(1,2)\,V(2,3)\,]_r + 2\,[\,V(2,3)\,V(3,4)\,]_r + 2\,[\,V(1,2)\,V(3,4)\,]_r\,.\end{aligned} \tag{3.3.40}$$

We can explicitly confirm that the equation (3.3.33) is satisfied. However, the coefficients in the basis

$$\begin{aligned}&\{\,[\,(V(1,2))^2\,]_r\,,\,[\,(V(2,3))^2\,]_r\,,\,[\,(V(3,4))^2\,]_r\,, \\ &\quad [\,V(1,2)\,V(2,3)\,]_r\,,\,[\,V(2,3)\,V(3,4)\,]_r\,,\,[\,V(1,2)\,V(3,4)\,]_r\,\}\end{aligned} \tag{3.3.41}$$

are guaranteed to match on both sides of (3.3.33) because they are the same as those in the regular case where the corresponding identity (3.3.32) has been shown.

This proof can be generalized to $U_{l+r} = U_l * U^{-1} * U_r$ at $\mathcal{O}(\lambda^n)$ for any positive integers l, r, and n. The state $U^{(n)}_{l+r}$ can be expressed in terms of $[\,V^{(n)}(1, l+r+n)\,]_r$ on $\mathcal{W}_{l+r+n}$. Because of the locality assumption (V), the terms of $U_l * U^{-1} * U_r$ at $\mathcal{O}(\lambda^n)$ can also be expressed in terms of products of the form

$$\prod_j [\,V^{(k_j)}(a_j, b_j)\,]_r \tag{3.3.42}$$

on $\mathcal{W}_{l+r+n}$, where positive integers k_j, a_j, and b_j satisfy $1 \le a_j < b_j \le l+r+n$, $b_j < a_{j+1}$ and $\sum_j k_j = n$. Using the factorization assumption (IV), the products can be written as

$$[\prod_j V^{(k_j)}(a_j, b_j)\,]_r \tag{3.3.43}$$

on $\mathcal{W}_{l+r+n}$. Finally, we use the replacement assumption (III) to expand both sides of the equation $U_{l+r} = U_l * U^{-1} * U_r$ in the basis

$$\Big\{[\prod_{i=1}^{l+r+n-1} V^{(\ell_i)}(i, i+1)\,]_r\Big\}, \tag{3.3.44}$$

where ℓ_i's are non-negative integers with $\sum_{i=1}^{l+r+n-1} \ell_i = n$. The coefficients in the basis are guaranteed to match on both sides of $U_{l+r} = U_l * U^{-1} * U_r$ because the equation holds in the regular case. This completes the proof of $U_{l+r} = U_l * U^{-1} * U_r$ in the singular case to all orders in λ.

The proof of $-Q_B A_L = A_L * U^{-1} * A_R$ is essentially parallel using the assumptions (III) and (IV) of replacement and factorization with additional insertions of O_L and O_R. For the details of the proof, we refer the reader to appendix A of [21]. We thus conclude that Ψ_L given by

$$\Psi_L = A_L * U^{-1} \tag{3.3.45}$$

solves the equation of motion for any exactly marginal deformations satisfying the assumptions (I)–(V).

3.3.4 Construction of a real solution

It is straightforward to construct a real solution Ψ from Ψ_L as we did in § 3.2.2 for marginal deformations with regular operator products. The state U satisfies $U^\ddagger = U$ under the assumption (VI) of reflection. It then follows from (3.2.30) that $(Q_B U)^\ddagger = -Q_B U$ and thus $(A_R - A_L)^\ddagger = A_L - A_R$. From this we conclude that the local operators O_L and O_R are mapped under the conjugation discussed in § 3.2.2 as follows:

$$O_L(t) \longrightarrow O_R(n+1-t), \quad O_R(t) \longrightarrow O_L(n+1-t) \quad \text{on} \quad \mathcal{W}_n . \tag{3.3.46}$$

We thus find

$$A_L^\ddagger = A_R , \qquad A_R^\ddagger = A_L . \tag{3.3.47}$$

In the case of marginal deformations with regular operator products, O_L and O_R are both λcV and are indeed mapped as (3.3.46).

We define Ψ_R by

$$\Psi_R \equiv U^{-1} * A_R . \tag{3.3.48}$$

As in the regular case, the state Ψ_R is the conjugate of Ψ_L:

$$\Psi_R = \Psi_L^\ddagger . \tag{3.3.49}$$

It satisfies the equation of motion and obeys the relation $Q_B U = U * \Psi_R - \Psi_L * U$. We conclude that Ψ given by

$$\begin{aligned} \Psi &= \frac{1}{\sqrt{U}} * \Psi_L * \sqrt{U} + \frac{1}{\sqrt{U}} * Q_B \sqrt{U} \\ &= \sqrt{U} * \Psi_R * \frac{1}{\sqrt{U}} + \sqrt{U} * Q_B \frac{1}{\sqrt{U}} \\ &= \frac{1}{2}\left[\frac{1}{\sqrt{U}} * \Psi_L * \sqrt{U} + \sqrt{U} * \Psi_R * \frac{1}{\sqrt{U}} + \frac{1}{\sqrt{U}} * Q_B \sqrt{U} - Q_B \sqrt{U} * \frac{1}{\sqrt{U}} \right] \end{aligned} \tag{3.3.50}$$

is real and satisfies the equation of motion. The solution Ψ can also be expressed in terms of A_L and A_R in the following way, which might be more convenient for an explicit expansion in λ:

$$\begin{aligned} \Psi &= \frac{1}{\sqrt{U}} * A_L * \frac{1}{\sqrt{U}} + \frac{1}{\sqrt{U}} * Q_B \sqrt{U} \\ &= \frac{1}{\sqrt{U}} * A_R * \frac{1}{\sqrt{U}} + \sqrt{U} * Q_B \frac{1}{\sqrt{U}} \\ &= \frac{1}{2}\left[\frac{1}{\sqrt{U}} * (A_L + A_R) * \frac{1}{\sqrt{U}} + \frac{1}{\sqrt{U}} * Q_B \sqrt{U} - Q_B \sqrt{U} * \frac{1}{\sqrt{U}} \right] . \end{aligned} \tag{3.3.51}$$

3.4 Explicit examples

We have separated the construction of solutions for marginal deformations in open string field theory into two steps. In the previous section, we have presented the general construction of solutions in

open string field theory from the operator $[e^{\lambda V(a,b)}]_r$. The second step is then to construct such properly renormalized operators satisfying the assumptions stated in the introduction for concrete examples of exactly marginal deformations. This is a problem in the BCFT and independent of string field theory. In this section, we present a class of marginal deformations with singular operator products for which the construction of $[e^{\lambda V(a,b)}]_r$ can be carried out explicitly. For the details of this construction, however, we refer the reader to section 4 of [21].

3.4.1 A class of marginal deformations with singular operator products

The dependence of the two-point function $\langle V(t_1)\,V(t_2)\rangle$ on t_1 and t_2 for a dimension-one primary field V is completely fixed by conformal symmetry. When the singular part of the operator product expansion (OPE) of V with itself is given by

$$V(t)\,V(0) \sim \frac{1}{t^2}\,, \tag{3.4.1}$$

the operator product $V(t_1)\,V(t_2)$ can be made finite in the limit $t_1 \to t_2$ by subtracting $\langle V(t_1)\,V(t_2)\rangle$ from it.[1] We define $\mathop{{}^{\circ}_{\circ}} V(t_1)\,V(t_2) \mathop{{}^{\circ}_{\circ}}$ for $t_1 \neq t_2$ by

$$\mathop{{}^{\circ}_{\circ}} V(t_1)\,V(t_2) \mathop{{}^{\circ}_{\circ}} \equiv V(t_1)\,V(t_2) - G(t_1,t_2)\,, \tag{3.4.2}$$

where

$$G(t_1,t_2) \equiv \langle V(t_1)\,V(t_2)\rangle\,. \tag{3.4.3}$$

Note that the correlation function $\langle V(t_1)\,V(t_2)\rangle$ depends on the Riemann surface where the BCFT is defined, and thus the definition of $\mathop{{}^{\circ}_{\circ}} V(t_1)\,V(t_2) \mathop{{}^{\circ}_{\circ}}$ also depends on the Riemann surface.

The OPE of V with itself, however, can have other singular terms. For example, the singular part of the OPE can be

$$V(t)\,V(0) \sim \frac{1}{t^2} + \frac{1}{t}\,\widetilde{V}(0) \tag{3.4.4}$$

with some dimension-one primary field $\widetilde{V}$, which can be proportional to V itself. The operator $\mathop{{}^{\circ}_{\circ}} V(t_1)\,V(t_2) \mathop{{}^{\circ}_{\circ}}$ is not finite if the single-pole term with $\widetilde{V}$ is nonvanishing.

The operator $\mathop{{}^{\circ}_{\circ}} V(t_1)\,V(t_2) \mathop{{}^{\circ}_{\circ}}$ coincides with the ordinary normal-ordered product $:V(t_1)\,V(t_2):$ and is thus manifestly finite for $V(t) = i\,\partial_t X^\mu(t)/\sqrt{2\alpha'}$, where X^μ is a space-like coordinate along the D-brane. However, it is in general different from $:V(t_1)\,V(t_2):$ when V is a composite operator. For example, when $V(t)$ is given by

$$V(t) = \sqrt{2}:\cos\!\left(\frac{X^\mu(t)}{\sqrt{\alpha'}}\right):, \tag{3.4.5}$$

we can write $\mathop{{}^{\circ}_{\circ}} V(t_1)\,V(t_2) \mathop{{}^{\circ}_{\circ}}$ as

$$\mathop{{}^{\circ}_{\circ}} V(t_1)\,V(t_2) \mathop{{}^{\circ}_{\circ}} = G(t_1,t_2)^{-1}:\cos\!\left(\frac{X^\mu(t_1)+X^\mu(t_2)}{\sqrt{\alpha'}}\right):+G(t_1,t_2)\left[:\cos\!\left(\frac{X^\mu(t_1)-X^\mu(t_2)}{\sqrt{\alpha'}}\right):-1\right], \tag{3.4.6}$$

[1] When the double-pole term $1/t^2$ in the OPE $V(t)\,V(0)$ is nonvanishing, we normalize $V(t)$ such that the coefficient of the double-pole term is unity. If the state $\Psi^{(1)}$ using V with this normalization is odd instead of even under the conjugation discussed in § 3.2.2, we set $\lambda = i\,\tilde{\lambda}$ and take $\tilde{\lambda}$ to be real when constructing the real solution Ψ in § 3.3.4.

which is not the same as the normal-ordered product:

$$\overset{\circ}{\circ} V(t_1)\, V(t_2) \overset{\circ}{\circ} \neq :V(t_1)\, V(t_2): = 2 : \cos\left(\frac{X^\mu(t_1)}{\sqrt{\alpha'}}\right) \cos\left(\frac{X^\mu(t_2)}{\sqrt{\alpha'}}\right) : . \tag{3.4.7}$$

We recursively define $\overset{\circ}{\circ} V(t_1)\, V(t_2) \ldots V(t_n) \overset{\circ}{\circ}$ for arbitrary n with $t_i \neq t_j$ as follows:

$$\begin{aligned} \overset{\circ}{\circ} V(t_1) \overset{\circ}{\circ} &\equiv V(t_1)\,, \\ \overset{\circ}{\circ} V(t_1)\, V(t_2) \ldots V(t_n) \overset{\circ}{\circ} &\equiv \overset{\circ}{\circ} V(t_1)\, V(t_2) \ldots V(t_{n-1}) \overset{\circ}{\circ}\, V(t_n) \\ &\quad - \sum_{i=1}^{n-1} G(t_i, t_n) \overset{\circ}{\circ} V(t_1)\, V(t_2) \ldots V(t_{i-1})\, V(t_{i+1}) \ldots V(t_{n-1}) \overset{\circ}{\circ} \end{aligned} \tag{3.4.8}$$

for $n > 1$ and $t_i \neq t_j$. This can be formally written in the following form:

$$\overset{\circ}{\circ} \prod_i V(t_i) \overset{\circ}{\circ} = \exp\left(-\frac{1}{2} \int dt_1 dt_2\, G(t_1, t_2) \frac{\delta}{\delta V(t_1)} \frac{\delta}{\delta V(t_2)}\right) \prod_i V(t_i) \quad \text{for} \quad t_i \neq t_j\,. \tag{3.4.9}$$

For $V(t) = i\,\partial_t X^\mu(t)/\sqrt{2\alpha'}$, the operator product $\overset{\circ}{\circ} V(t_1)\, V(t_2) \ldots V(t_n) \overset{\circ}{\circ}$ again coincides with $:V(t_1)\, V(t_2) \ldots V(t_n):$ and is regular. In general, however, $\overset{\circ}{\circ} V(t_1)\, V(t_2) \ldots V(t_n) \overset{\circ}{\circ}$ with $n \geq 3$ can be singular, even if it is finite in the limit $t_i \to t_j$ for any pair of i and j, when more than two operators simultaneously collide. In this section, we consider a class of marginal operators V which satisfy the following *finiteness condition.*

The finiteness condition. *The limit*

$$\lim_{t \to t'} \overset{\circ}{\circ} V(t)\, V(t')^n \overset{\circ}{\circ} \tag{3.4.10}$$

is finite for any positive integer n.

For this class of marginal operators, operators $[\, e^{\lambda V(a,b)}\,]_r$ satisfying the assumptions stated in the introduction were explicitly constructed in section 4 of [21]. .

3.4.2 Examples

Let us give some examples of such marginal deformations for D-branes in flat spacetime with Neumann or Dirichlet boundary conditions. As we have already mentioned, the finiteness condition (3.4.10) is satisfied for

$$V(t) = \frac{i}{\sqrt{2\alpha'}}\, \partial_t X^\mu(t)\,, \tag{3.4.11}$$

where X^μ is a space-like direction along the D-brane. The direction X^μ can be noncompact or can be compactified on a circle with any radius. Similarly, the operator

$$V(t) = \frac{1}{\sqrt{2\alpha'}}\, \partial_t X^0(t) \tag{3.4.12}$$

for the time-like direction also satisfies the finiteness condition.[2] Both of these deformations correspond to turning on a constant mode of the gauge field on the D-brane.

The finiteness condition is also satisfied for

$$V(t) = \frac{1}{\sqrt{2\alpha'}} \partial_\perp X^\alpha(t) , \tag{3.4.13}$$

where X^α is a direction transverse to the D-brane and $\partial_\perp$ is the derivative normal to the boundary. The direction X^α can be noncompact or can be compactified on a circle with any radius. This deformation corresponds to displacement of the position of the D-brane in the direction X^α. The condition (3.4.10) is satisfied because the operator $\overset{\circ}{\circ} V(t_1) V(t_2) \dots V(t_n) \overset{\circ}{\circ}$ again coincides with $: V(t_1) V(t_2) \dots V(t_n) :$ and is regular.

A more nontrivial example of V satisfying (3.4.10) is

$$V(t) = \sqrt{2} : \cos\left(\frac{X^\mu(t)}{\sqrt{\alpha'}} \right) : , \tag{3.4.14}$$

where X^μ is again a space-like direction along the D-brane. The direction X^μ can be noncompact or can be compactified on a circle whose radius is a multiple of the self-dual radius to be consistent with the periodicity of the cosine potential. This deformation is known to be exactly marginal [60–63] and interpolates Neumann and Dirichlet boundary conditions. If we start from a D25-brane and deform the background by this operator, we obtain a periodic array of D24-branes at some value of the deformation parameter. When we compactify the X^μ direction on a circle with the self-dual radius, the free boson for the X^μ direction can be described by a different free boson Y^μ because of the $SU(2) \times SU(2)$ symmetry, and the marginal operator $V(t)$ can be written in terms of Y^μ as follows:

$$V(t) = \sqrt{2} : \cos\left(\frac{X^\mu(t)}{\sqrt{\alpha'}} \right) : \; = \frac{i}{\sqrt{2\alpha'}} \partial_t Y^\mu(t) . \tag{3.4.15}$$

See, for example, § 3.1 of [58]. Finiteness of $\overset{\circ}{\circ} V(t_1) V(t_2) \dots V(t_n) \overset{\circ}{\circ}$ at the self-dual radius is then a consequence of Wick's theorem in the description in terms of Y^μ. On the other hand, the finiteness is highly nontrivial in the original description in terms of X^μ. The operator algebra of boundary operators necessary for the calculation of $\overset{\circ}{\circ} V(t_1) V(t_2) \dots V(t_n) \overset{\circ}{\circ}$, however, does not depend on the compactification radius. Thus $\overset{\circ}{\circ} V(t_1) V(t_2) \dots V(t_n) \overset{\circ}{\circ}$ is finite for any radius which is a multiple of the self-dual radius and for the noncompact case as well.

The operator algebra of boundary operators necessary for the calculation of the operator product $\overset{\circ}{\circ} V(t_1) V(t_2) \dots V(t_n) \overset{\circ}{\circ}$ is the same if we replace X^μ by iX^0. Therefore, the marginal operator

$$V(t) = \sqrt{2} : \cosh\left(\frac{X^0(t)}{\sqrt{\alpha'}} \right) : \tag{3.4.16}$$

also satisfies the finiteness condition. This deformation has been discussed in detail in the context of the rolling tachyon [50].

[2] We have to set $\lambda = i\tilde{\lambda}$ and take $\tilde{\lambda}$ to be real for this operator when constructing the real solution Ψ.

All the operators mentioned in this subsection are known to be exactly marginal. In section 4 of [21], solutions were constructed in terms of $\mathop{\circ}_{\circ} V(t_1)\, V(t_2) \ldots V(t_n) \mathop{\circ}_{\circ}$, and the construction depends on the explicit form of V only through these operator products. Thus all the marginal deformations discussed in this subsection are covered by this construction.

3.5 String field theory around the deformed background

3.5.1 Action

Now that we have constructed solutions for general marginal deformations, let us expand the string field theory action around the solutions. The string field theory action is given by

$$S[\Psi] = -\frac{1}{g^2}\left[\frac{1}{2}\langle \Psi\,,\, Q_B\Psi\rangle + \frac{1}{3}\langle \Psi\,,\, \Psi * \Psi\rangle\right], \tag{3.5.1}$$

where g is the open string coupling constant. In the case of a D25-brane in flat spacetime, g is related to the D25-brane tension T_{25} as $T_{25} = 1/(2\pi^2 g^2)$. We shift the string field Ψ as

$$\Psi = \Psi_\lambda + \delta\Psi\,, \tag{3.5.2}$$

where the solution Ψ_λ is the real solution derived in § 3.3.4,

$$\begin{aligned}\Psi_\lambda &= \frac{1}{2}\left[\frac{1}{\sqrt{U}} * \Psi_L * \sqrt{U} + \sqrt{U} * \Psi_R * \frac{1}{\sqrt{U}} + \frac{1}{\sqrt{U}} * Q_B\sqrt{U} - Q_B\sqrt{U} * \frac{1}{\sqrt{U}}\right] \\ &= \frac{1}{2}\left[\frac{1}{\sqrt{U}} * (A_L + A_R) * \frac{1}{\sqrt{U}} + \frac{1}{\sqrt{U}} * Q_B\sqrt{U} - Q_B\sqrt{U} * \frac{1}{\sqrt{U}}\right].\end{aligned} \tag{3.5.3}$$

We then expand the action and obtain

$$\begin{aligned}S[\Psi] &= S[\Psi_\lambda] + S[\delta\Psi] - \frac{1}{g^2}\langle \delta\Psi\,,\, \Psi_\lambda * \delta\Psi\rangle \\ &= S[\Psi_\lambda] + S[\delta\Psi] - \frac{1}{2g^2}\Big[\langle \delta\Psi\,,\, \frac{1}{\sqrt{U}} * (A_L + A_R) * \frac{1}{\sqrt{U}} * \delta\Psi\rangle \\ &\qquad + \langle \delta\Psi\,,\, \frac{1}{\sqrt{U}} * Q_B\sqrt{U} * \delta\Psi\rangle - \langle \delta\Psi\,,\, Q_B\sqrt{U} * \frac{1}{\sqrt{U}} * \delta\Psi\rangle\Big].\end{aligned} \tag{3.5.4}$$

The term linear in $\delta\Psi$ vanishes because Ψ_λ satisfies the equation of motion. The term $S[\Psi_\lambda]$ only shifts the action by an overall constant. In fact, it should vanish for solutions corresponding to exactly marginal deformations. The structure of the action suggests the following field redefinition:

$$\Phi \equiv \sqrt{U} * \delta\Psi * \sqrt{U} \qquad \Longrightarrow \qquad \delta\Psi = \frac{1}{\sqrt{U}} * \Phi * \frac{1}{\sqrt{U}}\,. \tag{3.5.5}$$

The term $S[\delta\Psi]$ can be expressed in terms of the new variable Φ as follows:

$$\begin{aligned}
S[\delta\Psi] &= S\left[\frac{1}{\sqrt{U}} * \Phi * \frac{1}{\sqrt{U}}\right] \\
&= -\frac{1}{2g^2}\left\langle \frac{1}{\sqrt{U}} * \Phi * \frac{1}{\sqrt{U}}, Q_B \cdot \left[\frac{1}{\sqrt{U}} * \Phi * \frac{1}{\sqrt{U}}\right]\right\rangle - \frac{1}{3g^2}\left\langle \Phi, U^{-1} * \Phi * U^{-1} * \Phi * U^{-1}\right\rangle \\
&= -\frac{1}{2g^2}\left\langle \Phi, U^{-1} * Q_B\Phi * U^{-1}\right\rangle - \frac{1}{3g^2}\left\langle \Phi, U^{-1} * \Phi * U^{-1} * \Phi * U^{-1}\right\rangle \\
&\quad -\frac{1}{2g^2}\left\langle \frac{1}{\sqrt{U}} * \Phi * \frac{1}{\sqrt{U}}, Q_B\frac{1}{\sqrt{U}} * \Phi * \frac{1}{\sqrt{U}}\right\rangle + \frac{1}{2g^2}\left\langle \frac{1}{\sqrt{U}} * \Phi * \frac{1}{\sqrt{U}}, \frac{1}{\sqrt{U}} * \Phi * Q_B\frac{1}{\sqrt{U}}\right\rangle .
\end{aligned} \tag{3.5.6}$$

Using the identity

$$Q_B\frac{1}{\sqrt{U}} = -\frac{1}{\sqrt{U}} * Q_B\sqrt{U} * \frac{1}{\sqrt{U}}, \tag{3.5.7}$$

it is easy to see that the last line of (3.5.6) precisely cancels the last two terms on the right-hand side of (3.5.4). The action around the deformed background in terms of Φ is thus given by

$$\begin{aligned}
S[\Psi] = S[\Psi_\lambda] &- \frac{1}{2g^2}\left[\left\langle \Phi, U^{-1} * Q_B\Phi * U^{-1}\right\rangle + \left\langle \Phi, U^{-1} * (A_L + A_R) * U^{-1} * \Phi * U^{-1}\right\rangle\right] \\
&- \frac{1}{3g^2}\left\langle \Phi, U^{-1} * \Phi * U^{-1} * \Phi * U^{-1}\right\rangle .
\end{aligned} \tag{3.5.8}$$

Note that $\sqrt{U}$ and $1/\sqrt{U}$ completely disappeared and the action is written in terms of U^{-1}, A_L, and A_R.

Let us now introduce the following deformed algebraic structures:

$$\begin{aligned}
A \star B &\equiv A * U^{-1} * B , \\
\mathcal{Q}A &\equiv Q_B A + A_L \star A - (-1)^A A \star A_R = Q_B A + \Psi_L * A - (-1)^A A * \Psi_R , \\
\langle\langle A, B\rangle\rangle &\equiv \langle A, U^{-1} * B * U^{-1}\rangle .
\end{aligned} \tag{3.5.9}$$

As $U = 1 + \mathcal{O}(\lambda^2)$. $A_L = \mathcal{O}(\lambda)$. and $A_R = \mathcal{O}(\lambda)$, these structures reduce to the original star product $*$, BRST operator Q_B, and inner product $\langle\ ,\ \rangle$ when $\lambda \to 0$. The shifted action $\mathcal{S}[\Phi] \equiv S[\Psi] - S[\Psi_\lambda]$ in terms of the new variable Φ can be written as follows:

$$\mathcal{S}[\Phi] = -\frac{1}{g^2}\left[\frac{1}{2}\langle\langle \Phi, \mathcal{Q}\Phi\rangle\rangle + \frac{1}{3}\langle\langle \Phi, \Phi \star \Phi\rangle\rangle\right], \tag{3.5.10}$$

where we have used

$$\begin{aligned}
&\langle \Phi, U^{-1} * (A_L + A_R) * U^{-1} * \Phi * U^{-1}\rangle \\
&= \langle \Phi, U^{-1} * A_L * U^{-1} * \Phi * U^{-1}\rangle + \langle \Phi, U^{-1} * \Phi * U^{-1} * A_R * U^{-1}\rangle .
\end{aligned} \tag{3.5.11}$$

Thus string field theory around the deformed background can be described by the star product $\star$, the operator $\mathcal{Q}$, and the inner product $\langle\langle\ ,\ \rangle\rangle$.

3.5.2 Properties of algebraic structures around the deformed background

Let us verify that the new algebraic structures obey the following relations necessary for a consistent formulation of string field theory:

$$\begin{aligned}
\mathcal{Q}^2 A &= 0\,, && (3.5.12)\\
\mathcal{Q}(A\star B) &= (\mathcal{Q}A)\star B + (-1)^A A\star(\mathcal{Q}B)\,, && (3.5.13)\\
\langle\!\langle A, B\rangle\!\rangle &= (-1)^{AB}\langle\!\langle B, A\rangle\!\rangle\,, && (3.5.14)\\
\langle\!\langle \mathcal{Q}A, B\rangle\!\rangle &= -(-1)^A\langle\!\langle A, \mathcal{Q}B\rangle\!\rangle\,, && (3.5.15)\\
\langle\!\langle A, B\star C\rangle\!\rangle &= \langle\!\langle A\star B, C\rangle\!\rangle\,. && (3.5.16)
\end{aligned}$$

Furthermore, we show that the generalized wedge states U_α satisfy

$$\mathcal{Q}U_\alpha = 0\,. \tag{3.5.17}$$

Let us begin with (3.5.12). It follows from the definition of $\mathcal{Q}$ that

$$\begin{aligned}
\mathcal{Q}^2 A &= \mathcal{Q}\left[Q_B A + \Psi_L * A - (-1)^A A * \Psi_R\right]\\
&= Q_B^2 A + Q_B\Psi_L * A - \Psi_L * Q_B A - (-1)^A Q_B A * \Psi_R - A * Q_B\Psi_R\\
&\quad + \Psi_L * \left(Q_B A + \Psi_L * A - (-1)^A A * \Psi_R\right) + (-1)^A\left(Q_B A + \Psi_L * A - (-1)^A A * \Psi_R\right) * \Psi_R\,.
\end{aligned} \tag{3.5.18}$$

Using $Q_B^2 = 0$ and the equation of motion for Ψ_L and Ψ_R, all the terms cancel and we find $\mathcal{Q}^2 A = 0$.

Similarly, we can prove (3.5.13) as follows:

$$\begin{aligned}
\mathcal{Q}_B(A\star B) &= Q_B A * U^{-1} * B + (-1)^A A * Q_B U^{-1} * B + (-1)^A A * U^{-1} * Q_B B\\
&\quad + \Psi_L * A * U^{-1} * B - (-1)^A(-1)^B A * U^{-1} * B * \Psi_R\\
&= \mathcal{Q}A\star B + (-1)^A A\star\mathcal{Q}B\\
&\quad + (-1)^A A * Q_B U^{-1} * B + (-1)^A A * \Psi_R * U^{-1} * B - (-1)^A A * U^{-1} * \Psi_L * B\,.
\end{aligned} \tag{3.5.19}$$

The terms in the last line cancel because of the identity

$$Q_B U^{-1} = -U^{-1} * Q_B U * U^{-1} = U^{-1} * (A_L - A_R) * U^{-1} = U^{-1} * \Psi_L - \Psi_R * U^{-1}\,. \tag{3.5.20}$$

This completes the proof of (3.5.13).

It is easy to verify (3.5.14) using the properties of the inner product $\langle\ ,\ \rangle$:

$$\begin{aligned}
\langle\!\langle A, B\rangle\!\rangle &= \langle A, U^{-1} * B * U^{-1}\rangle\\
&= \langle A * U^{-1}, B * U^{-1}\rangle\\
&= (-1)^{AB}\langle B * U^{-1}, A * U^{-1}\rangle\\
&= (-1)^{AB}\langle B, U^{-1} * A * U^{-1}\rangle\\
&= (-1)^{AB}\langle\!\langle B, A\rangle\!\rangle\,.
\end{aligned} \tag{3.5.21}$$

To show (3.5.15), we use the corresponding identity of Q_B and the properties of $\langle\ ,\ \rangle$. We find

$$\begin{aligned}\langle\langle\, \mathcal{Q}A, B\,\rangle\rangle &= \langle\, Q_B A + \Psi_L * A - (-1)^A\, A * \Psi_R\,,\, U^{-1} * B * U^{-1}\,\rangle \\ &= -(-1)^A \langle\, A\,,\, Q_B U^{-1} * B * U^{-1} + U^{-1} * Q_B B * U^{-1} + (-1)^B U^{-1} * B * Q_B U^{-1}\,\rangle \\ &\quad + (-1)^A (-1)^B \langle\, A\,,\, U^{-1} * B * U^{-1} * \Psi_L\,\rangle - (-1)^A \langle\, A\,,\, \Psi_R * U^{-1} * B * U^{-1}\,\rangle\,.\end{aligned} \tag{3.5.22}$$

Using the identity (3.5.20), we obtain

$$\begin{aligned}\langle\langle\, \mathcal{Q}A, B\,\rangle\rangle &= -(-1)^A \langle\, A\,,\, U^{-1} * \big(\, Q_B B + \Psi_L * B - (-1)^B\, B * \Psi_R\,\big) * U^{-1}\,\rangle \\ &= -(-1)^A \langle\langle\, A, \mathcal{Q}B\,\rangle\rangle\,.\end{aligned} \tag{3.5.23}$$

Finally, the relation (3.5.16) follows from the definitions of the deformed structures and the property of the inner product $\langle\ ,\ \rangle$:

$$\begin{aligned}\langle\langle\, A, B\star C\,\rangle\rangle &= \langle\, A\,,\, U^{-1} * B * U^{-1} * C * U^{-1}\,\rangle \\ &= \langle\, A * U^{-1} * B\,,\, U^{-1} * C * U^{-1}\,\rangle = \langle\langle\, A\star B, C\,\rangle\rangle\,.\end{aligned} \tag{3.5.24}$$

We have thus shown that the deformed algebraic structures satisfy all the algebraic relations required for a consistent formulation of string field theory.

Let us now show the equation (3.5.17), namely, that the generalized wedge states U_α are annihilated by $\mathcal{Q}$. We define the generalizations $A_{L,\alpha}$ and $A_{R,\alpha}$ of A_L and A_R, respectively, by

$$A_{L,\alpha} \equiv \sum_{n=1}^{\infty} \lambda^n\, A_{L,\alpha}^{(n)}\,, \qquad A_{R,\alpha} \equiv \sum_{n=1}^{\infty} \lambda^n\, A_{R,\alpha}^{(n)} \tag{3.5.25}$$

for $\alpha \geq 0$, where

$$\begin{aligned}\langle\, \phi\,,\, A_{L,\alpha}^{(n)}\,\rangle &= \sum_{l=1}^{n} \langle\, f\circ\phi(0)\,[\, O_L^{(l)}(1)\, V^{(n-l)}(1, n+\alpha)\,]_r\,\rangle_{\mathcal{W}_{n+\alpha}}\,, \\ \langle\, \phi\,,\, A_{R,\alpha}^{(n)}\,\rangle &= \sum_{r=1}^{n} \langle\, f\circ\phi(0)\,[\, V^{(n-r)}(1, n+\alpha)\, O_R^{(r)}(n+\alpha)\,]_r\,\rangle_{\mathcal{W}_{n+\alpha}}\,.\end{aligned} \tag{3.5.26}$$

Note that $A_L = A_{L,0}$ and $A_R = A_{R,0}$. The states $A_{L,\alpha}$ and $A_{R,\alpha}$ satisfy the following relations:

$$Q_B U_\alpha = A_{R,\alpha} - A_{L,\alpha}\,, \qquad A_{L,\alpha+\beta} = A_{L,\alpha} * U^{-1} * U_\beta\,, \qquad A_{R,\alpha+\beta} = U_\alpha * U^{-1} * A_{R,\beta}\,, \tag{3.5.27}$$

which are generalizations of $Q_B U = A_R - A_L$ and $U_{\alpha+\beta} = U_\alpha * U^{-1} * U_\beta$. The first relation in (3.5.27) immediately follows from the assumption (I). The second and third relations can be shown using the assumptions (III)–(V) as in the proofs of $U_{\alpha+\beta} = U_\alpha * U^{-1} * U_\beta$ and $-Q_B A_L = A_L * U^{-1} * A_R$ in § 3.3.3. Using these relations, it is easy to show that $\mathcal{Q}U_\alpha$ vanishes:

$$\begin{aligned}\mathcal{Q}U_\alpha &= A_{R,\alpha} - A_{L,\alpha} + \Psi_L * U_\alpha - U_\alpha * \Psi_R \\ &= U_\alpha * U^{-1} * A_R - A_L * U^{-1} * U_\alpha + A_L * U^{-1} * U_\alpha - U_\alpha * U^{-1} * A_R \\ &= 0\,.\end{aligned} \tag{3.5.28}$$

The state U_1 is expected to play the role of the $SL(2,R)$-invariant vacuum in the deformed theory, and $U = U_0$ is the identity state of the deformed star algebra. In fact,

$$U\star A = U * U^{-1} * A = A\,, \qquad A\star U = A * U^{-1} * U = A\,. \tag{3.5.29}$$

3.6 Discussion

The main result of this chapter was the construction of analytic solutions of open bosonic string field theory for general marginal deformations. We presented a procedure to construct a solution from the operator $[\, e^{\lambda V(a,b)} \,]_r$ satisfying the set of assumptions stated in the introduction. We believe that all of these assumptions are satisfied for any exactly marginal deformation and are thus necessary conditions for exact marginality of the deformation. We also believe that the set of assumptions provides a sufficient condition for marginality to all orders in λ because we have succeeded in constructing solutions of string field theory. This new characterization of exact marginality is another important result of this chapter, and we hope that our approach motivated by string field theory will provide new perspectives on the study of marginal deformations.

We believe that the finiteness condition (3.4.10) is a sufficient condition for marginality to all orders in λ. We can actually relax the condition because one actually only needs the finiteness of the operator $\circ(V(a,b))^n \circ$. Therefore, we can construct solutions even if the finiteness condition (3.4.10) is violated as long as the operator $\circ(V(a,b))^n \circ$ is well defined for any n.[3] It would be an interesting open problem whether the condition can be further relaxed. In particular, it is an interesting question whether the operators $O_L^{(n)}$ and $O_R^{(n)}$ with $n \geq 3$ can be nonvanishing by nontrivial collisions of more than two operators. In [62], Recknagel and Schomerus gave a sufficient condition for exact marginality which they called *self-locality* of the marginal operator. See § 2.4 of [62]. It would be also interesting to investigate the relation between their characterization of exact marginality in boundary conformal field theory and ours.

In [16], Fuchs, Kroyter and Potting constructed non-real solutions for the marginal deformation corresponding to turning on the constant mode of the gauge field. The relation between their solutions and the one presented here is discussed in appendix C of [21]. There, it was shown show that the solutions Ψ_L and Ψ_R for this particular marginal deformation coincide with [16].

The results of this chapter suggest a number of directions for future work. It would be interesting to study the solution corresponding to the deformation by the cosine potential in detail. The deformation at the value of λ describing lower-dimensional D-branes is particularly interesting. In the level-truncation analysis of marginal deformations, it has been demonstrated that the Siegel gauge condition is not globally well defined [64] and the branch of the marginal deformation corresponding to turning on the constant mode of the gauge field truncates at a finite value of the deformation parameter [47].[4] It is therefore important to study the convergence property of the expansion in λ for our solutions.

We expect that our work will play a role in further investigating background independence in string field theory by extending previous work [67–71]. The generalization of our construction to open superstring field theory formulated by Berkovits [72] is fairly straight-forward, and was explicitly carried out in [23]. Another important generalization is the construction of solutions

[3] We thank Ashoke Sen for discussions on this point and for explaining explicit examples.

[4] See [65, 66] for recent related studies.

corresponding to boundary conditions which are not connected by exactly marginal deformations. For example, consider the case where the original CFT flows to a different CFT by a marginally relevant deformation. We then expect that the operator $[\, e^{\lambda V(a,b)} \,]_r$ satisfying the assumptions (I) and (II) can be constructed at a special value of λ and our framework will be useful in constructing solutions for such marginally relevant deformations.

Chapter 4

Riemann surfaces in Schnabl gauge

4.1 Introduction

The sliver frame has played a central role in the construction and analysis of classical solutions in the previous chapters, but, as any projector frame, it is singular at the open string midpoint. Schnabl's tachyon vacuum solution and the solution in chapter 2, which represented regular marginal deformations, both satisfy the Schnabl gauge condition $B\Psi = 0$. Unlike in Siegel gauge [73], Ψ is not annihilated by the zero mode b_0 of the antighost field in the canonical open string frame. Rather, Ψ is annihilated by the zero mode B of the antighost field in the conformal frame of the sliver projector of the star algebra of open string fields.

One can wonder if the Schnabl gauge condition $B\Psi = 0$ defines a consistent open string perturbation theory. In this question, the singular behavior of the open string midpoint has brought interesting advantages but has also introduced some new subtleties.

At tree level, the sliver frame makes all conformal maps from the string diagrams to the upper-half plane very simple [45, 74]. This is remarkable, if we recall that in Siegel gauge these maps are extremely complicated and no closed form expressions are known except for four-string amplitudes [75]. The subtleties arise because there are delicate contributions whose origin can be traced to the singular behavior at the open string midpoint [45]. These contributions affect the off-shell part of four-string amplitudes and could affect higher-point functions on-shell. No Feynman rules are known that deal with these complications in general tree-level amplitudes.

This state of affairs prompted [46] to introduce a class of *regular linear b-gauges* that produce correct on-shell amplitudes. In this class, a propagator insertion with Schwinger parameter approaching infinity induces an open string degeneration of the Riemann surface associated with the string diagram– the desired behavior. Schnabl gauge does not belong to the class of regular b-gauges, but there is a simple one-parameter family of regular linear b-gauges that interpolates between Siegel and Schnabl gauge as its parameter λ goes from infinity to zero. This suggests that Schnabl gauge amplitudes can be obtained by taking the limit $\lambda \to 0$ of the well-behaved amplitudes in this λ-family.

While it is not yet proven that moduli space is covered for general tree amplitudes in Schnabl gauge, it is no mystery how the relevant Riemann surfaces – disks with boundary punctures – carry the moduli and how degenerations can be generated. Naive arguments, however, suggest that Schnabl gauge at loop level only produces surfaces with degenerate closed string moduli, thus making it impossible to reproduce the correct on-shell amplitudes. In a one-loop amplitude, for example, the line traced by the open string midpoint is a nontrivial closed curve. In the Schnabl propagator the open string midpoint does not move, thus naively suggesting a diagram with a zero-length closed curve that signals closed string degeneration.

It is the main purpose of this chapter to discuss the one-loop string diagrams in Schnabl gauge, following the analysis in [33]. Our results are quite encouraging. We find that the anticipated problems with closed string moduli are not present. Our main tool is the regulation provided by the λ-family of regular linear b-gauges that yield Schnabl gauge in the limit. Not only are closed string moduli produced but they are easily calculated, something that does not happen in Siegel gauge. Our work focuses only on the moduli problem; we do not attempt to fully compute any loop-amplitude. Such a computation, of course, would be quite interesting.

The analysis shows that closed string moduli arise because vertical lines in the sliver frame that are identified horizontally in tree diagrams, require slanted identifications in the case of loops. We recall that wedge surfaces [44, 49] are semi-infinite strips of fixed width whose vertical edges carry identical parameterizations. We are led to introduce *slanted* wedges, semi-infinite strips of fixed width whose vertical edges have parameterizations related by a scale factor. These slanted wedges are new, interesting objects in their own right. One can glue them and they are a natural ingredient in the construction of loop-diagrams. As opposed to the familiar wedges, however, there are no states associated to them. With the help of slanted wedges we develop a formalism that allows us to calculate the moduli (both open and closed) of arbitrary tree and one-loop amplitudes. Our analysis also shows that the BPZ-even gauge condition $B^+\Phi = (B + B^\star)\Phi = 0$ fails to generate the closed string modulus in one-loop diagrams because in this gauge the identifications in the sliver frame are not slanted. Unlike Schnabl gauge, the gauge $B^+\Phi = 0$ appears to be genuinely inadequate for loop calculations.

This chapter is organized as follows. In section 4.2, we will begin our analysis with the one-loop vacuum graph in general regular linear b-gauges, focusing on the Riemann surfaces generated by varying one of the two Schwinger parameters of the propagator. We see that the modulus of the annulus is an exactly calculable function of the Schwinger parameter and is, in fact, independent of the gauge choice. We then study the vacuum graph in Schnabl gauge as a limit in the family of regular interpolating gauges. The role of slanted identifications in Schnabl gauge first becomes apparent and the error in the presumption that diagrams are closed string degenerate is identified.

The situation becomes more nontrivial and challenging for the one-loop tadpole, i.e. the one-loop one-point function. We study this diagram in section 4.3 for the family of interpolating gauges parameterized by λ. The diagram only has a closed string modulus; the position of the open string

puncture can be adjusted using rotations. For any fixed λ, we can use extremal length methods to show that the full moduli space of annuli is produced as the Schwinger parameter is varied over its allowed range. In Siegel gauge the modulus of the annulus is a complicated function of the Schwinger parameter (defined implicitly by certain elliptic integrals, see, for example [76]). In the limit that we reach Schnabl gauge the modulus becomes a simple function of the Schwinger parameter. In this example one can glean the main geometrical insight that shows how the two components of the annulus, each one with its own open string boundary, are glued across a *hidden boundary* at infinity! The existence of such a hidden boundary leads us to conclude that the operator L (the Virasoro zero mode in the sliver frame) has an anomalous left/right decomposition, i.e. $[L_L, L_R] \neq 0$.

In section 4.4, we will introduce slanted wedges and show how to glue them together, as suggested by star multiplication, to produce a closed algebra. We discuss how the operators L_L and L_R and their BPZ conjugates act on slanted wedges and derive the action of the full Schnabl propagator. This formalism simplifies tremendously the construction of string diagrams, as we discuss for the case of trees in section 4.5. The moduli for tree diagrams are the positions of open string punctures and these can be calculated efficiently, as is demonstrated for the case of the 5-point diagram. We present the generalization to arbitrary tree diagrams, which is surprisingly straightforward using the algebra of slanted wedges.

In section 4.6 we discuss the Riemann surfaces for general one-loop string diagrams in Schnabl gauge. We show how to construct such a surface by gluing the hidden boundaries of the surfaces associated with each of the boundaries of the annulus. Both of these surfaces are naturally built with slanted wedges. We determine the closed string modulus and all open string moduli as simple functions of the Schwinger parameters. In particular, we find that the closed string modulus only depends on the Schwinger parameters of the propagators running in the loop. The computations are illustrated in section 4.7 where we work out the one-loop diagram with two external states. If both external states are placed on the same boundary component there are two string diagrams, and we discuss how they generate together the relevant open and closed string moduli.

In section 4.8 we use the family of λ-regularized gauges to justify our prescription for the calculation of one-loop moduli. There are three types of gluing operations that need to be justified in the Schnabl limit $\lambda \to 0$: (i) the star multiplication of slanted wedges corresponding to external states and propagator surfaces, (ii) the gluing along hidden boundaries that forms a single strip from the two slanted wedges each of which contains one boundary component of the one-loop diagram, and (iii) the identification of the edges of the resulting strip that creates the annulus. We show that all three types of operations can be justified rigorously in the Schnabl limit. We end in section 4.9 with some concluding remarks.

4.2 The vacuum graph

In this section we discuss the geometry of the vacuum graph. Our objectives are to set up notation and to calculate the modulus of the vacuum graph as a function of the Schwinger parameter for

general regular linear b-gauges.

4.2.1 Gauges, coordinate frames and the surface $\mathcal{R}(s)$

Reference [46] studied open string perturbation theory in a class of gauges called linear b-gauges. In these gauges, a linear combination of even moded antighost oscillators annihilates the classical string field $|\psi_{cl}\rangle$:

$$\mathcal{B}\,|\psi_{cl}\rangle = 0\,. \tag{4.2.1}$$

Here $\mathcal{B}$ is determined by a vector field $v(\xi)$ via

$$\mathcal{B} = \sum_{k\in\mathbb{Z}} v_{2k} b_{2k} = \oint \frac{d\xi}{2\pi i} v(\xi) b(\xi)\,, \qquad \text{with} \quad v(\xi) = \sum_{k\in\mathbb{Z}} v_{2k}\xi^{2k+1}\,, \quad v_{2k}\in\mathbb{R}\,. \tag{4.2.2}$$

A subset of linear b-gauges in which string perturbation is guaranteed to produce the correct on-shell amplitudes was identified in [46]. In this subset the vector field $v(\xi)$ is analytic in a neighborhood of the unit circle $|\xi| = 1$, and satisfies the condition

$$\Re\left(\bar{\xi} v(\xi)\right) > 0 \qquad \text{for} \quad |\xi| = 1\,. \tag{4.2.3}$$

These gauges were called *regular linear b-gauges*. One also defines

$$\mathcal{L} \equiv \{Q, \mathcal{B}\} = \oint \frac{d\xi}{2\pi i} v(\xi) T(\xi) = \sum_{k\in\mathbb{Z}} v_{2k} L_{2k}\,. \tag{4.2.4}$$

In a certain frame $w = g(\xi)$ the operator $\mathcal{L}$ generates translations [10,46]. The map $g(\xi)$ is related to the vector field $v(\xi)$ through

$$\frac{dg}{d\xi} = -\frac{1}{v(\xi)}\,. \tag{4.2.5}$$

Normalizing $v(\xi)$ appropriately, we can impose on $g(\xi)$ the convenient boundary conditions

$$g(-1) = 0\,, \quad g(1) = i\pi\,. \tag{4.2.6}$$

We also use the frame $z = f(\xi)$ where the operator $\mathcal{L}$ is the zero mode Virasoro operator and thus generates scaling. This frame is only determined up to an overall factor. We choose the normalization

$$f(\pm 1) = \pm\tfrac{1}{2}\,. \tag{4.2.7}$$

Given such a frame $z = f(\xi)$, one can determine the associated vector field $v(\xi)$ as

$$v(\xi) = \frac{f(\xi)}{f'(\xi)}\,. \tag{4.2.8}$$

The defining property of this vector field is that the operators $\mathcal{L}$ and $\mathcal{B}$ are, respectively, the zero modes of the Virasoro and antighost operators in the z frame. Use of (4.2.5) and (4.2.8) immediately

shows that the w and z frames are related by $g = -\ln f + c$, where c is a constant. This constant is determined by our boundary conditions on $g(\xi)$ and $f(\xi)$ in (4.2.6) and (4.2.7). We obtain

$$\boxed{w = g(\xi) = -\ln(2f(\xi)) + i\pi = -\ln(2z) + i\pi\,.} \tag{4.2.9}$$

In this map z is always in the upper-half plane and the branch of the logarithm is taken using $0 \leq \mathrm{Arg}\, z \leq \pi$. Inverting (4.2.9) we get

$$z = f(\xi) = -\tfrac{1}{2}\, e^{-w}\,. \tag{4.2.10}$$

Picking a gauge condition (4.2.1) for the classical string field $|\psi_{cl}\rangle$ of ghost number one is only the first step in the gauge fixing procedure [46, 77–80]. Appropriate vector fields $v(\xi)$ must be chosen for each ghost number and the gauge condition is that the corresponding $\mathcal{B}$ operator must annihilate the string field at the given ghost number. We will return to this issue when we address general one-loop amplitudes in section 4.6.

We noted above that the operator $\mathcal{L}$ generates rescalings in the z frame and translations in the w frame. As a differential operator we thus have

$$\mathcal{L} = -z\frac{d}{dz} = \frac{d}{dw}\,. \tag{4.2.11}$$

The operator $e^{-s\mathcal{L}}$ creates a strip $\mathcal{R}(s)$ of length s in the w frame with two horizontal open string boundaries [46], as depicted in Figure 4-1(a). The boundary conditions (4.2.6) ensure that the width of the strip is normalized to π. Furthermore, the strip domain $\mathcal{R}(s)$ has as right boundary the curve $w = g(\xi = e^{i\theta})$ with $0 \leq \theta \leq \pi$; this is just the w-plane image of the coordinate curve. It is clear from (4.2.11) that $e^{-s\mathcal{L}}$ translates by a distance s to the left. It follows that the left boundary of $\mathcal{R}(s)$ is the right boundary copied a distance s to the left.[1]

Using the relation (4.2.10), we can map the strip $\mathcal{R}(s)$ to the z frame. The right boundary of $\mathcal{R}(s)$ in the w frame becomes the *coordinate curve* $z = f(e^{i\theta})$ with $0 \leq \theta \leq \pi$ in the z frame. As $\mathcal{L}$ generates rescalings in this frame, the surface $\mathcal{R}(s)$ is swept out by rescalings of the coordinate curve with scale factors ranging from one to e^s. As we can decompose the operator $\mathcal{L}$ into left and right pieces,

$$\mathcal{L} = \mathcal{L}_L + \mathcal{L}_R\,, \tag{4.2.12}$$

we can similarly divide $\mathcal{R}(s)$ into two components, one associated with the action of $e^{-s\mathcal{L}_L}$ and the other associated with the action of $e^{-s\mathcal{L}_R}$. The component associated with $e^{-s\mathcal{L}_R}$ is the part of $\mathcal{R}(s)$ in the region $\Re(z) > 0$ and is shaded in light grey in Figure 4-1(b). It is swept out by rescalings of the right part of the coordinate curve, which we parameterize as

$$\tfrac{1}{2} + \gamma_R(\theta) \equiv f\big(e^{i\theta}\big)\,, \qquad 0 \leq \theta \leq \tfrac{\pi}{2}\,. \tag{4.2.13}$$

[1] This representation of $\mathcal{R}(s)$ differs from the representation in [46] by a rescaling of $\frac{1}{2}e^s$ in the z frame and by a translation of $-s$ in the w frame.

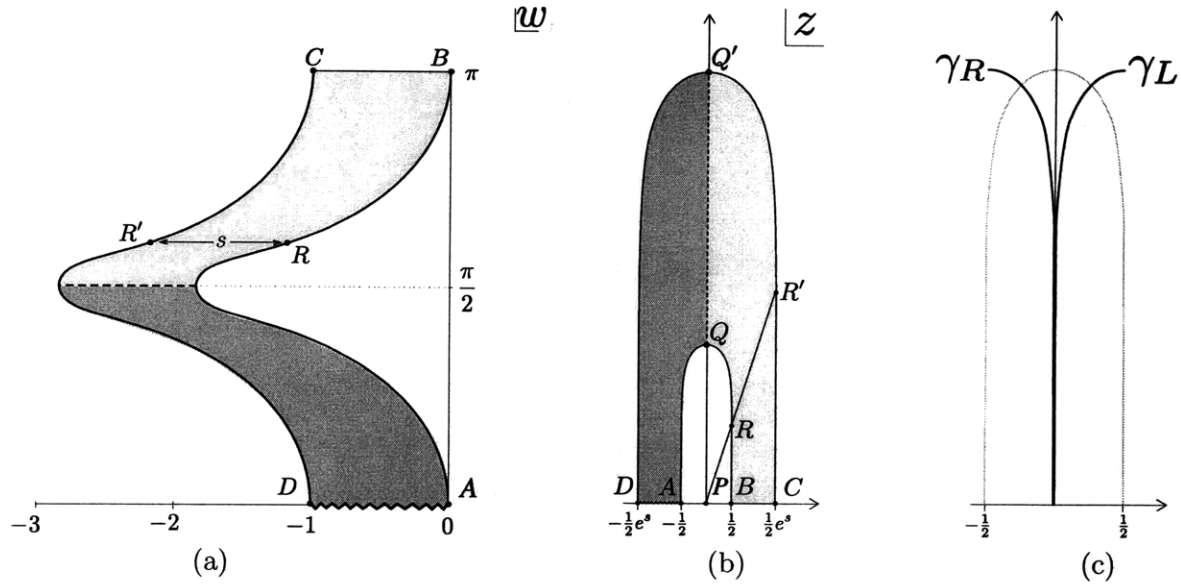

Figure 4-1: The surface $\mathcal{R}(s)$ created by $e^{-s\mathcal{L}}$ in the w frame (a) and in the z frame (b). Points R and R' related by horizontal translation $w \to w - s$ in the w frame are related by scaling $z \to e^s z$ in the z frame. The surface $\mathcal{R}(s)$ is displayed for $\mathcal{L} = L^\lambda$ with $\lambda = 10^{-4}$ and $s = 1$. The curves γ_L and γ_R arise from the coordinate curve $f(e^{i\theta})$, as illustrated in (c).

Similarly, the component of $\mathcal{R}(s)$ associated with $e^{-s\mathcal{L}_L}$, shaded in dark grey in the figure, is located in the region $\Re(z) < 0$, and is swept out by rescalings of the left part of the coordinate line, which we parameterize as

$$-\tfrac{1}{2} + \gamma_L(\theta) \equiv f\big(e^{i(\pi-\theta)}\big)\,, \qquad 0 \le \theta \le \tfrac{\pi}{2}\,. \tag{4.2.14}$$

Note that the curves $\gamma_R(\theta)$ and $\gamma_L(\theta)$ introduced above are, respectively, the right and left parts of the coordinate curve, displaced horizontally so that for $\theta = 0$ they are at the origin (Figure 4-1(c)). The left component of $\mathcal{R}(s)$ is simply a reflection of the right component around the axis $\Re(z) = 0$, because the general form (4.2.2) of the vector field $v(\xi)$ implies

$$\gamma_L(\theta) = -\overline{\gamma_R(\theta)}\,. \tag{4.2.15}$$

The left and right components of $\mathcal{R}(s)$ need to be glued on the imaginary axis along the line QQ', which stretches from $f(i)$ to $e^s f(i)$. For regular linear b-gauges $f(i)$ is finite, resulting in a finite boundary QQ' generated by $e^{-s\mathcal{L}_L}$ and $e^{-s\mathcal{L}_R}$. Thus, $e^{-s\mathcal{L}_L}$ and $e^{-s\mathcal{L}_R}$ do not give the surface associated with $e^{-s\mathcal{L}}$ until they are glued along QQ'. This can be traced to the non-commutativity of $\mathcal{L}_L$ and $\mathcal{L}_R$,

$$\big[\mathcal{L}_L\,,\,\mathcal{L}_R\big] \neq 0\,, \tag{4.2.16}$$

which in turn implies $e^{-s\mathcal{L}} \neq e^{-s\mathcal{L}_R} e^{-s\mathcal{L}_L}$ for regular linear b-gauges. The operators in (4.2.16) fail to commute because the vector field v does not vanish at the open string midpoint (see [6]).

In this chapter the family of λ-regulated gauges introduced in [46] plays an important role. This

family is defined through the one-parameter family of vector fields

$$v^\lambda(\xi) = e^\lambda(1+e^{-2\lambda}\xi^2)\tan^{-1}(e^{-\lambda}\xi)\,, \qquad \text{with} \qquad \lambda > 0\,. \tag{4.2.17}$$

The surface $\mathcal{R}(s)$ in this gauge is then generated by the operator

$$L^\lambda \equiv L_0 + 2\sum_{k=1}^{\infty} \frac{(-1)^{k+1}}{4k^2-1}\, e^{-2k\lambda}\, L_{2k}\,. \tag{4.2.18}$$

This family interpolates from Siegel gauge as $\lambda \to \infty$ to Schnabl gauge which arises in the limit $\lambda \to 0$. In fact, these gauges are regular linear b-gauges for all values $\lambda > 0$. Schnabl gauge is not regular – this is why there is no proof yet that amplitudes arise correctly.

For the λ-regulated z frames we have the λ-regulated functions

$$f^\lambda(\xi) = \frac{1}{2}\,\frac{\tan^{-1}(e^{-\lambda}\xi)}{\tan^{-1}(e^{-\lambda})}\,, \qquad \text{with} \qquad \lambda > 0\,. \tag{4.2.19}$$

While in general regular linear b-gauges the functions $f(\xi)$, just like $v(\xi)$, need only be analytic in a neighborhood of $|\xi| = 1$, the functions (4.2.19) have the nice property that they are analytic on the entire unit disk $|\xi| \le 1$. They map the real axis between $\xi = -1$ and $\xi = 1$ to the real axis between $z = -\frac{1}{2}$ and $z = \frac{1}{2}$, and map $\xi = 0$ to $z = 0$. The region in the z frame between the real axis and the curve $z = f(e^{i\theta})$ with $0 \le \theta \le \pi$ can thus be interpreted as a canonical coordinate patch that glues nicely to the boundary of $\mathcal{R}(s)$. The maps $f^\lambda(\xi)$ are thus *coordinate functions*. In the Schnabl limit $\lambda \to 0$, we obtain

$$f(\xi) \equiv \lim_{\lambda\to 0} f^\lambda(\xi) = \frac{2}{\pi}\tan^{-1}\xi\,. \tag{4.2.20}$$

This is the familiar coordinate function of the sliver frame which is well defined for all $|\xi| \le 1$ except for $\xi = i$. The open string midpoint $\xi = i$ is mapped to $i\infty$.

The behavior of the coordinate function $f^\lambda(\xi)$ for very small λ (near Schnabl gauge) will be of interest. We focus on the coordinate curve $f^\lambda(\xi = e^{i\theta})$ with $0 \le \theta \le \pi$. It is convenient to use the angular variable $\hat\theta$ that measures angles with respect to the imaginary axis

$$\hat\theta = \frac{\pi}{2} - \theta\,. \tag{4.2.21}$$

The coordinate function (4.2.19) admits a simple expansion when both λ and $\hat\theta$ are small, regardless of their ratio. One then finds[2]

$$f^\lambda(e^{i\theta}) = -\frac{i}{\pi}\ln\Big(\frac{\lambda + i\hat\theta}{2}\Big) + \mathcal{O}(\lambda) + \mathcal{O}(\hat\theta)\,. \tag{4.2.22}$$

We define $i\Lambda(\lambda)$ as the value of the coordinate function at $\xi = i$:

$$i\Lambda \equiv f^\lambda(i) = -\frac{i}{\pi}\ln\frac{\lambda}{2} + \mathcal{O}(\lambda)\,. \tag{4.2.23}$$

[2]We follow the convention that terms of order $\lambda\ln\lambda$ are written as $\mathcal{O}(\lambda)$.

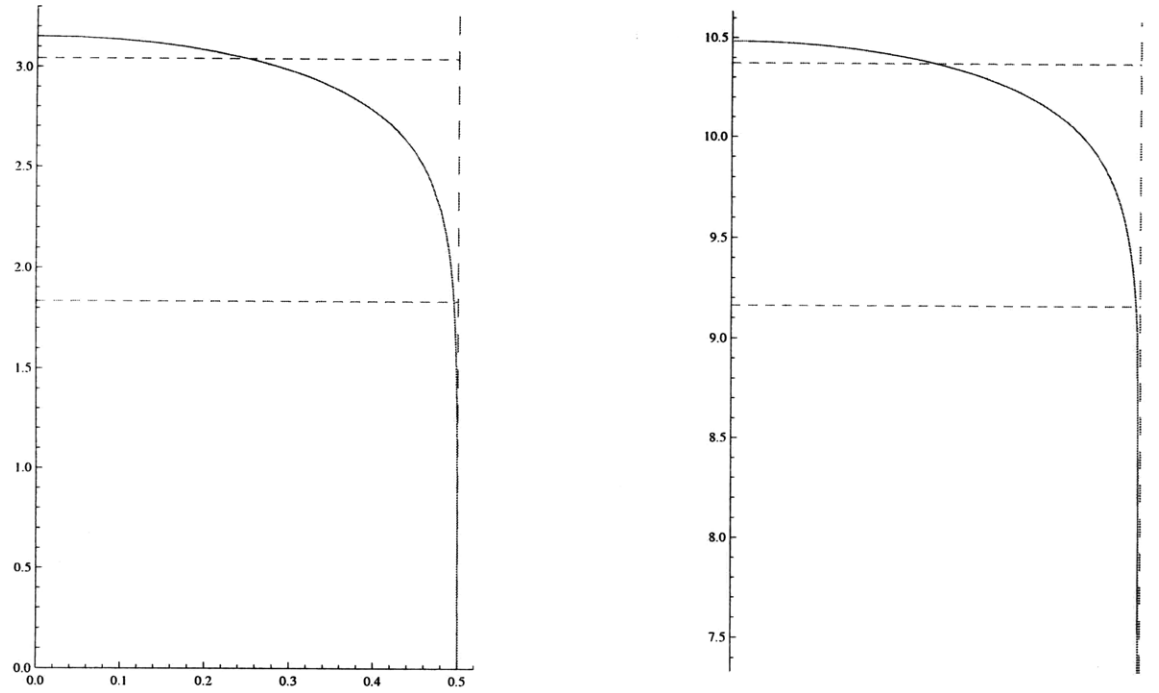

Figure 4-2: Left: The coordinate curve $f^\lambda(e^{i\theta})$ for $\theta \in [0, \pi/2]$ and $\lambda = 10^{-4}$. The intersection with the bottom dashed line indicates that by the time the curve has dropped about 1.32 from the top, it is within 1% of the vertical line $\Re(z) = 1/2$ that defines the sliver frame. Right: the same portion of the coordinate curve for $\lambda = 10^{-14}$. The top part of the coordinate curve is quite accurately the same as the one shown to the left, but is displaced upwards.

Happily, the regularized curve $f^\lambda(e^{i\theta})$ only differs appreciably from the sliver curve $f(e^{i\theta})$ for $\hat{\theta} = \mathcal{O}(\lambda)$. For $\lambda \ll 1$, the part of the curve $f^\lambda(e^{i\theta})$ which deviates significantly from $f(e^{i\theta})$ is thus entirely captured by (4.2.22). We can write the leading dependence as

$$f^\lambda(e^{i\theta}) \simeq i\Lambda(\lambda) - \frac{i}{2\pi} \ln\Big[1 + \Big(\frac{\hat{\theta}}{\lambda}\Big)^2\Big] + \frac{1}{\pi} \tan^{-1}\Big(\frac{\hat{\theta}}{\lambda}\Big) . \tag{4.2.24}$$

The nature of the curve $f^\lambda(e^{i\theta})$ is quite interesting. As illustrated in Figure 4-2, for any $\lambda \ll 1$ the coordinate curve near the top takes the *same* shape. This is so because, apart from the $i\Lambda(\lambda)$ term that sets the height, the rest of f^λ depends only on the ratio $\hat{\theta}/\lambda$, which spans the same values as $\hat{\theta}$ grows from zero to some multiple of λ. For $\hat{\theta} = \lambda$ the coordinate curve has come down about 0.11 from the top and is 50% of the way to the maximum real value of 1/2 (top dashed lines). For $\hat{\theta} = 64\lambda$ the coordinate curve has come down about 1.32 from the top and is 99% of the way to the maximum real value (lower dashed lines). Clearly, for sufficiently small λ, the coordinate curve deviates from the vertical lines that define the sliver frame only for $\hat{\theta} \ll 1$.

The curves γ_R^λ and γ_L^λ which parameterize the coordinate curve $f^\lambda(e^{i\theta})$ for λ-regulated gauges will play an important role in our analysis. They are defined by

$$\tfrac{1}{2} + \gamma_R^\lambda(\theta) \equiv f^\lambda\big(e^{i\theta}\big) , \qquad -\tfrac{1}{2} + \gamma_L^\lambda(\theta) \equiv f^\lambda\big(e^{i(\pi-\theta)}\big) , \tag{4.2.25}$$

a particular example of the general definitions (4.2.13) and (4.2.14). In the Schnabl limit $\lambda \to 0$, γ_R^λ and γ_L^λ coincide, and we therefore define

$$\gamma(\theta) \equiv \lim_{\lambda\to 0} \gamma_R^\lambda(\theta) = \lim_{\lambda\to 0} \gamma_L^\lambda(\theta) = i\,\frac{2}{\pi}\tanh^{-1}\Big(\tan\frac{\theta}{2}\Big)\,. \tag{4.2.26}$$

As expected, this is the parameterized vertical line that defines the left and right parts $\frac{1}{2}-\gamma$ and $\frac{1}{2}+\gamma$ of the coordinate curve of the sliver projector. Notice, however, that the limit (4.2.26) is not uniform in θ. In fact, for all $\lambda > 0$ we have

$$\lim_{\theta\to\frac{\pi}{2}} \Re\big(\gamma_{L/R}^\lambda(\theta)\big) = \pm\frac{1}{2}\,, \tag{4.2.27}$$

while $\Re(\gamma(\theta)) = 0$, independent of θ.

We now ask how much the coordinate curve of λ-regulated gauges still deviates from the vertical line that defines the sliver by the time its imaginary part has been reduced to $\Lambda/2$, that is, half the value it has at the top. To leading order in λ, the angle corresponding to this point on the curve is given by

$$\hat\theta_{\frac{1}{2}} = \sqrt{2\lambda} \quad\to\quad \theta_{\frac{1}{2}} = \tfrac{\pi}{2} - \sqrt{2\lambda}\,. \tag{4.2.28}$$

A short calculation then shows

$$\gamma_R^\lambda(\theta_{\frac{1}{2}}) = -\frac{1}{2\pi}\sqrt{2\lambda} + i\,\frac{\Lambda}{2} + \mathcal{O}(\lambda)\,. \tag{4.2.29}$$

As we can see, $\gamma_R^\lambda(\theta)$ only deviates by $\mathcal{O}(\sqrt{\lambda})$ from the imaginary axis by the time its height has dropped by half.

4.2.2 The annulus and its modulus

The surfaces associated with the one-loop vacuum graph are obtained by gluing the two parameterized edges of the propagator to itself. The propagator associated with regular linear b-gauges is in general a complicated object. Its geometric interpretation depends on the ghost number of the state it acts on. In alternating gauge, which was introduced in [46], the surface of the propagator is built by gluing the strips associated with $e^{-s\mathcal{L}}$ and $e^{-s^\star\mathcal{L}^\star}$ in some order (that depends on ghost number) and by including the action of the BRST operator Q, that acts as a total derivative on moduli. The details of this construction will be important for our general analysis in section 4.6. For now, we focus on one term that arises from the propagator: it can be described by setting $s^\star = 0$ and gives the strip $\mathcal{R}(s)$ associated with $e^{-s\mathcal{L}}$. The generalization to the full propagator will not introduce further conceptual problems in our Riemann surface analysis. We restrict ourselves to the simplified propagator in the discussion of the vacuum and the tadpole diagrams because it suffices to demonstrate the main features of loop diagrams in Schnabl gauge.

For any regular linear b-gauge, the gluing of the simplified propagator $\mathcal{R}(s)$ to itself is implemented in the w frame by the identification $w \sim w - s$. The result, for each value of s, is an annulus. In this annulus the boundaries are the horizontal segments BC and AD, shown in Figure 4-1(a)

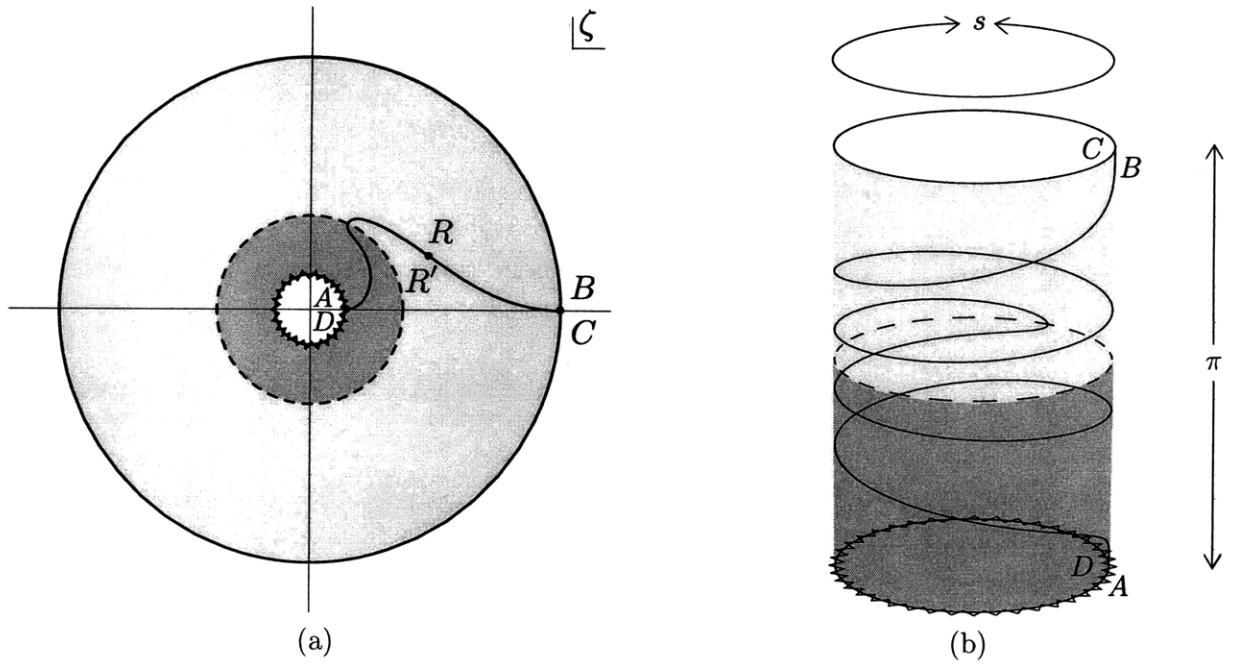

Figure 4-3: The vacuum graph obtained from gluing the edges of $\mathcal{R}(s)$, illustrated for $\mathcal{L} = L^\lambda$ with $\lambda = 10^{-4}$. In (a) the surface is displayed as a canonical annulus in the ζ frame for $s = 10$. The cutting curve is shown explicitly. In (b) the surface is displayed as a cylinder obtained from the identification $w \sim w - s$ in the w frame for $s = 1$. This should be compared to Figure 4-1(a).

for λ-regularized gauges. The map from this annulus to a canonically presented annulus in the ζ frame is

$$\zeta = \exp\Big(-\frac{2\pi i}{s}(w - i\pi)\Big) = \exp\Big(-\frac{2\pi^2}{s}\Big)\exp\Big(-\frac{2\pi i w}{s}\Big)\,. \tag{4.2.30}$$

See Figure 4-3(a). We can also write, using (4.2.9),

$$\zeta = \exp\Big(\frac{2\pi i}{s}\ln 2z\Big)\,. \tag{4.2.31}$$

The map (4.2.30) takes BC into the unit circle $|\zeta| = 1$ and AD into the inner circle $|\zeta| = \exp(-2\pi^2/s)$. Since the strip $\mathcal{R}(s)$ is foliated in the w frame by horizontal lines of length s at heights that go from zero to π it is clear that the map (4.2.30) takes the interior of the strip to the region between the two ζ circles mentioned above. The shape of the edges of $\mathcal{R}(s)$ is irrelevant to the map; their image under the map is a cutting curve for the annulus. Shown to the right in Figure 4-3(b) is the w-frame picture of $\mathcal{R}(s)$ rolled up into a cylinder of height π and circumference s. The cutting curve is shown in both presentations.

The modulus M of an annulus with radii r_{in} and r_{out} with $r_{\text{in}} < r_{\text{out}}$ is usually defined by

$$M \equiv \frac{1}{2\pi}\ln\frac{r_{\text{out}}}{r_{\text{in}}}\,. \tag{4.2.32}$$

The moduli space of annuli is the set

$$0 \le M \le \infty\,. \tag{4.2.33}$$

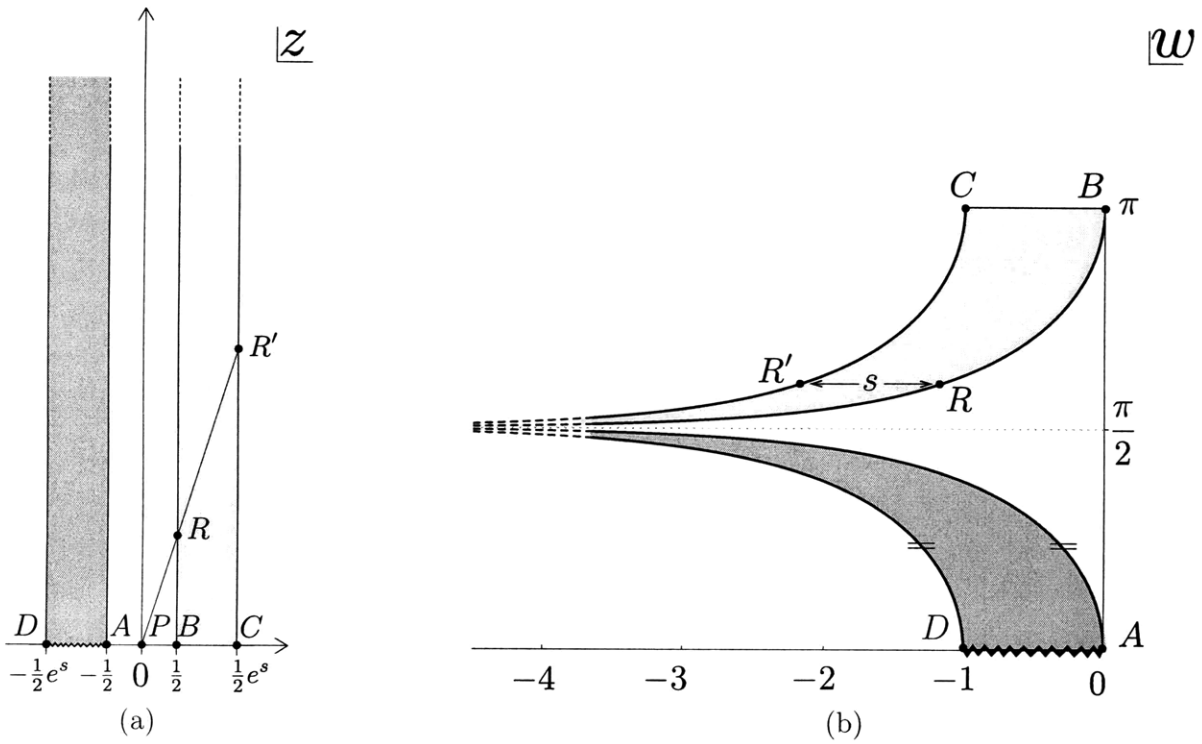

Figure 4-4: The $\mathcal{R}(s)$ strip in the Schnabl limit $\lambda = 0$ both in the w and in the z frames, displayed for $s = 1$. The gluing of the free edges of the strip gives rise to an annulus of finite modulus (see Figure 4-5). The gluing identification in the z frame is that induced by radial lines emerging from the origin.

For our annulus the modulus is

$$M = \frac{\pi}{s}\,. \tag{4.2.34}$$

This result for the annulus modulus is valid for any regular linear b-gauge. In particular, the modulus M of the annulus produced by the gluing of the edges of $\mathcal{R}(s)$ is the same for all values of λ in the λ-regularized gauges and depends only on s. As $s \to 0$, $M \to \infty$, the inner circle goes to zero size, and we approach closed string degeneration. As $s \to \infty$ the inner circle approaches the outer circle, M goes to zero, and we approach open string degeneration. The full moduli space (4.2.33) is therefore covered. It thus follows that in the Schnabl limit $\lambda \to 0$ the gluing of $\mathcal{R}(s)$ also gives an annulus of $M = \pi/s$ and that moduli space is covered in this case as well. The limit $\lambda \to 0$ of Figure 4-1 is shown in Figure 4-4. Moreover, Figure 4-5 shows the map to the ζ plane and the cylinder view of the w-presentation. Note that we could have calculated the annulus modulus in Schnabl gauge using any other family of regular linear b-gauges which approaches Schnabl gauge when the regulator is removed. The result for M would have been the same.

A few remarks about this construction in the Schnabl limit are in order.

- The map (4.2.30) still takes the shaded domain in the w plane to the circular annulus because the identification $w \sim w - s$ still holds. The cutting curve is infinitely long (Figure 4-5).

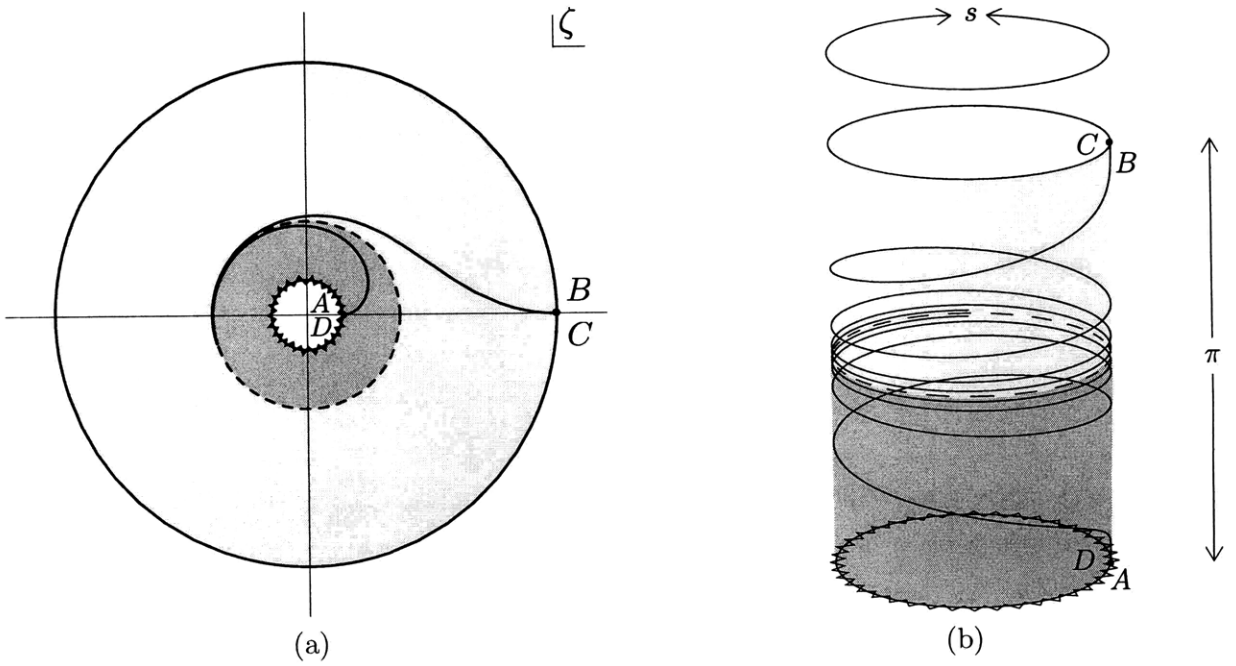

Figure 4-5: The vacuum graph obtained from gluing the edges of $\mathcal{R}(s)$ in the Schnabl limit $\lambda \to 0$. In (a) the surface is displayed as a canonical annulus in the ζ frame for $s = 10$. In (b) the surface is displayed as a cylinder obtained from the identification $w \sim w - s$ in the w frame for $s = 1$. These surfaces differ from the corresponding finite-λ surfaces in Figure 4-3 only through the shape of the cutting curve.

- In the z plane the vertical strip to the right produces the upper half of the annulus (the upper half of the vertical cylinder of height π and circumference s). The vertical strip to the left produces the lower half of the annulus. The two halves are glued.

- The identifications $w \sim w - s$ become *slanted* identifications $z \sim e^s z$ of the vertical lines through B and C, and of the vertical lines through A and D. If the identifications had been horizontal ($z \sim z - \frac{1}{2} + \frac{1}{2}e^s$) both the right and left strips would have each given rise to a (closed string) degenerate annulus. In fact, such a problematic horizontal identification happens for the gauge condition $B^+\Phi = 0$ in the sliver frame. It is the slanted identification that makes the z frame picture in Schnabl gauge consistent with a finite modulus annulus.

In the previous section we remarked that the propagator strip $\mathcal{R}(s)$ for regular linear b-gauges can be decomposed into two components associated with $e^{-s\mathcal{L}_L}$ and $e^{-s\mathcal{L}_R}$, respectively. These components are glued along the boundary QQ' in Figure 4-1(b). $\mathcal{L}_L$ and $\mathcal{L}_R$ generate this unmatched boundary that needs to be glued by hand because they do not commute. The operators L and $L^\star$ in Schnabl gauge can also be decomposed into left and right parts. We write $L = L_L + L_R$, $L^\star = L^\star_L + L^\star_R$. In the Schnabl limit, the unmatched boundary is hidden at $i\infty$ in the z- frame, but arises in the annulus frame ζ as the circle $|\zeta| = \exp(-\pi^2/s)$, shown dashed in Figure 4-5(a). We are led to conclude that while both L and $L^\star$ arise from vector fields that vanish at the open string midpoint, they do not vanish fast enough to ensure that L_L and L_R commute and that $L^\star_L$

and $L_R^\star$ commute:[3]

$$\boxed{[L_L, L_R] \neq 0\,, \qquad [L_L^\star, L_R^\star] \neq 0\,.} \tag{4.2.35}$$

We conclude this subsection by recalling the relation of the modulus M with the conformal invariant known as the extremal length [81]. The extremal length is an invariant associated to a given set of curves Γ on a Riemann surface. Let ρ denote a conformal metric (a metric for which $ds = \rho(z,\bar{z})|dz|$) on the Riemann surface. The length $\ell(\gamma,\rho)$ of a curve $\gamma \in \Gamma$ and the area $A(\Omega,\rho)$ of the Riemann surface Ω are given by:

$$\ell(\gamma,\rho) = \int_\gamma \rho|dz|\,, \quad A(\Omega,\rho) = \iint_\Omega \rho^2\, dxdy\,. \tag{4.2.36}$$

We define $\ell(\Gamma,\rho)$ as the length of the shortest curve in Γ with respect to the metric ρ:

$$\ell(\Gamma,\rho) = \inf_{\gamma\in\Gamma} \ell(\gamma,\rho)\,. \tag{4.2.37}$$

The extremal length λ_Γ is defined as [81]

$$\lambda_\Gamma = \sup_\rho \left(\frac{\ell^2(\Gamma,\rho)}{A(\Omega,\rho)}\right). \tag{4.2.38}$$

To evaluate λ_Γ one must search over metrics until the quantity inside parenthesis on the right-hand side is maximized. The extremal metric ρ for which the maximum is attained is a minimal area metric: it is the metric with least area consistent with all curves in the set having a length greater than or equal to a certain prescribed value. From the definition (4.2.38) it is clear that the extremal length λ_Γ is a conformal invariant.

Let us now return to the vacuum graph of regular linear b-gauges. Imagine the domain $\mathcal{R}(s)$, glued to itself to form the vacuum graph, as a cylinder of circumference s and height π. This is, in fact, the w frame picture in Figure 4-3(b). There are two types of curves on this cylinder (or annulus): open curves that stretch from one boundary to the other and closed curves that go around the cylinder. We thus have an extremal length λ_{open} associated with the set of open curves and an extremal length λ_{closed} associated with the set of closed curves. It is a familiar result that in the w frame the *same* metric $\rho = 1$ is extremal for *both* open and closed curves [82]. It is clear that in this flat metric the shortest open curves have length π and the shortest closed curves have length s. The area, moreover, is πs. It follows that the extremal lengths are

$$\lambda_{\text{open}} = \frac{\pi^2}{\pi s} = \frac{\pi}{s}\,, \qquad \lambda_{\text{closed}} = \frac{s^2}{\pi s} = \frac{s}{\pi}\,. \tag{4.2.39}$$

It is interesting to note that

$$\lambda_{\text{open}}\lambda_{\text{closed}} = 1\,, \quad \text{and} \quad M = \lambda_{\text{open}} = \frac{1}{\lambda_{\text{closed}}}\,. \tag{4.2.40}$$

The relations (4.2.40) are general and valid for any annulus. Note that degeneration of a given type means vanishing extremal length for the curves of associated type. Thus closed string degeneration ($s \to 0$) happens for $\lambda_{\text{closed}} \to 0$ and open string degeneration ($s \to \infty$) happens for $\lambda_{\text{open}} \to 0$.

[3] In fact the linear combination $L^+ = L + L^*$ arises from a vector that, as we approach the midpoint, vanishes sufficiently fast to ensure that L_L^+ and L_R^+ commute.

4.3 One-loop tadpole graph

In this section we discuss the one-loop tadpole graph. The underlying Riemann surface is an annulus with an open string puncture, that is, a puncture on one of the boundary components of the annulus. The puncture, which represents the external state, introduces significant complications in the geometry. Indeed, it is well known that in Siegel gauge the map of the string diagram to the round annulus is nontrivial and the modulus of the annulus cannot be calculated in simple closed form.

As in the previous section we restrict ourselves to the contribution from the propagator surface $\mathcal{R}(s)$ generated by $e^{-s\mathcal{L}}$. We discuss the graph for the family of interpolating gauges. We first show that for any value of the regulator λ the moduli space of annuli is generated when the Schwinger parameter s covers the range from zero to infinity. We then study the geometry as the regulator parameter λ goes to zero and we approach Schnabl gauge. We present a construction which allows us to exactly map the tadpole string diagram to the round annulus in the limit $\lambda \to 0$. The modulus of the annulus becomes exactly calculable in Schnabl gauge.

4.3.1 Covering moduli space in the λ-regulated gauges

Let us consider the one-loop tadpole graph with propagator $e^{-s\mathcal{L}}$. It is useful to first examine the surface obtained in the λ-regulated gauges. The way to assemble the surface is illustrated using Figure 4-6. We need the part of the surface associated with the external state and the propagator strip $\mathcal{R}(s)$.

As we can see in Figure 4-6(b), the placement of $\mathcal{R}(s)$ in the z frame is the same one used for the vacuum graph in the last section (Figure 4-1(b)). As discussed above equation (4.2.35), it is convenient to view the surface $\mathcal{R}(s)$ as built by gluing together two pieces – one associated with $e^{-sL_R^\lambda}$ and one associated with $e^{-sL_L^\lambda}$. These two pieces are glued along the dashed line QQ' to form the complete surface $\mathcal{R}(s)$.

The two curved boundaries of $e^{-sL_L^\lambda}$ are identified, just as for the vacuum graph. This time, however, the two curved boundaries of $e^{-sL_R^\lambda}$ are not glued to each other. To form the tadpole, we need to glue these two boundaries to the left and right boundaries of the external state. As the functions $f^\lambda(\xi)$ are coordinate functions and thus well defined for all $|\xi| \leq 1$, we can conveniently place this external state in the region between the real axis and the coordinate curve $f^\lambda(e^{i\theta})$. The operator insertion is then located at $z = f(0) = 0$ (see Figure 4-6(b)).

The gluing patterns both in the z and w frames are readily obtained from the graph in Figure 4-6(a). The only slightly nontrivial gluing operation is that identifying the curves AQ and CQ' in the z plane (the lines with triple arrows). We can express these two curves using $\gamma_{L/R}^\lambda$ defined in (4.2.25):

$$AQ = -\tfrac{1}{2} + \gamma_L^\lambda\,, \qquad CQ' = e^s(\tfrac{1}{2} + \gamma_R^\lambda)\,. \tag{4.3.1}$$

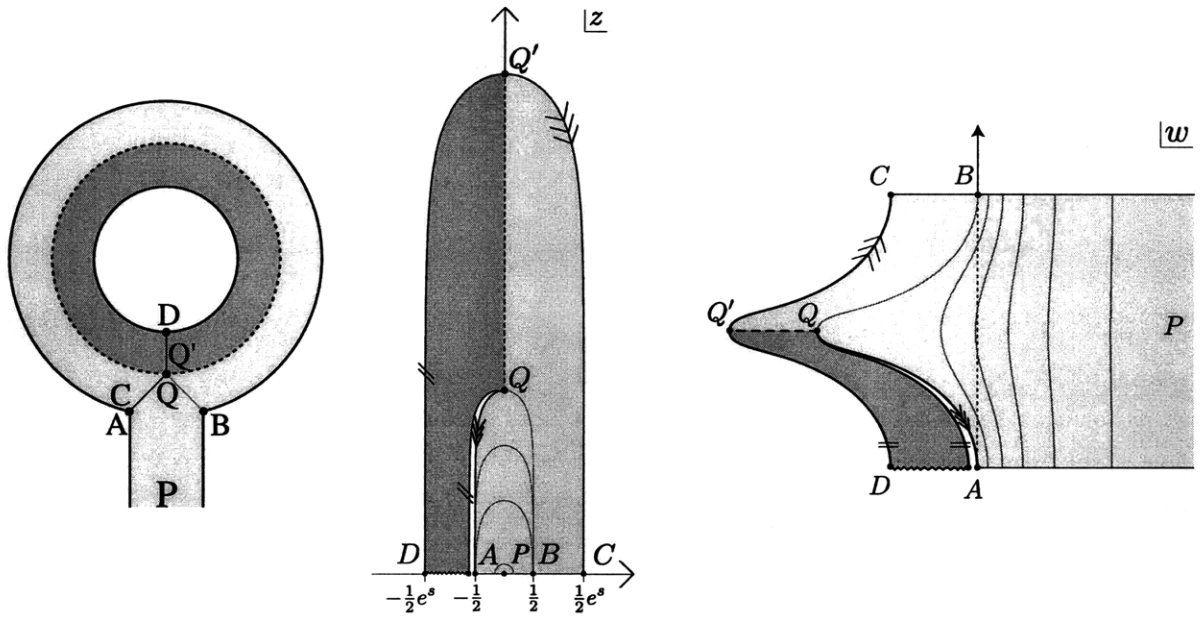

(a) (b) (c)

Figure 4-6: (a) The topology of the one-loop tadpole diagram obtained by gluing the external strip for the Fock space state to the propagator strip. (b) The tadpole diagram for a λ-regulated gauge in the z frame, displayed for $\lambda = 10^{-4}$ and $s = 1$. Note the cut from Q to A that separates the two boundary components. (c) The tadpole diagram in the w frame.

It then follows that the identification between AQ and CQ' is given by the map

$$z = -\tfrac{1}{2} + \gamma_L^\lambda(\theta) \;\rightarrow\; z' = e^s\big(\tfrac{1}{2} + \gamma_R^\lambda(\theta)\big)\,. \tag{4.3.2}$$

Recalling $\gamma_L(\theta) = -\overline{\gamma_R(\theta)}$, we find that a point $z \in AQ$ is identified with the point $z' \in CQ'$, where z' is obtained by first reflecting z across the vertical axis $z \rightarrow -\bar{z}$, and then applying the expansion factor e^s:

$$z \rightarrow z' = -e^s\,\bar{z}\,. \tag{4.3.3}$$

There should be no concern that z' appears to be a non-analytic function of z. The above relation is not a *sewing* relation, but just a relation valid on the curve (for example, the analytic relation $\xi\xi' = -1$ becomes $\xi' = -\bar{\xi}$ on the unit circle). The analytic gluing relation is determined by the sequence of conformal maps $z \rightarrow f^{-1}(z)$ back to the coordinate circle, $\xi \rightarrow -1/\xi$, followed by the action of f and, finally, multiplication by e^s. The analytic gluing relation corresponding to the identification (4.3.3) is thus

$$z \sim e^s f\Big(-\frac{1}{f^{-1}(z)}\Big)\,. \tag{4.3.4}$$

Since there is no simple closed form expression for the modulus $M(s)$ of the annulus in Siegel gauge, we cannot hope to calculate explicitly $M(s)$ for arbitrary finite λ. Extremal length, however, gives a very simple proof that moduli space will be covered. Consider the w-frame picture in Figure 4-6(c). The extremal metric cannot be found, but let us use the metric $\rho = 1$ on the lower

half of the strip $\mathcal{R}(s)$ (below $Q'Q$) and $\rho = 0$ elsewhere. In other words, we are setting $\rho = 1$ only on the part of the surface corresponding to $e^{-sL_L^\lambda}$ (shaded in dark grey in the figure). The area of the surface in this metric is $A = \frac{1}{2}\pi s$. In this metric the shortest open curves have length $\frac{\pi}{2}$. This gives the following inequality for the open string extremal length

$$\lambda_{\text{open}} \geq \frac{\left(\frac{\pi}{2}\right)^2}{\frac{\pi s}{2}} = \frac{\pi}{2s}\,. \tag{4.3.5}$$

For closed curves we take $\rho = 1$ all over the propagator strip $\mathcal{R}(s)$ *and* over the portion of the external state strip that lies to the left of the vertical line AB in Figure 4-6(c). In other words, we set $\rho = 1$ in the region $\Re(w) < 0$. We set $\rho = 0$ elsewhere. A little thought shows that in this metric the shortest closed curve has length s. The area is $\pi s + A(\lambda)$, where $A(\lambda)$ is the area of the external state strip in the chosen metric. We thus get

$$\lambda_{\text{closed}} \geq \frac{s^2}{\pi s + A(\lambda)} \quad \rightarrow \quad \lambda_{\text{open}} \leq \frac{\pi}{s} + \frac{A(\lambda)}{s^2}\,. \tag{4.3.6}$$

In the Siegel limit $\lambda \to \infty$, the vertical line AB in the w frame coincides with the right boundary of $\mathcal{R}(s)$ so that the area $A(\infty) = 0$. It is easy to see that the area $A(\lambda)$ grows as λ decreases, but it stays finite even in the limit $\lambda \to 0$. In fact, the relevant integral can be exactly calculated and one finds that

$$A_0 \equiv \lim_{\lambda \to 0} A(\lambda) = \pi \ln 2\,. \tag{4.3.7}$$

Back in (4.3.6), we use $A(\lambda) \leq A_0$ and find

$$\lambda_{\text{open}} \leq \frac{\pi}{s} + \frac{A_0}{s^2} = \frac{\pi}{s} + \frac{\pi \ln 2}{s^2}\,. \tag{4.3.8}$$

Combining (4.3.5) and (4.3.8) and recalling that $M = \lambda_{\text{open}}$ we get

$$\frac{\pi}{2s} \leq M(s) \leq \frac{\pi}{s}\left(1 + \frac{\ln 2}{s}\right). \tag{4.3.9}$$

The above inequalities imply that $M(s) \to 0$ as $s \to \infty$ and $M(s) \to \infty$ as $s \to 0$, so the full moduli space will be covered for $s \in [0, \infty)$. This is consistent with the results of [46] which showed that regular linear b-gauges, such as the λ-regulated gauges, give correct on-shell string amplitudes. The inequalities (4.3.9) hold for all $\lambda > 0$. We thus conclude that moduli space is covered in the Schnabl limit $\lambda \to 0$.

4.3.2 Modulus in Schnabl gauge

The estimates done in the previous subsection bound $M(s)$ and allow us to confirm that moduli space is covered for any value of the deformation parameter λ. We now claim that the value of the modulus $M(s)$ becomes calculable in simple closed form in the Schnabl limit $\lambda \to 0$. The derivation requires careful analysis of a conformal map in the limit $\lambda \to 0$. Since the final result is simple, we will present it here, without proof. In the following subsection we justify our claim.

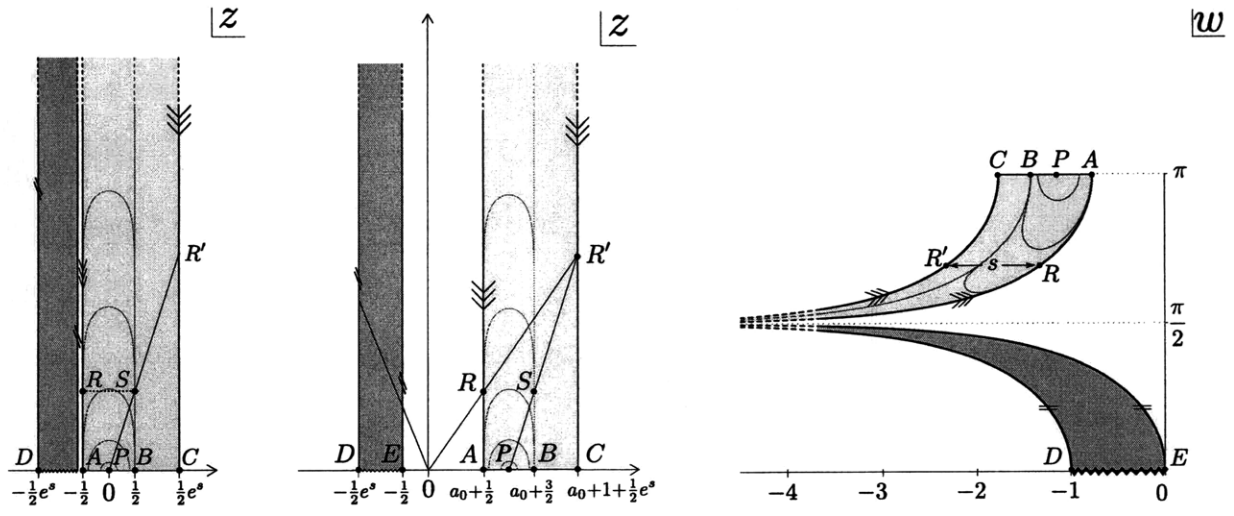

(a) (b) (c)

Figure 4-7: (a) The one-loop tadpole in the z frame. The surface is composed of two separate strips: one above $z \in [-\frac{1}{2}e^s, -\frac{1}{2}]$ and the other above $z \in [-\frac{1}{2}, \frac{1}{2}e^s]$. These two strips are joined at $i\infty$. The figure is displayed for $s = 1$. (b) The same surface with the right strip translated to the right by a distance $a_0 + 1$, which depends on s and makes the identifications of the left and right boundaries work with rays through the origin. (c) The middle figure mapped to the w frame with $w = -\ln 2z + i\pi$.

We begin with Figure 4-7(a), where we see that the surface of the tadpole diagram appears as two *disconnected* vertical strips in the z frame. The strip above the real segment $[-\frac{1}{2}e^s, -\frac{1}{2}]$ represents e^{-sL_L} and the strip above the real segment $[-\frac{1}{2}, \frac{1}{2}e^s]$ represents the external state and e^{-sL_R}. These real segments are the boundaries of the annulus. On the left strip the identification of the edges is $z \sim e^s z$. On the right strip the identification is more nontrivial. Its left boundary carries the ordinary sliver parameterization and is given by $-\frac{1}{2}+\gamma(\theta)$, with $\gamma(\theta)$ defined in (4.2.26). The right boundary of the right strip is given by $e^s(\frac{1}{2} + \gamma(\theta))$ and thus carries a parameterization which is rescaled by e^s. It follows that a point R on the line above $z = -\frac{1}{2}$ and a point R' on the line above $z = \frac{1}{2}e^s$ are identified if the copy S of R on the line above $z = \frac{1}{2}$ is related to R' via the scaling $z \sim e^s z$. This is, in fact, the gluing prescription discussed around equation (4.3.3). The two separate strips are supposed to be glued together at $i\infty$ but it is not obvious how to glue these hidden boundaries.

We could proceed as we did in the previous section and map this configuration of surfaces directly to the w frame via (4.2.9). Just like in Figure 4-6(c)), the external state would be represented in the w frame by an infinite strip of height π. In Schnabl gauge, however, we can construct a different map of the tadpole diagram to the w frame, one in which the whole surface is foliated by horizontal lines of length s. It is then possible to use the map $\zeta(w)$ in (4.2.30) to get a round annulus. We will now show how this is done.

In the z frame we translate the right strip towards the right by a distance that makes the line

through the identified points R and R' go through the origin. Since the heights of R and R' are related by e^s it follows, by similar triangles, that $R \sim R'$ are related by $z \sim e^s z$ (see Figure 4-7(b)). The requisite displacement, called $a_0 + 1$ for later convenience, is determined from the similar triangles:

$$e^s = \frac{CR'}{AR} = \frac{a_0 + 1 + \frac{1}{2}e^s}{a_0 + \frac{1}{2}} \,. \tag{4.3.10}$$

One readily finds that

$$a_0 = \frac{1}{e^s - 1} \,, \quad a_0 + 1 = \frac{1}{1 - e^{-s}} \,. \tag{4.3.11}$$

With this result one can check that the two vertical lines for the right strip are located at

$$\Re(z) = a_0 + \frac{1}{2} = \frac{1}{2}\coth\left(\frac{s}{2}\right) \,, \quad \text{and} \quad \Re(z) = a_0 + 1 + \frac{1}{2}e^s = e^s \cdot \frac{1}{2}\coth\left(\frac{s}{2}\right) \,. \tag{4.3.12}$$

The map $w = -\ln(2z) + i\pi$ in (4.2.9) takes the full left and right strips to the w-frame picture in Figure 4-7(c). This picture is similar to that in Figure 4-4(b), which refers to the vacuum graph. There is only one minor difference: the image of the right strip in Figure 4-7(c) is displaced some distance to the left. This happens because the coordinate $z(A)$ of the point A satisfies

$$z(A) = a_0 + \frac{1}{2} > \frac{1}{2} \quad \rightarrow \quad \Re\big(w(A)\big) < 0 \,. \tag{4.3.13}$$

Since both strips in Figure 4-7(b) work with identification $z \sim e^s z$, the w plane Figure 4-7(c) has the identification $w \sim w - s$. This w presentation is different from the earlier w presentation in which the coordinate half-disk for the external state appears as a semi-infinite strip (Figure 4-6(c)); the coordinate half-disk has been pushed up! The identification $w \sim w - s$ ensures that the map (4.2.30) takes the w-plane region to the annulus with modulus

$$\boxed{M = \frac{\pi}{s} \,.} \tag{4.3.14}$$

Inserting an external state to form the tadpole graph therefore did not affect the modulus of the annulus – the modulus (4.3.14) coincides with our result (4.2.34) for the modulus of the vacuum graph. The only evidence of the external state is that the top boundary of the annulus is split between the boundary AB of the coordinate half-disk with the puncture and the boundary BC generated by e^{-sL_R}. The surprisingly simple form of the modulus will turn out to be generic for one-loop diagrams in Schnabl gauge. In fact, we will find that the annulus modulus of a general one-loop diagram is a simple function that depends only on the Schwinger parameters of the propagators running in the loop; the Schwinger parameters of trees attached to the loop do not affect the modulus of the annulus.

4.3.3 Taking the $\lambda \to 0$ limit

We will now justify our construction of the map of the Schnabl tadpole diagram to the round annulus. Let us consider the λ-regulated version of the one-loop tadpole graph, first shown in Figure 4-6(b). We cut the diagram along the QQ' line to produce two disconnected pieces. Just

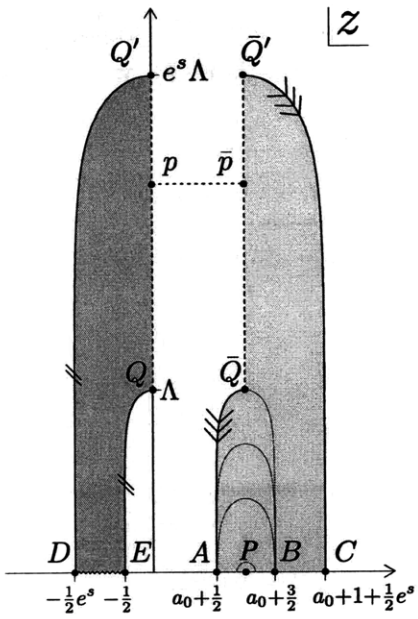

Figure 4-8: The z-frame λ-regulated one-loop tadpole of Figure 4-6 cut along QQ' and with the right piece translated to the right a distance a_0+1 so that the identification of A and C is through scaling by e^s. The figure is displayed for $\lambda = 10^{-4}$ and $s = 1$.

like we did for the Schnabl tadpole, we displace the right part of the figure to the right a distance $a_0 + 1$. The identifications on the left part of the surface still work with $z \sim e^s z$, but on the right they do not anymore. Choosing a_0 as before (see (4.3.11)) we ensure that the points A and C are still identified with $z \sim e^s z$, but this identification is only approximate for the other points on the curves $A\bar{Q}$ and $C\bar{Q}'$.

As before, the map $w = -\ln(2z) + i\pi$ takes the left part of Figure 4-8 (the surface associated with $e^{-sL_L^\lambda}$) to the familiar annular domain with identifications exactly given by $w \sim w - s$ (see Figure 4-9). Since $z(Q) = i\Lambda$ (see (4.2.23)) the image of QQ' in the w frame is shifted $\ln 2\Lambda$ to the left with respect to the image of the inner boundary DE.

For the map of the right part of Figure 4-8 we have to be a bit more careful. We will use the same map $w = -\ln(2z) + i\pi$, which results in a surface whose identification is not quite $w \sim w - s$ and thus cannot be interpreted as an annular region for general λ. Furthermore, the image of $\bar{Q}\bar{Q}'$ in the w frame does not quite coincide with the image of QQ'. What we are going to show is that in the limit as $\lambda \to 0$ (and consequently $\Lambda \to \infty$) the identifications needed to form the full annulus become exact. More precisely, as $\lambda \to 0$ two things should happen:

1. All points $p \in QQ'$ and $\bar{p} \in \bar{Q}\bar{Q}'$ that are at the same height (and should therefore be identified), are mapped to points on the w frame that approach each other as $\lambda \to 0$. This convergence is uniform on QQ' ensuring that the top and bottom parts of the annulus glue well.

2. Points $q \in A\bar{Q}$ and $q' \in A\bar{Q}'$ that must be identified will map to coordinates w that satisfy

$w(q) - w(q') = s$ in the limit $\lambda \to 0$. This convergence is uniform on $A\bar{Q}$, ensuring that the top part of the annulus works with the same identification $w \sim w - s$ as the bottom part.

If these two claims hold, it justifies the prescription given in the previous subsection for the Schnabl limit. In the remainder of this subsection we will prove (1) and (2).

Consider first claim (1) regarding the gluing of QQ' to $\bar{Q}\bar{Q}'$. Let $ix\Lambda$, with x a real number, denote the imaginary part of a point $p \in QQ'$ that must be identified with a point $\bar{p} \in \bar{Q}\bar{Q}'$ with the same imaginary part. Since the imaginary part of any point p (or $\bar{p}$) ranges between Λ and $e^s\Lambda$ we have

$$1 \le x \le e^s \quad \to \quad \Lambda \le x\Lambda \le e^s\Lambda\,. \tag{4.3.15}$$

We then have

$$z(p) = \imath\, x\Lambda\,, \quad z(\bar{p}) = a_0 + 1 + i\, x\Lambda = \frac{1}{1-e^{-s}} + i\, x\Lambda\,, \tag{4.3.16}$$

where we made use of (4.3.11). Using (4.2.9) we get

$$w(\bar{p}) - w(p) = -\ln\Big[\frac{z(\bar{p})}{z(p)}\Big] = -\ln\Big[1 + \frac{1}{ix\Lambda(1-e^{-s})}\Big] \tag{4.3.17}$$

As $\lambda \to 0$ we have $\Lambda \to \infty$. It is then clear that for any fixed value of $s > 0$ and any $x \in [1, e^s]$ the above gives $w(\bar{p}) - w(p) \to 0$. Furthermore, it follows from (4.3.17) and $x \ge 1$ that the convergence of $\bar{Q}\bar{Q}'$ to QQ' is uniform. This proves claim (1).

It is interesting to discuss the above result in more detail. We show in Figure 4-9 two examples of the w plane surface, both for $s = 1$. The top figure uses $\lambda = 10^{-4}$ and the bottom one uses $\lambda = 10^{-14}$. One can see the image of $\bar{Q}\bar{Q}'$ as the sloping edge that approaches (as we go from the top figure to the bottom figure) the horizontal image of QQ'. Expanding the logarithm in (4.3.17) we get

$$w(\bar{p}) - w(p) = i\,\frac{1}{x\Lambda(1-e^{-s})} - \frac{1}{2}\,\frac{1}{x^2\Lambda^2(1-e^{-s})^2} + \mathcal{O}(\Lambda^{-3})\,. \tag{4.3.18}$$

The vertical distance between the images of p and $\bar{p}$ vanishes as Λ^{-1}. The horizontal distance vanishes faster, as fast as Λ^{-2}. These features are clearly seen in the figure for the pair $\bar{Q}$, Q, and for the pair $\bar{Q}'$, Q'. Furthermore, the vertical convergence of Q' to $\bar{Q}'$ in the w frame is faster by a factor of e^s than the vertical convergence of Q to Q'. This is due to the suppression factor $\frac{1}{x}$ in the imaginary part of (4.3.18), and is clearly visible in the figure.

Let us now address claim (2). Before the translation is performed (see Figure 4-6(b)), the identified curves AQ and CQ' are parameterized as shown in (4.3.1). After the translation by $a_0 + 1$, we obtain Figure 4-8 with the curves $A\bar{Q}$ and $C\bar{Q}'$ given by

$$A\bar{Q} = a_0 + \tfrac{1}{2} + \gamma_L^\lambda\,, \qquad C\bar{Q}' = a_0 + 1 + e^s\big(\tfrac{1}{2} + \gamma_R^\lambda\big)\,. \tag{4.3.19}$$

These parameterized curves are identified. The (complex) ratio $r(\theta)$ between identified points on the curves is given by

$$r(\theta) = \frac{a_0 + 1 + e^s\big(\frac{1}{2} + \gamma_R^\lambda(\theta)\big)}{a_0 + \frac{1}{2} + \gamma_L^\lambda(\theta)} = e^s \cdot \frac{\gamma_R(\theta) + \frac{1}{2}\coth\frac{s}{2}}{\gamma_L(\theta) + \frac{1}{2}\coth\frac{s}{2}}\,, \tag{4.3.20}$$

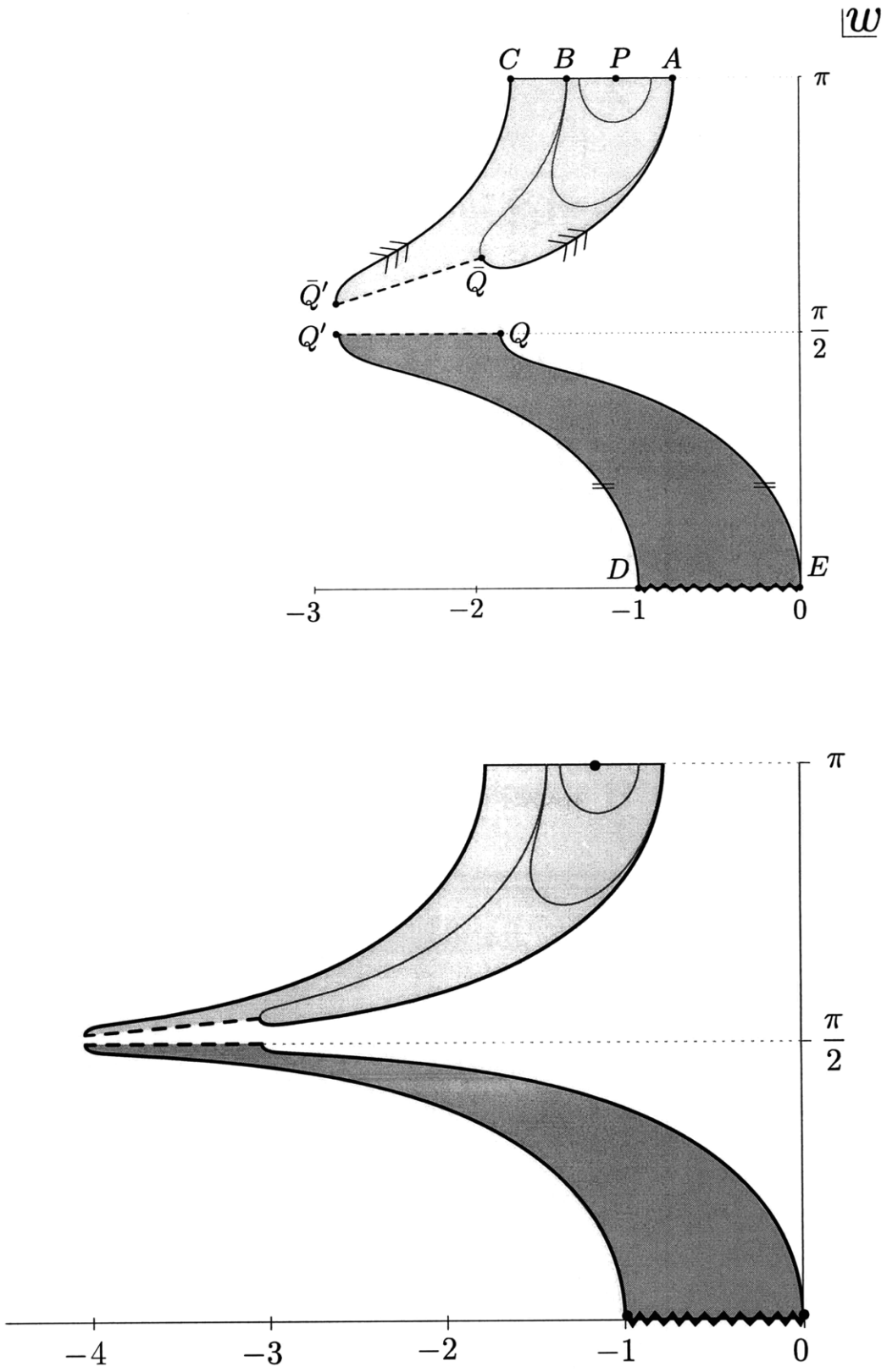

Figure 4-9: The λ-regulated one-loop tadpole in the plane $w = -\ln(2z) + i\pi$. The top figure arises for $\lambda = 10^{-4}$ and the bottom figure arises for $\lambda = 10^{-14}$. Both figures use $s = 1$.

where we used the definition (4.3.11) of the shift $a_0 + 1$ as well as (4.3.12). We must show that this ratio has the limit

$$r(\theta) \to e^s \qquad \text{for} \quad \lambda \to 0\,, \quad 0 \le \theta \le \tfrac{\pi}{2}\,. \tag{4.3.21}$$

If this is so, the map to the w plane (via the logarithm) will imply that the points corresponding to θ are separated by a horizontal translation by s. To make the map to the annulus well defined in the limit $\lambda \to 0$, we need this horizontal separation by s to hold to arbitrary precision for all points on the identified curves, i.e. we need the limit (4.3.21) to hold *uniformly* on $0 \le \theta \le \frac{\pi}{2}$.

One finds $r(\theta = 0) = e^s$, exactly, as expected for the ratio of the base points A and C of the two curves. Indeed, the translation was designed to make the identification $z \sim e^s z$ work on the real axis. For general θ, a short calculation gives

$$r(\theta) = e^s \cdot \frac{1 + \delta(\theta)}{1 - \delta(\theta)}\,, \quad \text{with} \quad \delta = \frac{\gamma_R - \gamma_L}{\gamma_R + \gamma_L + \coth\frac{s}{2}} = \frac{\Re\big(\gamma_R\big)}{i\Im\big(\gamma_R\big) + \frac{1}{2}\coth\frac{s}{2}}\,, \tag{4.3.22}$$

where we used $\gamma_L = -\overline{\gamma_R}$ in the last step. As we map the two points in question to the w plane, their separation is given by $\ln r$. We obtain

$$\ln r = s + \ln\Big(\frac{1-\delta}{1+\delta}\Big)\,. \tag{4.3.23}$$

We want to show that δ goes to zero uniformly on $0 \le \theta \le \frac{\pi}{2}$ when $\lambda \to 0$. We are going to break the curve γ_R into two parts: (i) the top part for which $\Im(\gamma_R) \in [\Lambda/2, \Lambda]$ and (ii) the bottom part for which $\Im(\gamma_R) \in [0, \Lambda/2]$. We recall from (4.2.29), that this corresponds to splitting the range of θ at $\theta = \theta_{\frac{1}{2}}$. Consider the top part (i). In this region we estimate

$$\big|\delta\big| = \left|\frac{\Re\big(\gamma_R\big)}{i\Im\big(\gamma_R\big) + \frac{1}{2}\coth\frac{s}{2}}\right| \le \frac{\operatorname{Max}\Re\big(\gamma_R\big)}{\operatorname{Min}\Im\big(\gamma_R\big)} = \frac{\frac{1}{2}}{\frac{\Lambda}{2}} = \frac{1}{\Lambda} \tag{4.3.24}$$

so that

$$\big|\delta(\theta)\big| \le \frac{1}{\Lambda} \qquad \text{for} \quad \theta \in \big[\theta_{\frac{1}{2}}, \tfrac{\pi}{2}\big]\,. \tag{4.3.25}$$

Now consider region (ii), i.e. $0 \le \theta \le \theta_{\frac{1}{2}}$. Recall our earlier estimate (4.2.29) that at $\theta = \theta_{\frac{1}{2}}$ the coordinate curve has indeed risen to a height of $\Lambda/2$ and that

$$\Re\Big(\gamma_R\big(\theta_{\frac{1}{2}}\big)\Big) = -\frac{1}{2\pi}\sqrt{2\lambda}\,. \tag{4.3.26}$$

In this region $\Im(\gamma_R)$ can be arbitrarily small, and $|\Re(\gamma_R)|$ reaches its maximal value at $\theta = \theta_{\frac{1}{2}}$. We thus estimate

$$|\delta| = \left|\frac{\Re(\gamma_R)}{i\Im(\gamma_R) + \frac{1}{2}\coth\frac{s}{2}}\right| \le \left|\frac{\Re(\gamma_R)}{\frac{1}{2}\coth\frac{s}{2}}\right| \le \frac{\frac{1}{2\pi}\sqrt{2\lambda}}{\frac{1}{2}} = \frac{1}{\pi}\sqrt{2\lambda} \tag{4.3.27}$$

for region (ii), so that

$$\big|\delta(\theta)\big| \le \frac{1}{\pi}\sqrt{2\lambda} \qquad \text{for} \quad \theta \in \big[0, \theta_{\frac{1}{2}}\big]\,. \tag{4.3.28}$$

We now have upper bounds on δ valid for the regions (i) and (ii). For any $\lambda < 1$ the upper bound in (4.3.25) for region (i) is larger than that in (4.3.28) for region (ii). Therefore we obtain the uniform upper bound

$$\big|\delta(\theta)\big| \le \frac{1}{\Lambda} \quad \text{for all} \quad \theta \in \big[0, \tfrac{\pi}{2}\big]\,, \quad \lambda < 1\,. \tag{4.3.29}$$

This means that $\delta(\theta)$ will vanish uniformly on $0 \leq \theta \leq \frac{\pi}{2}$ as $\lambda \to 0$, as we wanted to prove. This establishes the second claim, and thus completes the argument that shows that regulation leads to the claimed simple map in Schnabl gauge.

We conclude with a comment concerning the Schnabl gauge limit. In the unregulated case, shown in Figure 4-7(b), we see that the left and right cylinders are supposed to be glued at $i\infty$. It may seem as if the gluing involves both the coordinate patch strip of the external state and the strip to the right of it. The regulation shows that this is not quite the way things work. The coordinate frame for the external state tapers out and does not glue to the bottom part of the diagram, which arises from the left cylinder. The tip $\bar{Q}$ of the local coordinate frame (the string midpoint) lies at the end of the gluing line. As can be seen in Figure 4-9, at $\bar{Q}$ the coordinate curve goes both up towards B and down to eventually reach A. The behavior at $\bar{Q}$ follows from conformality to the z frame, as shown in Figure 4-8.

4.4 Slanted wedges: A family of surfaces

Loop amplitudes in Schnabl gauge use surfaces that do not feature in tree amplitudes. As we have seen in the previous sections, we sometimes deal with semi-infinite strips that look like the familiar wedge surfaces, except that the vertical edges are subject to identifications that are slanted. For wedge surfaces, presented as vertical semi-infinite strips, the natural identification of the vertical edges is a horizontal translation by the width a of the wedge.

It turns out to be convenient to introduce a set of surfaces that generalize the wedge surfaces. They will be called *slanted* wedges and are characterized by two parameters: the width a of the underlying wedge and the slant b, to be defined below. There is one important difference between wedges and slanted wedges. Associated with wedges there are wedge states but there are no surface states associated with slanted wedges.

For wedge surfaces, the surface states are based on once-punctured disks. The disk is formed by attaching the left edge of the wedge surface to the right edge of a unit-width wedge coordinate frame (with a marked point, or puncture) and gluing the two remaining vertical edges with a horizontal identification. The resulting surface is a semi-infinite cylinder with a puncture on the boundary at the real axis. This surface can be conformally mapped to a disk. More precisely, the disk has an inner puncture because it misses one point, the image of $i\infty$ on the wedges. This missing point can be ignored. The situation is far more serious for slanted wedges. As we have seen in the construction of the one-loop tadpole, a wedge with a slanted identification has a hidden boundary at $i\infty$, a boundary that must be glued to another surface. Instead of having a vanishingly small additional boundary associated with a missing point, as in the case for wedges, slanted wedges have an additional boundary that cannot be ignored. As a result there are no canonical surface states associated with slanted wedges. The hidden boundaries of slanted wedges can be brought into the open by λ-regularization.

Even without associated states, we can define a kind of star algebra of slanted wedges. While not strictly needed for tree diagrams, slanted wedges simplify significantly the construction of the associated Riemann surfaces. For loop diagrams slanted wedges are key to the construction of the relevant Riemann surfaces.

4.4.1 Definition and examples

The slanted wedge $[a;b]$, with $a, b \geq 0$, is defined on the upper-half plane z as the semi-infinite strip between $\Re(z) = \frac{1}{2}$ and $\Re(z) = \frac{1}{2} + a$:

$$[a;b] \equiv \left\{ z \,\middle|\, \frac{1}{2} \leq \Re(z) \leq \frac{1}{2} + a\,,\ \Im(z) \geq 0 \right\}. \tag{4.4.1}$$

The above states that, as a region, $[a;b]$ is the wedge of width a, positioned so that the left boundary is $\Re(z) = \frac{1}{2}$. By definition, the left boundary $\Re(z) = \frac{1}{2}$ carries the parameterization induced by the sliver map $z = \frac{2}{\pi}\tan^{-1}\xi$. More explicitly, the point $\xi = e^{\imath\theta}$ is mapped to

$$\text{Left Boundary:}\quad e^{\imath\theta} \to \tfrac{1}{2} + \gamma(\theta) \qquad\qquad \text{with}\quad 0 \leq \theta \leq \frac{\pi}{2}\,, \tag{4.4.2}$$

where the curve $\gamma(\theta)$ was defined in (4.2.26). It follows that the left boundary of $[a;b]$ glues naturally to a coordinate patch $-\frac{1}{2} \leq \Re(z) \leq \frac{1}{2}$ of the sliver frame. The slant parameter $b > 0$ is a scaling factor for the parameterization of the right boundary $\Re(z) = \frac{1}{2} + a$ of $[a;b]$. We have

$$\text{Right Boundary:}\quad e^{\imath\theta} \to \tfrac{1}{2} + a + b\cdot\gamma(\theta) \quad \text{with}\quad 0 \leq \theta \leq \frac{\pi}{2}\,. \tag{4.4.3}$$

This implies that the parameterization of the right boundary is obtained by stretching that of the left boundary by the factor b. See Figure 4-10(a) for a representation of the slanted wedge $[a;b]$. For $b = 1$ both boundaries of the slanted wedge carry the same parameterization and are thus horizontal translations of each other. Thus $[a;1]$ is just the familiar ordinary wedge surface of width a:

$$[a;1] = W_a\,. \tag{4.4.4}$$

Fock space states are described as $[1;1]$ with a local operator insertion at $z = 1$ between the two boundaries. The Fock space state insertion is mapped from $\xi = 0$ to $[1;1]$ via $z = 1 + \frac{2}{\pi}\tan^{-1}\xi$. In general, slanted wedges can carry operator insertions or line integrals.

Since slanted wedges are Riemann surfaces we have some equivalence relations that must be noted. First, the position of the slanted wedge can be altered. While $[a;b]$ is always assumed to have a left boundary $\Re(z) = \frac{1}{2}$, a translation by a real constant can be used to position the slanted wedge elsewhere. This is useful to form star products, for example. Sometimes we have to deal with wedge regions where both edges carry scaled parameterizations. We could call such surfaces $[b_L;a;b_R]$ with b_L and b_R denoting the scaling factors for the left and the right edges, respectively. Explicitly, this means that the parameterizations of the left and right boundaries in (4.4.2) and (4.4.3) are replaced by $\frac{1}{2} + b_L\gamma(\theta)$ and $\frac{1}{2} + a + b_R\gamma(\theta)$, respectively. This surface, under the map $z \to z/b_L$ and a possible translation, gives us the conformal identification

$$[b_L;a;b_R] \ \sim\ [a/b_L\,;b_R/b_L]\,. \tag{4.4.5}$$

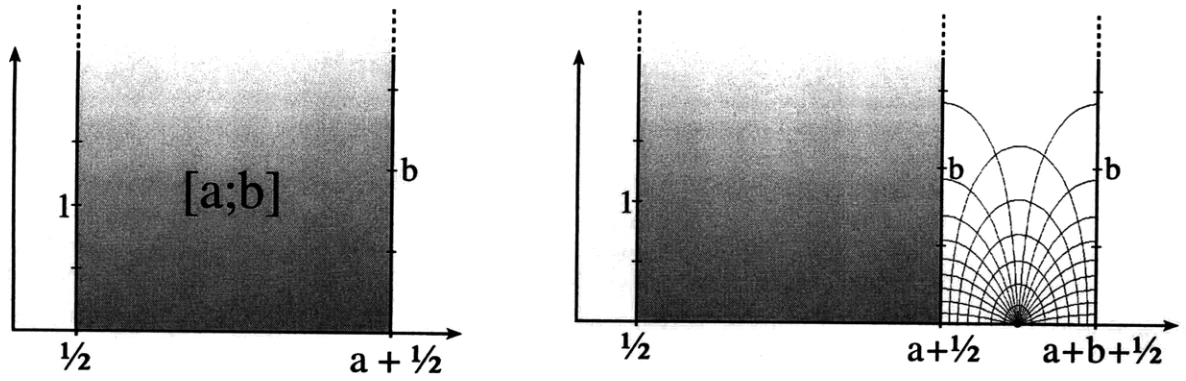

(a) (b)

Figure 4-10: (a) The slanted wedge $[a;b]$ in the sliver frame z. (b) Illustration of the star multiplication of a slanted wedge $[a;b]$ with a Fock space state $[1;1]$. The result is a slanted wedge $[a+b;b]$.

We obtain a wedge of width a/b_L with unit scaling on the left boundary and scaling b_R/b_L on the right boundary. The above shows that we do not have to define slanted wedges with scaled parameterizations on both edges.

4.4.2 Operations on slanted wedges

In order to create the surfaces relevant to the Feynman rules we need to introduce the "star-multiplication" of slanted wedges. For plain wedges the star multiplication is homomorphic to the star multiplication of the corresponding wedge states. Since we have no states associated with slanted wedges, their star multiplication is only a device to construct interesting surfaces.

As for surface states, we define star multiplication as the gluing of the right boundary of the first surface to the left boundary of the second surface. This gluing, however, requires identical parameterizations. For two slanted wedges $[a_1;b_1]$ and $[a_2;b_2]$, we define

$$\boxed{[a_1;b_1] * [a_2;b_2] \equiv [\,a_1 + b_1 a_2\,;\, b_1 b_2\,]\,.} \tag{4.4.6}$$

The logic behind this is clear: since the right boundary of the first slanted wedge carries a scaling b_1, the second slanted wedge must be fully scaled by b_1 so that its left boundary carries the same scaling. In this process its width becomes $b_1 a_2$ and the scaling of its right boundary $b_1 b_2$. Once the surfaces are glued, we get a total width of $a_1 + b_1 a_2$ and a scaling factor $b_1 b_2$, which applies to the right boundary.

Clearly, slanted wedges form a closed algebra under the star multiplication and plain wedges form a commutative subalgebra. The algebra (4.4.6) of slanted wedges $[a;b]$ can also be represented as the algebra of matrices of the form

$$[a;b] \leftrightarrow \begin{pmatrix} b & a \\ 0 & 1 \end{pmatrix}\,. \tag{4.4.7}$$

Indeed, in agreement with (4.4.6) we then have

$$\begin{pmatrix} b_1 & a_1 \\ 0 & 1 \end{pmatrix} \begin{pmatrix} b_2 & a_2 \\ 0 & 1 \end{pmatrix} = \begin{pmatrix} b_1 b_2 & a_1 + b_1 a_2 \\ 0 & 1 \end{pmatrix} . \tag{4.4.8}$$

A simple and useful particular case of (4.4.6) involves a Fock space state and a slanted wedge:

$$[a; b] * [1; 1] = [a + b\,; b] . \tag{4.4.9}$$

This example is illustrated in Figure 4-10(b). Note that in the final surface the puncture lies at $z = \frac{1}{2} + a + \frac{1}{2}b$, the first $\frac{1}{2}$ for the conventional offset, the a due to the first surface and $\frac{1}{2}b$ because the slanting required scaling the unit width of the Fock state surface by b.

We now consider the Schnabl gauge propagator. As we will see, its various ingredients act naturally on slanted wedges and can be themselves represented by slanted wedges. The classical propagator is given by

$$\mathcal{P} = \int ds ds^\star \, e^{-sL} \, B \, Q \, B^\star e^{-s^\star L^\star} = \int ds ds^\star \; B \, Q \, e^{-sL} e^{-s^\star L^\star} B^\star . \tag{4.4.10}$$

We will focus solely on the Riemann surface interpretation of this propagator, namely the action of $e^{-sL} e^{-s^\star L^\star}$ on surfaces. The presence of line integral insertions from B, Q, and $B^\star$ will not play a role in the following analysis.

We will construct the action of the propagator step by step, treating the operators e^{-sL_R}, e^{-sL_L}, $e^{-s^\star L_R^\star}$, and $e^{-s^\star L_L^\star}$ separately. As discussed in section 4.2.2 these operators generate hidden boundaries, which will now be associated with slanted wedges. For loop diagrams these boundaries require special attention.

Let us first consider the action of e^{-sL_R} on a general Fock space state $|F\rangle$. We represent $|F\rangle$ in the sliver frame z as the semi-infinite strip between $\Re(z) = -\frac{1}{2}$ and $\Re(z) = \frac{1}{2}$. The operator insertion of the Fock space state is mapped to $z = 0$ in the sliver frame via the map $z = \frac{2}{\pi} \tan^{-1} \xi$. Recalling the discussion of $\mathcal{R}(s)$ in section 4.3, we see that $e^{-sL_R}|F\rangle$ is represented in the z frame by gluing a strip of width $\frac{1}{2}(e^s - 1)$ to the right boundary of $|F\rangle$ (Figure 4-4). The parametrization of the right boundary on the resulting surface, however, has a scaling factor e^s. We conclude that e^{-sL_R} attaches to the right of $|F\rangle$ the slanted wedge $[\frac{1}{2}(e^s - 1); e^s]$ (see Figure 4-11(a)). Having determined that e^{-sL_R} is represented by the right attachment of the slanted wedge $[\frac{1}{2}(e^s - 1); e^s]$, it follows that, more generally,

$$e^{-sL_R} \, [a; b] = [a; b] * [\tfrac{1}{2}(e^s - 1); e^s] . \tag{4.4.11}$$

The slanted wedge $[a; b]$ has hidden boundaries and the action of e^{-sL_R} introduces an additional one that stems from cutting the propagator surface $\mathcal{R}(s)$. We have seen this hidden boundary emerge through λ-regularization as the line $\bar{Q}\bar{Q}'$ displayed in Figure 4-8.

Similarly, e^{-sL_L} glues a strip of width $\frac{1}{2}(e^s - 1)$ to the left boundary of $|F\rangle$. Now the *left* boundary of the resulting surface has a parametrization which is scaled by e^s (see Figure 4-11(a)).

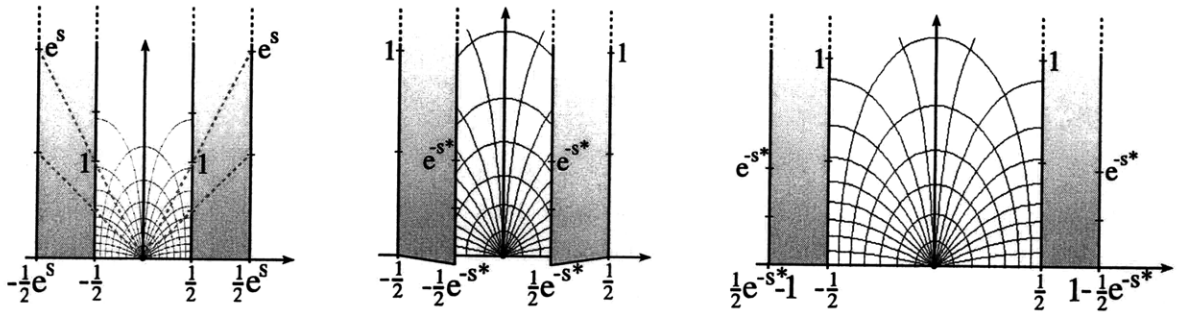

Figure 4-11: (a) The action of e^{-sL} on a Fock space state adds the shaded strips on both sides of the Fock space state. The shaded strip on the right represents e^{-sL_R}, the shaded strip on the left represents e^{-sL_L}. The dashed grey lines illustrate the rescaling of the parameterizations from the inner to the outer boundaries. (b) The action of $e^{-s^\star L^\star}$ on a Fock space state creates the shaded strips which lie on top of the Fock space state surface. (c) The action of $e^{-s^\star L^\star}$ on a Fock space state after flipping the strips of the propagator.

To interpret this added piece of strip as a slanted wedge, we need to rescale it by a factor e^{-s} so that its left boundary has canonical parameterization. We conclude that the action e^{-sL_L} on $|F\rangle$ glues the slanted wedge $[\frac{1}{2}(1-e^{-s}); e^{-s}]$ to the left boundary of $|F\rangle$. This generalizes to

$$e^{-sL_L}\,[a;b] = [\tfrac{1}{2}(1-e^{-s}); e^{-s}] * [a;b]\,. \tag{4.4.12}$$

It follows from (4.4.11) and (4.4.12) that

$$e^{-s_R L_R} e^{-s_L L_L}[a;b] = e^{-s_L L_L} e^{-s_R L_R}[a;b]\,, \tag{4.4.13}$$

for all values of s_L and s_R. We thus conclude that acting on slanted wedges the operators L_L and L_R commute. The action of e^{-sL} on a given slanted wedge can be calculated as follows

$$\begin{aligned} e^{-sL}[a;b] &= e^{-s(L_L+L_R)}[a;b] = e^{-sL_L} e^{-sL_R}[a;b] \\ &= [\tfrac{1}{2}(1-e^{-s}); e^{-s}] * [a;b] * [\tfrac{1}{2}(e^{s}-1); e^{s}]\,, \end{aligned} \tag{4.4.14}$$

and therefore

$$e^{-sL}[a;b] = [\tfrac{1}{2}(1+b)(1-e^{-s}) + ae^{-s}\,; b]\,. \tag{4.4.15}$$

For the particularly important case of $b=1$, the above reduces to

$$\boxed{e^{-sL}\,[a;1] = [1+(a-1)e^{-s}\,;\,1]\,.} \tag{4.4.16}$$

Since $[a;1]$ is a wedge state, this identity can be readily confirmed by familiar methods (see eqn. (A.27) of [45]).

The geometric interpretation of $e^{-s^\star L^\star}|F\rangle$ is somewhat more intricate. In the construction of $e^{-sL}|F\rangle$ we glue the *right* boundary of the w-frame strip $\mathcal{R}(s)$ to the coordinate curve of $|F\rangle$. This

boundary of $\mathcal{R}(s)$ is mapped by (4.2.10) to the coordinate curve $\Re(z) = \pm\frac{1}{2}$ and the gluing to the Fock space state works out naturally, as shown in Figure 4-11(a). It follows from the discussion in [46] that the surface corresponding to $e^{-s^\star L^\star}$ can be obtained by gluing the *left* boundary of the w-frame $\mathcal{R}(s^\star)$ to the coordinate curve of $|F\rangle$. This left boundary of $\mathcal{R}(s^\star)$ is mapped by (4.2.10) to $\Re(z) = \pm\frac{1}{2}e^{s^\star}$ and the strip develops inwards up to $\Re(z) = \pm\frac{1}{2}$. To glue the chosen boundary of $\mathcal{R}(s^\star)$ to the coordinate curve at $\Re(z) = \pm\frac{1}{2}$, we rescale $\mathcal{R}(s^\star)$ by $z \to e^{-s^\star} z$. The result, illustrated in Figure 4-11(b), is that $e^{-s^\star L_R^\star}$ acting on the sliver-frame $|F\rangle$ introduces a strip between $\frac{1}{2}e^{-s^\star}$ and $\frac{1}{2}$, which is glued to the Fock space state at $\Re(z) = \frac{1}{2}$. In this presentation the surface added by $e^{-s^\star L_R^\star}$ lies on top of the Fock state surface. The parameterization of the left boundary of this added strip is shrunk by a factor of $e^{-s^\star}$. We can flip the surface of $e^{-s^\star L_R^\star}$ around the axis $\Re(z) = \frac{1}{2}$ to obtain the result shown in Figure 4-11(c). We have thus found that $e^{-s^\star L_R^\star}$ attaches the left boundary of the slanted wedge $[\frac{1}{2}(1-e^{-s^\star}); e^{-s^\star}]$ to the right boundary of $|F\rangle$. On general slanted wedges

$$e^{-s^\star L_R^\star}\,[a;b] = [a;b] * [\tfrac{1}{2}(1-e^{-s^\star}); e^{-s^\star}]\,. \tag{4.4.17}$$

Similarly, we obtain

$$e^{-s^\star L_L^\star}\,[a;b] = [\tfrac{1}{2}(e^{s^\star}-1); e^{s^\star}] * [a;b]\,. \tag{4.4.18}$$

We notice from (4.4.11), (4.4.12), (4.4.17), and (4.4.18) that the slanted wedges associated with $e^{-s^\star L_L^\star}$ and $e^{-s^\star L_R^\star}$ can be obtained from those associated with e^{-sL_R} and e^{-sL_L}, respectively, by letting $s \to s^\star$. This is not a peculiarity of Schnabl gauge; it follows because the surface $\mathcal{R}^\star(s^\star)$ generated $e^{-s^\star \mathcal{L}^\star}$ can be obtained from the surface $\mathcal{R}(s)$ generated by $e^{-s\mathcal{L}}$ from a reflection in the w frame [46].

The action of $e^{-s^\star L^\star}$ on a given slanted wedge can be calculated from

$$e^{-s^\star L^\star}[a;b] \equiv e^{-s^\star L_L^\star} e^{-s^\star L_R^\star}[a;b] = [\tfrac{1}{2}(e^{s^\star}-1); e^{s^\star}] * [a;b] * [\tfrac{1}{2}(1-e^{-s^\star}); e^{-s^\star}] \tag{4.4.19}$$

and gives

$$e^{-s^\star L^\star}[a;b] = [\tfrac{1}{2}(1+b)(e^{s^\star}-1) + ae^{s^\star}\,; b]\,. \tag{4.4.20}$$

For the case of surface states the above reduces to the identity

$$\boxed{e^{-s^\star L^\star}\,[a;1] = [(1+a)e^{s^\star} - 1; 1]\,.} \tag{4.4.21}$$

that is readily confirmed by familiar methods (see eqn. (A.28) of [45]).

From (4.4.11), (4.4.12), (4.4.17), and (4.4.18) we find that the left and right parts of the classical propagator act on a slanted wedge $[a;b]$ as

$$\boxed{\begin{aligned} e^{-sL_R} e^{-s^\star L_R^\star}\,[a;b] &= [a;b] * [\tfrac{1}{2}(1+e^{s-s^\star}) - e^{-s^\star}\,;\, e^{s-s^\star}]\,, \\ e^{-sL_L} e^{-s^\star L_L^\star}\,[a;b] &= [\tfrac{1}{2}(1+e^{s^\star-s}) - e^{-s}\,;\, e^{s^\star-s}] * [a;b]\quad. \end{aligned}} \tag{4.4.22}$$

It now follows that the action of the classical propagator (4.4.10) on a slanted wedge $[a;b]$ is given by:

$$e^{-sL}e^{-s^\star L^\star}[a;b] = [\,\tfrac{1}{2}(1+b)(1+e^{s^\star-s}-2e^{-s})+a\,e^{s^\star-s}\,;\,b\,]\,. \tag{4.4.23}$$

On wedge states $[a;1]$, this simplifies to

$$\boxed{e^{-sL}e^{-s^\star L^\star}[a;1] = \big[1-2e^{-s}+(1+a)e^{s^\star-s}\,;\,1\big]\,.} \tag{4.4.24}$$

As we have emphasized, there are no states associated with slanted wedges $[a;b]$ for $b \neq 1$. Such surfaces are incomplete, they have a *hidden* vertical boundary segment at $i\infty$. Since eventually no hidden boundary can remain, a surface $[a;b]$ with $b \neq 1$, will have its hidden boundary glued to that of a compensating surface $[\hat{a};1/b]$ with inverse slant factor. This will be especially relevant when we build general one-loop diagrams in section 4.6. There we construct compensating slanted wedges $[a;e^{s_{\rm eff}}]$ and $[\hat{a};e^{-s_{\rm eff}}]$ which can then be mapped to the annulus. For tree diagrams the situation is simpler: the total surface representing the diagram is always of the form $[a;1]$, with horizontal identifications applied to the vertical edges.

4.4.3 Keeping track of insertions on slanted wedges

The open string moduli are encoded in the positions of punctures on the corresponding Riemann surfaces. As we will use slanted wedges to describe these surfaces, we need to keep track of operator insertions on slanted wedges. We denote by

$$[\,a;b\,|x_1,x_2,\ldots,x_k]\,,\quad \text{with}\quad \tfrac{1}{2}\le x_1\le x_2\le\ldots\le x_k\le\tfrac{1}{2}+a\,, \tag{4.4.25}$$

a slanted wedge with marked points at real coordinates x_i. The wedge is presented, as usual, with its left boundary above $z=\frac{1}{2}$. When star multiplying two slanted wedges, the position x of a marked point on the first slanted wedge is unaffected:

$$[\,a;b\,|x]*[\,a';b'] = [a+ba';bb'\,|\,x\,]\,. \tag{4.4.26}$$

A puncture at x' on the second wedge, on the other hand, is displaced and experiences scaling:

$$[\,a;b\,]*[\,a';b'\,|x'] = [a+ba';bb'\,|\,\tfrac{1}{2}+a+b(x'-\tfrac{1}{2})\,]\,. \tag{4.4.27}$$

From this one can readily verify that

$$\begin{aligned}
e^{-sL_L}[\,a;b\,|x] &= [\,\ldots;\ldots\,|\,1-e^{-s}+e^{-s}x\,]\,,\\
e^{-sL_R}[\,a;b\,|x] &= [\,\ldots;\ldots\,|\,x\,]\,,\\
e^{-s^\star L^\star_L}[\,a;b\,|x] &= [\,\ldots;\ldots\,|\,e^{s^\star}x\,]\,,\\
e^{-s^\star L^\star_R}[\,a;b\,|x] &= [\,\ldots;\ldots\,|\,x\,]\,.
\end{aligned} \tag{4.4.28}$$

We put dots ... on the width and slant parameters of the resulting wedges because these values are unaffected by the punctures and were given earlier. Note that the exponentials of right operators

do not affect the position since they add a slanted wedge from the right. It follows from the above relations that

$$e^{-sL}\, e^{-s^\star L^\star}\, [\, a; b\,|x] = [\ \dots\ ;\ \dots\ \mid 1 - e^{-s} + e^{s^\star - s} x\,]\,. \tag{4.4.29}$$

This formula generalizes easily to the case of additional punctures: all $x_i \to 1 - e^{-s} + e^{s^\star - s} x_i$.

4.4.4 Representation of the L, $L^\star$ algebra on slanted wedges

It is known that one can view $L, L^\star, L^+ = L + L^\star$ as well as L_L^+ and L_R^+ as differential operators acting on the familiar wedge states. As we have learned, the left and right parts of L and $L^\star$ only act naturally on slanted wedges (acting on an ordinary wedge they will give a slanted wedge). In this section we represent $L_L, L_R, L_L^\star$ and $L_R^\star$, as differential operators on slanted wedges. This provides some further insight into slanted wedges, a check of this formalism and, as a by product, a tool to derive (or rederive) some identities.

Let us focus on the right part of the L and $L^\star$ operators. From (4.4.11) and (4.4.17) we have

$$\begin{aligned} L_R[a;b] &= -\frac{d}{ds}\Big|_{s=0} e^{-sL_R}\ [a;b] = (-\tfrac{1}{2} b\partial_a - b\partial_b)[a;b]\,, \\ L_R^\star[a;b] &= -\frac{d}{ds^\star}\Big|_{s^\star=0} e^{-s^\star L_R^\star}[a;b] = (-\tfrac{1}{2} b\partial_a + b\partial_b)[a;b]\,, \end{aligned} \tag{4.4.30}$$

and we identify the representation

$$L_R = -\tfrac{1}{2} b\partial_a - b\partial_b\,, \qquad L_R^\star = -\tfrac{1}{2} b\partial_a + b\partial_b\,. \tag{4.4.31}$$

For the left counterparts a similar calculation gives

$$L_L = (a - \tfrac{1}{2})\partial_a + b\partial_b\,, \qquad L_L^\star = -(a + \tfrac{1}{2})\partial_a - b\partial_b\,. \tag{4.4.32}$$

One can readily confirm that acting on slanted wedges the operators L_R and L_L commute, and so do $L_R^\star$ and $L_L^\star$. One can now recover the more familiar differential operators

$$L = -(\tfrac{1}{2}(1+b) - a)\partial_a\,, \quad L^\star = -(\tfrac{1}{2}(1+b) + a)\partial_a\,, \quad L^+ = L + L^\star = -(1+b)\partial_a\,. \tag{4.4.33}$$

It is now possible to calculate the commutator $[L, L^\star]$ by imagining it acting on a wedge state,

$$[L, L^\star] = [-(\tfrac{1}{2}(1+b) + a)\partial_a\,, -(\tfrac{1}{2}(1+b) - a)\partial_a] = -(1+b)\partial_a = L^+\,, \tag{4.4.34}$$

which is the expected result. In fact, even the right parts of $L, L^\star$, and L^+ obey the same equation, as one would expect,

$$[L_R, L_R^\star] = \left[-\tfrac{1}{2} b\partial_a + b\partial_b\,, -\tfrac{1}{2} b\partial_a - b\partial_b\right] = -b\partial_a = L_R^+\,. \tag{4.4.35}$$

Let us illustrate how one derives identities using the above representation of operators. Note first that

$$L_R^+ \equiv L_R + L_R^\star = -b\partial_a\,. \tag{4.4.36}$$

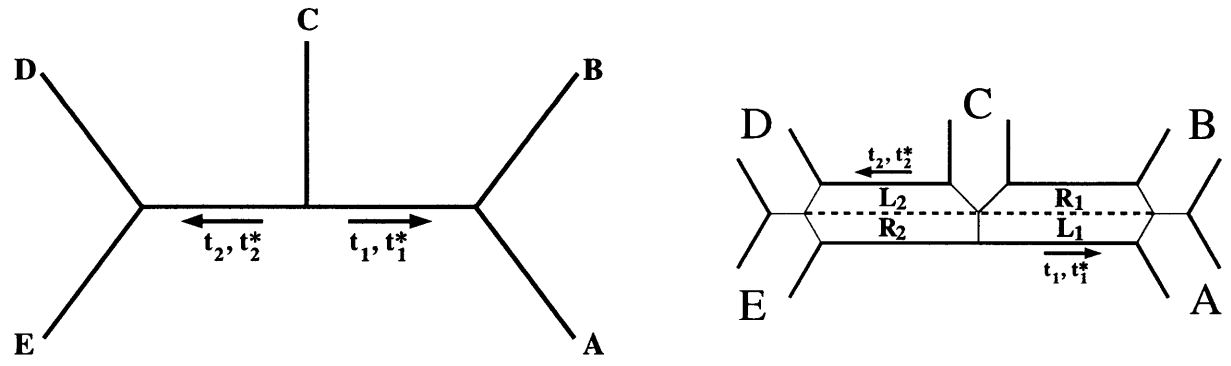

(a) (b)

Figure 4-12: (a) A Feynman diagram for a five-point amplitude. (b) The topology of the corresponding Riemann surface.

It then follows that

$$e^{-s^+L_R^+}[a;b] = [a + bs^+; b] = [a;b] * [s^+;1]\,, \tag{4.4.37}$$

showing that $e^{-s^+L_R^+}$ acts by right multiplying a wedge of length s^+. Additionally, for wedge states $[a;1]$ of width a we have

$$-L_R^+[a;1] = \partial_a[a;1]\,, \qquad [a;1] = e^{-aL_R^+}[0;1]\,, \tag{4.4.38}$$

where the zero-length wedge $[0;1]$ is the identity state $|\mathcal{I}\rangle$. Another example uses (4.4.22) and (4.4.37):

$$e^{-tL_R}e^{-tL_R^\star}[a;b] = [a;b] * [1 - e^{-t}\,;1] = e^{-(1-e^{-t})L_R^+}[a;b]\,, \tag{4.4.39}$$

leading us to conclude that $e^{-tL_R}e^{-tL_R^\star} = e^{-(1-e^{-t})L_R^+}$.

4.5 Riemann surfaces for tree-level diagrams

In this section we will use the technology of slanted wedges developed in the previous section to construct the punctured disks associated with tree diagrams. We start with the particularly simple case of a diagram with five external lines. We then sketch the construction for arbitrary tree-level diagrams.

4.5.1 The five-point diagram

Let us use the formalism of section 4.4 to construct the surface corresponding to the tree-level five-point diagram shown in Figure 4-12. Our goal is to determine the relative angles of the operator insertions on the unit disk. These are the open string moduli. There are, of course, no closed string moduli. All other diagrams contributing to the five point function are permutations of the external states in the diagram of Figure 4-12.

The diagram contains two internal propagators, parameterized by the Schwinger parameters $t_i, t_i^\star$ with $i = 1, 2$. Here and in the following we use the letter t for Schwinger parameters of propagators in tree diagrams (or subtrees of loop diagrams). As this is a tree-level diagram, the classical propagator (4.4.10) must be used on both lines. We use arrows to assign a direction to each propagator line in the diagram. At fixed Schwinger parameters the classical propagator on the $\imath$-th line acts as the operator $e^{-t_\imath L} BQB^\star e^{-t_\imath^\star L^\star}$ in the indicated direction, *i.e.* on the state representing the surface in the direction of the arrow. Equivalently, it acts as the BPZ conjugate operator $e^{-t_\imath^\star L} BQB^\star e^{-t_\imath L^\star}$ in the direction opposite to the arrow. Since the full propagator is BPZ invariant, amplitudes do not depend on this assignment after integration over Schwinger parameters. The selection of specific arrows is simply a convention that fixes which Schwinger parameter we call $t_\imath$ and which one we call $t_\imath^\star$.

Let us consider the part of the diagram consisting of the first propagator (t_1,$t_1^\star$) and the Fock space states $|F_A\rangle$, $|F_B\rangle$. Each Fock space state is of the form $[1; 1|1]$. Together, and acted by the propagator, they form the twice-punctured surface state

$$\begin{aligned} [a_1; 1 \,|\, x_A, x_B] &\equiv e^{-t_1 L} e^{-t_1^\star L^\star} \big([1; 1|1]_A * [1; 1\,|1]_B \big) \\ &= e^{-t_1 L} e^{-t_1^\star L^\star} \, [2; 1|1, 2] \\ &= [1 - 2e^{-t_1} + 3e^{t_1^\star - t_1}; 1 \,|\, x_A, x_B] \,, \\ \text{with} \qquad x_A &= 1 - e^{-t_1} + e^{t_1^\star - t_1} \\ x_B &= 1 - e^{-t_1} + 2e^{t_1^\star - t_1} \,, \end{aligned} \tag{4.5.1}$$

where we used (4.4.24) to calculate the wedge parameters and (4.4.29) to calculate the positions x_A and x_B of the punctures on the resulting wedge. Similarly, we can analyze the part of the diagram with the second propagator (t_2,$t_2^\star$) and the Fock space states $|F_D\rangle$, $|F_E\rangle$. They form the surface state

$$[a_2; 1 \,|\, x_D, x_E] \equiv e^{-t_2 L} e^{-t_2^\star L^\star} \big([1; 1|1]_D * [1; 1|1]_E \big) = [1 - 2e^{-t_2} + 3e^{t_2^\star - t_2}; 1|x_D, x_E \,] \,, \tag{4.5.2}$$

with the operator insertions corresponding to $|F_D\rangle$ and $|F_E\rangle$ located at

$$\begin{aligned} x_D &= 1 - e^{-t_2} + e^{t_2^\star - t_2} \,, \\ x_E &= 1 - e^{-t_2} + 2e^{t_2^\star - t_2} \,. \end{aligned} \tag{4.5.3}$$

To assemble the Riemann surface corresponding to the five-point diagram we glue the surfaces $[a_1; 1|x_A, x_B]$, $[1; 1|1]_C$ (corresponding to $|F_C\rangle$) and $[a_2; 1|x_D, x_E]$. We obtain the surface Σ given by

$$\begin{aligned} \Sigma &\equiv [a_1; 1|x_A, x_B] * [1; 1|1]_C * [a_2; 1|\, x_D, x_E] \\ &= [a_1 + a_2 + 1; 1|\, x_A,\, x_B,\; a_1 + 1,\; a_1 + 1 + x_D,\, a_1 + 1 + x_E] \,. \end{aligned} \tag{4.5.4}$$

In particular, we notice that the wedge Σ is not slanted. The two vertical boundaries of Σ are thus identified horizontally and the resulting surface is mapped to the unit disk η via

$$\eta = \exp\left(\frac{2\pi i z}{a}\right) \,, \quad a = a_1 + a_2 + 1 \,. \tag{4.5.5}$$

A horizontal distance Δx along the boundary of Σ translates into an angular separation $\Delta\phi$ on the unit disk given by

$$\frac{\Delta\phi}{2\pi} = \frac{\Delta x}{a} \,. \tag{4.5.6}$$

For the relative angles of the operator insertions on the boundary of the unit disk we thus obtain

$$\begin{aligned}
\frac{\phi_B - \phi_A}{2\pi} &= \frac{x_B - x_A}{a} &&= \frac{e^{t_1^\star - t_1}}{3 - 2e^{-t_1} - 2e^{-t_2} + 3e^{t_1^\star - t_1} + 3e^{t_2^\star - t_2}} \,, \\
\frac{\phi_C - \phi_A}{2\pi} &= \frac{a_1 + 1 - x_A}{a} &&= \frac{1 - e^{-t_1} + 2e^{t_1^\star - t_1}}{3 - 2e^{-t_1} - 2e^{-t_2} + 3e^{t_1^\star - t_1} + 3e^{t_2^\star - t_2}} \,, \\
\frac{\phi_D - \phi_A}{2\pi} &= \frac{a_1 + 1 + x_D - x_A}{a} &&= \frac{2 - e^{-t_1} + 2e^{t_1^\star - t_1} - e^{-t_2} + e^{t_2^\star - t_2}}{3 - 2e^{-t_1} - 2e^{-t_2} + 3e^{t_1^\star - t_1} + 3e^{t_2^\star - t_2}} \,, \\
\frac{\phi_E - \phi_A}{2\pi} &= \frac{a_1 + 1 + x_E - x_A}{a} &&= \frac{2 - e^{-t_1} + 2e^{t_1^\star - t_1} - e^{-t_2} + 2e^{t_2^\star - t_2}}{3 - 2e^{-t_1} - 2e^{-t_2} + 3e^{t_1^\star - t_1} + 3e^{t_2^\star - t_2}} \,.
\end{aligned} \tag{4.5.7}$$

This concludes the computation of angles for the string diagram in Figure 4-12. Of course, the positions of three of the punctures can be fixed arbitrarily, so there are just two open string moduli. As usual for amplitudes in non BPZ-invariant gauges, we have twice as many Schwinger parameters as moduli of the corresponding Riemann surface. Indeed, we have four Schwinger parameters (t_1, $t_1^\star$, t_2, $t_2^\star$). This is not a problem because each of the two propagators is accompanied by a BRST operator Q. In [45, 74], the classical propagator (4.4.10) was rewritten as

$$\mathcal{P} = \frac{B}{L} + \text{ other terms } \,, \tag{4.5.8}$$

and it turned out that the B/L term by itself covered the moduli space of on-shell amplitudes for the four-point function. All other terms only contributed off-shell.

It is therefore interesting to ask if there is an assignment of B/L and $B^\star/L^\star$ to the propagator lines in the five-point diagram which produces all the requisite open string degenerations: as a Schwinger parameter becomes large the associated line produces the degeneration represented by a long strip. That degeneration, moreover, must occur independent of the values of the other Schwinger parameters, even if they also go to infinity. Not every assignment works. If we assign $B^\star/L^\star$ to *both* propagators (namely, $t_1 = t_2 = 0$) making one Schwinger parameter large is not sufficient to guarantee an open string degeneration. In fact, for $t_1^\star = t_2^\star \to \infty$ the angles of the five insertions on the unit circle spread out over the circle, a configuration that is clearly not degenerate. This is not too surprising. If we had regarded the left propagator as acting to the right, we would have encountered the operator combination $e^{-t_2^\star L_L} e^{-t_1^\star L_L^\star}$ acting on the Fock space state $|F_A\rangle$. This product of operators has been noticed to produce interesting subtleties in [45]. Although both Schwinger parameters in the operator diverge, the resulting Riemann surface is perfectly regular. Indeed, acting on any slanted wedge we have from (4.4.22):

$$\begin{aligned}
\lim_{t_1^\star = t_2^\star \to \infty} e^{-t_2^\star L_L} e^{-t_1^\star L_L^\star} [a;b] &= \lim_{t_1^\star = t_2^\star \to \infty} [\tfrac{1}{2} + \tfrac{1}{2} e^{t_1^\star - t_2^\star} - e^{-t_2^\star} \,; e^{t_1^\star - t_2^\star}] * [a;b] = [1;1] * [a;b] \\
&= [a+1;b] \,.
\end{aligned} \tag{4.5.9}$$

In this limit the operator simply inserts the unit wedge $[1;1]$. This is a surface of finite width and finite rescaling and cannot induce an open string degeneration in any diagram. For all other

choices of assignments of B/L and $B^\star/L^\star$ to the two propagator lines, open string degenerations are always produced when we make any Schwinger parameter large. Details of this analysis are given in appendix A of [33].

4.5.2 General tree diagrams

The construction of the surface for the five-string diagram was particularly simple. For general tree-level diagrams we need to be more systematic. As we did for the five-string diagram we assign an arrow to each propagator, indicating the direction in which it acts. This assignment is arbitrary and will not affect the total set of surfaces created as the Schwinger parameters vary over their full range because the propagator is BPZ-invariant.

We now rewrite the five-string diagram in a way that makes the case for the general rules to be stated below. Let us revisit the surface considered in (4.5.1):

$$e^{-t_1 L} e^{-t_1^\star L^\star} \big([1;1|1]_A * [1;1\,|1]_B\big) = e^{-t_1 L_L} e^{-t_1^\star L_L^\star} e^{-t_1 L_R} e^{-t_1^\star L_R^\star} \big([1;1|1]_A * [1;1\,|1]_B\big)\,. \tag{4.5.10}$$

Recalling (4.4.22), we then find

$$\begin{aligned} & e^{-t_1 L} e^{-t_1^\star L^\star} \big([1;1|1]_A * [1;1\,|1]_B\big) \\ & = [\tfrac{1}{2}(1+e^{t_1^\star - t_1}) - e^{-t_1}\,;\, e^{t_1^\star - t_1}] * [1;1|1]_A * [1;1\,|1]_B * [\tfrac{1}{2}(1+e^{t_1 - t_1^\star}) - e^{-t_1^\star}\,;\, e^{t_1 - t_1^\star}] \\ & = L_1 * [1;1|1]_A * [1;1\,|1]_B * R_1\,, \end{aligned} \tag{4.5.11}$$

where we have defined the slanted wedges L_i and R_i associated with the left and right part of the i-th propagator:

$$L_i \equiv [\tfrac{1}{2}(1+e^{t_i^\star - t_i}) - e^{-t_i}\,;\, e^{t_i^\star - t_i}]\,, \qquad R_i \equiv [\tfrac{1}{2}(1+e^{t_i - t_i^\star}) - e^{-t_i^\star}\,;\, e^{t_i - t_i^\star}]\,. \tag{4.5.12}$$

It is now clear that (4.5.2) becomes:

$$e^{-t_2 L} e^{-t_2^\star L^\star} \big([1;1|1]_D * [1;1|1]_E\big) = L_2 * [1;1|1]_D * [1;1\,|1]_E * R_2\,. \tag{4.5.13}$$

Assembling now the full surface Σ as in (4.5.4) we have

$$\Sigma = L_1 * [1;1|1]_A * [1;1\,|1]_B * R_1 * [1;1|1]_C * L_2 * [1;1|1]_D * [1;1\,|1]_E * R_2\,. \tag{4.5.14}$$

Note that Σ is a wedge of unit slant factor (an ordinary wedge) because the slant factors of L_i and R_i are multiplicative inverses of each other. Since the right and left edges of Σ are to be identified, we can slide part of the wedge state from left to right, cyclically. We write, for convenience,

$$\Sigma = [1;1|1]_A * [1;1\,|1]_B * R_1 * [1;1|1]_C * L_2 * [1;1|1]_D * [1;1\,|1]_E * R_2 * L_1\,. \tag{4.5.15}$$

The rule for building the surface Σ for general tree diagrams is now clear: *Begin at some external state and trace around the diagram in the counterclockwise direction. For each external state add the factor* $[1;1|1]$. *For each line i traversed against the propagator arrow add a factor R_i. For each*

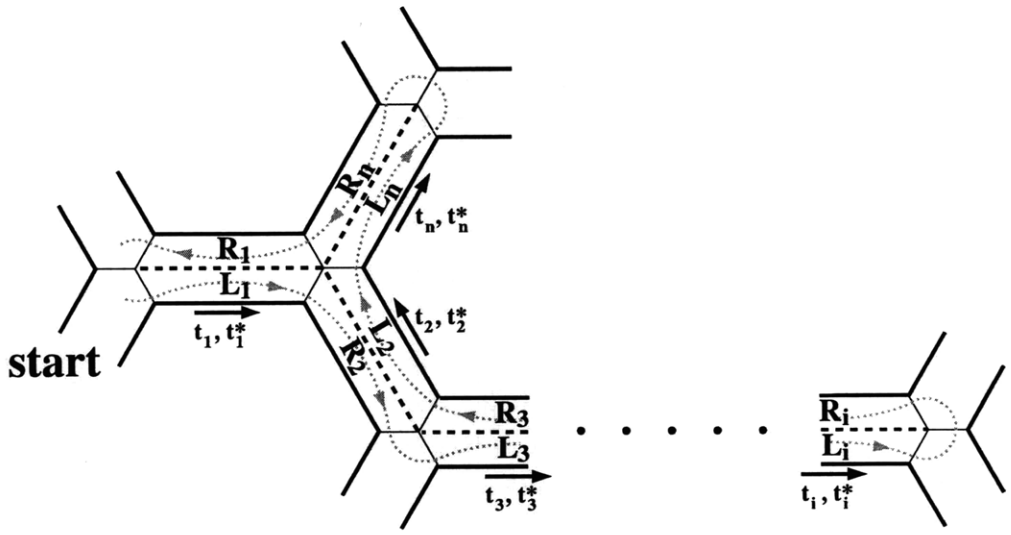

Figure 4-13: The surface Σ for general tree diagrams is built by tracing the grey dotted line counterclockwise around the diagram, starting at an arbitrary external state. When tracing along the i-th propagator one picks up either the slanted wedge corresponding to the left part (L_i) or right part (R_i) of the propagator. This depends on the direction of the propagator (black arrows).

line i traversed along the propagator arrow add a factor L_i. All factors are added from the right. The formula in (4.5.15) results from the application of this rule to the diagram in Figure 4-12, starting at the external state $|F_A\rangle$. Note that the rules build the surface using half strings. If we are tracing in the direction of the arrow on the i line, we multiply by the surface L_i because the propagator acts from the left on the surface to be built. If we are tracing against the arrow of the propagator, we multiply by the surface R_i because, in this case, the propagator acts from the right on the surface we have already built.

For the more complicated diagram in Figure 4-13 the rules are still simple to follow. Although it is redundant information, the labels L_i and R_i in Figure 4-13 represent the factors that must be included, as a result of the chosen assignment of arrows, when we follow the grey dotted curve along the diagram. We have,

$$\begin{aligned}\Sigma = [1;1|1] * L_1 * R_2 * [1;1|1] * L_3 * \ldots * L_i * [2;1|1,2] * R_i * \ldots \\ \ldots * R_3 * L_2 * L_n * [2;1|1,2] * R_n * R_1 * [1;1|1]\,.\end{aligned} \tag{4.5.16}$$

The resulting surface is of unit slant (for each L_i there is an R_i) and takes the form

$$\Sigma = [a;1\,|\,x_1, x_2, \ldots x_k\,]\,, \tag{4.5.17}$$

for some calculable width a and some calculable positions x_i. The left and right boundaries of Σ are identified through translation by a. We can therefore map the glued Σ surface to a unit disk using $\eta = \exp(2\pi i z/a)$. To determine the moduli of the surface, we only need to know the angular separation between operator insertions on the unit circle. If insertions are separated by Δx on Σ,

their relative angle $\Delta\phi$ on the unit circle is simply given by

$$\frac{\Delta\phi}{2\pi} = \frac{\Delta x}{a}\,. \tag{4.5.18}$$

This concludes our discussion of Riemann surfaces for general tree-level diagrams.

4.6 Riemann surfaces for general one-loop diagrams

In section 4.3 we built the surface corresponding to the tadpole diagram in Schnabl gauge using the simplified propagator B/L (i.e. $s^\star = 0$). Using the z frame we built separately the parts of the surface that contain the inner and outer boundary components of the annulus, as displayed in Figure 4-7(b). Let us now review this construction using the algebra of slanted wedges.

On the outer boundary (the right strip in the z frame) there is a Fock space state $[1;1|1]$. It is acted by the right part e^{-sL_R} of the propagator so we get a slanted wedge Σ given by

$$\Sigma = e^{-sL_R}[1;1|1] = [\tfrac{1}{2}(1+e^s); e^s|1\,]\,, \tag{4.6.1}$$

where we made use of (4.4.11) and (4.4.28). On the inner boundary there is only the remaining left part e^{-sL_L} of the propagator so the resulting slanted wedge $\widehat{\Sigma}$ is just

$$\widehat{\Sigma} \equiv [\tfrac{1}{2}(1-e^{-s}); e^{-s}]\,, \tag{4.6.2}$$

making use of (4.4.12). The slanted wedges Σ and $\widehat{\Sigma}$ are glued to each other at their hidden boundaries at $i\infty$, as discussed in section 4.3 using λ-regularization.

We need to place the surfaces Σ and $\widehat{\Sigma}$ in the z-plane in such a way that: (i) their hidden boundaries at $i\infty$ glue correctly, and (ii) the slanted identifications become translations in the w frame ($z = -\frac{1}{2}e^{-w}$). We refer to the result as the natural w-picture. For the identifications on Σ to be simple translations in the w frame, we shift Σ horizontally, so that the position of its right boundary is a rescaling by e^s of its left boundary. The translation is uniquely determined and Σ lands between the vertical lines given in (4.3.12). Similarly, we need to shift the position of $\widehat{\Sigma}$ in such a way that the position of its right boundary is a rescaling by e^{-s} of its left boundary. As $e^{-s} < 1$, this implies that we need to position $\widehat{\Sigma}$ in the region $\Re(z) < 0$. In fact, we readily see that $\widehat{\Sigma}$ must be placed as the region between $\Re(z) = -\frac{1}{2}$ and $\Re(z) = -\frac{1}{2}e^{-s}$.

But we are not done yet. The boundaries at $i\infty$ now do *not* glue correctly. By the definition of slanted wedges, the parameterizations of the left boundaries of Σ and $\widehat{\Sigma}$ match – indeed, they both have unit scaling factor. But for the hidden boundaries at $i\infty$ to glue nicely in the w frame, the parameterizations of the left boundary of Σ needs to match the parametrization of the *right* boundary of $\widehat{\Sigma}$.[4] We can achieve this simply by rescaling the shifted $\widehat{\Sigma}$ by e^s. Then $\widehat{\Sigma}$ is positioned between $\Re(z) = -\frac{1}{2}e^s$ and $\Re(z) = -\frac{1}{2}$. This is precisely the configuration of surfaces that we ended up with and fully justified in section 4.3.

[4]This requirement will lead to the established result for this diagram, but will be justified in more generality using λ-regularization in section 4.8.3.

The above steps can easily be generalized to one-loop diagrams of arbitrary complexity. We will now show how this is done. A detailed justification of the procedure is given in section 4.8, where we discuss the λ-regulation explicitly.

4.6.1 The natural w-picture

For a one-loop diagram, we construct two complementary surfaces

$$\Sigma \equiv [a; e^{s_{\rm eff}} | \vec{x}] \quad \text{and} \quad \widehat{\Sigma} \equiv [\hat{a}; e^{-s_{\rm eff}} | \vec{\hat{x}}], \tag{4.6.3}$$

where $\vec{x}$ and $\vec{\hat{x}}$ collectively represent the positions of all punctures on Σ and $\widehat{\Sigma}$, respectively. These surfaces are said to be complementary because their scaling factors multiply to one. On each surface, the left and the right boundaries are identified, and the two surfaces are glued to each other at their hidden boundaries at $i\infty$.

The *natural w picture* is one in which the hidden boundaries of Σ and $\widehat{\Sigma}$ glue nicely and the identifications on Σ and $\widehat{\Sigma}$ are horizontal translations by $s_{\rm eff}$. To obtain this picture we need to place the surfaces Σ and $\widehat{\Sigma}$ correctly in the z frame. First, we shift the surfaces Σ and $\widehat{\Sigma}$ by real constants a_0 and $\hat{a}_0$, respectively, so that the position of their right boundaries is a rescaling of the left boundaries by $e^{s_{\rm eff}}$ and $e^{-s_{\rm eff}}$, respectively. Recall that by definition all slanted wedges start out with their left boundary at $\Re(z) = \frac{1}{2}$. The required shifts are thus determined by the relations

$$e^{s_{\rm eff}} = \frac{a_0 + a + \frac{1}{2}}{a_0 + \frac{1}{2}}, \qquad e^{-s_{\rm eff}} = \frac{\hat{a}_0 + \hat{a} + \frac{1}{2}}{\hat{a}_0 + \frac{1}{2}}. \tag{4.6.4}$$

Thus

$$a_0 = \frac{a}{e^{s_{\rm eff}} - 1} - \tfrac{1}{2}, \qquad \hat{a}_0 = -\frac{\hat{a}}{1 - e^{-s_{\rm eff}}} - \tfrac{1}{2}. \tag{4.6.5}$$

This shift places the surface Σ at

$$\text{Final } \Sigma \text{ region:} \quad a_0 + \tfrac{1}{2} \le \Re(z) \le e^{s_{\rm eff}}(a_0 + \tfrac{1}{2}). \tag{4.6.6}$$

As we discussed for the tadpole example above, we then rescale $\widehat{\Sigma}$ by a factor of $e^{s_{\rm eff}}$ so that it has the canonical parametrization on its *right* boundary. With this scaling $\widehat{\Sigma}$ ends up in the location

$$\text{Final } \widehat{\Sigma} \text{ region:} \quad e^{s_{\rm eff}}(\hat{a}_0 + \tfrac{1}{2}) \le \Re(z) \le \hat{a}_0 + \tfrac{1}{2}. \tag{4.6.7}$$

After positioning Σ and $\widehat{\Sigma}$ in this way we map to the w frame via (4.2.9) and to the annulus frame ζ via

$$\zeta = e^{-\frac{2\pi\imath}{s_{\rm eff}}(w - \imath\pi)}. \tag{4.6.8}$$

The modulus M of the annulus was defined in (4.2.32). We can read it off from (4.6.8) as

$$M = \frac{\pi}{|s_{\rm eff}|}. \tag{4.6.9}$$

A point x on Σ with $\frac{1}{2} \le x \le \frac{1}{2} + a$ is located at $z = x + a_0$ in the shifted Σ region (4.6.6). Using (4.2.31), we see that it ends on a boundary of the annulus at an angle

$$\phi = \frac{2\pi}{s_{\text{eff}}} \ln(2|a_0 + x|) = \frac{2\pi}{s_{\text{eff}}} \ln\Big(2\Big|x - \tfrac{1}{2} + \frac{a}{e^{s_{\text{eff}}} - 1}\Big|\Big) . \tag{4.6.10}$$

Similarly, any point $\hat{x}$ on $\widehat{\Sigma}$ is located at $z = e^{s_{\text{eff}}}(\hat{x} + \hat{a}_0)$ in the final $\widehat{\Sigma}$ region (4.6.7) and lands at an angle

$$\hat{\phi} = \frac{2\pi}{s_{\text{eff}}} \ln(2e^{s_{\text{eff}}}|\hat{x} + \hat{a}_0|) = \frac{2\pi}{s_{\text{eff}}} \ln\Big(2\Big|\tfrac{1}{2} - \hat{x} + \frac{\hat{a}}{1 - e^{-s_{\text{eff}}}}\Big|\Big) . \tag{4.6.11}$$

All points in $\vec{x}$ land on the same boundary component and all points in $\vec{\hat{x}}$ land on the other boundary component. With the maps written here, if $s_{\text{eff}} > 0$ the points in $\vec{x}$ lie on the outer component and if $s_{\text{eff}} < 0$ they lie on the inner component. Of course, there is no invariant distinction between these components as they can be exchanged by a conformal map.

4.6.2 General one-loop diagrams

Let us now build the complementary surfaces Σ and $\widehat{\Sigma}$ in (4.6.3) for a general one-loop diagram. Let n be the number of propagators running in the loop. It follows that there are also n vertices within the loop. These vertices will be labeled 1 to n as we move counterclockwise in the loop (see Figure 4-14(a)). Two lines of each cubic vertex in the loop connect to loop propagators. The remaining line can lead to a single external state or to a subtree diagram with a set of external states. In either case, the additional external state(s) at this vertex are all on one specific boundary of the annulus. We let Σ represent the part of the diagram which is drawn on the outer side of the loop and $\widehat{\Sigma}$ represent the part of the diagram on the inside of the loop. Eventually, we will glue the surfaces Σ and $\widehat{\Sigma}$ along their hidden boundaries, shown as dashed lines in Figure 4-14(b). In section 4.6.1 we have learned how to perform this gluing.

If the external states at the i-th vertex are on the Σ-side of the annulus, they add to Σ a surface

$$[a_i; 1 \,|\, \vec{y_i}\,] = [a_i; 1 \,|\, y_i^1, \ldots, y_i^{m_i}] \quad \text{with } a_i > 0 , \tag{4.6.12}$$

where the y_i^α are the positions of the punctures and $\alpha = 1, \ldots m_i$ is an index that enumerates them. If only a Fock space state is connected to vertex i, the surface in (4.6.12) is $[1; 1|1]$. As shown in Figure 4-14(a), the surface in (4.6.12) can in general represent a complicated subtree diagram. The slant factor is one because the subdiagram is a tree. As the external states of the i-th vertex are on the Σ-side of the diagram, they do not affect the $\widehat{\Sigma}$-side. In order to treat both Σ and $\widehat{\Sigma}$ symmetrically, we also insert a surface on $\widehat{\Sigma}$, the trivial "identity surface"

$$[\hat{a}_i; 1] = [0; 1] . \tag{4.6.13}$$

If, on the other hand, the external states are on the boundary corresponding to $\widehat{\Sigma}$, we have a surface insertion

$$[\hat{a}_i; 1 \,|\, \vec{\hat{y}_i}\,] = [\hat{a}_i; 1 \,|\, \hat{y}_i^1, \ldots, \hat{y}_i^{\hat{m}_i}] \quad \text{with } \hat{a}_i > 0 \tag{4.6.14}$$

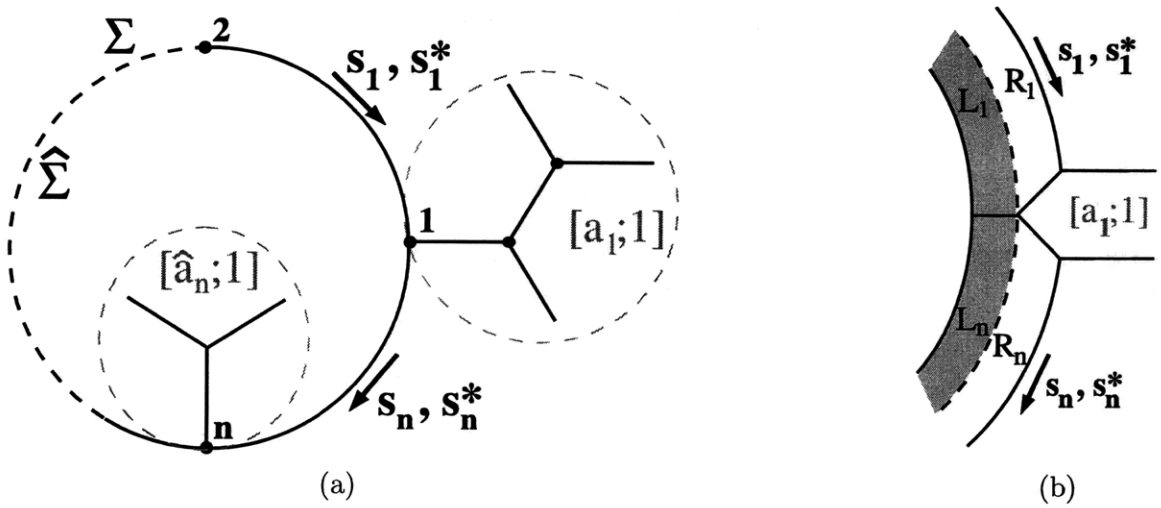

(a) (b)

Figure 4-14: (a) A general one-loop diagram with n vertices and n propagators in the loop. At each vertex the external states can either contribute to Σ or $\widehat{\Sigma}$ and thus end up on either boundary of the annulus. (b) The topology of the surfaces at vertex one. The right part R_i of the i-th propagator contributes to Σ. The left part L_i of the i-th propagator (shaded) contributes to $\widehat{\Sigma}$. Σ and $\widehat{\Sigma}$ are glued along the hidden boundaries represented by the dashed lines.

on $\widehat{\Sigma}$ accompanied by a trivial insertion $[a_i; 1] = [0; 1]$ on the Σ side. Thus the n vertices in the loop are described by $2n$ wedges, only n of which are non-trivial.

The propagators in the loop are in general complicated, because their geometric action depends on the ghost number of the state that they act on [46]. Since states of all ghost numbers circulate in the loop we cannot use the classical propagator (4.4.10). We choose the alternating gauge introduced in [46] for the FP gauge fixing procedure of Schnabl gauge. This yields the propagator

$$\mathcal{P} = \mathcal{P}_+ \, \Pi_+ + \mathcal{P}_- \, \Pi_- \,, \tag{4.6.15}$$

where Π_+ (Π_-) is the projector on even (odd) ghost number, and $\mathcal{P}_\pm$, for the i-th propagator, are defined by

$$\mathcal{P}_+ = \int ds_i ds_i^\star \, e^{-s_i L} \, B \, Q \, B^\star e^{-s_i^\star L^\star} \,, \qquad \mathcal{P}_- = \int ds_i ds_i^\star \, e^{-s_i^\star L^\star} \, B^\star \, Q \, B e^{-s_i L} \,. \tag{4.6.16}$$

The classical propagator is $\mathcal{P}_+$ since it acts on ghost number two sources to give ghost number one classical states. With external physical states of ghost number one, all non-trivial surface insertions at the loop insert states of ghost number one. Since the three string vertex couples states whose ghost numbers add up to three, the states on the two loop-propagators that attach to the vertex must both have either even or odd ghost number. Consequently the states running over *all* the propagators in the loop are either of even ghost number or odd ghost number. It follows that in alternating gauge we only need to consider two types of Riemann surfaces for every diagram at one loop level. The first surface is constructed by including a projector onto states of even ghost number anywhere in the loop and using $\mathcal{P}_+$ for all lines in the loop. The second surface is constructed with a projector onto odd ghost numbers in the loop and using $\mathcal{P}_-$ for all lines in the loop.

As mentioned before, the final set of surfaces is independent of the chosen direction on the propagator on each line. For simplicity, however, we orient all propagators in the loop clockwise. Tracing the outer loop counterclockwise, the right part of the propagator contributes to the surface Σ on each line. The inner loop must be traced clockwise so the left part of the propagator contributes to the surface $\widehat{\Sigma}$ on each line. This has been illustrated in Figure 4-14(b).

At fixed Schwinger parameters, the right part of $\mathcal{P}_+$ adds to Σ the slanted wedge corresponding to the operator $e^{-s_i L_R} e^{-s_i^\star L_R^\star}$, which is calculated in (4.4.22). The right part of $\mathcal{P}_-$, on the other hand, adds the slanted wedge corresponding to $e^{-s_i^\star L_R^\star} e^{-s_i L_R}$ to Σ, which is calculated using (4.4.11) and (4.4.17). We conclude that the i-th propagator contributes to Σ the slanted wedge R_i given by

$$R_i \equiv [r_i; e^{s_i - s_i^\star}] \quad \text{with} \quad \begin{cases} r_i = \frac{1}{2}(1 + e^{s_i - s_i^\star}) - e^{-s_i^\star} & \text{for even ghost number } (\mathcal{P}_+) \\ r_i = e^{s_i} - \frac{1}{2}(1 + e^{s_i - s_i^\star}) & \text{for odd ghost number } (\mathcal{P}_-)\,. \end{cases} \tag{4.6.17}$$

Similarly, the left part of the propagator contributes to $\widehat{\Sigma}$ the slanted wedge L_i given by $e^{-s_i L_L} e^{-s_i^\star L_L^\star}$ for $\mathcal{P}_+$ and $e^{-s_i^\star L_L^\star} e^{-s_i L_L}$ for $\mathcal{P}_-$. We readily find

$$L_i \equiv [l_i; e^{s_i^\star - s_i}] \quad \text{with} \quad \begin{cases} l_i = \frac{1}{2}(1 + e^{s_i^\star - s_i}) - e^{-s_i} & \text{for even ghost number } (\mathcal{P}_+) \\ l_i = e^{s_i^\star} - \frac{1}{2}(1 + e^{s_i^\star - s_i}) & \text{for odd ghost number } (\mathcal{P}_-)\,. \end{cases} \tag{4.6.18}$$

The definitions (4.6.17) and (4.6.18) generalize (4.5.12) from the classical propagators of tree diagrams to loop propagators in alternating gauge.

We now assemble the complete surfaces Σ and $\widehat{\Sigma}$. We construct Σ by gluing the surfaces of propagators and external states counterclockwise, starting at vertex 1. We obtain

$$\Sigma \equiv [a; e^{s_{\text{eff}}} | \vec{x}\,] = [a_1; 1 | \vec{y}_1] * R_1 * \cdots * [a_n; 1 | \vec{y}_n] * R_n\,, \tag{4.6.19}$$

Similarly, we construct $\widehat{\Sigma}$ by gluing the surfaces of propagators and external states. We trace clockwise starting right below vertex 1 and get

$$\widehat{\Sigma} \equiv [\hat{a}; e^{-s_{\text{eff}}} | \vec{\hat{x}}\,] = L_n * [\hat{a}_n; 1 | \vec{\hat{y}}_n\,] * \cdots * L_1 * [\hat{a}_1; 1 | \vec{\hat{y}}_1\,]\,. \tag{4.6.20}$$

It is clear from (4.6.19) and (4.6.20) that

$$s_{\text{eff}} = \sum_{i=1}^{n} (s_i - s_i^\star)\,. \tag{4.6.21}$$

It follows that the modulus M of the annulus is given by

$$\boxed{M = \frac{\pi}{|s_{\text{eff}}|}\,.} \tag{4.6.22}$$

To calculate the positions of the punctures we first determine the total lengths a and $\hat{a}$ of Σ and $\widehat{\Sigma}$. Looking at (4.6.19) we see that

$$a = a_1 + r_1 + e^{s_1 - s_1^\star}\big(a_2 + r_2 + e^{s_2 - s_2^\star}(a_3 + r_3 + \ldots\ . \tag{4.6.23}$$

This is readily seen to give

$$a = \sum_{i=1}^{n} e^{\sum_{j=1}^{i-1} s_j - s_j^\star} (a_i + r_i) = \sum_{i=1}^{n} b_i \, (a_i + r_i) \, . \tag{4.6.24}$$

where we defined

$$b_i \equiv e^{\sum_{j=1}^{i-1} s_j - s_j^\star} \, . \tag{4.6.25}$$

We can view b_i as a *local scaling factor.* It is the product of the slant factors of the surfaces R_1, $R_2, \ldots$, up to R_{i-1}. It is the scaling factor that must apply to R_i when it is glued in to form Σ in (4.6.19).

The value of $\hat{a}$ is computed similarly. Looking at (4.6.20) we write

$$\hat{a} = e^{s_n^\star - s_n} \hat{a}_n + l_n + e^{s_n^\star - s_n} \big(e^{s_{n-1}^\star - s_{n-1}} \, \hat{a}_{n-1} + l_{n-1} + \ldots \, , \tag{4.6.26}$$

which gives

$$\hat{a} = \sum_{i=1}^{n} e^{\sum_{j=i+1}^{n} s_j^\star - s_j} (e^{s_i^\star - s_i} \hat{a}_i + l_i) \, . \tag{4.6.27}$$

Noticing that $e^{s_i - s_i^\star} l_i = r_i$ (see (4.6.17) and (4.6.18)) we can also rewrite $\hat{a}$ as

$$\hat{a} = e^{-s_{\text{eff}}} \sum_{i=1}^{n} e^{\sum_{j=1}^{i-1} s_j - s_j^\star} (\hat{a}_i + r_i) = e^{-s_{\text{eff}}} \sum_{i=1}^{n} b_i \, (\hat{a}_i + r_i) \, . \tag{4.6.28}$$

For insertions at positions y_k^α and $\hat{y}_k^\alpha$ we denote by x_k^α and $\hat{x}_k^\alpha$ their final coordinates on Σ and $\widehat{\Sigma}$. The collection of these insertions were represented by $\vec{x}$ and $\vec{\hat{x}}$ in (4.6.19) and (4.6.20). Short calculations using (4.4.27) show that these positions are given by

$$\begin{aligned} x_k^\alpha - \tfrac{1}{2} &= b_k \, (y_k^\alpha - \tfrac{1}{2}) + \sum_{i=1}^{k-1} b_i \, (a_i + r_i) \, , \\ \hat{x}_k^\alpha - \tfrac{1}{2} &= e^{-s_{\text{eff}}} \Big(b_k \, (\hat{y}_k^\alpha - \tfrac{1}{2} + r_k) + \sum_{i=k+1}^{n} b_i \, (\hat{a}_i + r_i) \Big) \, . \end{aligned} \tag{4.6.29}$$

It follows immediately from (4.6.10) and (4.6.11) that in the annulus frame ζ these positions translate into the angles

$$\boxed{\phi_k^\alpha = \frac{2\pi}{s_{\text{eff}}} \ln\Big(2\Big|x_k^\alpha - \tfrac{1}{2} + \frac{a}{e^{s_{\text{eff}}} - 1}\Big|\Big) \, , \qquad \hat{\phi}_k^\alpha = \frac{2\pi}{s_{\text{eff}}} \ln\Big(2\Big|\tfrac{1}{2} - \hat{x}_k^\alpha + \frac{\hat{a}}{1 - e^{-s_{\text{eff}}}}\Big|\Big) \, .} \tag{4.6.30}$$

Up to a trivial overall rotation of the annulus, the angles (4.6.30) represent the open string moduli of the one-loop diagram. This concludes our construction of moduli for general one-loop diagrams in Schnabl gauge.

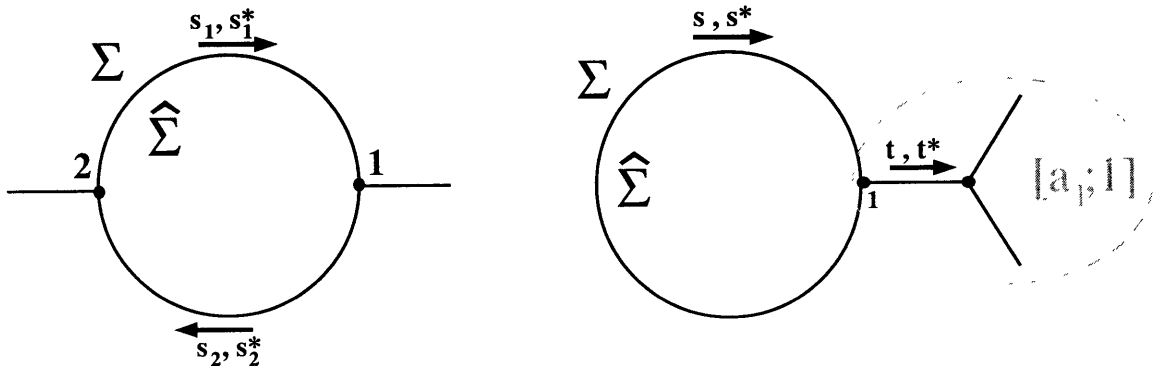

(a) (b)

Figure 4-15: The two diagrams contributing to the two-point function with both insertions on the same boundary.

4.7 The one-loop two-point diagram

We now apply the general construction of section 4.6 to the one-loop two-point diagram. In the following analysis we will restrict ourselves to the Riemann surfaces generated by even ghost-number propagators running in the loop, i.e. we use the propagator $\mathcal{P}_+$ in the loop. The other Riemann surface, which is generated by putting $\mathcal{P}_-$ on all loop propagator lines, can be calculated analogously.

4.7.1 Riemann surfaces with both insertions on the same boundary

Let us consider the one-loop two-point function with both insertions on the same boundary component of the annulus – the so-called planar contributions. There are two diagrams that contribute, as shown in Figure 4-15.

First diagram

In the first diagram (Figure 4-15(a)) we have two propagators in the loop ($n = 2$) and two Fock space surfaces $[1;1|1]$ connected directly to vertices in the loop, on the side that we choose to call the surface Σ. The Fock space surfaces do not contribute to $\widehat{\Sigma}$. In the notation of (4.6.12)

$$a_1 = a_2 = 1\,, \qquad y_1^1 = y_2^1 = 1\,, \qquad \hat{a}_1 = \hat{a}_2 = 0\,. \tag{4.7.1}$$

We label the Schwinger parameters of the two propagators by s_1, $s_1^\star$, s_2, $s_2^\star$ and (4.6.21) gives

$$s_{\text{eff}} = s_1 - s_1^\star + s_2 - s_2^\star\,. \tag{4.7.2}$$

The length a of the Σ surface follows from (4.6.24) and (4.6.17). We find

$$a = \tfrac{3}{2} + 2e^{s_1 - s_1^\star} - e^{-s_1^\star} + \tfrac{1}{2}\, e^{s_{\text{eff}}} - e^{s_1 - s_1^\star - s_2^\star}\,. \tag{4.7.3}$$

The position of the punctures on Σ are found using (4.6.29) and (4.6.17). We obtain:

$$x_1^1 = 1\,, \qquad x_2^1 = 2 + e^{s_1 - s_i^\star} - e^{-s_1^\star}\,. \tag{4.7.4}$$

The relevant open string modulus is the relative angle between the insertions. Making use of (4.6.30) a short calculation gives

$$\Delta\phi = \phi_2^1 - \phi_1^1 = \frac{2\pi}{s_{\rm eff}} \ln \frac{2 - e^{-s_1^\star} + e^{s_1 - s_1^\star} + e^{s_2^\star - s_2} - e^{-s_2}}{1 - e^{-s_1^\star} + 2e^{s_1 - s_1^\star} - e^{s_1 - s_1^\star - s_2^\star} + e^{s_{\rm eff}}}\,. \tag{4.7.5}$$

Just like for the five-point diagram, let us consider the Riemann surfaces generated by the simplified propagator B/L. We thus set $s_1^\star = s_2^\star = 0$ and (4.7.5) becomes

$$\Delta\phi = \frac{2\pi}{s_1 + s_2} \ln\Big(\frac{1 + e^{s_1}}{e^{s_1} + e^{s_1 + s_2}}\Big) = \pi + \frac{2\pi}{s_1 + s_2} \ln\Big(\frac{\cosh\frac{s_1}{2}}{\cosh\frac{s_2}{2}}\Big)\,. \tag{4.7.6}$$

It is convenient to study this angle for fixed modulus of the annulus: $s_{\rm eff} = s_1 + s_2 = \text{const}$. We then have

$$\Delta\phi = \pi + \frac{2\pi}{s_{\rm eff}} \ln\Big(\frac{\cosh\frac{s_1}{2}}{\cosh\frac{s_{\rm eff} - s_1}{2}}\Big)\,. \tag{4.7.7}$$

For $s_1 = \frac{1}{2} s_{\rm eff}$ the two punctures are maximally separated: $\Delta\phi = \pi$. As we vary s_1 the separation angle varies within an interval centered at π. The maximal (minimal) angle $\Delta\phi_+$ ($\Delta\phi_-$) is obtained for $s_1 = s_{\rm eff}$ ($s_1 = 0$), and it is given by

$$\Delta\phi_\pm = \pi \pm \frac{2\pi}{s_{\rm eff}} \ln\cosh\tfrac{s_{\rm eff}}{2}\,. \tag{4.7.8}$$

Close to closed string degeneration, i.e. for $s_{\rm eff} \ll 1$, we obtain the simplified expression

$$\Delta\phi_\pm = \pi \pm \frac{\pi}{4} s_{\rm eff} \qquad \text{for} \quad s_{\rm eff} \ll 1\,. \tag{4.7.9}$$

Thus near closed string degeneration the diagram just generates a region of moduli in which the punctures are nearly opposite. Close to open string degeneration ($s_{\rm eff} \to \infty$) equation (4.7.8) shows that almost the entire range of the position modulus is covered. In general, not all of the range of the position modulus is obtained. In Figure 4-16 we show the region of the complete two-dimensional moduli space ($s_{\rm eff}, \Delta\phi$) that the present, first diagram covers. The remaining region, as we will see now, is generated by second diagram contributing to the amplitude.

Second diagram

In the second diagram (Figure 4-15(b)) there is only one propagator in the loop ($s^\star$, s) and both external states are connected to the loop through another internal propagator (t, $t^\star$). We then have

$$[a_1; 1|\, y_1^1, y_1^2] = e^{-tL} e^{-t^\star L^\star} [2; 1|1, 2] = [1 - 2e^{-t} + 3e^{t^\star - t}; 1|y_1^1, y_1^2]\,, \tag{4.7.10}$$

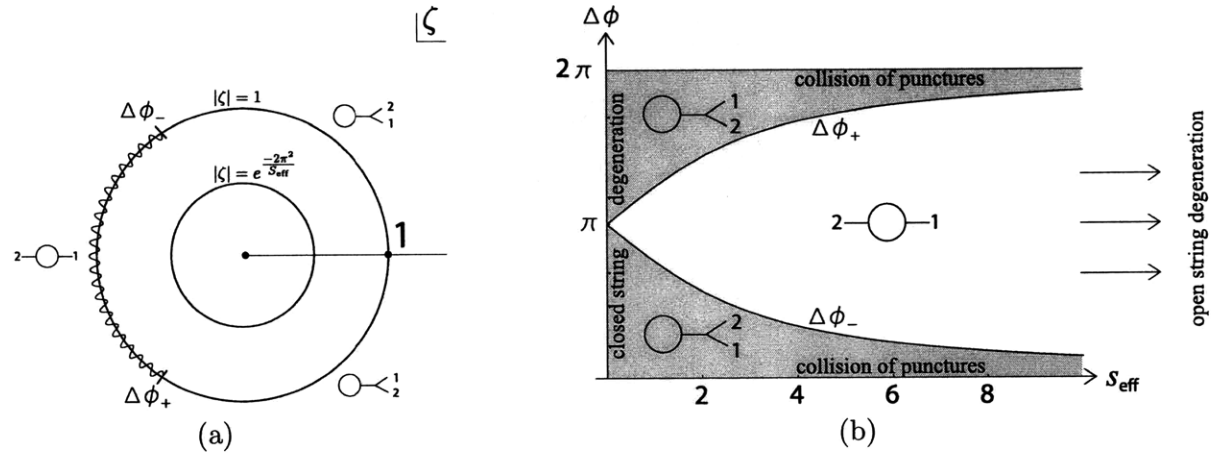

Figure 4-16: (a) The ζ-frame annulus for the planar one-loop two-point function. Insertion 1 is fixed at angle $\phi = 0$ and the position modulus is the angle $\Delta\phi$ for insertion 2. Both string diagrams in Figure 4-15 are needed to generate the full position range $0 \leq \Delta\phi \leq 2\pi$. (b) The space $(s_{\text{eff}}, \Delta\phi)$ of closed and open moduli is covered fully by the indicated string diagrams.

where we use (4.4.23) and (4.4.29) to obtain

$$a_1 = 1 - 2e^{-t} + 3e^{t^\star - t}, \quad y_1^1 = 1 - e^{-t} + e^{t^\star - t}, \quad y_1^2 = 1 - e^{-t} + 2e^{t^\star - t}, \quad \hat{a}_1 = 0\,. \tag{4.7.11}$$

To build Σ we use (4.6.19) with $n = 1$ and find

$$\Sigma \equiv [a; e^{s-s^\star}|x_1^1, x_1^2] = [a_1; 1|\, y_1^1, y_1^2] * [r_1; e^{s-s^\star}]\,, \qquad r_1 = \tfrac{1}{2}(1 + e^{s-s^\star}) - e^{-s^\star}\,, \tag{4.7.12}$$

and thus

$$a = a_1 + r_1 = \tfrac{3}{2} - 2e^{-t} + 3e^{t^\star - t} - e^{-s^\star} + \tfrac{1}{2}e^{s-s^\star}\,. \tag{4.7.13}$$

As $[a_1; 1|\, y_1^1, y_1^2]$ is the left-most surface in Σ, the positions of insertions on Σ coincide with the positions of insertions on $[a_1; 1]$: we have $x_1^1 = y_1^1$ and $x_1^2 = y_1^2$. For the relative angle $\Delta\phi$ between the two insertions we use (4.6.30) to obtain

$$\Delta\phi = \frac{2\pi}{s_{\text{eff}}} \ln\left(\frac{1 - e^{-s^\star} + e^{s-s^\star} - e^{-t} + e^{t^\star - t} - e^{s-s^\star-t} + 2e^{s-s^\star+t^\star-t}}{1 - e^{-s^\star} + e^{s-s^\star} - e^{-t} + 2e^{t^\star-t} - e^{s-s^\star-t} + e^{s-s^\star+t^\star-t}}\right), \tag{4.7.14}$$

with $s_{\text{eff}} = s - s^\star$.

Let us again focus on the surfaces generated by the simplified propagators $B^\star/L^\star$ or B/L. We have two options.

- $s^\star = t = 0$ (The case $s = t = 0$ gives similar results)
  In this case $s_{\text{eff}} = s$ and $\Delta\phi$ reduces to

$$\Delta\phi = \frac{2\pi}{s_{\text{eff}}} \ln\left(\frac{e^{t^\star} + 2e^{s_{\text{eff}}+t^\star} - 1}{2e^{t^\star} + e^{s_{\text{eff}}+t^\star} - 1}\right). \tag{4.7.15}$$

  For $t^\star \to 0$, this gives

$$\Delta\phi = \frac{2\pi}{s_{\text{eff}}} \ln\left(\frac{2e^{s_{\text{eff}}}}{1 + e^{s_{\text{eff}}}}\right) = \pi - \frac{2\pi}{s_{\text{eff}}} \ln\cosh\tfrac{s_{\text{eff}}}{2} \quad \text{for } t^\star \to 0\,, \tag{4.7.16}$$

and matches smoothly to the first diagram's $\Delta\phi_-$ as given in (4.7.8).

For $t^\star \to \infty$, however, there is no collision between the insertions. Instead, we obtain

$$\Delta\phi = \frac{2\pi}{s_{\rm eff}} \ln\left(\frac{1+2e^{s_{\rm eff}}}{2+e^{s_{\rm eff}}}\right) \quad \text{for} \quad t^\star \to \infty\,. \tag{4.7.17}$$

Thus diagram two with propagator $B^\star/L^\star$ in the subtree does *not* cover moduli space together with diagram one. This is not surprising because tracing along the Σ boundary of the Feynman diagram we encounter the operator combination $e^{-t^\star L_L} e^{-s_{\rm eff} L^\star_L} e^{-t^\star L^\star_L}$. At fixed annulus modulus, i.e. for $s_{\rm eff} = const$, this operator does not produce open string degeneration for $t^\star \to \infty$. In fact,

$$\lim_{t^\star\to\infty} e^{-t^\star L_L} e^{-s_{\rm eff} L^\star_L} e^{-t^\star L^\star_L}[a;b] = [a + \tfrac{1}{2}(e^{s_{\rm eff}}+1); e^{s_{\rm eff}} b]\,, \tag{4.7.18}$$

which is a perfectly regular surface.

- $s^\star = t^\star = 0$ (The case $s = t^\star = 0$ gives similar results)
  Again, $s_{\rm eff} = s$ and this choice corresponds to B/L as the propagator in the tree. This time we obtain

$$\Delta\phi = \frac{2\pi}{s_{\rm eff}} \ln\left(\frac{e^{s_{\rm eff}} + e^{s_{\rm eff}-t}}{e^{s_{\rm eff}} + e^{-t}}\right) = \pi - \frac{2\pi}{s_{\rm eff}} \ln\left(\frac{\cosh\frac{t+s_{\rm eff}}{2}}{\cosh\frac{t}{2}}\right). \tag{4.7.19}$$

  For $t = 0$ we again match to $\Delta\phi_-$ in the first diagram. This time, all angles $0 < \Delta\phi < \Delta\phi_-$ are covered. Indeed,

$$\Delta\phi \to 0 \quad \text{for} \quad t \to \infty\,. \tag{4.7.20}$$

  This is sufficient to cover moduli space together with diagram one, as shown in Figure 4-16. The diagram gives the shaded region $0 < \Delta\phi < \Delta\phi_-$. Of course, since external states are distinguishable, the region $\Delta\phi_+ < \Delta\phi < 2\pi$ is generated by the string diagram in which the order of the Fock space state insertions is reversed.

4.7.2 Riemann surfaces with insertions on both boundaries

Let us consider a one-loop amplitude with one Fock space state insertion on the outer boundary and one Fock space state insertion on the inner boundary. This nonplanar string diagram in shown in Figure 4-17. As $[a_1;1|1]$ and $[\hat{a}_2;1|1]$ are the Fock space surfaces, we have

$$a_1 = \hat{a}_2 = 1\,, \qquad a_2 = \hat{a}_1 = 0\,, \qquad y^1_1 = 1\,, \qquad \hat{y}^1_2 = 1\,. \tag{4.7.21}$$

We have two propagators running in the loop. The relevant surfaces, using (4.6.19) and (4.6.20) are

$$\begin{aligned} \Sigma &\equiv [a;1|x^1_1] = [1;1|1] * R_1 * R_2 \\ \widehat{\Sigma} &\equiv [\hat{a};1|\hat{x}^1_2] = L_2 * [1;1|1] * L_1\,. \end{aligned} \tag{4.7.22}$$

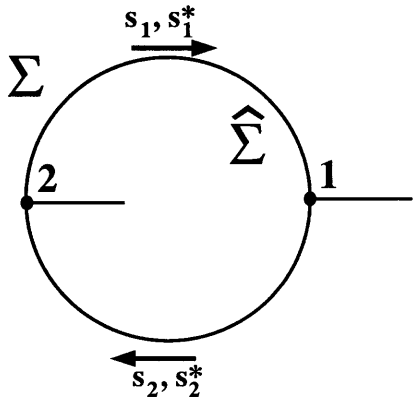

Figure 4-17: The diagram of the two-point function with insertions on both boundaries.

The relevant parameters above are readily calculated:

$$\begin{aligned} a &= \tfrac{3}{2} - e^{-s_1^\star} + e^{s_1 - s_1^\star}(1 - e^{-s_2^\star} + \tfrac{1}{2}e^{s_2 - s_2^\star}) \\ \hat{a} &= e^{-s_{\text{eff}}}\left(\tfrac{1}{2} - e^{-s_1^\star} + e^{s_1 - s_1^\star}(2 - e^{-s_2^\star} + \tfrac{1}{2}e^{s_2 - s_2^\star})\right), \\ s_{\text{eff}} &= s_1 - s_1^\star + s_2 - s_2^\star, \\ x_1^1 &= 1, \qquad \hat{x}_2^1 = e^{s_2^\star - s_2} - e^{s_2} + 1. \end{aligned} \tag{4.7.23}$$

A calculation using the above results and (4.6.30) gives us the difference in insertion angles

$$\Delta\phi = \hat{\phi}_2^1 - \phi_1^1 = \frac{2\pi}{s_{\text{eff}}} \ln \frac{1 - e^{-s_1^\star} + e^{s_1 - s_1^\star} - e^{-s_2} + e^{s_2^\star - s_2}}{1 - e^{-s_1^\star} + e^{s_1 - s_1^\star} - e^{s_1 - s_1^\star - s_2^\star} + e^{s_{\text{eff}}}}. \tag{4.7.24}$$

Let us consider two cases of simplified propagators. If both propagators are B/L, then we can set $s_1^\star = s_2^\star = 0$ (similarly for $B^\star/L^\star$ and $s_1 = s_2 = 0$) and obtain

$$\Delta\phi = \frac{2\pi}{s_1 + s_2} \ln \frac{e^{s_1}}{e^{s_{\text{eff}}}} = 2\pi \frac{s_1}{s_1 + s_2}. \tag{4.7.25}$$

Moduli space is covered: for fixed $s_{\text{eff}} = s_1 + s_2$, $\Delta\phi$ takes on all values between 0 and 2π.

To examine the case of mixed propagators B/L and $B^\star/L^\star$ we set $s_1^\star = s_2 = 0$. Then,

$$\Delta\phi = \frac{2\pi}{s_1 - s_2^\star} \ln(e^{s_1 - s_2^\star} - e^{-s_2^\star} + 1). \tag{4.7.26}$$

Since $s_1 = s_{\text{eff}} + s_2^\star$ and $s_1, s_2^* \geq 0$, for fixed $s_{\text{eff}} > 0$ we have a constraint in the range of s_1. Moduli space is not fully covered. In fact, for $s_{\text{eff}} \to \infty$ we have $\Delta\phi \to 2\pi$ for the entire range of permissible s_1, $s_2^\star$. In this limit the open string modulus is stuck at the collision of punctures.

4.8 A regularized view on one-loop diagrams

In section 4.6 we presented a prescription to map the Riemann surface of a general one-loop diagram to the annulus while keeping track of the operator insertions of external states. This allowed us

to calculate the closed and open string moduli of the surface as simple functions of the Schwinger parameters. The treatment was entirely in Schnabl gauge and used the formalism of slanted wedges. To justify our prescription, however, we need to revisit the construction by regularizing Schnabl gauge. This analysis extends the proof for the one-loop tadpole given in section 4.3.3 to general one-loop diagrams. Again, we use the λ-regularization introduced in [46]. To confirm our prescription we need to examine the three types of operations that are used. These operations are the multiplication of slanted wedges, the gluing between left and right boundaries on both Σ and $\widehat{\Sigma}$, and the gluing of Σ and $\widehat{\Sigma}$ to each other at their hidden boundaries. Before we check these operations, let us analyze the relevant gluing boundaries in more detail.

4.8.1 The boundaries of regularized slanted wedges

To examine the gluing curves, it is convenient to represent the coordinate curve $f^\lambda(e^{i\theta})$ in the z frame in terms of the parameterized curves γ_R^λ and γ_L^λ defined in (4.2.25) and shown in Figure 4-1(c). Regarded as the regulated surface $[1;1|1]$, a Fock space state is then bounded by $\frac{1}{2}+\gamma_L^\lambda$ and $\frac{3}{2}+\gamma_R^\lambda$. The boundaries touch at the midpoint $\theta=\pi/2$.

Similarly, the regularized slanted wedge corresponding to $e^{-sL_R^\lambda}$ is bounded by the curves $\frac{1}{2}+\gamma_R^\lambda$ and $e^s(\frac{1}{2}+\gamma_R^\lambda)$. Its left boundary glues nicely to a Fock space state. The right boundary is a simple rescaling of the left boundary by e^s. This was illustrated in the context of the tadpole graph in Figure 4-6(b). The two boundaries of $e^{-sL_R^\lambda}$ do not touch for $\theta=\frac{\pi}{2}$. In fact, $e^{-sL_R^\lambda}$ has a vertical boundary on the imaginary axis from $i\Lambda$ to $ie^s\Lambda$, as discussed in section 4.3. This vertical line segment connects the endpoints of the left and right boundary of $e^{-sL_R^\lambda}$.

The regularized slanted wedge corresponding to $e^{-s^\star(L_R^\lambda)^\star}$ is more delicate. Recall that in Figure 4-11 we *flipped* the surface around its right vertical boundary to be able to interpret $e^{-s^\star L_R^\star}$ as the slanted wedge $[\frac{1}{2}(1-e^{-s^\star});e^{-s^\star}]$. We conclude that the regularized boundaries of $e^{-s^\star(L_R^\lambda)^\star}$ are given by $\frac{1}{2}+\gamma_L^\lambda$ and $\frac{1}{2}+\frac{1}{2}(1-e^{-s^\star})+e^{-s^\star}\gamma_L^\lambda$. The surface of $e^{-s^\star(L_R^\lambda)^\star}$ also has a hidden vertical boundary. It is located between $1+ie^{-s^\star}\Lambda$ and $1+i\Lambda$. These facts are illustrated in Figure 4-18, where we also show the surface for $e^{-s^\star(L_L^\lambda)^\star}$, which needs further displacement and rescaling to be presented as a regularization of a conventional slanted wedge.

In our construction, we build surfaces from slanted wedges associated with propagators and Fock space states. From this it is clear, that the slanted wedges $[a;b]$ relevant to our construction will, after regularization, be bounded on the left by either $\frac{1}{2}+\gamma_L^\lambda$ or $\frac{1}{2}+\gamma_R^\lambda$ and will be bounded on the right by either $\frac{1}{2}+a+b\gamma_L^\lambda$ or by $\frac{1}{2}+a+b\gamma_R^\lambda$. Furthermore, the slanted wedges associated with the left and right parts of e^{-sL} and $e^{-s^\star L^\star}$ carry a hidden boundary that needs to be glued to the hidden boundary of a complementary surface.

For $\lambda\to 0$, the curves $\gamma_{L/R}^\lambda(\theta)$ both approach the canonical vertical sliver parametrization $\gamma(\theta)$ defined in (4.2.26). One may therefore wonder why it is not trivial that regularized slanted wedges glue nicely for $\lambda\to 0$. The problem is that the convergence of $\gamma_{L/R}^\lambda(\theta)$ to the curve $\gamma(\theta)$ in the limit $\lambda\to 0$ is not *uniform* on the full interval $0\le\theta\le\frac{\pi}{2}$. In fact, for any $\lambda>0$, the curves $\gamma_{L/R}^\lambda$ start

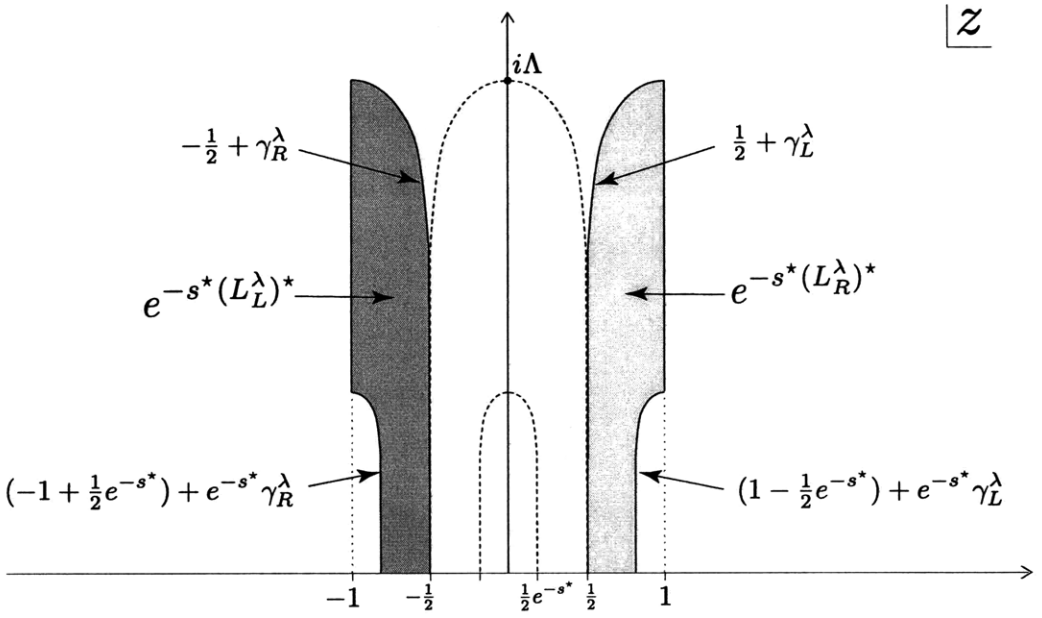

Figure 4-18: The regularized version of the slanted wedges corresponding to $e^{-s^\star(L_L^\lambda)^\star}$ and $e^{-s^\star(L_R^\lambda)^\star}$.

deviating significantly from γ in the region where $\Im(z)$ is of order Λ, as discussed in section 4.2.1. This effect can be neglected for tree-level amplitudes. In fact, the relevant frame for the calculation of moduli and correlators in tree amplitudes is the disk frame η, which is related to the z frame through

$$\eta = \exp\left(\frac{2\pi i z}{a}\right) . \tag{4.8.1}$$

Here, $a > 0$ is a function of the Schwinger parameters and independent of λ. All points with large imaginary values in the z frame converge to the point $\eta = 0$. In the η-frame, the deviations of $\gamma_{L/R}^\lambda$ from γ are thus suppressed by a factor of $e^{-\frac{2\pi\Lambda}{a}}$, which vanishes for $\lambda \to 0$.

For one-loop diagrams the natural frame to consider for the gluing is either the ζ-frame of the annulus or the w frame, in which the annulus is "unwrapped". The w coordinate is given by

$$w = -\ln(2z) + i\pi . \tag{4.8.2}$$

Clearly, not all points z with large imaginary values converge to a single point in the w frame. Therefore the analysis for one-loop diagrams is more subtle than for trees. The mapping of the boundary curves $\gamma_{L/R}^\lambda$ to the w frame have been analyzed in the context of the simplified tadpole diagram. Indeed, in section 4.3 we have proven that when mapped to the w frame, the left boundary of the Fock space state is a translation by s of the right boundary of e^{-sL_R}. Concretely, we showed in claim (2) of section 4.3.3 that

$$\lim_{\lambda\to 0} w\Big(a_0 + \tfrac{1}{2} + \gamma_L^\lambda\Big) - w\Big(e^s\big(a_0 + \tfrac{1}{2} + \gamma_R^\lambda\big)\Big) = s . \tag{4.8.3}$$

The limit holds uniformly on $0 \le \theta \le \frac{\pi}{2}$. This result can be easily generalized to the uniform

convergence

$$\boxed{\begin{array}{l}\lim\limits_{\lambda\to 0}\; w\big(e^{s'}(d+\gamma^\lambda_{L/R})\big) - w\big(e^{s''}(d+\gamma^\lambda_{R/L})\big) = s''-s' \\ \quad \forall\; d,s',s''\in\mathbb{R} \text{ independent of } \lambda\,;\; d\neq 0\,.\end{array}} \tag{4.8.4}$$

Note that only this case of mixed curves γ_L and γ_R is non-trivial. If both curves are either of the type γ_L or of the type γ_R, the identity analogous to (4.8.4) is exact for all λ:

$$w\big(e^{s'}(d+\gamma^\lambda_{L/R})\big) - w\big(e^{s''}(d+\gamma^\lambda_{L/R})\big) = s''-s' \quad \text{for all} \quad \lambda\geq 0\,. \tag{4.8.5}$$

This follows from the definition of the map (4.2.9) to the w frame.

4.8.2 Gluings and identifications on Σ

For one-loop diagrams, we know from (4.6.19) that the surface Σ is constructed by the multiplication of $2n$ slanted wedges. Let as analyze the validity of the gluing between any pair of neighboring slanted wedges in this product. To this end, we split the surface Σ into two slanted wedges. One of them comprises all the surfaces to the left of the gluing we are interested in, the other one comprises all the surfaces to the right of this gluing. We thus have

$$\Sigma = [a; e^{s_{\text{eff}}}] = [a_1; b_1] * [a_2; b_2]\,. \tag{4.8.6}$$

When multiplying the slanted wedges $[a_1; b_1]$ and $[a_2; b_2]$, we need to glue the right boundary of $[a_1; b_1]$ to the left boundary $[a_2; b_2]$. To see that our usual multiplication prescription is valid, we analyze this gluing of the two boundaries using λ-regulated slanted wedges. If these boundaries are either both of the type γ^λ_L or both of the type γ^λ_R, the gluing is natural for all λ and no limit needs to be taken. If the boundaries are of mixed type, the gluing curves do not match for $\Im(z)$ of order Λ. The surfaces thus either start overlapping or separating in this region. But using (4.8.4) in the form

$$\lim_{\lambda\to 0}\; w\big(\tfrac{1}{2}+a_0+a_1+b_1\gamma^\lambda_L\big) - w\big(\tfrac{1}{2}+a_0+a_1+b_1\gamma^\lambda_R\big) = 0\,, \tag{4.8.7}$$

we see that the boundaries match in the w frame for $\lambda\to 0$. The shift a_0, defined in (4.6.5), is independent of λ so that uniform convergence is guaranteed. We have thus shown that all the slanted wedges which are multiplied in the construction of Σ glue nicely to each other in the w frame when $\lambda\to 0$.

Eventually, we also have to glue the left and right boundaries of Σ to each other. This is done by the map from the w frame to the annulus ζ through (4.6.8). This map has the periodicity $w\sim w-s_{\text{eff}}$. It is thus sufficient to show that in the limit $\lambda\to 0$, the left and right boundaries of Σ are related through a translation by s_{eff} in the w frame. As shown in (4.8.5), if both boundaries of Σ are of type γ^λ_L or both are of type γ^λ_R, this relation in the w frame is exact by construction, even for finite λ. If one boundary is of the type γ^λ_L and the other boundary is of the type γ^λ_R, we can use (4.8.4) in the form

$$\lim_{\lambda\to 0}\; w\big(\tfrac{1}{2}+a_0+\gamma^\lambda_{L/R}\big) - w\big(e^{s_{\text{eff}}}(\tfrac{1}{2}+a_0+\gamma^\lambda_{R/L})\big) = s_{\text{eff}} \tag{4.8.8}$$

to see that the two boundaries of Σ are related through a translation by s_{eff} in the w frame.

In summary, we have shown that the w-frame image of Σ, as $\lambda \to 0$, represents a smooth surface which is foliated by horizontal lines of length $|s_{\text{eff}}|$. Clearly, the same arguments as above also apply to the surface $\widehat{\Sigma}$. To complete the proof of our prescription, we still need to show that the surfaces Σ and $\widehat{\Sigma}$ also glue smoothly to each other at their hidden boundaries.

4.8.3 Gluing the hidden boundaries

In constructing one-loop amplitudes for Schnabl gauge, we cut the surfaces associated with $e^{-s_i L}$ and $e^{-s_i^\star L^\star}$ into two pieces associated with their left and right parts. As we saw using λ-regularization, these surfaces really have a hidden boundary at $i\infty$ at which they were cut, and we need to ensure that these hidden boundaries glue nicely when we form the annulus.

In the λ-regularized construction the hidden boundaries are of the general form

$$\boxed{z = d + ix\Lambda \qquad \text{with} \quad e^{s'} \le x \le e^{s''}, \qquad d, s', s'' \in \mathbb{R} \ \text{ independent of } \lambda.} \tag{4.8.9}$$

The parameters d, s', and s'' are thus suitable to characterize general hidden boundaries of slanted wedges. They emerge as actual vertical boundary segments once the slanted wedge is regularized, but we will still call them hidden boundaries, to avoid confusion with other types of boundaries. The hidden boundary of $e^{-s^\star (L^\lambda)^\star_R}$, for example, stretches from $1+ie^{-s^\star}\Lambda$ to $1+i\Lambda$, as we can see in Figure 4-18. We thus have $d = 1$, $s' = -s^\star$, and $s'' = 0$ as the parameters of the hidden boundary of $e^{-s^\star L^\star_R}$. Note also that the parameters s' and s'' are just the logarithms of the scaling factors that apply to the left or right boundaries of the surface associated with $e^{-s^\star L^\star_R}$. The parameter s'' that defines the top endpoint of the hidden boundary arises from the left boundary which has a scale factor of one, thus $s'' = 0$. The parameter s' that defines the bottom endpoint of the hidden boundary arises from the right boundary, which has a scale factor of $e^{-s^\star}$, thus $s' = -s^\star$.

Let us summarize the parameters of hidden boundaries for slanted wedges associated with propagators:

$$d = 0 \qquad s' = 0 \qquad s'' = s \qquad \text{for the hidden boundary of } e^{-sL_R}, \tag{4.8.10}$$

$$d = 1 \qquad s' = -s \qquad s'' = 0 \qquad \text{for the hidden boundary of } e^{-sL_L}, \tag{4.8.11}$$

$$d = 1 \qquad s' = -s^\star \qquad s'' = 0 \qquad \text{for the hidden boundary of } e^{-s^\star L^\star_R}, \tag{4.8.12}$$

$$d = 0 \qquad s' = 0 \qquad s'' = s^\star \qquad \text{for the hidden boundary of } e^{-s^\star L^\star_L}. \tag{4.8.13}$$

When we multiply regulated slanted wedges to form the surfaces Σ and $\widehat{\Sigma}$, hidden boundaries get shifted and rescaled. Of course they are then still of the general form (4.8.9).

In proving claim (1) of section 4.3.3 –that the hidden boundaries of e^{-sL_L} and e^{-sL_R} glue nicely in the tadpole graph– we showed that

$$\lim_{\lambda \to 0} \ w(ix\Lambda) - w(a_0 + 1 + ix\Lambda) = 0 \qquad \text{for all} \quad 1 \le x \le e^s. \tag{4.8.14}$$

More generally, consider two hidden boundaries of the form (4.8.9) with identical ranges of x so that they are related by just a horizontal translation. If the horizontal distance $\Delta d \in \mathbb{R}$ that separates these hidden boundaries is independent of λ, they glue nicely in the w frame in the limit $\lambda \to 0$. A straightforward generalization of the proof in section 4.3.3 indeed shows that the following limit holds uniformly

$$\boxed{\lim_{\lambda\to 0} \; w(d+ix\Lambda) - w(d+\Delta d+ix\Lambda) = 0 \quad \forall\, e^{s'} \le x \le e^{s''} \;\text{ with }\; d, \Delta d, s', s'' \in \mathbb{R}\,.} \tag{4.8.15}$$

We now show that for one-loop diagrams all gluings of hidden boundaries work nicely in the w frame. Each propagator in the loop has two hidden boundaries, one from cutting e^{-sL} and one from cutting $e^{-s^\star L^\star}$. For definiteness, we analyze the k-th propagator in the loop and assume it is of type $\mathcal{P}_+$. This propagator is responsible for the insertion of the slanted wedge associated with

$$e^{-s_k L_R}\, \underline{e^{-s_k^\star L_R^\star}} \qquad \text{into } \Sigma\,. \tag{4.8.16}$$

The same propagator will be responsible for the insertion of the slanted wedge associated with

$$e^{-s_k L_L}\, \underline{e^{-s_k^\star L_L^\star}} \qquad \text{into } \widehat{\Sigma}\,. \tag{4.8.17}$$

We will focus on the underlined operators in the two expressions above. The first produces a hidden boundary in Σ and the second a hidden boundary in $\widehat{\Sigma}$. We aim to show that these hidden boundaries appear at the same height and have the same vertical range so that (4.8.15) implies that they glue correctly as the regulator is removed. More concretely, we want to show that these two hidden boundaries are characterized by (4.8.9) with identical parameters s' and s'', both independent of λ. The value of d for each boundary must also be λ-independent.

Let us begin with the hidden boundary generated by $e^{-s_k^\star L_R^\star}$ in Σ. Just before Σ is mapped to the w frame, the associated slanted wedge has its left boundary at a position x_L^k that is independent of λ (as is familiar from our calculations of positions in section 4.6, positions just depend on Schwinger parameters). According to (4.8.12), the hidden boundary of $e^{-s_k^\star L_R^\star}$, as a canonically presented slanted wedge is positioned a distance $d - \frac{1}{2} = \frac{1}{2}$ to the right of its left boundary. We conclude that on Σ, it is positioned a distance $\frac{1}{2} b_k$ from its left boundary, i.e. at $d = x_L^k + \frac{1}{2} b_k$. The factor of b_k is necessary because it represents the *local scale factor*: it is the product of the scale factors of all the slanted wedges that precede the insertion of $e^{-s_k^\star L_R^\star}$ in Σ (see (4.6.19)). Note that the first operator in (4.8.16) does not contribute to the local scale factor because its slanted wedge ends up to the right of the one we are looking at. As both x_L^k and b_k are manifestly λ independent, so is the location d of the hidden boundary. This is all that matters, its specific value is not needed.

The parameters s' and s'' for $e^{-s_k^\star L_R^\star}$ listed in (4.8.12) get a contribution from the logarithm of the local scale factor b_k at the insertion. We thus have:

$$s' = -s_k^\star + \ln b_k\,, \quad s'' = 0 + \ln b_k = \ln b_k\,, \qquad \text{for } e^{-s_k^\star L_R^\star} \text{ on } \Sigma\,. \tag{4.8.18}$$

Let us now consider the insertion of $e^{-s_k^\star L_L^\star}$ on $\widehat{\Sigma}$, just before $\widehat{\Sigma}$ is mapped to the w frame. The position $\hat{x}_L^k$ of the associated slanted wedge, defined as the real value of its left boundary, is

independent of λ. What we need is the local scale factor $b_{\rm loc}$ at this position. For this we recall that $\widehat{\Sigma}$ is rescaled by $e^{s_{\rm eff}}$ in such a way that its left boundary has scaling factor $e^{s_{\rm eff}}$ and the right boundary has unit scaling factor. It then follows from (4.6.20) that, in addition to $e^{s_{\rm eff}}$, we get the multiplicative contribution from the slant parameters of $L_n, L_{n-1}, \ldots, L_{k+1}$ *and* the slant parameter of the first operator in (4.8.17). This gives

$$b_{\rm loc} = e^{s_{\rm eff}} \cdot e^{\sum_{j=k+1}^{n}(s_j^\star - s_j)} \cdot e^{-s_k} = e^{\sum_{j=1}^{k}(s_j - s_j^\star)} \cdot e^{-s_k} = b_k e^{-s_k^\star} \,. \tag{4.8.19}$$

This time the s' and s'' parameters in (4.8.13) are modified by the addition of the logarithm of $b_{\rm loc}$. We thus get

$$s' = 0 + \ln b_{\rm loc} = -s_k^\star + \ln b_k \,, \quad s'' = s_k^\star + \ln b_{\rm loc} = \ln b_k \,, \qquad \text{for } e^{-s_k^\star L_L^\star} \text{ on } \widehat{\Sigma} \,. \tag{4.8.20}$$

Comparing (4.8.18) with (4.8.20), we see that the parameters s' and s'' match precisely. Therefore we conclude from (4.8.15) that the hidden boundaries of $e^{-s_k^\star L_R^\star}$ and $e^{-s_k^\star L_L^\star}$ glue nicely in the w frame.

A few remarks are in order.

- The hidden boundaries of $e^{-s_k L_R}$ and $e^{-s_k L_L}$ also glue seamlessly in the w frame. The proof is completely analogous to the one presented above.

- The propagators in subtrees also have hidden boundaries. The hidden boundaries associated with a subtree propagator are either both on Σ or both on $\widehat{\Sigma}$. These boundaries cannot be simply ignored because unlike in tree-amplitudes, the subtree is mapped to the annulus and *not* to the disk. Still, it is easy to see by a similar analysis as for loop propagators that these hidden boundaries glue nicely in the w frame.

- One might wonder if the question of gluing hidden boundaries could have been ignored. After all, these hidden boundaries are pushed off to $i\infty$ in the z frame and to $\frac{\pi}{2} - i\infty$ in the w frame and these seem to be well defined points. This naive argument, however, leads to wrong conclusions. It would allow *independent* z-frame rescalings of Σ and $\widehat{\Sigma}$, which is equivalent to shifting their relative horizontal position in the w frame. On the annulus, this corresponds to rotating the inner and outer boundaries of the annulus with respect to each other. But if we have insertions on both the inner and the outer boundary, the configuration after such a relative rotation is *not* conformally equivalent to the original one. We conclude that the naive expectation that the gluing in Schnabl gauge works out correctly automatically, leaves an ambiguity in the open string moduli. This ambiguity is fixed when we regulate and demand the gluing to work out nicely in the limit $\lambda \to 0$.

- While we did our analysis of the gluing of hidden boundaries using the λ-regulated gauges, any other family of regular linear b-gauges associated with zero modes in the frames $z = \tilde{f}^\lambda(\xi)$

could have been used, as long as this family approaches Schnabl gauge in the limit $\lambda \to 0$. By construction, for such a family the frames satisfy

$$\lim_{\lambda \to 0} \tilde{\Lambda} = \infty \quad \text{with} \quad i\tilde{\Lambda} \equiv \tilde{f}^{\lambda}(i)\,. \tag{4.8.21}$$

The proof of consistent gluing of hidden boundaries goes through with $\Lambda \to \tilde{\Lambda}$.

This concludes the proof of our prescription for the construction of general one-loop Riemann surfaces in Schnabl gauge.

4.9 Discussion

The open string midpoint has played a very subtle and important role in covariant open string field theory. The midpoint makes it non-trivial to formulate open string field theory as a theory of half-strings (see [83]). Spacetime diffeomorphisms are not quite open-string gauge symmetries because of the special status of the midpoint in the star product [84]. Nevertheless, closed string poles appear in open string loop diagrams, again because of the special role of the midpoint. Naively, the star algebra was expected to have no projectors. But again, open string surface states with singular behavior at the midpoint give rise to projectors that seem to be completely consistent.

It is perhaps no surprise then that the tachyon vacuum solution uses a gauge, Schnabl gauge, that is described by the conformal frame of a projector. So does the rolling tachyon solution that describes the decay of a D-brane. Since observables associated with these solutions probe closed string physics [30, 85, 86] it is natural to ask if the use of Schnabl gauge allows the correct incorporation of closed string physics. As a first step, in this chapter we asked whether Schnabl gauge, just like Siegel gauge, leads to correct loop amplitudes. Indeed, naive arguments suggested that the singular midpoint behavior in Schnabl gauge could ruin the validity of the gauge at loop level, precisely where closed string physics is revealed. In a nutshell, the string diagrams for one loop appeared to give a surface that is disconnected into two pieces, each of which contains one of the boundary components of the annulus.

The analysis presented in this chapter gives reason for optimism and teaches us a few facts:

- The left and right parts of the operator L (the Virasoro zero-mode in sliver frame) fail to commute. This non-commutation is required by consistency: it introduces a finite hidden boundary to each of the two disconnected surfaces that form the annulus. The gluing across the hidden boundaries restores the closed string moduli.

- Schnabl gauge string diagrams at one loop cover the (one-dimensional) closed string moduli space. This is no proof of complete consistency, but dispels the fear of inconsistency due to subtle midpoint effects.

- All moduli, open and closed, of one-loop amplitudes with arbitrary numbers of open string states are calculable in closed form. Schnabl gauge off-shell amplitudes may ultimately be recognized as simpler than those in the familiar Siegel or light-cone gauges.

- Wedge surfaces have a natural generalization in the form of *slanted* wedges. Only on slanted wedges we have a natural action of the left and right parts of the operators L and $L^\star$. The use of these surfaces allows us to give (for the first time) an explicit algorithm to construct arbitrarily complicated tree and one-loop diagrams.

The focus in this chapter has been narrow. We have studied the moduli of the diagrams generated in Schnabl gauge. We have not calculated any loop amplitude in detail. For this one must, of course, deal with the antighost and BRST insertions. Even regarding moduli we have not answered everything. Though the specific examples we have analyzed in this chapter are encouraging, it is not yet clear whether open string moduli are covered in general. This problem is in fact still unsolved at tree-level. We are lacking proof that even tree amplitudes are correctly reproduced in Schnabl gauge. The open string propagator has moduli associated with the operators B/L and $B^\star/L^\star$, but also contains the BRST operator Q, which acts as a total derivative on moduli space. Our analysis of the tree-level five-point function and the one-loop two-point function suggests that there might be an assignment of simplified propagators B/L and $B^\star/L^\star$ to the propagator lines so that the string diagram has all the requisite degenerations. Finding such an assignment could be the next step in a proof of consistency of Schnabl gauge.

The λ-regularized gauges are fully consistent and Schnabl gauge amplitudes can in principle be defined by the limit $\lambda \to 0$ of λ-regulated amplitudes. Calculating regularized amplitudes is problematic, because even at small (but fixed) λ, the geometry differs significantly from the Schnabl geometry when any Schwinger parameter becomes large, i.e. of order $\mathcal{O}(\log\log\lambda^{-1})$. When one imposes cutoffs on the integration region of Schwinger parameters, the limit of removing these cutoffs and the limit $\lambda \to 0$ do not, in general, commute. It would be interesting to determine a cutoff prescription for which these limits commute and thus define consistent amplitudes for Schnabl gauge. A possible candidate for such a prescription is a generalization of the symmetric limit defined for the four-point amplitude in [45]. Note that, in this chapter, we took the limit $\lambda \to 0$ at fixed Schwinger parameters and any amplitude calculated using these surfaces is thus a true Schnabl-gauge amplitude and needs to be supplemented with a suitable prescription on the integration over Schwinger parameters.

The conformal field theory boundary state of the rolling tachyon has been studied to extract the time-dependent pressure profile of tachyon condensation (see [58] and references therein). The result suggests that the pressure goes to zero at late times, consistent with the expectation that the D-brane decays into heavy non-relativistic closed strings. The conformal field theory analysis of the closed string production in the background of the rolling tachyon encounters UV divergences [53]. As the corresponding analytic solution of string field theory has been found, this problem can now

also be studied within open string field theory.[5] It would be interesting to extract a boundary state from the one-loop open-string vacuum amplitude in the background of the rolling tachyon solution. This string field theory boundary state may confirm the expected late time behavior of the pressure and could help us understand the role of observables in open string field theory. A big step in this direction has been achieved in [38], and we will present the findings there in the next chapter.

[5]For an interesting recent analysis of observables associated with on-shell closed string states, see [30].

Chapter 5

The boundary state from open string fields

5.1 Introduction

The current formulation of open string field theory [1] requires a choice of a consistent open string background described by a boundary conformal field theory (BCFT).[1] Other boundary conformal field theories are expected to be described by classical solutions to the equation of motion of the open string field theory based on the original BCFT. As discussed in previous chapters, there have been remarkable developments in open string field theory since Schnabl's discovery of an analytic solution for tachyon condensation [43], and various analytic solutions have been constructed and studied. It still remains difficult, however, to extract information on the BCFT represented by a solution of open string field theory.

A useful object that contains information on a BCFT is the boundary state $|B\rangle$. The one-point function of a closed string vertex operator ϕ_c inserted at the origin of a unit disk can be written using the boundary state $|B\rangle$ as

$$\langle\, (c_0 - \tilde{c}_0)\, \phi_c(0)\, \rangle_{\text{disk}} = \langle B|(c_0 - \tilde{c}_0)|\phi_c\rangle\,, \tag{5.1.1}$$

where $|\phi_c\rangle$ is the state corresponding to ϕ_c and the operator $c_0 - \tilde{c}_0$ is associated with a conformal Killing vector on the disk. A classical solution Ψ of open string field theory is expected to describe a consistent open string background and thus a boundary conformal field theory, which we denote by BCFT$_*$. If we can construct the boundary state $|B_*\rangle$ for BCFT$_*$ from the solution Ψ, we can extract all information contained in bulk one-point functions in the new background. Interesting progress in that direction was recently reported by Ellwood [30]. It was argued that for *on-shell* closed string vertex operators $\mathcal{V}$, the one-point functions on the disk with BCFT$_*$ boundary conditions can be calculated from the gauge-invariant observables $W(\mathcal{V}, \Psi)$ introduced in [85, 86] as follows:

$$\langle B_*|(c_0 - \tilde{c}_0)|\mathcal{V}\rangle - \langle B|(c_0 - \tilde{c}_0)|\mathcal{V}\rangle = -4\pi i\, W(\mathcal{V}, \Psi)\,. \tag{5.1.2}$$

[1] See [35, 87–89] for reviews.

This remarkable observation means that the on-shell part of the information encoded in the BCFT boundary state $|B_*\rangle$ can be extracted from the corresponding solution of open string field theory.

The restriction to on-shell closed string states arises because the operator $\mathcal{V}$ in $W(\mathcal{V}, \Psi)$ is inserted at a point with a conical singularity on a Riemann surface. Therefore $W(\mathcal{V}, \Psi)$ is not well defined when $\mathcal{V}$ is not a primary field of weight $(0, 0)$. Unfortunately, there are few on-shell vertex operators with nonvanishing one-point functions on a disk. On the other hand, the boundary state is well defined when it is contracted with an arbitrary off-shell closed string state and contains more information on the BCFT. If we can relax the on-shell restriction on the closed string state in $W(\mathcal{V}, \Psi)$, we will be able to extract much more information on the BCFT$_*$ from the solution Ψ. This is our motivation.

In this chapter we construct, for any open string field theory solution Ψ, a class of closed string states $|B_*(\Psi)\rangle$ of ghost number three. Their contraction with arbitrary off-shell closed string states is regular. The states $|B_*(\Psi)\rangle$ are BRST invariant, namely,

$$Q\,|B_*(\Psi)\rangle = 0\,. \tag{5.1.3}$$

Under a gauge transformation $\delta_\chi\Psi$ of the solution Ψ, the states $|B_*(\Psi)\rangle$ change at most by a BRST-exact term:

$$|B_*(\Psi + \delta_\chi\Psi)\rangle \;=\; |B_*(\Psi)\rangle \;+\; (\,Q - \text{exact}\,)\,. \tag{5.1.4}$$

Therefore, a gauge-invariant observable can be constructed from $|B_*(\Psi)\rangle$ by its contraction with an on-shell closed string state $\mathcal{V}$:

$$\langle\mathcal{V}|(c_0 - \tilde{c}_0)|B_*(\Psi + \delta_\chi\Psi)\rangle = \langle\mathcal{V}|(c_0 - \tilde{c}_0)|B_*(\Psi)\rangle\,. \tag{5.1.5}$$

The novelty in the construction of these observables is that they admit a perfectly regular off-shell extension and, as we will show, the state $|B_*(\Psi)\rangle$ is explicitly calculable in certain cases. We claim that the state $|B_*(\Psi)\rangle$ coincides with the boundary state $|B_*\rangle$ up to a possible BRST-exact term. In fact, they precisely coincide in all calculable examples that we examined.

Our construction of $|B_*(\Psi)\rangle$ is inspired by Ellwood's paper [30] and by recent developments in the calculation of Feynman diagrams in Schnabl gauge [33,45] and in a class of gauges called linear b-gauges [46].[2] In the construction of $|B_*(\Psi)\rangle$, we first choose a propagator strip associated with a linear b-gauge. The shape of the strip is determined by the operator $\mathcal{B}$ used in the gauge-fixing condition on the open string field of ghost number one. The length of the strip is determined by a choice of a Schwinger parameter $s > 0$. Then the chosen propagator strip can be represented as the surface generated by the operator $e^{-s\mathcal{L}}$, where $\mathcal{L}$, defined by $\mathcal{L} = \{Q, \mathcal{B}\}$, is the BRST transformation of $\mathcal{B}$.

The main ingredient for the construction of $|B_*(\Psi)\rangle$ is a *half-propagator strip*. We cut the chosen propagator strip in half along the line traced by the open string midpoint. We then take one of the resulting half-propagator strips and form an annulus by identifying its initial and final

[2]For progress related to other gauge choices, see [36,65,74].

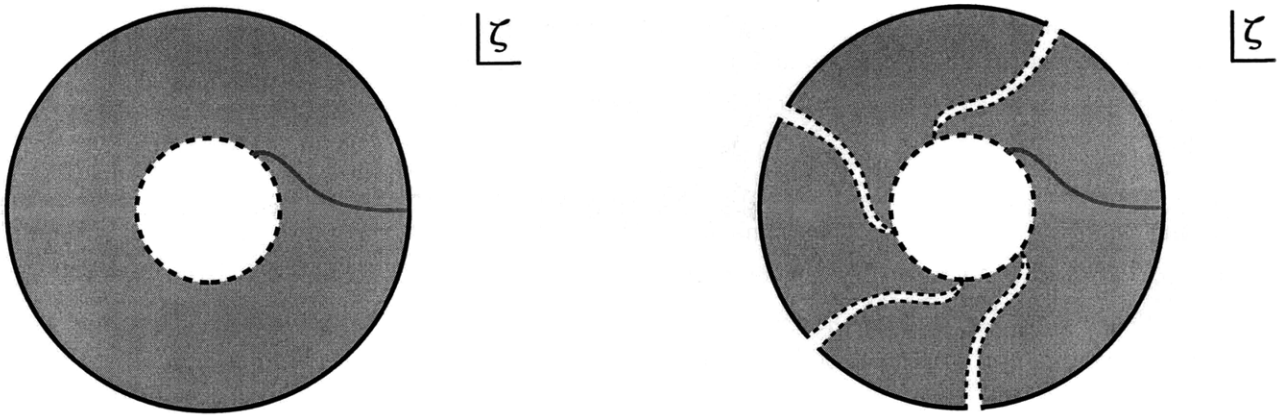

(a) (b)

Figure 5-1: (a) An annulus constructed from a half-propagator strip. The boundary conditions of the original BCFT are imposed on the outer boundary. The grey line in the figure represents the identified half-string edges of the half-propagator strip. The path integral over this annulus defines a closed string state at the inner boundary depicted as a dashed line in the figure. (b) An annulus with four slits. The classical solution Ψ is glued to each slit. The path integral over this annulus after gluing classical solutions defines a closed string state at the inner boundary.

half-string edges. Imposing the original BCFT boundary conditions at the open string boundary of this annulus, the path integral over the annulus defines a closed string state at the other boundary where we originally cut the propagator strip. See Figure 5-1(a). It is clear that this closed string state, after an appropriate exponential action of $L_0 + \tilde{L}_0$, reproduces the boundary state $|B\rangle$ of the original BCFT. We can thus construct the boundary state $|B\rangle$ for any choices of $\mathcal{B}$ and s. It should be pointed out, however, that the propagator for non-BPZ-even gauges ($\mathcal{B}^\star \neq \mathcal{B}$) is a complicated object, while our construction is based on $e^{-s\mathcal{L}}$ which in these cases is not the full propagator surface.

Let us now repeat the construction with the above half-propagator strip replaced by the one for the background associated with Ψ. The modified half-propagator strip can be constructed by gluing the solution Ψ to slits which are inserted at various positions along the annulus. See Figure 5-1(b). The shape of the slits is correlated with the shape of the half-propagator strip before the identification of the half-string edges and is determined by the operator $\mathcal{B}$. The slits are accompanied by appropriate b-ghost line integrals, and the positions of the slits are integrated over. A closed string state is again defined by the path integral over this annulus. After an appropriate exponential action of $L_0 + \tilde{L}_0$ and summing over the number of solution insertions, this defines the state $|B_*(\Psi)\rangle$.

The resulting state $|B_*(\Psi)\rangle$ depends on $\mathcal{B}$ and s, but the gauge-invariant observables $\langle\mathcal{V}|(c_0 - \tilde{c}_0)|B_*(\Psi)\rangle$ are independent of $\mathcal{B}$ and s. Indeed, we can show that as we vary $\mathcal{B}$ and s, the closed string state $|B_*(\Psi)\rangle$ changes at most by a possible BRST-exact term. While it is difficult to calculate the state $|B_*(\Psi)\rangle$ for generic choices of $\mathcal{B}$, it is explicitly calculable for solutions based on

the familiar wedge surfaces [44,49] if we choose Schnabl's propagator strip. In fact, in this case the methods developed in chapter 4 to map Riemann surfaces for one-loop amplitudes in Schnabl gauge to an annulus can be used to construct the Riemann surfaces which define $|B_*(\Psi)\rangle$. We explicitly calculate $|B_*(\Psi)\rangle$ based on the Schnabl propagator strip of arbitrary length s for various known solutions of string field theory such as Schnabl's tachyon vacuum solution and the solutions for marginal deformations with regular operator products constructed in [12,13] and in [21]. We find that $|B_*(\Psi)\rangle$ vanishes identically for the tachyon vacuum solution, which is consistent with Sen's conjecture that the D-brane disappears at the tachyon vacuum. For the marginal deformations, $|B_*(\Psi)\rangle$ *precisely* reproduces the BCFT boundary state $|B_*\rangle$. Both results hold independent of the length s of the propagator strip used in the construction. At least for these examples the exact BCFT boundary state can be obtained from the corresponding open string field theory solution!

Our results imply, in particular, that the boundary state $|B_*(\Psi)\rangle$ calculated from the known rolling tachyon solutions of open string field theory coincides with the BCFT boundary state discussed in [50,51,57,58,90,91]. This boundary state describes a regular behavior of D-brane decay in the far future. For example, the pressure decreases monotonically and vanishes in the far future. The rolling tachyon solution Ψ, on the other hand, exhibits ever-growing oscillations for the component fields of the open string [12,13]. It has been a long-standing puzzle whether such wildly oscillatory solutions describe a regular time-dependent process in the far future [52,56,92]. Our explicit construction of the boundary state from the rolling tachyon solution confirms that the solution represents the expected regular physics. Our interpretation is that the wild oscillatory behavior is due to the description of the regular physics in the *closed* string channel in terms of the *open* string degrees of freedom.

The chapter is organized as follows. In section 5.2 we introduce the half-propagator strips and explain the construction of closed string states using half-propagator strips. In section 5.3 we define the closed string state $|B_*(\Psi)\rangle$. We show its BRST invariance and prove that it changes at most by a BRST-exact term under a gauge transformation of Ψ. We show in section 5.4 that as we vary $\mathcal{B}$ and s, the state $|B_*(\Psi)\rangle$ changes at most by a BRST-exact term.

In sections 5.5 and 5.6 we demonstrate that the state $|B_*(\Psi)\rangle$ is calculable for solutions based on wedge states if we choose Schnabl's propagator strip. We then explicitly calculate $|B_*(\Psi)\rangle$ for various known solutions and find that it coincides with the BCFT boundary state for arbitrary s. In these cases, the state $|B_*(\Psi)\rangle$ factorizes into matter and ghost sectors, and the ghost sector coincides with the boundary state of the bc CFT. It is important to understand when this factorization holds because the state $|B_*(\Psi)\rangle$ factorized in this way can be a consistent BCFT boundary state without any BRST-exact term. In section 5.6.2 we discuss this factorization and show that for solutions based on wedge states with a certain class of ghost insertions and arbitrary matter insertions, the state $|B_*(\Psi)\rangle$ constructed from the Schnabl propagator always factorizes in this way. In section 5.7 we end with concluding remarks.

5.2 Half-propagator strips and closed string states

We begin this section by reviewing the construction of propagator strips in linear b-gauges [46]. We then introduce half-propagator strips by cutting the full strips along the line traced by the open string midpoint. We further introduce various ingredients to be used in section 5.3 for the construction of $|B_*(\Psi)\rangle$, such as the star multiplication of half-propagator strips and operator insertions on the strips. Finally, we construct closed string states from half-propagator strips by identifying the half-string edges. The coordinate curve of the closed string is the curve traced by the open string midpoint.

5.2.1 Half-propagator strips for regular linear b-gauges

A large class of gauge choices for string perturbation theory was discussed in [46]. These so-called *linear b-gauges*, which we reviewed above in section 4.2.1, impose a gauge condition

$$\mathcal{B}\,|\psi_{cl}\rangle = 0 \tag{5.2.1}$$

on the classical open string field $|\psi_{cl}\rangle$ of ghost number one.[3] The operator $\mathcal{B}$ is a linear combination of even-moded b-ghost oscillators that is determined by a vector field $v(\xi)$ (see eq. (4.2.2)). If the associated vector field $v(\xi)$ is analytic in a neighborhood of the unit circle $|\xi| = 1$ and furthermore satisfies the condition (4.2.3), the gauge choice is called *regular*. It was shown in [46] that regular linear b-gauges correctly reproduce open string on-shell amplitudes and that pure-gauge external states decouple.

The propagator of a regular linear b-gauge is characterized by the strip surface generated by $e^{-s\mathcal{L}}$, where $\mathcal{L} = \{Q, \mathcal{B}\}$. In a certain conformal frame w, this strip surface is generated by horizontal translations. See Figure 5-2(a). The w frame is obtained from the vector field $v(\xi)$ through

$$\frac{dw(\xi)}{d\xi} = \frac{1}{v(\xi)}\,, \quad w(1) = 0\,. \tag{5.2.2}$$

Normalizing $v(\xi)$ appropriately, we can impose the additional condition[4]

$$w(-1) = i\pi\,. \tag{5.2.3}$$

The horizontal boundaries of the strip are then located at $\Im(w) = 0$ and $\Im(w) = \pi$. The left boundary is the parameterized curve $\gamma(\theta) = w(e^{i\theta})$ for $0 \le \theta \le \pi$. It follows from (5.2.2) and (5.2.3) that

$$\gamma(0) = 0\,, \qquad \Im\big(\gamma(\tfrac{\pi}{2})\big) = \tfrac{\pi}{2}\,, \qquad \gamma(\pi) = i\pi\,, \tag{5.2.4}$$

where the middle equation holds because of (4.2.2).

[3] String fields of different ghost numbers are introduced in the process of gauge fixing. See [46] for detailed discussions about gauge conditions on such quantum string fields.

[4] This definition of the w frame differs slightly from the conventions of chapter 4. They are related by $w_{\text{here}} = -w_{\text{there}} + i\pi$.

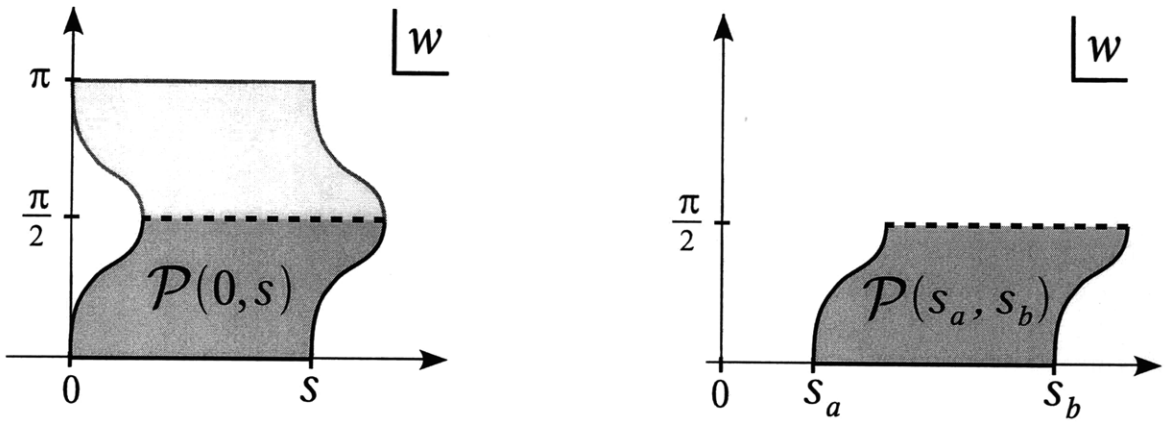

Figure 5-2: (a) Illustration of the surface associated with $e^{-s\mathcal{L}}$. It is generated by horizontal translations in the w frame. The half-propagator strip $\mathcal{P}(0,s)$ is obtained by cutting the surface $e^{-s\mathcal{L}}$ along the line $\Im(w) = \frac{\pi}{2}$. (b) The surface $\mathcal{P}(s_a, s_b)$ is a horizontal translation of the surface $\mathcal{P}(0, s_b - s_a)$ by s_a.

When $e^{-s\mathcal{L}}$ acts on an open string state A, the parameterization on γ is used to glue the strip associated with $e^{-s\mathcal{L}}$ to the coordinate curve of A. In the w frame, the right boundary of the strip $e^{-s\mathcal{L}}$ is a horizontal translation by s of its left boundary. It is therefore parameterized by the curve $s + \gamma(\theta)$ with $0 \leq \theta \leq \pi$. This fixes the horizontal position of the strip surface $e^{-s\mathcal{L}}$ in the w frame. We will now consider the surfaces which arise when we cut the strip $e^{-s\mathcal{L}}$ along the line $\Im(w) = \frac{\pi}{2}$. This line is generated by horizontal translations of $\gamma(\frac{\pi}{2})$ and is thus associated with the open string midpoint. The resulting surfaces from this particular cut are of interest for a number of reasons. In the annulus amplitude, we cut the propagator surface along a closed string curve to read off the boundary state along the boundary generated by the cut. Choosing the open string midpoint for this cut is natural because of the special role of the midpoint in open string field theory. Furthermore, if one chooses this cut for the strip $e^{-s\mathcal{L}}$ in Schnabl gauge, the resulting surfaces are the so-called slanted wedges introduced in chapter 4. As we explained there, the remarkable algebraic properties of these slanted wedges under gluing allowed the explicit map of one-loop Riemann surfaces to an annulus frame, which is expected to facilitate the explicit calculation of off-shell amplitudes. The analysis in the current chapter will experience a similarly drastic simplification in the Schnabl gauge limit.

The cutting of the strip $e^{-s\mathcal{L}}$ along the line $\Im(w) = \frac{\pi}{2}$ yields two surfaces. We will denote the bottom one, located in the region $0 \leq \Im(w) \leq \frac{\pi}{2}$, by $\mathcal{P}(0,s)$. See Figure 5-2(a). The arguments 0 and s remind us that the open string boundary of $\mathcal{P}(0,s)$ is located on the real axis between $w = 0$ and $w = s$. More generally, we use the notation $\mathcal{P}(s_a, s_b)$ with $s_b \geq s_a$ for the surface $\mathcal{P}(0, s_b - s_a)$ shifted horizontally by s_a in the w frame. See Figure 5-2(b). The left and right boundaries of $\mathcal{P}(s_a, s_b)$ are parameterized by $s_a + \gamma(\theta)$ and $s_b + \gamma(\theta)$, respectively, where the range of θ is now restricted to $0 \leq \theta \leq \frac{\pi}{2}$. Finally, $\mathcal{P}(s_a, s_b)$ has a boundary induced by the cut. This boundary is neither an open string boundary nor the coordinate line of an open string state.

For reasons that will become apparent later, we will refer to this boundary as the *closed string boundary*.[5]

Naively, the surface $\mathcal{P}(0,s)$ is generated by the operator $e^{-s\mathcal{L}_R}$, where $\mathcal{L}_R$ is the right half of $\mathcal{L}$. This notation, however, is misleading. It suggests, incorrectly, that the surface $\mathcal{P}(0,s)$ with $\mathcal{L}_R$ inserted at the left edge is the same as $\mathcal{P}(0,s)$ with $\mathcal{L}_R$ inserted at the right edge because $[\mathcal{L}_R, e^{-s\mathcal{L}_R}] = 0$. This is not the case because the line integral $\mathcal{L}_R$ has an endpoint on the closed string boundary and this endpoint cannot be moved by contour deformation. Let us denote by $\mathcal{L}_R(t)$ the line integral $\mathcal{L}_R$ along the contour $t+\gamma(\theta)$ with $0 \le \theta \le \frac{\pi}{2}$. As $\mathcal{L}_R$ generates translations in the w frame, we have

$$\mathcal{L}_R(t) \equiv \int_t^{\gamma(\frac{\pi}{2})+t} \left[\frac{dw}{2\pi i}\, T(w) + \frac{d\bar{w}}{2\pi i}\, \widetilde{T}(\bar{w})\right]. \tag{5.2.5}$$

The surface $\mathcal{P}(s_a, s_b)$ can then be properly expressed as the path-ordered exponential:

$$\mathcal{P}(s_a, s_b) = \mathrm{Pexp}\left[-\int_{s_a}^{s_b} dt\, \mathcal{L}_R(t)\right]. \tag{5.2.6}$$

Our convention for the path-ordering is $\mathcal{L}_R(t_1)\,\mathcal{L}_R(t_2)$ for $t_1 < t_2$. It is now clear that

$$\mathcal{L}_R(s_a)\,\mathcal{P}(s_a, s_b) - \mathcal{P}(s_a, s_b)\,\mathcal{L}_R(s_b) \neq 0 \tag{5.2.7}$$

because the left-hand side represents a surface with two disconnected contour integrals. It is therefore natural to introduce an operator that supplements the remaining line integral on $\mathcal{P}(s_a, s_b)$ along the closed string boundary. We thus define

$$\widehat{\mathcal{L}} = \int_{\gamma(\frac{\pi}{2})+s_a}^{\gamma(\frac{\pi}{2})+s_b} \left[\frac{dw}{2\pi i}\, T(w) + \frac{d\bar{w}}{2\pi i}\, \widetilde{T}(\bar{w})\right] \tag{5.2.8}$$

for $\widehat{\mathcal{L}}$ acting on $\mathcal{P}(s_a, s_b)$. We then have the identity

$$\mathcal{L}_R(s_a)\,\mathcal{P}(s_a, s_b) - \mathcal{P}(s_a, s_b)\,\mathcal{L}_R(s_b) + \widehat{\mathcal{L}}\,\mathcal{P}(s_a, s_b) = 0\,, \tag{5.2.9}$$

which follows from first connecting the three line integrals in (5.2.9)

and then shrinking the resulting integral contour to zero size. Furthermore, we have

$$\partial_{s_b}\,\mathcal{P}(s_a, s_b) = -\mathcal{P}(s_a, s_b)\,\mathcal{L}_R(s_b)\,, \qquad \partial_{s_a}\,\mathcal{P}(s_a, s_b) = \mathcal{L}_R(s_a)\,\mathcal{P}(s_a, s_b)\,, \tag{5.2.10}$$

which follow from the definition (5.2.6).

Following the definitions (5.2.5) and (5.2.8) of the line integrals of the energy-momentum tensor, we define the corresponding b-ghost line integrals as follows:

$$\begin{aligned} \mathcal{B}_R(t) &= \int_t^{\gamma(\frac{\pi}{2})+t} \left[\frac{dw}{2\pi i}\, b(w) + \frac{d\bar{w}}{2\pi i}\, \tilde{b}(\bar{w})\right], \\ \widehat{\mathcal{B}} &= \int_{\gamma(\frac{\pi}{2})+s_a}^{\gamma(\frac{\pi}{2})+s_b} \left[\frac{dw}{2\pi i}\, b(w) + \frac{d\bar{w}}{2\pi i}\, \tilde{b}(\bar{w})\right] \end{aligned} \tag{5.2.11}$$

[5]For the particular case of Schnabl gauge, this boundary is the so-called *hidden boundary* introduced in chapter 4.

for $\widehat{\mathcal{B}}$ acting on $\mathcal{P}(s_a, s_b)$. We also define the corresponding line integrals of the BRST current

$$\begin{aligned} \mathcal{Q}_R(t) &= \int_t^{\gamma(\frac{\pi}{2})+t} \left[\frac{dw}{2\pi i} j_B(w) - \frac{d\bar{w}}{2\pi i} \tilde{j}_B(\bar{w}) \right], \\ \widehat{\mathcal{Q}} &= \int_{\gamma(\frac{\pi}{2})+s_a}^{\gamma(\frac{\pi}{2})+s_b} \left[\frac{dw}{2\pi i} j_B(w) - \frac{d\bar{w}}{2\pi i} \tilde{j}_B(\bar{w}) \right] \end{aligned} \tag{5.2.12}$$

for $\widehat{\mathcal{Q}}$ acting on $\mathcal{P}(s_a, s_b)$. Just as in (5.2.9), we connect line integrals of the BRST current and the b ghost to find

$$\begin{aligned} &\mathcal{B}_R(s_a)\mathcal{P}(s_a, s_b) - \mathcal{P}(s_a, s_b)\mathcal{B}_R(s_b) + \widehat{\mathcal{B}}\,\mathcal{P}(s_a, s_b) = 0\,, \\ &\mathcal{Q}_R(s_a)\mathcal{P}(s_a, s_b) - \mathcal{P}(s_a, s_b)\mathcal{Q}_R(s_b) + \widehat{\mathcal{Q}}\,\mathcal{P}(s_a, s_b) = 0\,. \end{aligned} \tag{5.2.13}$$

5.2.2 Star multiplication of half-propagator strips

The surface $\mathcal{P}(s_a, s_b)$ is equipped with two parameterized boundaries which can be glued to open string states A or to other surfaces $\mathcal{P}(s'_a, s'_b)$. For the latter, we require that the glued boundaries in the w frame match. As for regular star multiplication of open string states, we use the symbol $*$ to denote this gluing.[6] For the special case of Schnabl gauge, this type of gluing operation was discussed extensively in chapter 4, and it lead to the algebra of slanted wedges (see section 4.4). From the definition of $\mathcal{P}(s_a, s_b)$ it immediately follows that

$$\mathcal{P}(s_a, s_b) * \mathcal{P}(s_b, s_c) = \mathcal{P}(s_a, s_c)\,. \tag{5.2.14}$$

Open string states A do not carry a closed string boundary. Therefore the gluing operation

$$\mathcal{P}(s_a, s_b) * A * \mathcal{P}(s_b, s_c) \tag{5.2.15}$$

is well defined and yields a surface with one connected closed string boundary between $\gamma(\frac{\pi}{2}) + s_a$ and $\gamma(\frac{\pi}{2}) + s_c$. It can be thought of as the surface $\mathcal{P}(s_a, s_c)$ with a *slit* along the curve $s_b + \gamma(\theta)$, where the open string state A is to be inserted. See Figure 5-3. It follows from (5.2.10) that a change in s_b on the surface (5.2.15) is generated by

$$\begin{aligned} &\partial_{s_b} \left[\mathcal{P}(s_a, s_b) * A * \mathcal{P}(s_b, s_c) \right] \\ &= -\mathcal{P}(s_a, s_b)\,\mathcal{L}_R(s_b) * A * \mathcal{P}(s_b, s_c) + \mathcal{P}(s_a, s_b) * A * \mathcal{L}_R(s_b)\,\mathcal{P}(s_b, s_c) \\ &\equiv -\mathcal{P}(s_a, s_b) * [\mathcal{L}_R(s_b), A] * \mathcal{P}(s_b, s_c)\,. \end{aligned} \tag{5.2.16}$$

Note the location of the star symbols in the second line, which is implicit in the commutator defined in the last line. This definition applies to any commutator or anticommutator of a line integral up to the closed string boundary with an open string state. For example,

$$\begin{aligned} &\mathcal{P}(s_a, s_b) * \{ \mathcal{B}_R(s_b), A \} * \mathcal{P}(s_b, s_c) \\ &\equiv \mathcal{P}(s_a, s_b)\,\mathcal{B}_R(s_b) * A * \mathcal{P}(s_b, s_c) + \mathcal{P}(s_a, s_b) * A * \mathcal{B}_R(s_b)\,\mathcal{P}(s_b, s_c)\,. \end{aligned} \tag{5.2.17}$$

[6] We will suppress explicit $*$ symbols in later sections.

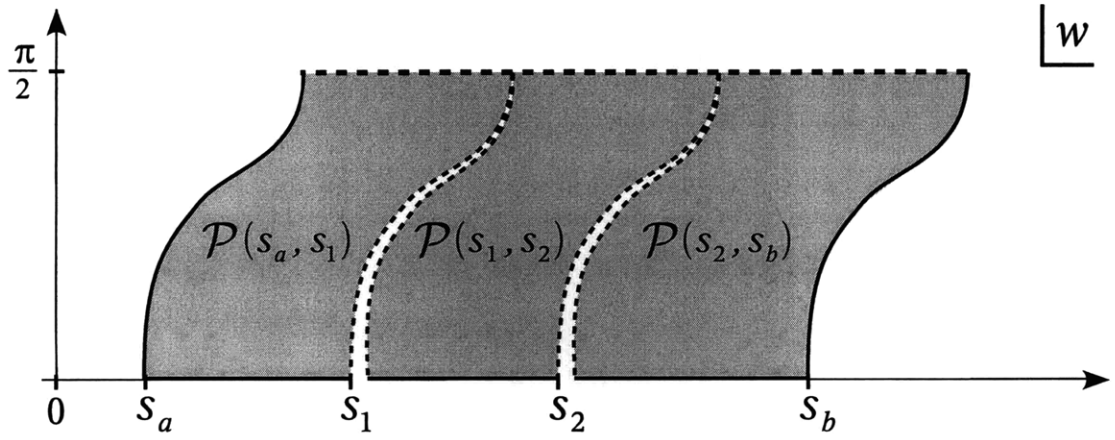

Figure 5-3: Illustration of the surface $\Sigma(s_a, s_b)$ for $k = 2$. It is obtained from the surface $\mathcal{P}(s_a, s_b)$ by inserting k open string states along the parameterized slits $s_i + \gamma(\theta)$.

In the case of $\mathcal{Q}_R(t)$, we have

$$\begin{aligned} &\mathcal{P}(s_a, s_b) * \{\, \mathcal{Q}_R(s_b), A \,\} * \mathcal{P}(s_b, s_c) \\ &\equiv \mathcal{P}(s_a, s_b)\, \mathcal{Q}_R(s_b) * A * \mathcal{P}(s_b, s_c) + \mathcal{P}(s_a, s_b) * A * \mathcal{Q}_R(s_b)\, \mathcal{P}(s_b, s_c) \\ &= -\mathcal{P}(s_a, s_b) * (QA) * \mathcal{P}(s_b, s_c) \end{aligned} \tag{5.2.18}$$

for any Grassmann-odd state A because the BRST current is a primary field of weight one so that its integral in the w frame can be deformed and easily mapped to the frame for A. Similar relations do not hold for $\mathcal{L}_R(t)$ and $\mathcal{B}_R(t)$ because the energy-momentum tensor and the b ghost are not primary fields of weight one:

$$\begin{aligned} \mathcal{P}(s_a, s_b) * [\,\mathcal{L}_R(s_b), A\,] * \mathcal{P}(s_b, s_c) &\neq -\mathcal{P}(s_a, s_b) * (\mathcal{L}A) * \mathcal{P}(s_b, s_c)\,, \\ \mathcal{P}(s_a, s_b) * \{\,\mathcal{B}_R(s_b), A\,\} * \mathcal{P}(s_b, s_c) &\neq -\mathcal{P}(s_a, s_b) * (\mathcal{B}A) * \mathcal{P}(s_b, s_c)\,. \end{aligned} \tag{5.2.19}$$

More generally, we will consider surfaces $\Sigma(s_a, s_b)$ resulting from multiple insertions of open string states $A_1, A_2, \ldots, A_k$ into $\mathcal{P}(s_a, s_b)$ in the following form:

$$\Sigma(s_a, s_b) = \mathcal{P}(s_a, s_1) * A_1 \ldots \mathcal{P}(s_{i-1}, s_i) * A_i * \mathcal{P}(s_i, s_{i+1}) \ldots A_k * \mathcal{P}(s_k, s_b) \tag{5.2.20}$$

with $s_a \leq s_1$, $s_i \leq s_{i+1}$, and $s_k \leq s_b$. The surface $\Sigma(s_a, s_b)$ is illustrated in Figure 5-3 for $k = 2$. The surface $\Sigma(s_a, s_b)$ is $\mathcal{P}(s_a, s_b)$ with k parameterized slits along the curves $s_i + \gamma(\theta)$ where the states A_i are to be glued. We denote the Grassmann property of Σ by $(-)^\Sigma$:

$$(-)^\Sigma = \prod_{i=1}^{k} (-)^{A_i}\,. \tag{5.2.21}$$

The operators $\widehat{\mathcal{L}}$, $\widehat{\mathcal{B}}$, and $\widehat{\mathcal{Q}}$ are derivations when acting on products of the form (5.2.20). For

example, we have

$$\begin{aligned}
&\widehat{\mathcal{L}}\left[\,\mathcal{P}(s_a,s_b)*A*\mathcal{P}(s_b,s_c)\,\right]\\
&=\left[\,\widehat{\mathcal{L}}\,\mathcal{P}(s_a,s_b)\right]*A*\mathcal{P}(s_b,s_c)+\mathcal{P}(s_a,s_b)*\left[\,\widehat{\mathcal{L}}\,A\,\right]*\mathcal{P}(s_b,s_c)+\mathcal{P}(s_a,s_b)*A*\left[\,\widehat{\mathcal{L}}\,\mathcal{P}(s_b,s_c)\right]\\
&=\left[\,\widehat{\mathcal{L}}\,\mathcal{P}(s_a,s_b)\right]*A*\mathcal{P}(s_b,s_c)+\mathcal{P}(s_a,s_b)*A*\left[\,\widehat{\mathcal{L}}\,\mathcal{P}(s_b,s_c)\right].
\end{aligned}\tag{5.2.22}$$

Here we used the fact that an open string state A does not have a closed string boundary and it is therefore annihilated by $\widehat{\mathcal{L}}$, $\widehat{\mathcal{B}}$, and $\widehat{\mathcal{Q}}$:

$$\widehat{\mathcal{L}}\,A=0\,,\qquad \widehat{\mathcal{B}}\,A=0\,,\qquad \widehat{\mathcal{Q}}\,A=0\,.\tag{5.2.23}$$

We define the BRST operator $\mathcal{Q}$ acting on a surface $\Sigma(s_a,s_b)$ of the form (5.2.20) by

$$\mathcal{Q}\,\Sigma(s_a,s_b)\equiv(-)^{\Sigma}\,\Sigma(s_a,s_b)\,\mathcal{Q}_R(s_b)-\widehat{\mathcal{Q}}\,\Sigma(s_a,s_b)-\mathcal{Q}_R(s_a)\,\Sigma(s_a,s_b)\,.\tag{5.2.24}$$

Note that the three integral contours can be connected. We have

$$\{\mathcal{Q},\mathcal{B}_R(t)\}=\mathcal{L}_R(t)\,,\qquad \{\mathcal{Q},\widehat{\mathcal{B}}\,\}=\widehat{\mathcal{L}}\,.\tag{5.2.25}$$

From (5.2.13) we know that $\mathcal{P}(s_a,s_b)$ is annihilated by this operator:

$$\mathcal{Q}\,\mathcal{P}(s_a,s_b)=0\,.\tag{5.2.26}$$

On an open string state A, inserted along a slit $s_a+\gamma(\theta)$ in the w frame, the definition of $\mathcal{Q}$ in (5.2.24) reduces to the usual BRST transformation Q:

$$\mathcal{Q}\,A=(-)^{A}A\,\mathcal{Q}_R(s_a)-\widehat{\mathcal{Q}}A-\mathcal{Q}_R(s_a)\,A=Q\,A\,.\tag{5.2.27}$$

Here we have used $\widehat{\mathcal{Q}}A=0$. Combining (5.2.26), (5.2.27), and the fact that the BRST current is a primary field of weight one, we find that the BRST transformation of a product $\Sigma(s_a,s_b)$ of the form (5.2.20) reduces to BRST transformations of the Fock-space states A_i. We have

$$\mathcal{Q}\,\Sigma(s_a,s_b)=\sum_{i=1}^{k}(-)^{\sum_{j=1}^{i-1}A_j}\mathcal{P}(s_a,s_1)*A_1\,\ldots\,\mathcal{P}(s_{i-1},s_i)*(QA_i)*\mathcal{P}(s_i,s_{i+1})\,\ldots\,A_k*\mathcal{P}(s_k,s_b)\,.\tag{5.2.28}$$

Similarly, the properties (5.2.9), (5.2.22) and (5.2.23) can be used to show

$$\begin{aligned}
&\mathcal{L}_R(s_a)\,\Sigma(s_a,s_b)-\Sigma(s_a,s_b)\,\mathcal{L}_R(s_b)+\widehat{\mathcal{L}}\,\Sigma(s_a,s_b)\\
&=\sum_{i=1}^{k}\mathcal{P}(s_a,s_1)*A_1\,\ldots\,\mathcal{P}(s_{i-1},s_i)*[\mathcal{L}_R(s_i),A_i]*\mathcal{P}(s_i,s_{i+1})\,\ldots\,A_k*\mathcal{P}(s_k,s_b)\\
&=-\sum_{i=1}^{k}\partial_{s_i}\Sigma(s_a,s_b)\,,
\end{aligned}\tag{5.2.29}$$

where we used (5.2.16) in the last step. The corresponding identity for b-ghost line integrals is

$$\begin{aligned}
&\mathcal{B}_R(s_a)\,\Sigma(s_a,s_b)-(-)^{\Sigma}\,\Sigma(s_a,s_b)\,\mathcal{B}_R(s_b)+\widehat{\mathcal{B}}\,\Sigma(s_a,s_b)\\
&=\sum_{i=1}^{k}(-)^{\sum_{j=1}^{i-1}A_j}\mathcal{P}(s_a,s_1)*A_1\,\ldots\,\left(\mathcal{B}_R(s_i)A_i-(-)^{A_i}A_i\mathcal{B}_R(s_i)\right)\,\ldots\,A_k*\mathcal{P}(s_k,s_b)\,.
\end{aligned}\tag{5.2.30}$$

5.2.3 Closed string states from half-propagator strips

A surface $\Sigma(s_a, s_b)$ of the form (5.2.20) can be used to construct a *closed string* surface state. To do this, we first introduce the identification $w \sim w + (s_b - s_a)$ in the w frame. This identifies the left boundary $s_a + \gamma(\theta)$ with the right boundary $s_b + \gamma(\theta)$ of $\Sigma(s_a, s_b)$. We are left with the closed string boundary at $\Im(w) = \frac{\pi}{2}$, whose name we are now doing justice by gluing it to the coordinate line $0 \leq \sigma \leq 2\pi$ of a closed string coordinate patch. The map from σ to the closed string boundary $\Im(w) = \frac{\pi}{2}$ of $\Sigma(s_a, s_b)$ is given by

$$\sigma \;\rightarrow\; w = i\,\frac{\pi}{2} + (s_b - s_a)\,\frac{\sigma}{2\pi}\,. \tag{5.2.31}$$

This map is consistent with the identifications $w \sim w+(s_b-s_a)$ and $\sigma \sim \sigma+2\pi$. The resulting surface is a closed string surface state with its coordinate line at $\Im(w) = \frac{\pi}{2}$ parameterized by (5.2.31). We denote this closed string surface state by

$$\oint_{s_b-s_a} \Sigma(s_b, s_a)\,. \tag{5.2.32}$$

We have represented the operation that turns the surface $\Sigma(s_b, s_a)$ into a closed string surface state by the symbol $\oint_{s_b-s_a}$. This notation is somewhat reminiscent of the notation $\int A$, often used in open string field theory, which glues the left and right parts of the open string state A. The subscript $s_b - s_a$ is a reminder that the width $s_b - s_a$ of the strip $\Sigma(s_a, s_b)$ explicitly enters the gluing prescription (5.2.31).

A natural representation of $\oint_{s_b-s_a} \Sigma(s_a, s_b)$ can be obtained in the ζ frame defined by

$$\zeta = \exp\Big(\frac{2\pi i}{s_b - s_a}\,w\Big)\,. \tag{5.2.33}$$

This maps the surface Σ to an annulus with the open string boundary placed at $|\zeta| = 1$ and the closed string coordinate line located at $|\zeta| = e^{-\frac{\pi^2}{s_b-s_a}}$. The surface state $\oint_{s_b-s_a} \Sigma(s_a, s_b)$ is then defined through inner products with arbitrary closed string states $|\phi_c\rangle$ in the Fock space by

$$\Big\langle\, \phi_c\,,\, \oint_{s_b-s_a} \Sigma(s_a, s_b)\,\Big\rangle \;=\; \Big\langle\, d_{s_b-s_a} \circ \phi_c(0)\,[\,\ldots\,]\,\Big\rangle_{\text{disk}}\,, \tag{5.2.34}$$

where the operator $\phi_c(0)$ corresponding to $|\phi_c\rangle$ is mapped from its canonical coordinate patch $|\xi| \leq 1$ to the shrunk coordinate patch $|\zeta| \leq e^{-\frac{\pi^2}{s_b-s_a}}$ by the retraction

$$d_{s_b-s_a}(\xi) = e^{-\frac{\pi^2}{s_b-s_a}}\,\xi\,. \tag{5.2.35}$$

The dots $[\ldots]$ in (5.2.34) represent the slits where the open string states A_i are inserted. They are also mapped from the w frame to the ζ frame via (5.2.33). For the case of $k = 4$ slits, the ζ-frame representation of the closed string surface state $\oint_{s_b-s_a} \Sigma(s_a, s_b)$ was illustrated in Figure 5-1(b).

The identification $w \sim w + (s_b - s_a)$ allows us to move line integrals cyclically in $\oint_{s_b-s_a}$. We have

$$\begin{aligned}
&\oint_{s_b-s_a} \mathcal{L}_R(s_a)\,\Sigma(s_a,s_b) = \oint_{s_b-s_a} \Sigma(s_a,s_b)\,\mathcal{L}_R(s_b)\,,\\
&\oint_{s_b-s_a} \mathcal{B}_R(s_a)\,\Sigma(s_a,s_b) = (-)^{\Sigma} \oint_{s_b-s_a} \Sigma(s_a,s_b)\,\mathcal{B}_R(s_b)\,,\\
&\oint_{s_b-s_a} \mathcal{Q}_R(s_a)\,\Sigma(s_a,s_b) = (-)^{\Sigma} \oint_{s_b-s_a} \Sigma(s_a,s_b)\,\mathcal{Q}_R(s_b)\,.
\end{aligned} \tag{5.2.36}$$

Let us examine how operators acting on the closed string state $\oint_{s_b-s_a} \Sigma(s_a,s_b)$ translate into line integrals on $\Sigma(s_a,s_b)$. The BRST operator is invariant under conformal transformations, and we find

$$\begin{aligned}
Q \oint_{s_b-s_a} \Sigma(s_a,s_b) &= -\oint_{s_b-s_a} \widehat{\mathcal{Q}}\,\Sigma(s_a,s_b)\\
&= -\oint_{s_b-s_a} \Big(\widehat{\mathcal{Q}}\,\Sigma(s_a,s_b) + \mathcal{Q}_R(s_a)\,\Sigma(s_a,s_b) - (-)^{\Sigma}\Sigma(s_a,s_b)\,\mathcal{Q}_R(s_b)\Big)\\
&= \oint_{s_b-s_a} \mathcal{Q}\,\Sigma(s_a,s_b)\,,
\end{aligned} \tag{5.2.37}$$

where we used (5.2.36) in the second step and (5.2.24) in the last step. Let us now consider the action of $L_0 - \tilde{L}_0$ on $\oint_{s_b-s_a} \Sigma(s_a,s_b)$. As $L_0 - \tilde{L}_0$ generates rotations in the ζ frame, we expect it to generate horizontal translations in the w frame. As a first step we note that

$$\begin{aligned}
L_0 - \tilde{L}_0 &= \int_{|\zeta|=\exp(-\frac{\pi^2}{s_b-s_a})} \left[\frac{d\zeta}{2\pi i}\,\zeta\,T(\zeta) - \frac{d\bar{\zeta}}{2\pi i}\,\bar{\zeta}\,\widetilde{T}(\bar{\zeta})\right]\\
&= \frac{s_b-s_a}{2\pi i} \int_{\gamma(\frac{\pi}{2})+s_a}^{\gamma(\frac{\pi}{2})+s_b} \left[\frac{dw}{2\pi i}\,T(w) + \frac{d\bar{w}}{2\pi i}\,\widetilde{T}(\bar{w})\right],
\end{aligned} \tag{5.2.38}$$

and therefore

$$(L_0 - \tilde{L}_0) \oint_{s_b-s_a} \Sigma(s_a,s_b) = \frac{s_b-s_a}{2\pi i} \oint_{s_b-s_a} \widehat{\mathcal{L}}\,\Sigma(s_a,s_b)\,. \tag{5.2.39}$$

For $\Sigma(s_a,s_b)$ of the form (5.2.20) we can use (5.2.36) and (5.2.29) to find

$$\begin{aligned}
(L_0 - \tilde{L}_0) \oint_{s_b-s_a} \Sigma(s_a,s_b) &= \frac{s_b-s_a}{2\pi i} \oint_{s_b-s_a} \Big([\,\mathcal{L}_R, \Sigma(s_a,s_b)\,] + \widehat{\mathcal{L}}\,\Sigma(s_a,s_b)\Big)\\
&= -\frac{s_b-s_a}{2\pi i} \oint_{s_b-s_a} \left[\sum_{i=1}^{k} \partial_{s_i}\Sigma(s_a,s_b)\right].
\end{aligned} \tag{5.2.40}$$

This result is consistent with the intuition that the generator of rotations in the ζ frame, $L_0 - \tilde{L}_0$, should generate horizontal translations on the positions s_i of the slits where the open string states A_i are glued. The translation in the w frame is proportional to the total length of the strip $s_b - s_a$,

as expected. The corresponding identity for $b_0 - \tilde{b}_0$ reads

$$\begin{aligned}(b_0 - \tilde{b}_0) \oint_{s_b - s_a} \Sigma(s_a, s_b) &= \frac{s_b - s_a}{2\pi i} \oint_{s_b - s_a} \widehat{\mathcal{B}}\, \Sigma(s_a, s_b) \\ = \frac{s_b - s_a}{2\pi i} \oint_{s_b - s_a} \sum_{i=1}^{k} (-)^{\sum_{j=1}^{i-1} A_j} &\mathcal{P}(s_a, s_1) * A_1 \ \dots \\ &\times \left(\mathcal{B}_R(s_i) A_i - (-)^{A_i} A_i\, \mathcal{B}_R(s_i)\right) \ \dots \ A_k * \mathcal{P}(s_k, s_b)\,.\end{aligned} \tag{5.2.41}$$

We can move an open string state A cyclically within $\oint_{s_b - s_a}$ just as we did for line integrals in (5.2.36). We have

$$\oint_{s_b - s_a} A * \Sigma(s_a, s_b) = (-)^{A\Sigma} \oint_{s_b - s_a} \Sigma(s_a, s_b) * A\,. \tag{5.2.42}$$

Similarly, we can cyclically move half-propagator strips in $\oint_{s_b - s_a}$, but all surfaces must attach to the same segment of the closed string boundary after using the cyclicity. We conclude that

$$\begin{aligned}&\oint_{s_b - s_a} \mathcal{P}(s_a, s_1) * A_1 * \mathcal{P}(s_1, s_2) \ \dots \ A_k * \mathcal{P}(s_k, s_b) \\ &= \oint_{s_b - s_a} A_1 * \mathcal{P}(s_1, s_2) \ \dots \ A_k * \mathcal{P}(s_k, s_b) * \mathcal{P}(s_b, s_1 + s_b - s_a) \\ &= \oint_{s_b - s_a} A_1 * \mathcal{P}(s_1, s_2) \ \dots \ A_k * \mathcal{P}(s_k, s_1 + s_b - s_a)\,,\end{aligned} \tag{5.2.43}$$

where the position of $\mathcal{P}(s_a, s_1)$ was translated by $s_b - s_a$, which is consistent with the periodicity $w \sim w + (s_b - s_a)$ in the w frame.

5.3 Construction of BRST-invariant closed string states

In this section we construct a class of closed string states from a solution of open string field theory using the half-propagator strips we discussed in section 5.2. We then show that the closed string states are BRST invariant and change by BRST-exact terms under gauge transformations of the classical solution.

5.3.1 The boundary state from the half-propagator strip

The surface $\mathcal{P}(0, s)$ is closely related to the BCFT boundary state $|B\rangle$. Recall from (5.1.1) that a one-point function of a closed string vertex operator at the origin on a unit disk can be expressed in terms of $|B\rangle$ as follows:

$$\langle B|(c_0 - \tilde{c}_0)|\phi_c\rangle\,, \tag{5.3.1}$$

where $|\phi_c\rangle$ is the closed string state corresponding to the vertex operator. When we cut the unit disk along a circle of radius $e^{-\frac{\pi^2}{s}}$, the one-point function can be thought of as an inner product of $\langle B|\, e^{-\frac{\pi^2}{s}(L_0 + \tilde{L}_0)}$ and $e^{\frac{\pi^2}{s}(L_0 + \tilde{L}_0)}(c_0 - \tilde{c}_0)|\phi_c\rangle$:

$$\langle B|(c_0 - \tilde{c}_0)|\phi_c\rangle = \langle B|\, e^{-\frac{\pi^2}{s}(L_0 + \tilde{L}_0)} e^{\frac{\pi^2}{s}(L_0 + \tilde{L}_0)}(c_0 - \tilde{c}_0)|\phi_c\rangle\,. \tag{5.3.2}$$

The half-propagator strip of length s with the initial and final half-string boundaries identified can be mapped to the annulus region on the unit disk bounded by the unit circle and the circle of radius $e^{-\frac{\pi^2}{s}}$. We therefore have

$$\oint_s \mathcal{P}(0,s) = e^{-\frac{\pi^2}{s}(L_0+\tilde{L}_0)} |B\rangle \,. \tag{5.3.3}$$

The boundary state $|B\rangle$ can thus be expressed in terms of the half-propagator strip as follows:

$$|B\rangle = e^{\frac{\pi^2}{s}(L_0+\tilde{L}_0)} \oint_s \mathcal{P}(0,s) \,. \tag{5.3.4}$$

This definition reproduces the BCFT boundary state for any value of s. In particular, we conclude

$$\partial_s \left[e^{\frac{\pi^2}{s}(L_0+\tilde{L}_0)} \oint_s \mathcal{P}(0,s) \right] = \partial_s |B\rangle = 0 \,. \tag{5.3.5}$$

Later we will confirm this explicitly in section 5.4.2.

5.3.2 Construction of the closed string state $|B_*(\Psi)\rangle$

We now define a closed string state that is expected to be a generalization of $|B\rangle$ to the background associated with a solution to the equation of motion of open string field theory. In (5.3.4) the boundary state $|B\rangle$ was expressed in terms of the surface $\mathcal{P}(0,s)$ which is the right half of the propagator strip generated by $e^{-s\mathcal{L}}$. Since $\{Q,\mathcal{B}\} = \mathcal{L}$, we can write

$$e^{-s\mathcal{L}} = e^{-s\{Q,\mathcal{B}\}} \,. \tag{5.3.6}$$

We generalize $e^{-s\mathcal{L}}$ by replacing Q in this expression by the BRST operator associated with the new background.

When we expand the open string field theory action around a solution Ψ of the equation of motion

$$Q\Psi + \Psi^2 = 0 \,, \tag{5.3.7}$$

the BRST operator Q_* associated with the new background is given by

$$Q_* A \equiv QA + \Psi A - (-)^A A\,\Psi \tag{5.3.8}$$

for any state A. Thus the operator $e^{-s\mathcal{L}}$ should be modified as

$$e^{-s\mathcal{L}} \;\to\; e^{-s\{Q_*,\mathcal{B}\}} \,. \tag{5.3.9}$$

To define a modified half-propagator strip $\mathcal{P}_*(0,s)$, we have to extract the right half of the surface associated with $e^{-s\{Q_*,\mathcal{B}\}}$. To do this, we first examine the action of $\{Q_*,\mathcal{B}\}$ on an arbitrary state A. Making use of (5.3.8), we readily find

$$\{Q_*,\mathcal{B}\}\,A = \mathcal{L}A + \Psi\,(\mathcal{B}A) + (-)^A\,(\mathcal{B}A)\,\Psi + \mathcal{B}\,(\Psi A) - (-)^A \mathcal{B}\,(A\Psi) \,. \tag{5.3.10}$$

If we write $\mathcal{L} = \mathcal{L}_R + \mathcal{L}_L$ and $\mathcal{B} = \mathcal{B}_R + \mathcal{B}_L$, we find that the action of $\{Q_*, \mathcal{B}\}$ on A decomposes into right and left pieces as

$$\{Q_*, \mathcal{B}\}A = \Big[\, \mathcal{L}_R A + (-)^A(\mathcal{B}_R A)\Psi - (-)^A \mathcal{B}_R(A\Psi) \,\Big] + \Big[\, \mathcal{L}_L A + \Psi(\mathcal{B}_L A) + \mathcal{B}_L(\Psi A) \,\Big]\,, \quad (5.3.11)$$

where terms with a mixed action on both right and left halves of the state A have canceled as follows:

$$\Psi(\mathcal{B}_R A) + \mathcal{B}_R(\Psi A) = 0\,, \quad (-)^A(\mathcal{B}_L A)\Psi - (-)^A \mathcal{B}_L(A\Psi) = 0\,. \quad (5.3.12)$$

Therefore the operator $\mathcal{L}_R(t)$ in the half-propagator strip $\mathcal{P}(s_a, s_b)$ defined in (5.2.6) should be modified as

$$\mathcal{L}_R(t) \;\to\; \mathcal{L}_R(t) + \{\mathcal{B}_R(t), \Psi\}\,. \quad (5.3.13)$$

The sign factors of $(-)^A$ in (5.3.11) have disappeared because of our path-ordering convention stated after (5.2.6). We thus define the modified half-propagator strip by

$$\mathcal{P}_*(s_a, s_b) \equiv \mathrm{Pexp}\Big[-\int_{s_a}^{s_b} dt \,\Big[\, \mathcal{L}_R(t) + \{\mathcal{B}_R(t), \Psi\} \,\Big]\Big]\,. \quad (5.3.14)$$

It is useful to explicitly expand $\mathcal{P}_*(s_a, s_b)$ in powers of the classical solution. We obtain

$$\begin{aligned}
\mathcal{P}_*(s_a, s_b) &= \mathcal{P}(s_a, s_b) - \int_{s_a}^{s_b} ds_1\, \mathcal{P}(s_a, s_1)\, \{\mathcal{B}_R(s_1), \Psi\}\, \mathcal{P}(s_1, s_b) \\
&\quad + \int_{s_a}^{s_b} ds_1 \int_{s_1}^{s_b} ds_2\, \mathcal{P}(s_a, s_1)\, \{\mathcal{B}_R(s_1), \Psi\}\, \mathcal{P}(s_1, s_2)\, \{\mathcal{B}_R(s_2), \Psi\}\, \mathcal{P}(s_2, s_b) + \dots \\
&= \sum_{k=0}^{\infty} (-1)^k \int_{s_a}^{s_b} ds_1 \dots \int_{s_{i-1}}^{s_b} ds_i \dots \int_{s_{k-1}}^{s_b} ds_k\, \mathcal{P}(s_a, s_1)\, \{\mathcal{B}_R(s_1), \Psi\}\, \mathcal{P}(s_1, s_2) \dots \\
&\qquad \times \dots \mathcal{P}(s_{i-1}, s_i)\, \{\mathcal{B}_R(s_i), \Psi\}\, \mathcal{P}(s_i, s_{i+1}) \dots \mathcal{P}(s_{k-1}, s_k)\, \{\mathcal{B}_R(s_k), \Psi\}\, \mathcal{P}(s_k, s_b)\,.
\end{aligned} \quad (5.3.15)$$

The modified half-propagator strip obeys the following relations:

$$\begin{aligned}
\partial_{s_b} \mathcal{P}_*(s_a, s_b) &= -\mathcal{P}_*(s_a, s_b)\, (\, \mathcal{L}_R(s_b) + \{\mathcal{B}_R(s_b), \Psi\}\,)\,, \\
\partial_{s_a} \mathcal{P}_*(s_a, s_b) &= (\, \mathcal{L}_R(s_a) + \{\mathcal{B}_R(s_a), \Psi\}\,)\, \mathcal{P}_*(s_a, s_b)\,.
\end{aligned} \quad (5.3.16)$$

The formula (5.2.16) is generalized as follows:

$$\partial_t \big[\, \mathcal{P}_*(s_a, t)\, A\, \mathcal{P}_*(t, s_b) \,\big] = -\mathcal{P}_*(s_a, t) \,\big[\, \mathcal{L}_R(t) + \{\mathcal{B}_R(t), \Psi\}\,,\, A \,\big]\, \mathcal{P}_*(t, s_b)\,. \quad (5.3.17)$$

By analogy with the expression (5.3.4) of the original boundary state $|B\rangle$, we now introduce the following background-dependent state:

$$\boxed{\,|B_*(\Psi)\rangle \equiv e^{\frac{\pi^2}{s}(L_0 + \tilde{L}_0)} \oint_s \mathcal{P}_*(0, s)\,.\,} \quad (5.3.18)$$

For future use we expand $|B_*(\Psi)\rangle$ in powers of the solution:

$$|B_*(\Psi)\rangle = \sum_{k=0}^{\infty} |B_*^{(k)}(\Psi)\rangle\,, \quad (5.3.19)$$

where

$$
\begin{aligned}
|B_*^{(0)}(\Psi)\rangle &= |B\rangle\,,\\
|B_*^{(1)}(\Psi)\rangle &= -\,e^{\frac{\pi^2}{s}(L_0+\tilde{L}_0)}\oint_s\int_0^s ds_1\,\mathcal{P}(0,s_1)\,\{\mathcal{B}_R(s_1),\Psi\}\,\mathcal{P}(s_1,s)\,,\\
|B_*^{(2)}(\Psi)\rangle &= e^{\frac{\pi^2}{s}(L_0+\tilde{L}_0)}\oint_s\int_0^s ds_1\int_{s_1}^s ds_2\,\mathcal{P}(0,s_1)\,\{\mathcal{B}_R(s_1),\Psi\}\,\mathcal{P}(s_1,s_2)\,\{\mathcal{B}_R(s_2),\Psi\}\,\mathcal{P}(s_2,s)\,,\\
&\;\;\vdots\\
|B_*^{(k)}(\Psi)\rangle &= (-1)^k\,e^{\frac{\pi^2}{s}(L_0+\tilde{L}_0)}\oint_s\int_0^s ds_1\ldots\int_{s_{i-1}}^s ds_i\ldots\int_{s_{k-1}}^s ds_k\,\mathcal{P}(0,s_1)\,\{\mathcal{B}_R(s_1),\Psi\}\,\mathcal{P}(s_1,s_2)\ldots\\
&\qquad\times\ldots\mathcal{P}(s_{i-1},s_i)\,\{\mathcal{B}_R(s_i),\Psi\}\,\mathcal{P}(s_i,s_{i+1})\ldots\mathcal{P}(s_{k-1},s_k)\,\{\mathcal{B}_R(s_k),\Psi\}\,\mathcal{P}(s_k,s)\,.
\end{aligned}
\tag{5.3.20}
$$

We expect that $|B_*(\Psi)\rangle$ is related to the boundary state of the BCFT described by the solution Ψ. In the following we study various properties of $|B_*(\Psi)\rangle$ and in section 5.6 we explicitly calculate it for analytic solutions.

5.3.3 BRST invariance of $|B_*(\Psi)\rangle$

We show that the closed string state $|B_*(\Psi)\rangle$ is BRST closed when Ψ satisfies the equation of motion of open string field theory. The BRST transformation of $\{\mathcal{B}_R(t),\Psi\}$ is

$$
\begin{aligned}
\mathcal{Q}\,\{\mathcal{B}_R(t),\Psi\} &= \mathcal{Q}\,(\mathcal{B}_R(t)\,\Psi+\Psi\,\mathcal{B}_R(t)) = \mathcal{L}_R(t)\,\Psi+\mathcal{B}_R(t)\,\Psi^2-\Psi^2\,\mathcal{B}_R(t)-\Psi\,\mathcal{L}_R(t)\\
&= [\,\mathcal{L}_R(t),\Psi\,]+\{\mathcal{B}_R(t),\Psi\}\,\Psi-\Psi\,\{\mathcal{B}_R(t),\Psi\} = [\,\mathcal{L}_R(t)+\{\mathcal{B}_R(t),\Psi\},\Psi\,]\,,
\end{aligned}
\tag{5.3.21}
$$

where we have used the equation of motion $Q\Psi+\Psi^2=0$. Using (5.3.17), we conclude

$$
\begin{aligned}
\mathcal{Q}\,\mathcal{P}_*(s_a,s_b) &= -\int_{s_a}^{s_b} dt\,\mathcal{P}_*(s_a,t)\,\big(\mathcal{Q}\,\{\mathcal{B}_R(t),\Psi\}\big)\,\mathcal{P}_*(t,s_b)\\
&= -\int_{s_a}^{s_b} dt\,\mathcal{P}_*(s_a,t)\,[\,\mathcal{L}_R(t)+\{\mathcal{B}_R(t),\Psi\},\Psi\,]\,\mathcal{P}_*(t,s_b)\\
&= \int_{s_a}^{s_b} dt\,\partial_t\big[\mathcal{P}_*(s_a,t)\,\Psi\,\mathcal{P}_*(t,s_b)\big]\\
&= -\big[\,\Psi,\mathcal{P}_*(s_a,s_b)\,\big]\,.
\end{aligned}
\tag{5.3.22}
$$

It is instructive to derive this relation explicitly from the expansion (5.3.15) of the path-ordered exponential which defines $\mathcal{P}_*(s_a,s_b)$. It follows from (5.3.21) that

$$
\begin{aligned}
&\mathcal{Q}\Big[\,\mathcal{P}(s_{i-1},s_i)\,\{\mathcal{B}_R(s_i),\Psi\}\,\mathcal{P}(s_i,s_{i+1})\,\Big] = \mathcal{P}(s_{i-1},s_i)\,(\mathcal{Q}\{\mathcal{B}_R(s_i),\Psi\})\,\mathcal{P}(s_i,s_{i+1})\\
&= -\partial_{s_i}\Big[\,\mathcal{P}(s_{i-1},s_i)\,\Psi\,\mathcal{P}(s_i,s_{i+1})\,\Big]+\mathcal{P}(s_{i-1},s_i)\,[\,\{\mathcal{B}_R(s_i),\Psi\},\Psi\,]\,\mathcal{P}(s_i,s_{i+1})\,,
\end{aligned}
\tag{5.3.23}
$$

where we have used (5.2.16) and (5.2.28). Let us consider the term in the expansion of $\mathcal{P}_*(s_a, s_b)$ with k insertions of the classical solution. We need to calculate its BRST transformation

$$(-1)^k \mathcal{Q} \int_{s_a}^{s_b} ds_1 \,.. \int_{s_{i-1}}^{s_b} ds_i \,.. \int_{s_{k-1}}^{s_b} ds_k \, \mathcal{P}(s_a, s_1) \,.. \mathcal{P}(s_{i-1}, s_i) \, \{\mathcal{B}_R(s_i), \Psi\} \, \mathcal{P}(s_i, s_{i+1}) \,.. \mathcal{P}(s_k, s_b) \,. \tag{5.3.24}$$

Using (5.3.23) and the formula

$$\begin{aligned} &\int_{s_{i-1}}^{s_b} ds_i \int_{s_i}^{s_b} ds_{i+1} \, \partial_{s_i} f(s_{i-1}, s_i, s_{i+1}) \\ &= \int_{s_{i-1}}^{s_b} ds_i \, \partial_{s_i} \left[\int_{s_i}^{s_b} ds_{i+1} \, f(s_{i-1}, s_i, s_{i+1}) \right] + \int_{s_{i-1}}^{s_b} ds_i \, f(s_{i-1}, s_i, s_i) \\ &= - \int_{s_{i-1}}^{s_b} ds_{i+1} \, f(s_{i-1}, s_i, s_{i+1}) \Big|_{s_i = s_{i-1}} + \int_{s_{i-1}}^{s_b} ds_i \, f(s_{i-1}, s_i, s_{i+1}) \Big|_{s_{i+1} = s_i} , \end{aligned} \tag{5.3.25}$$

we calculate (5.3.24) as

$$\begin{aligned} &(-1)^k \sum_{i=1}^{k} \int_{s_a}^{s_b} ds_1 \,.. \int_{s_{i-1}}^{s_b} ds_i \,.. \int_{s_{k-1}}^{s_b} ds_k \\ &\qquad \times \mathcal{P}(s_a, s_1) \ldots \mathcal{P}(s_{i-1}, s_i) \left[\{\mathcal{B}_R(s_i), \Psi\} \, , \, \Psi \right] \mathcal{P}(s_i, s_{i+1}) \ldots \mathcal{P}(s_k, s_b) \\ &- (-1)^{k-1} \int_{s_a}^{s_b} ds_1 \,.. \int_{s_{i-1}}^{s_b} ds_i \,.. \int_{s_{k-2}}^{s_b} ds_{k-1} \\ &\qquad \times \Bigg[\sum_{i=1}^{k-1} \mathcal{P}(s_a, s_1) \ldots \mathcal{P}(s_{i-1}, s_i) \left[\{\mathcal{B}_R(s_i), \Psi\} \, , \, \Psi \right] \mathcal{P}(s_i, s_{i+1}) \ldots \mathcal{P}(s_{k-1}, s_b) \\ &\qquad\quad + \Big[\Psi \, , \, \mathcal{P}(s_a, s_1) \ldots \mathcal{P}(s_{i-1}, s_i) \, \{\mathcal{B}_R(s_i), \Psi\} \, \mathcal{P}(s_i, s_{i+1}) \ldots \mathcal{P}(s_{k-1}, s_b) \Big] \Bigg] \,. \end{aligned} \tag{5.3.26}$$

Here we relabeled the indices in the last two terms so that the $k-1$ integration variables are $s_1, \ldots, s_{k-1}$. We see that after summing over all k, the first term at order $k-1$ cancels the second term at order k, and we are left with contributions from the last term. As in (5.3.22), we conclude that

$$\mathcal{Q} \mathcal{P}_*(s_a, s_b) = - \left[\Psi, \mathcal{P}_*(s_a, s_b) \right] . \tag{5.3.27}$$

Recalling the definition of the modified BRST operator Q_* in (5.3.8), this is in fact a natural modification of (5.2.26). We then find

$$Q \oint_{s_b - s_a} \mathcal{P}_*(s_a, s_b) = \oint_{s_b - s_a} \mathcal{Q} \mathcal{P}_*(s_a, s_b) = - \oint_{s_b - s_a} \left[\Psi, \mathcal{P}_*(s_a, s_b) \right] = 0 \,, \tag{5.3.28}$$

where we used (5.2.37) in the first step and (5.2.42) in the last step. Since the BRST operator commutes with $L_0 + \tilde{L}_0$, we obtain

$$Q \, |B_*(\Psi)\rangle = 0 \,. \tag{5.3.29}$$

We have thus constructed a BRST-invariant closed string state for a given solution Ψ.

It is easy to see that the closed string state $|B_*(\Psi)\rangle$ is annihilated by $b_0 - \tilde{b}_0$. It follows from (5.2.41) and $[\mathcal{B}_R(t), \{\mathcal{B}_R(t), \Psi\}] = 0$ that

$$(b_0 - \tilde{b}_0) \oint_{s_b - s_a} \mathcal{P}_*(s_a, s_b) = 0 \,. \tag{5.3.30}$$

Since $b_0 - \tilde{b}_0$ commutes with $L_0 + \tilde{L}_0$, we conclude that

$$(b_0 - \tilde{b}_0) \, |B_*(\Psi)\rangle = 0 \,. \tag{5.3.31}$$

The state $|B_*(\Psi)\rangle$ is also annihilated by $L_0 - \tilde{L}_0$ because

$$(L_0 - \tilde{L}_0) \, |B_*(\Psi)\rangle = \{Q, \, b_0 - \tilde{b}_0\} \, |B_*(\Psi)\rangle = 0 \,. \tag{5.3.32}$$

In summary, we have found that the state $|B_*(\Psi)\rangle$ satisfies three consistency requirements for its interpretation as a boundary state, namely,

$$\boxed{Q \, |B_*(\Psi)\rangle = 0 \,, \qquad (b_0 - \tilde{b}_0) \, |B_*(\Psi)\rangle = 0 \,, \qquad (L_0 - \tilde{L}_0) \, |B_*(\Psi)\rangle = 0 \,.} \tag{5.3.33}$$

5.3.4 Variation of $|B_*(\Psi)\rangle$ under open string gauge transformations

Consider an infinitesimal gauge transformation of the solution:

$$\delta_\chi \Psi = Q \, \chi + [\, \Psi, \chi \,] \,. \tag{5.3.34}$$

It follows from the path-ordered expression of $\mathcal{P}_*(s_a, s_b)$ that it changes under the gauge transformation as follows:

$$\begin{aligned} \delta_\chi \mathcal{P}_*(s_a, s_b) &= - \int_{s_a}^{s_b} dt \, \mathcal{P}_*(s_a, t) \, \{\mathcal{B}_R(t), \delta_\chi \Psi\} \, \mathcal{P}_*(t, s_b) \\ &= - \int_{s_a}^{s_b} dt \, \mathcal{P}_*(s_a, t) \, \{\mathcal{B}_R(t), Q\chi\} \, \mathcal{P}_*(t, s_b) - \int_{s_a}^{s_b} dt \, \mathcal{P}_*(s_a, t) \, \{\mathcal{B}_R(t), [\, \Psi, \chi \,]\} \, \mathcal{P}_*(t, s_b) \,. \end{aligned} \tag{5.3.35}$$

The first term in the second line can be written as

$$\begin{aligned} & - \int_{s_a}^{s_b} dt \, \mathcal{P}_*(s_a, t) \, \{\mathcal{B}_R(t), Q\chi\} \, \mathcal{P}_*(t, s_b) \\ &= \mathcal{Q} \int_{s_a}^{s_b} dt \, \mathcal{P}_*(s_a, t) \, [\, \mathcal{B}_R(t), \chi \,] \, \mathcal{P}_*(t, s_b) - \int_{s_a}^{s_b} dt \, (\mathcal{Q} \, \mathcal{P}_*(s_a, t)) \, [\, \mathcal{B}_R(t), \chi \,] \, \mathcal{P}_*(t, s_b) \\ & \quad - \int_{s_a}^{s_b} dt \, \mathcal{P}_*(s_a, t) \, [\, \mathcal{L}_R(t), \chi \,] \, \mathcal{P}_*(t, s_b) + \int_{s_a}^{s_b} dt \, \mathcal{P}_*(s_a, t) \, [\, \mathcal{B}_R(t), \chi \,] \, (\mathcal{Q} \, \mathcal{P}_*(t, s_b)) \,. \end{aligned} \tag{5.3.36}$$

The first term on the right-hand side of (5.3.36) is BRST exact. The second and fourth terms on the right-hand side can be written using (5.3.27) as follows:

$$\begin{aligned} & - \int_{s_a}^{s_b} dt \, (\mathcal{Q} \, \mathcal{P}_*(s_a, t)) \, [\, \mathcal{B}_R(t), \chi \,] \, \mathcal{P}_*(t, s_b) + \int_{s_a}^{s_b} dt \, \mathcal{P}_*(s_a, t) \, [\, \mathcal{B}_R(t), \chi \,] \, (\mathcal{Q} \, \mathcal{P}_*(t, s_b)) \\ &= \left\{ \Psi, \int_{s_a}^{s_b} dt \, \mathcal{P}_*(s_a, t) \, [\, \mathcal{B}_R(t), \chi \,] \, \mathcal{P}_*(t, s_b) \right\} - \int_{s_a}^{s_b} dt \, \mathcal{P}_*(s_a, t) \, \{\, \Psi, [\, \mathcal{B}_R(t), \chi \,]\, \} \, \mathcal{P}_*(t, s_b) \,. \end{aligned} \tag{5.3.37}$$

Since

$$\{\mathcal{B}_R(t), [\,\Psi, \chi\,]\} + \{\,\Psi, [\,\mathcal{B}_R(t), \chi\,]\,\} = [\,\{\mathcal{B}_R(t), \Psi\,\}, \chi\,]\,, \tag{5.3.38}$$

we find

$$\begin{aligned}\delta_\chi \mathcal{P}_*(s_a, s_b) = \mathcal{Q} \int_{s_a}^{s_b} dt\, \mathcal{P}_*(s_a, t)\, [\,\mathcal{B}_R(t), \chi\,]\, \mathcal{P}_*(t, s_b) \\ + \left\{\, \Psi, \int_{s_a}^{s_b} dt\, \mathcal{P}_*(s_a, t)\, [\,\mathcal{B}_R(t), \chi\,]\, \mathcal{P}_*(t, s_b) \right\} \\ - \int_{s_a}^{s_b} dt\, \mathcal{P}_*(s_a, t)\, [\,\mathcal{L}_R(t) + \{\mathcal{B}_R(t), \Psi\}, \chi\,]\, \mathcal{P}_*(t, s_b)\,.\end{aligned} \tag{5.3.39}$$

Using (5.3.17), we obtain the following final expression:

$$\begin{aligned}\delta_\chi \mathcal{P}_*(s_a, s_b) = \mathcal{Q} \int_{s_a}^{s_b} dt\, \mathcal{P}_*(s_a, t)\, [\,\mathcal{B}_R(t), \chi\,]\, \mathcal{P}_*(t, s_b) \\ + \left\{\, \Psi, \int_{s_a}^{s_b} dt\, \mathcal{P}_*(s_a, t)\, [\,\mathcal{B}_R(t), \chi\,]\, \mathcal{P}_*(t, s_b) \right\} - [\,\chi, \mathcal{P}_*(s_a, s_b)\,]\,.\end{aligned} \tag{5.3.40}$$

It follows from this and (5.2.42) that

$$\delta_\chi \oint_{s_b - s_a} \mathcal{P}_*(s_a, s_b) = Q \oint_{s_b - s_a} \int_{s_a}^{s_b} dt\, \mathcal{P}_*(s_a, t)\, [\,\mathcal{B}_R(t), \chi\,]\, \mathcal{P}_*(t, s_b)\,. \tag{5.3.41}$$

We thus have

$$\delta_\chi |B_*(\Psi)\rangle = Q \left[\, e^{\frac{\pi^2}{s}(L_0 + \tilde{L}_0)} \oint_s \int_0^s dt\, \mathcal{P}_*(0, t)\, [\,\mathcal{B}_R(t), \chi\,]\, \mathcal{P}_*(t, s) \right] \tag{5.3.42}$$

and conclude that

$$\boxed{\delta_\chi |B_*(\Psi)\rangle \;=\; Q - \text{exact}\,.} \tag{5.3.43}$$

The inner product $\langle \mathcal{V}|\,(c_0 - \tilde{c}_0)|B_*(\Psi)\rangle$ is then invariant under gauge transformations of open string field theory for any closed string state $|\mathcal{V}\rangle$ that is annihilated by the BRST operator because $\langle \mathcal{V}|\,(c_0 - \tilde{c}_0)\, Q\,|\Omega\rangle = 0$ for any closed string state $|\Omega\rangle$. This can be shown in the following way Any closed string state has to be annihilated by $b_0 - \tilde{b}_0$. Thus $|\Omega\rangle$ can be written as

$$|\Omega\rangle = (b_0 - \tilde{b}_0)\,|\widetilde{\Omega}\rangle\,. \tag{5.3.44}$$

Since $|\mathcal{V}\rangle$ is annihilated by both Q and $b_0 - \tilde{b}_0$, we have

$$\begin{aligned}\langle \mathcal{V}|\,(c_0 - \tilde{c}_0)\, Q\,|\Omega\rangle &= \langle \mathcal{V}|\,(c_0 - \tilde{c}_0)\, Q\,(b_0 - \tilde{b}_0)\,|\widetilde{\Omega}\rangle \\ &= \langle \mathcal{V}|\,\{c_0 - \tilde{c}_0,\, Q\}\,(b_0 - \tilde{b}_0)\,|\widetilde{\Omega}\rangle = \langle \mathcal{V}|\,[\,\{c_0 - \tilde{c}_0,\, Q\},\, b_0 - \tilde{b}_0\,]\,|\widetilde{\Omega}\rangle\,.\end{aligned} \tag{5.3.45}$$

Using the Jacobi identity, we find

$$\begin{aligned}[\,\{c_0 - \tilde{c}_0,\, Q\},\, b_0 - \tilde{b}_0\,] &= -\,[\,\{Q,\, b_0 - \tilde{b}_0\},\, c_0 - \tilde{c}_0\,] - [\,\{b_0 - \tilde{b}_0,\, c_0 - \tilde{c}_0\},\, Q\,] \\ &= -\,[\,L_0 - \tilde{L}_0,\, c_0 - \tilde{c}_0\,] = 0\,.\end{aligned} \tag{5.3.46}$$

Therefore $\langle \mathcal{V}|\,(c_0 - \tilde{c}_0)\, Q\,|\Omega\rangle$ vanishes for any closed string state $|\Omega\rangle$ and thus we conclude that $\langle \mathcal{V}|\,(c_0 - \tilde{c}_0)|B_*(\Psi)\rangle$ is gauge-invariant for any closed string state $|\mathcal{V}\rangle$ annihilated by the BRST operator.

5.4 Dependence on the choice of the propagator strip

The closed string state $|B_*(\Psi)\rangle$ for a given solution Ψ depends on the total strip length s and the operator $\mathcal{B}$ for the gauge-fixing condition. In this section we study the dependence of the state $|B_*(\Psi)\rangle$ on s and $\mathcal{B}$.

5.4.1 Variation of the propagator

Let us consider an infinitesimal change of the gauge-fixing condition (5.2.1) for the propagator. The corresponding changes of $\mathcal{B}_R$ and $\mathcal{L}_R$ are

$$\mathcal{B}_R(t) \;\to\; \mathcal{B}_R(t) + \delta\mathcal{B}_R(t)\,, \qquad \mathcal{L}_R(t) \;\to\; \mathcal{L}_R(t) + \{\mathcal{Q}_R(t), \delta\mathcal{B}_R(t)\}\,. \tag{5.4.1}$$

Thus the modified half-propagator strip $\mathcal{P}_*(s_a, s_b)$ changes as follows:

$$\begin{aligned}
\delta\mathcal{P}_*(s_a,s_b) &= -\int_{s_a}^{s_b} dt\, \mathcal{P}_*(s_a,t)\,\delta[\,\mathcal{L}_R(t) + \{\mathcal{B}_R(t),\Psi\}\,]\,\mathcal{P}_*(t,s_b) \\
&= -\int_{s_a}^{s_b} dt\, \mathcal{P}_*(s_a,t)\,\{\mathcal{Q}_R(t),\delta\mathcal{B}_R(t)\}\,\mathcal{P}_*(t,s_b) - \int_{s_a}^{s_b} dt\, \mathcal{P}_*(s_a,t)\,\{\delta\mathcal{B}_R(t),\Psi\}\,\mathcal{P}_*(t,s_b) \\
&= -\mathcal{Q}\int_{s_a}^{s_b} dt\, \mathcal{P}_*(s_a,t)\,\delta\mathcal{B}_R(t)\,\mathcal{P}_*(t,s_b) - \left\{\Psi, \int_{s_a}^{s_b} dt\, \mathcal{P}_*(s_a,t)\,\delta\mathcal{B}_R(t)\,\mathcal{P}_*(t,s_b)\right\},
\end{aligned} \tag{5.4.2}$$

where we used (5.3.27) in the last step. We therefore find that

$$\delta \oint_{s_b-s_a} \mathcal{P}_*(s_a,s_b) = -\,Q \oint_{s_b-s_a} \int_{s_a}^{s_b} dt\, \mathcal{P}_*(s_a,t)\,\delta\mathcal{B}_R(t)\,\mathcal{P}_*(t,s_b)\,. \tag{5.4.3}$$

We conclude that the closed string state $|B_*(\Psi)\rangle$ changes by a BRST-exact term under a variation (5.4.1) of the gauge-fixing condition:

$$\boxed{\delta|B_*(\Psi)\rangle \;=\; Q - \text{exact}\,.} \tag{5.4.4}$$

5.4.2 Change of the strip length and the action of $L_0 + \tilde{L}_0$

To understand the s dependence of $|B_*(\Psi)\rangle$, let us begin by relating closed string states of the type $\oint_{s_b-s_a}\Sigma(s_a,s_b)$ defined in (5.2.20) with different values for s_b. Consider an infinitesimal change in s_b. A change in the strip length $s_b - s_a$ affects the gluing of the strip to the closed string coordinate, as can be seen from (5.2.31). We thus need to reparameterize the closed string boundary. Infinitesimally, we account for this change by inserting a line integral of the energy-momentum tensor along the closed string boundary. From (5.2.31) it follows that the vector field u which adjusts the parameterization of the closed string boundary to an infinitesimal change in s_b is given by

$$u(w) = \frac{w - \big(\gamma(\frac{\pi}{2}) + s_a\big)}{s_b - s_a}\,. \tag{5.4.5}$$

This vector field is tangential to the closed string boundary $\Im(w) = \frac{\pi}{2}$, vanishes at $w = \gamma(\frac{\pi}{2}) + s_a$, and satisfies

$$u\left(\gamma(\tfrac{\pi}{2}) + s_b\right) = 1\,. \tag{5.4.6}$$

It thus follows that the corresponding line integral of the energy-momentum tensor,

$$\widehat{\mathcal{L}}^{\text{rep}} = \int_{\gamma(\frac{\pi}{2})+s_a}^{\gamma(\frac{\pi}{2})+s_b} \left[\frac{dw}{2\pi i}\,\frac{w-\gamma(\frac{\pi}{2})-s_a}{s_b-s_a}\,T(w) + \frac{d\bar{w}}{2\pi i}\,\frac{\bar{w}-\overline{\gamma(\frac{\pi}{2})}-s_a}{s_b-s_a}\,\widetilde{T}(\bar{w})\right], \tag{5.4.7}$$

generates the desired linear stretching of the closed string boundary:

$$\partial_{s_b}\oint_{s_b-s_a}\Sigma(s_a,s_b) = \oint_{s_b-s_a}\partial_{s_b}\Sigma(s_a,s_b) + \oint_{s_b-s_a}\widehat{\mathcal{L}}^{\text{rep}}\,\Sigma(s_a,s_b)\,. \tag{5.4.8}$$

Note that the constant part of the vector field $u(w)$ has an imaginary contribution $\frac{-\imath\pi}{2(s_b-s_a)}$ arising from $\gamma(\frac{\pi}{2})$ and thus we cannot immediately derive a useful identity analogous to (5.2.9). This contribution to the operator $\widehat{\mathcal{L}}^{\text{rep}}$ is proportional to $L_0+\tilde{L}_0$, which can be written in the w frame as

$$\begin{aligned} L_0+\tilde{L}_0 &= \int_{|\zeta|=\exp(-\frac{\pi^2}{s_b-s_a})}\left[\frac{d\zeta}{2\pi i}\,\zeta\,T(\zeta) + \frac{d\bar{\zeta}}{2\pi i}\,\bar{\zeta}\,\widetilde{T}(\bar{\zeta})\right] \\ &= \frac{s_b-s_a}{2\pi i}\int_{\gamma(\frac{\pi}{2})+s_a}^{\gamma(\frac{\pi}{2})+s_b}\left[\frac{dw}{2\pi i}\,T(w) - \frac{d\bar{w}}{2\pi i}\,\widetilde{T}(\bar{w})\right]. \end{aligned} \tag{5.4.9}$$

Therefore, if we define

$$\widehat{\mathcal{L}}^{\text{rep}'} = \int_{\gamma(\frac{\pi}{2})+s_a}^{\gamma(\frac{\pi}{2})+s_b}\left[\frac{dw}{2\pi i}\,\frac{w-\Re\left(\gamma(\frac{\pi}{2})\right)-s_a}{s_b-s_a}\,T(w) + \frac{d\bar{w}}{2\pi i}\,\frac{\bar{w}-\Re\left(\gamma(\frac{\pi}{2})\right)-s_a}{s_b-s_a}\,\widetilde{T}(\bar{w})\right] \tag{5.4.10}$$

for $\widehat{\mathcal{L}}^{\text{rep}'}$ acting on $\Sigma(s_a,s_b)$, we have

$$\partial_{s_b}\oint_{s_b-s_a}\Sigma(s_a,s_b) = \oint_{s_b-s_a}\partial_{s_b}\Sigma(s_a,s_b) + \oint_{s_b-s_a}\widehat{\mathcal{L}}^{\text{rep}'}\Sigma(s_a,s_b) + \frac{\pi^2}{(s_b-s_a)^2}(L_0+\tilde{L}_0)\oint_{s_b-s_a}\Sigma(s_a,s_b)\,. \tag{5.4.11}$$

We introduce $\mathcal{L}_R^{\text{rep}'}(t)$ with the same integrand as $\widehat{\mathcal{L}}^{\text{rep}'}$ by

$$\mathcal{L}_R^{\text{rep}'}(t) = \int_t^{\gamma(\frac{\pi}{2})+t}\left[\frac{dw}{2\pi i}\,\frac{w-\Re\left(\gamma(\frac{\pi}{2})\right)-s_a}{s_b-s_a}\,T(w) + \frac{d\bar{w}}{2\pi i}\,\frac{\bar{w}-\Re\left(\gamma(\frac{\pi}{2})\right)-s_a}{s_b-s_a}\,\widetilde{T}(\bar{w})\right], \tag{5.4.12}$$

and we have the following identity analogous to (5.2.9):

$$\mathcal{L}_R^{\text{rep}'}(s_a)\,\mathcal{P}(s_a,s_b) - \mathcal{P}(s_a,s_b)\,\mathcal{L}_R^{\text{rep}'}(s_b) + \widehat{\mathcal{L}}^{\text{rep}'}\,\mathcal{P}(s_a,s_b) = 0\,. \tag{5.4.13}$$

Note that unlike the line integrals $\mathcal{L}_R$, $\mathcal{B}_R$ and $\mathcal{Q}_R$, the integrand of $\mathcal{L}_R^{\text{rep}'}$ is not invariant under the identification $w \sim w + (s_b - s_a)$. We instead have

$$\oint_{s_b-s_a}\mathcal{L}_R^{\text{rep}'}(s_a)\Sigma(s_a,s_b) - \oint_{s_b-s_a}\Sigma(s_a,s_b)\mathcal{L}_R^{\text{rep}'}(s_b) + \oint_{s_b-s_a}\Sigma(s_a,s_b)\mathcal{L}_R(s_b) = 0\,. \tag{5.4.14}$$

Adding the left-hand side of (5.4.14) to (5.4.11) allows us to localize the integration contour around the slits where the open strings are inserted. We obtain

$$\partial_{s_b}\oint_{s_b-s_a}\Sigma(s_a,s_b)=\oint_{s_b-s_a}\big[\partial_{s_b}\Sigma(s_a,s_b)+\Sigma(s_a,s_b)\mathcal{L}_R(s_b)\big]+\frac{\pi^2}{(s_b-s_a)^2}(L_0+\tilde{L}_0)\oint_{s_b-s_a}\Sigma(s_a,s_b)$$
$$+\sum_{i=1}^{k}\oint_{s_b-s_a}\mathcal{P}(s_a,s_1)*A_1\cdots[\mathcal{L}_R^{\mathrm{rep}'}(s_i),A_i]\cdots A_k*\mathcal{P}(s_k,s_b)\,. \tag{5.4.15}$$

Let us apply this result to the expression on the right-hand side of (5.3.4) for the boundary state $|B\rangle$. The last term in (5.4.15) vanishes for this case as $\mathcal{P}(0,s)$ does not contain any open string state insertions A_i. Furthermore, the first term in (5.4.15) also vanishes because of (5.2.10). We find

$$\partial_s|B\rangle=\partial_s\Big[e^{\frac{\pi^2}{s}(L_0+\tilde{L}_0)}\oint_s\mathcal{P}(0,s)\Big]=-\frac{\pi^2}{s^2}(L_0+\tilde{L}_0)|B\rangle+e^{\frac{\pi^2}{s}(L_0+\tilde{L}_0)}\,\partial_s\oint_s\mathcal{P}(0,s)=0\,. \tag{5.4.16}$$

We have thus confirmed (5.3.5), and the right-hand side of (5.3.4) reproduces the BCFT boundary state of the original theory independent of s.

5.4.3 Variation of s

We now use the results of the previous subsection to study the s dependence of the closed string state $|B_*(\Psi)\rangle$. Recalling that

$$\partial_s\mathcal{P}_*(0,s)=-\mathcal{P}_*(0,s)\big(\mathcal{L}_R(s)+\{\mathcal{B}_R(s),\Psi\}\big)\,, \tag{5.4.17}$$

we find

$$\begin{aligned}\partial_s|B_*(\Psi)\rangle&=-\frac{\pi^2}{s^2}\,(L_0+\tilde{L}_0)\,e^{\frac{\pi^2}{s}(L_0+\tilde{L}_0)}\oint_s\mathcal{P}_*(0,s)+e^{\frac{\pi^2}{s}(L_0+\tilde{L}_0)}\,\partial_s\oint_s\mathcal{P}_*(0,s)\\&=e^{\frac{\pi^2}{s}(L_0+\tilde{L}_0)}\oint_s\Big[\widehat{\mathcal{L}}^{\mathrm{rep}'}\,\mathcal{P}_*(0,s)-\mathcal{P}_*(0,s)\big(\mathcal{L}_R(s)+\{\mathcal{B}_R(s),\Psi\}\big)\Big]\,,\end{aligned} \tag{5.4.18}$$

where we have used (5.4.11). We define the b-ghost line integral $\widehat{\mathcal{B}}^{\mathrm{rep}'}$ as $\widehat{\mathcal{L}}^{\mathrm{rep}'}$ in (5.4.10) with $T(z)$ and $\widetilde{T}(\bar{z})$ replaced by $b(z)$ and $\tilde{b}(\bar{z})$, respectively. It follows that $\{\mathcal{Q},\,\widehat{\mathcal{B}}^{\mathrm{rep}'}\}=\widehat{\mathcal{L}}^{\mathrm{rep}'}$. Consider now the first term on the above right-hand side. We have

$$\oint_s\widehat{\mathcal{L}}^{\mathrm{rep}'}\,\mathcal{P}_*(0,s)=\oint_s\{\mathcal{Q},\,\widehat{\mathcal{B}}^{\mathrm{rep}'}\}\mathcal{P}_*(0,s)=Q\oint_s\widehat{\mathcal{B}}^{\mathrm{rep}'}\,\mathcal{P}_*(0,s)+\oint_s\widehat{\mathcal{B}}^{\mathrm{rep}'}[\Psi\,,\,\mathcal{P}_*(0,s)]\,. \tag{5.4.19}$$

The commutator term vanishes using the cyclicity property (5.2.42),[7] and we conclude that the first term in (5.4.18) is BRST exact:

$$e^{\frac{\pi^2}{s}(L_0+\tilde{L}_0)}\oint_s\widehat{\mathcal{L}}^{\mathrm{rep}'}\,\mathcal{P}_*(0,s)=Q\left[e^{\frac{\pi^2}{s}(L_0+\tilde{L}_0)}\oint_s\widehat{\mathcal{B}}^{\mathrm{rep}'}\,\mathcal{P}_*(0,s)\right]. \tag{5.4.20}$$

[7]The cyclicity property is unaffected by the presence of the line integral $\widehat{\mathcal{B}}^{\mathrm{rep}'}$ along the closed string boundary

The second term in (5.4.18) is also BRST exact. In fact, we again use the cyclicity property to find

$$\begin{aligned}\oint_s \mathcal{P}_*(0,s)\big(\mathcal{L}_R(s)+\{\mathcal{B}_R(s),\Psi\}\big) &= \oint_s\Big(\mathcal{P}_*(0,s)\{\mathcal{Q}_R(s),\mathcal{B}_R(s)\}-\big[\,\Psi\,,\,\mathcal{P}_*(0,s)\,\big]\,\mathcal{B}_R(s)\Big)\\ &= Q\oint_s \mathcal{P}_*(0,s)\mathcal{B}_R(s)\,.\end{aligned} \tag{5.4.21}$$

As both terms in (5.4.18) are BRST exact, we conclude that $|B_*(\Psi)\rangle$ changes by a BRST exact piece under a variation of s:

$$\boxed{\partial_s|B_*(\Psi)\rangle \;=\; Q-\text{exact}\,.} \tag{5.4.22}$$

Using the formula

$$\oint_s \mathcal{B}_R^{\text{rep}'}(0)\,\mathcal{P}_*(0,s)-\oint_s \mathcal{P}_*(0,s)\,\mathcal{B}_R^{\text{rep}'}(s)+\oint_s \mathcal{P}_*(0,s)\,\mathcal{B}_R(s)=0\,, \tag{5.4.23}$$

which can be derived in the same way as (5.4.14), the total BRST-exact term in (5.4.22) can be written as

$$\partial_s|B_*(\Psi)\rangle = Q\left[e^{\frac{\pi^2}{s}(L_0+\tilde{L}_0)}\oint_s\Big(\,\widehat{\mathcal{B}}^{\,\text{rep}'}\,\mathcal{P}_*(0,s)+\mathcal{B}_R^{\text{rep}'}(0)\,\mathcal{P}_*(0,s)-\mathcal{P}_*(0,s)\,\mathcal{B}_R^{\text{rep}'}(s)\Big)\right] \tag{5.4.24}$$

so that the three b-ghost contours can be connected.

5.4.4 The $s\to 0$ limit

Let us now consider the limit $s\to 0$ of the state $|B_*(\Psi)\rangle$. The first term in the expansion (5.3.19) is the original boundary state $|B\rangle$. It is independent of s and thus the limit $s\to 0$ is trivial. The next term $|B_*^{(1)}(\Psi)\rangle$ can be written as

$$\begin{aligned}|B_*^{(1)}(\Psi)\rangle &= -\,e^{\frac{\pi^2}{s}(L_0+\tilde{L}_0)}\int_0^s ds_1\oint_s \mathcal{P}(0,s_1)\,\{\mathcal{B}_R(s_1),\Psi\}\mathcal{P}(s_1,s)\\ &= -\,e^{\frac{\pi^2}{s}(L_0+\tilde{L}_0)}\,\frac{2\pi i}{s}\int_0^s ds_1\,(b_0-\tilde{b}_0)\oint_s \mathcal{P}(0,s_1)\,\Psi\,\mathcal{P}(s_1,s)\,,\end{aligned} \tag{5.4.25}$$

where we used (5.2.41). We can further transform it using an integrated version of (5.2.40) as follows:

$$\begin{aligned}|B_*^{(1)}(\Psi)\rangle &= -\,e^{\frac{\pi^2}{s}(L_0+\tilde{L}_0)}\,\frac{2\pi i}{s}\int_0^s ds_1\,(b_0-\tilde{b}_0)\,e^{-s_1\frac{2\pi i}{s}(L_0-\tilde{L}_0)}\oint_s \Psi\,\mathcal{P}(0,s)\\ &= -i\,e^{\frac{\pi^2}{s}(L_0+\tilde{L}_0)}\int_0^{2\pi} d\theta\,(b_0-\tilde{b}_0)\,e^{-i\theta(L_0-\tilde{L}_0)}\oint_s \Psi\,\mathcal{P}(0,s)\,,\end{aligned} \tag{5.4.26}$$

where in the last step we defined $\theta=2\pi s_1/s$. One might have suspected that the state

$$\lim_{s\to 0}\int_0^s ds_1\oint_s \mathcal{P}(0,s_1)\,\{\mathcal{B}_R(s_1),\Psi\}\mathcal{P}(s_1,s) \tag{5.4.27}$$

vanishes because the integration region of s_1 collapses in the limit $s\to 0$. We see from (5.4.26), however, that the integration over s_1 effectively rotates the surface state once around the closed

string coordinate. The vanishing integration region over s_1 was only a coordinate effect of our parameterization of the integral over the rotational modulus, and the final expression in (5.4.26) is clearly nonvanishing in the limit $s \to 0$ for generic Ψ.

Let us next consider inner products $\langle \mathcal{V} \,|\, (c_0 - \tilde{c}_0)|B_*^{(k)}(\Psi)\rangle$ with $k \geq 2$, where $\mathcal{V}$ is an arbitrary on-shell closed string state:

$$\begin{aligned}
&\langle \mathcal{V} \,|\, (c_0 - \tilde{c}_0)|B_*^{(k)}(\Psi)\rangle \\
&= (-1)^k \,\langle \mathcal{V} \,|\, (c_0 - \tilde{c}_0) \,|\, \oint_s \int_0^s ds_1 \int_{s_1}^s ds_2 \ldots \int_{s_{k-1}}^s ds_k \, \mathcal{P}(0, s_1) \, \{\mathcal{B}_R(s_1), \Psi\} \, \mathcal{P}(s_1, s_2) \ldots \\
&\qquad\qquad \times \mathcal{P}(s_{k-1}, s_k) \, \{\mathcal{B}_R(s_k), \Psi\} \, \mathcal{P}(s_k, s) \,\rangle \,.
\end{aligned} \tag{5.4.28}$$

The factor $e^{\frac{\pi^2}{s}(L_0 + \tilde{L}_0)}$ did not contribute because $\mathcal{V}$ is a primary field of weight $(0, 0)$. The limit $s \to 0$ of these inner products were essentially discussed in section 4 of [30], where it was argued that the terms with $k \geq 2$ vanish for a certain regular class of solutions. Let us review the argument in [30].[8]

As we did in (5.4.25), one can extract a factor of $b_0 - \tilde{b}_0$ from the expression in (5.4.28). It is accompanied by a factor of $2\pi\imath/s$, thus the integrand in (5.4.28) is singular in the limit $s \to 0$. However, the k dimensional integral should be transmuted into one integral for the overall rotation and a $k-1$ dimensional integral, and the Jacobian should cancel the singularity of the factor $2\pi\imath/s$ as in (5.4.26). It was argued in [30] that the resulting integrand is finite in the limit $s \to 0$, while the $k-1$ dimensional integration region vanishes. Then the inner products in (5.4.28) vanish in the limit $s \to 0$ for $k \geq 2$.

As was remarked in one of the footnotes of [30], however, it is difficult to identify necessary regularity conditions on the solution for the finiteness of the resulting integrand in the limit $s \to 0$ and thus difficult to prove rigorously that the inner products in (5.4.28) vanish in the limit $s \to 0$ for $k \geq 2$. For example, the open string midpoint of the solution approaches the closed string vertex operator in the limit $s \to 0$, and we may find singular operator products. In fact, the analytic solutions in Schnabl gauge constructed in [12, 13, 43] contain b-ghost integrals extending up to the open string midpoint, and their operator products with $\mathcal{V}$ can potentially be singular. Furthermore, we have to be careful when we judge whether expressions are finite using the w frame because conformal factors associated with the map to a disk coordinate can potentially be singular in the limit $s \to 0$. In fact, we have seen that the singular factor in (5.4.25) arose from such a conformal factor. Similarly, we have

$$\begin{aligned}
&\oint_s \mathcal{P}(0, s_1) \, \{\mathcal{B}_R(s_1), \Psi\} \, \mathcal{P}(s_1, s_2) \, \{\mathcal{B}_R(s_2), \Psi\} \, \mathcal{P}(s_2, s) \\
&= \frac{2\pi i}{s} \, (b_0 - \tilde{b}_0) \oint_s \mathcal{P}(0, s_1) \, \Psi \, \mathcal{P}(s_1, s_2) \, \{\mathcal{B}_R(s_2), \Psi\} \, \mathcal{P}(s_2, s) \,.
\end{aligned} \tag{5.4.29}$$

[8] The analysis in [30] was based on the Siegel propagator strip, but this choice does not enter the following argument in an essential way.

This is also singular in the limit $s \to 0$, but we expect that

$$\oint_s \mathcal{P}(0,s_1)\,\Psi\,\mathcal{P}(s_1,s_2)\,\{\mathcal{B}_R(s_2),\Psi\}\,\mathcal{P}(s_2,s) \tag{5.4.30}$$

is finite in the limit $s \to 0$ if the solution Ψ is regular. The difference in the behavior as $s \to 0$ between (5.4.29) and (5.4.30) is not so obvious.

We therefore do not make a general claim that the inner products in (5.4.28) vanish in the limit $s \to 0$ for $k \geq 2$. On the other hand, an advantage of our approach is that the state $|B_*(\Psi)\rangle$ is explicitly calculable for solutions based on wedge states if we choose the propagator strip of Schnabl gauge, as we demonstrate in section 5.5. We can thus examine this suppression of higher-order terms explicitly in section 5.6 for various known analytic solutions. We indeed find that the states $|B_*^{(k)}(\Psi)\rangle$ with $k \geq 2$ vanish in the limit $s \to 0$ for all explicit examples that we consider.

If the inner products $\langle\,\mathcal{V}\,|\,(c_0-\tilde{c}_0)|B_*^{(k)}(\Psi)\rangle$ with $k \geq 2$ vanish in the limit $s \to 0$ for a given regular solution Ψ, we find

$$\begin{aligned}
&\lim_{s\to 0}\,\langle\mathcal{V}|(c_0-\tilde{c}_0)|B_*(\Psi)\rangle - \langle\mathcal{V}|(c_0-\tilde{c}_0)|B\rangle = \lim_{s\to 0}\,\langle\mathcal{V}|(c_0-\tilde{c}_0)|B_*^{(1)}(\Psi)\rangle \\
&= -i\,\lim_{s\to 0}\int_0^{2\pi} d\theta\,\langle\,\mathcal{V}\,|\,(c_0-\tilde{c}_0)\,(b_0-\tilde{b}_0)\,|\,\oint_s \Psi\,\mathcal{P}(0,s)\,\rangle \\
&= -4\pi i\,\lim_{s\to 0}\langle\,\mathcal{V}\,|\,\oint_s \Psi\,\mathcal{P}(0,s)\,\rangle\,.
\end{aligned} \tag{5.4.31}$$

Here we used that $|\mathcal{V}\rangle$ is annihilated by $L_0 \pm \tilde{L}_0$ and $b_0 - \tilde{b}_0$. The parameter s in (5.4.31) is simply a regularization of a contraction of Ψ with the identity state. In the limit $s \to 0$, the closed string vertex operator is inserted at the open string midpoint of Ψ, and we recover the familiar string field theory observables $W(\mathcal{V},\Psi)$:

$$\lim_{s\to 0}\big\langle\mathcal{V}|(c_0-\tilde{c}_0)|B_*(\Psi)\big\rangle - \big\langle\mathcal{V}|(c_0-\tilde{c}_0)|B\big\rangle \;=\; -4\pi i\,W(\mathcal{V},\Psi)\,, \tag{5.4.32}$$

where $W(\mathcal{V},\phi)$ for a generic open string state $|\phi\rangle$ in the Fock space is defined by

$$W(\mathcal{V},\phi) = \langle\,\mathcal{V}(i)\,f_I\circ\phi(0)\,\rangle_{\rm UHP}\,. \tag{5.4.33}$$

We denote by $f_I \circ \phi(0)$ the conformal transformation of the operator $\phi(0)$ corresponding to the state $|\phi\rangle$ under the identity map

$$f_I(\xi) = \frac{2\,\xi}{1-\xi^2}\,. \tag{5.4.34}$$

As is well known, the observables $W(\mathcal{V},\Psi)$ are gauge-invariant. The vanishing of terms with two or more solution insertions in the limit $s \to 0$ is thus consistent because $|B_*^{(0)}(\Psi)\rangle + |B_*^{(1)}(\Psi)\rangle$ is gauge-invariant in this limit. Furthermore, when we vary s, the state $|B_*(\Psi)\big\rangle$ only changes by a BRST-exact term which has a vanishing inner product with $\langle\mathcal{V}|(c_0-\tilde{c}_0)$, and thus we conclude that (5.4.32) holds even for finite s:

$$\big\langle\mathcal{V}|(c_0-\tilde{c}_0)|B_*(\Psi)\big\rangle - \big\langle\mathcal{V}|(c_0-\tilde{c}_0)|B\big\rangle \;=\; -4\pi i\,W(\mathcal{V},\Psi) \quad \text{for any } s\,. \tag{5.4.35}$$

It was argued in [30] that the observables $W(\mathcal{V},\Psi)$ represent the difference between the original boundary state $|B\rangle$ and the boundary state $|B_*\rangle$ contracted with $\langle\mathcal{V}|(c_0-\tilde{c}_0)$:[9]

$$\langle\mathcal{V}|(c_0-\tilde{c}_0)|B_*\rangle - \langle\mathcal{V}|(c_0-\tilde{c}_0)|B\rangle = -4\pi i\, W(\mathcal{V},\Psi)\,. \tag{5.4.36}$$

This implies that

$$\langle\mathcal{V}|(c_0-\tilde{c}_0)|B_*(\Psi)\rangle \;=\; \langle\mathcal{V}|(c_0-\tilde{c}_0)|B_*\rangle \tag{5.4.37}$$

and thus

$$|B_*(\Psi)\rangle \;=\; |B_*\rangle \;+\; Q-\text{exact}\,. \tag{5.4.38}$$

To summarize, if the inner products $\langle\,\mathcal{V}\,|\,(c_0-\tilde{c}_0)|B_*^{(k)}(\Psi)\rangle$ with $k\geq 2$ vanish for a given regular solution Ψ, the relation (5.4.36) which was argued in [30] to hold in general implies that the closed string state $|B_*(\Psi)\rangle$ coincides with the BCFT boundary state $|B_*\rangle$ up to a possible BRST-exact term. Again, instead of attempting to prove this relation in general, we explicitly calculate $|B_*(\Psi)\rangle$ for various known analytic solutions in section 5.6. We find, surprisingly, that the possible BRST-exact term *vanishes* for arbitrary s, and we precisely obtain the BCFT boundary state for all the solutions we consider in section 5.6.

5.5 Regular and calculable boundary states

For any choice of parameter s, propagator gauge-fixing condition $\mathcal{B}$, and classical solution Ψ, we can construct the closed string state $|B_*(\Psi)\rangle$. In general, however, it is difficult to calculate $|B_*(\Psi)\rangle$ explicitly because the gluing of insertions of classical solutions to the slits in the w frame generically requires calculations of correlation functions on a complicated Riemann surface. A drastic simplification occurs if we choose Schnabl's gauge condition.[10], Here, B is the antighost zero mode in the sliver frame as defined in (2.2.7). If we choose $\mathcal{B}=B$ and a classical solution Ψ based on wedge states, we can use the results of chapter 4 to map the resulting surface to an annulus and calculate the state $|B_*(\Psi)\rangle$ explicitly. In this section we assemble the main ingredients necessary for this calculation.

As in previous chapters, we define the wedge region $\mathcal{W}_\alpha$ by the semi-infinite strip on the upper-half plane of z between the vertical lines $\Re(z)=-\frac{1}{2}$ and $\Re(z)=\frac{1}{2}+\alpha$ with these lines identified by translation. Recall that the wedge states W_α are defined by

$$\langle\,\phi,W_\alpha\,\rangle = \langle\; f\circ\phi(0)\,\rangle_{\mathcal{W}_\alpha}\,. \tag{5.5.1}$$

Here and in what follows we denote a generic open string state in the Fock space by $|\phi\rangle$ and its corresponding operator by $\phi(0)$. When a solution is made of wedge states with operator insertions, we call it a wedge-based solution.

[9]The relation in the notation of [30] is $W(\mathcal{V},\Psi)=\mathcal{A}_\Psi^{\text{disk}}(\mathcal{V})-\mathcal{A}_0^{\text{disk}}(\mathcal{V})$, where $\mathcal{A}_\Psi^{\text{disk}}(\mathcal{V})$ and $\mathcal{A}_0^{\text{disk}}(\mathcal{V})$ are related to the inner products as $\langle\mathcal{V}|(c_0-\tilde{c}_0)|B_*\rangle=-4\pi i\mathcal{A}^{\text{disk}}(\mathcal{V})$ and $\langle\mathcal{V}|(c_0-\tilde{c}_0)|B\rangle=-4\pi i\mathcal{A}_0^{\text{disk}}(\mathcal{V})$.

[10]The simplification also occurs for $\mathcal{B}\propto(B+\alpha B^\star)$ with $\alpha\neq 1$.

We now map the w-frame geometry with its parameterized slits to a frame which is convenient for the propagator choice $\mathcal{B} = B$. It is related to the w frame via

$$z = \frac{1}{2} e^w . \tag{5.5.2}$$

The z frame is closely related to the familiar sliver frame. In fact, the image of the curve $\gamma(\theta)$ in the z frame coincides with the sliver-frame coordinate line $f(e^{\imath\theta})$. More generally, $s_i + \gamma(\theta)$, which parameterizes a slit in a half-propagator strip or its boundary, becomes vertical in this frame and is located at $\Re(z) = \frac{1}{2} e^{s_i}$. The parameterization in the z frame is given by

$$s_i + \gamma(\theta) \;\to\; z = e^{s_i} f(e^{\imath\theta}) = \frac{1}{2} e^{s_i} + i\, e^{s_i} \left[\frac{2}{\pi} \operatorname{arctanh}\left(\tan \frac{\theta}{2} \right) \right] . \tag{5.5.3}$$

Since the slits are infinite, the closed string boundary is *hidden* at $z \to i\infty$. This property can be traced back to the fact that Schnabl gauge is not a *regular* linear b gauge. In fact, the vector field $v(\xi)$ associated with Schnabl's B vanishes at $\xi = i$ and thus violates the condition (4.2.3) at the open string midpoint. This simplifies the analysis in Schnabl gauge, but all manipulations of surfaces must be justified by regularizing the propagator and taking the Schnabl limit. Fortunately, all manipulations that our analysis requires were already justified in chapter 4, so we can simply apply the prescriptions developed there. In particular, it is important to understand the contour of the integrals $\mathcal{B}_R(t)$ and $\mathcal{L}_R(t)$ in the z frame as a limit of a regulated curve. We denote the contour after using the doubling trick by $C(t)$:

$$\mathcal{B}_R(t) \to \int_{C(t)} \frac{dz}{2\pi i}\, z\, b(z) , \qquad \mathcal{L}_R(t) \to \int_{C(t)} \frac{dz}{2\pi i}\, z\, T(z) . \tag{5.5.4}$$

In the regularized analysis, the closed string boundary is a finite segment on the imaginary z axis, and t parameterizes the endpoint of the contour $C(t)$ on that line segment.[11] In the Schnabl limit, the location of the closed string boundary diverges to $i\infty$. The contour $C(t)$ in this limit naively runs from $-i\,\infty$ to $i\,\infty$ along the vertical line $\Re(z) = \frac{e^t}{2}$ and the t dependence of its endpoints on the imaginary axis is hidden. As we discussed in section 5.2, however, it *does* depend on t even in the limit, namely,

$$\int_{C(t)} \frac{dz}{2\pi i}\, z\, b(z) \;-\; \int_{C(t')} \frac{dz}{2\pi i}\, z\, b(z) \;\neq 0 \tag{5.5.5}$$

for $t' > t$ even when there are no operator insertions between the two contours. This is the z-frame representation of

$$\mathcal{B}_R(t)\, \mathcal{P}(t,t') - \mathcal{P}(t,t')\, \mathcal{B}_R(t') \neq 0 \tag{5.5.6}$$

which follows from the inequality (5.2.7). Let us now consider a calculation of

$$(-1)^k \oint_s \prod_{i=1}^{k} \left[\int_{s_{i-1}}^{s} ds_i\, \mathcal{P}(s_{i-1}, s_i)\, \{\mathcal{B}_R(s_i), A_{\alpha_i}\} \right] \mathcal{P}(s_k, s) , \tag{5.5.7}$$

[11] In the notation of chapter 4, the endpoints of the contour $C(t)$ are $\pm ie^t\Lambda$. In the Schnabl limit we have $\Lambda \to \infty$.

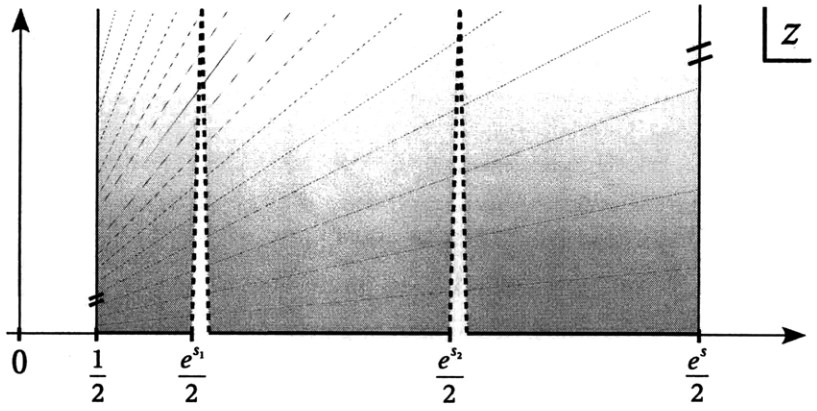

Figure 5-4: Illustration of (5.5.7) for $k = 2$ before inserting the states A_{α_1} and A_{α_2}. The two slits are depicted as dashed lines in the figure. The grey lines illustrate the rescaling of the parameterization from the left boundary to the right boundary. The double lines indicate the identification between these two boundaries.

where A_{α_i} is a Grassmann-odd state made of the wedge state W_{α_i} with operator insertions, and $s_0 = 0$. Before gluing the states A_{α_i} to the parameterized slits, the total surface is located in the region

$$\frac{1}{2} \leq \Re(z) \leq \frac{1}{2} e^s , \tag{5.5.8}$$

and the parameterizations of its vertical boundaries are given by $f(e^{i\theta})$ for the left boundary and $e^s f(e^{i\theta})$ for the right boundary. These boundaries are glued by the operation $\oint_s$ which forms a closed string state from the surface, and this gluing is compatible with the identification $z \sim e^s z$. See Figure 5-4. Recall from (4.2.31), that the map to the annulus frame ζ is given by

$$\zeta = \exp\Big(\frac{2\pi i}{s} \ln 2z\Big) , \tag{5.5.9}$$

which is compatible with the identification $z \sim e^s z$.

From the parameterization (5.5.3) it is obvious how to insert the wedge-based state A_{α_1} to the slit at $\Re(z) = \frac{e^{s_1}}{2}$: simply translate the remaining surface in the region $\Re(z) > \frac{e^{s_1}}{2}$ horizontally to the right by $e^{s_1}\alpha_1$ and map A_{α_1} from its sliver frame $z^{(1)}$ used in (5.5.1) to the resulting gap in the z frame via

$$z = e^{s_1} z^{(1)} . \tag{5.5.10}$$

The next slit is now located at $\Re(z) = e^{s_1}\alpha_1 + \frac{1}{2}e^{s_2}$. We translate the remaining surface in the region $\Re(z) > e^{s_1}\alpha_1 + \frac{1}{2}e^{s_2}$ by $e^{s_2}\alpha_2$, and map the state A_{α_2} into the resulting gap via

$$z = e^{s_1}\alpha_1 + e^{s_2} z^{(2)} . \tag{5.5.11}$$

See Figure 5-5. The construction iterates. For the insertion of A_{α_i} after having inserted the previous $i-1$ states, the slit is located at

$$\Re(z) = \sum_{j=1}^{i-1} e^{s_j}\alpha_j + \frac{1}{2} e^{s_i} , \tag{5.5.12}$$

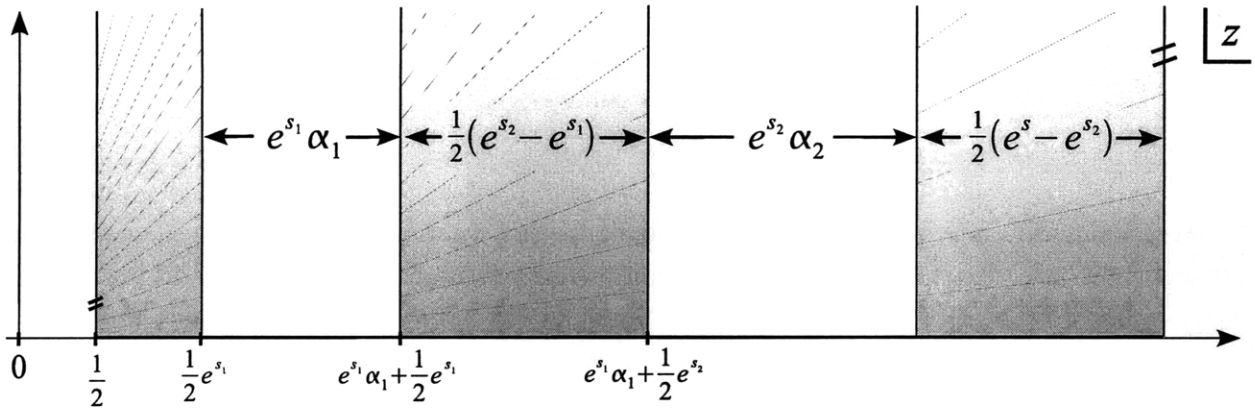

Figure 5-5: Illustration of (5.5.7) for $k = 2$ with gaps of width $e^{s_1}\alpha_1$ and of width $e^{s_2}\alpha_2$ inserted at the two slits. Compare this with Figure 5-4. The states A_{α_1} and A_{α_2} are then mapped into these gaps.

and we translate the remaining surface to the right of the slit by $e^{s_i}\alpha_i$. Then we map the state A_{α_i} into the resulting gap via

$$z = \sum_{j=1}^{i-1} e^{s_j}\alpha_j + e^{s_i} z^{(i)} \,. \tag{5.5.13}$$

At the end of the process, the whole surface corresponding to (5.5.7), which we denote by Σ, is located in the z frame in the region

$$\frac{1}{2} \le \Re(z) \le \sum_{j=1}^{k} e^{s_j}\alpha_j + \frac{1}{2}\, e^{s} \,. \tag{5.5.14}$$

The parameterization of the identified left and right boundaries of this resulting surface Σ are not related by scaling $z \sim e^s z$, so we cannot map Σ directly to the annulus frame via (5.5.9). To restore this relation, we use the prescription given in section 4.6.1. We shift the entire surface Σ horizontally by

$$a_0 = \frac{1}{e^s - 1} \sum_{j=1}^{k} e^{s_j}\alpha_j \,. \tag{5.5.15}$$

With this value of the shift, Σ is then located in the region

$$\frac{1}{2} + a_0 \le \Re(z) \le e^s\Big(\frac{1}{2} + a_0\Big) \,, \tag{5.5.16}$$

and the gluing of the left to the right boundary of Σ is now compatible with the identification $z \sim e^s z$. In chapter 4, this translated frame was called *the natural z frame.* The total map from the coordinate $z^{(i)}$ of the wedge surface on which A_{α_i} is defined to the natural z frame is a combination of the map (5.5.13) and a horizontal translation by a_0. It is thus given by

$$\boxed{z = \ell_i + e^{s_i} z^{(i)} \,,} \tag{5.5.17}$$

where

$$\ell_i = \sum_{j=1}^{i-1} \alpha_j \, e^{s_j} + a_0 \,, \quad \ell_1 = a_0 \,. \tag{5.5.18}$$

It is consistent with the identification $z \sim e^s z$ in the natural z frame to map Σ to the annulus frame ζ via (5.5.9). The gluing to the closed string coordinate patch is unaffected by our manipulations in the z frame, as was shown in chapter 4. One may worry that the horizontal translations of the surfaces may have resulted in a relative rotation in the ζ frame. This is not the case, as can be easily seen from the regularized analysis of section 4.8. We can thus analytically map the surface that defines the closed string state (5.5.7) to an annulus that has exactly the same modulus as the annulus that defines $\oint_s \mathcal{P}(0,s)$. In particular, all closed string surface states contributing to $|B_*(\Psi)\rangle$ for wedge-based solutions are represented on exactly the *same Riemann surface.* This remarkable property of the Schnabl propagator strip will be crucial for our explicit calculations in section 5.6.

The b-ghost line integrals $\mathcal{B}_R(s_i)$ in (5.5.7) have a simple representation in the natural z frame. Indeed, mapping the line integrals $\mathcal{B}_R(s_i)$ from their initial z-frame representation (5.5.4) in the presence of slits to their final location in the natural z frame, we find

$$-\{\mathcal{B}_R(s_i).\, A_{\alpha_i}\} \;\to\; -\int_{C(s_i)} \frac{dz}{2\pi i}\,(z-\ell_i)b(z)\,[\ldots] \,-\, [\ldots] \int_{C(s_i)} \frac{dz}{2\pi i}\,(z-\ell_{i+1})b(z)\,. \tag{5.5.19}$$

The dots $[\ldots]$ in (5.5.19) represent the operator insertions for A_{α_i}. Note that the difference in the endpoints of the contour $C(s_i)$ generated by translation of the contour in the direction of the real axis vanishes in the Schnabl limit, as discussed in chapter 4. Since both contours in (5.5.19) have the same endpoint on the closed string boundary, the contours can be connected. From the relation $\ell_{i+1} = \ell_i + e^{s_i}\alpha_i$ we find

$$\boxed{-\{\mathcal{B}_R(s_i), A_{\alpha_i}\} \;\to\; \oint \frac{dz}{2\pi i}\,(z-\ell_i)b(z)\,[\ldots] \,+\, e^{s_i}\alpha_i\,[\ldots]\,\mathcal{B}_R^+\,,} \tag{5.5.20}$$

where the contour encircles the operators $[\ldots]$ counterclockwise and

$$\mathcal{B}_R^+ = \int_{-i\infty}^{i\infty} \frac{dz}{2\pi i}\, b(z)\,. \tag{5.5.21}$$

We do not write the t dependence on the endpoints of the integration contour of $\mathcal{B}_R^+$ because the integral does not depend on the choice of t. To see this, note that

$$\mathcal{L}_R^+ \equiv \{Q, \mathcal{B}_R^+\} \tag{5.5.22}$$

generates horizontal translations in the z frame. It was shown in chapter 4 that the closed string boundary is unaffected by such translations in the Schnabl limit. It follows that the integrand in (5.5.21) vanishes along the closed string boundary.[12] Thus the operator $\mathcal{B}_R^+$ does not depend on

[12]This can also be explicitly confirmed by mapping (5.5.21) to the annulus frame ζ and evaluating the integrand at $|\zeta| = e^{-\frac{\pi^2}{s}}$.

the choice of t. The position of this insertion is given implicitly by the operator ordering in the correlator.

We have assembled all the ingredients required to explicitly calculate $|B_*(\Psi)\rangle$ with $\mathcal{B} = B$ for wedge-based solutions. In fact, the map from the wedge surfaces on which the solutions are defined to the natural z frame are explicitly given in (5.5.17) and the positions and conformal factors of operator insertions on the surface Σ can be explicitly calculated. The b-ghost line integrals $\mathcal{B}_R(s_i)$ have the simple representation (5.5.20) in the natural z frame. Finally, the map from the natural z frame to the annulus frame is explicitly given in (5.5.9). We conclude that the boundary state $|B_*(\Psi)\rangle$ is explicitly calculable for wedge-based solutions if we use the half-propagator strips associated with Schnabl's B.

5.6 The BCFT boundary state from analytic solutions

In this section we explicitly calculate $|B_*(\Psi)\rangle$ constructed using the Schnabl propagator strips for various known wedge-based solutions. We analyze Schnabl's tachyon vacuum solution and the two known analytic solutions for marginal deformations with regular operator products. We find that

$$|B_*(\Psi)\rangle = 0 \quad \text{for all } s \tag{5.6.1}$$

in the case of the tachyon vacuum solution and

$$|B_*(\Psi)\rangle = |B_*\rangle \quad \text{for all } s \tag{5.6.2}$$

with no additional BRST-exact term in the case of marginal deformations.

5.6.1 Schnabl's solution for tachyon condensation

Schnabl's solution $\Psi_{\mathcal{S}}$ for tachyon condensation is given by [43]

$$\Psi_{\mathcal{S}} = \lim_{N\to\infty}\left[\sum_{n=0}^{N}\psi'_n - \psi_N\right], \qquad \psi'_n \equiv \frac{d}{dn}\psi_n\,, \tag{5.6.3}$$

where

$$\langle\phi,\psi_{n-1}\rangle = -\langle\, f\circ\phi(0)\, c(1)\, \mathcal{B}_R^+\, c(n)\,\rangle_{\mathcal{W}_n} \quad \text{for } n>1 \tag{5.6.4}$$

and

$$\langle\,\phi,\psi_0\rangle \equiv \lim_{n\to 1}\langle\,\phi,\psi_{n-1}\rangle = \langle\, f\circ\phi(0)\, c(1)\,\rangle_{\mathcal{W}_1}\,. \tag{5.6.5}$$

The goal of this subsection is the calculation of $|B_*(\Psi_{\mathcal{S}})\rangle$. As a warm-up exercise, it is instructive to calculate

$$|B_*^{(1)}(\psi_0)\rangle = -\,e^{\frac{\pi^2}{s}(L_0+\tilde{L}_0)}\oint_s\int_0^s ds_1\,\mathcal{P}(0,s_1)\,\{\mathcal{B}_R(s_1),\psi_0\}\,\mathcal{P}(s_1,s)\,. \tag{5.6.6}$$

The required shift a_0 from (5.5.15) is given by

$$a_0 = \frac{e^{s_1}}{e^s - 1}\,, \tag{5.6.7}$$

and the operator $c(1)$ in (5.6.5) is mapped to $e^{-s_1} c(e^{s_1} + a_0)$. The operator insertions in the natural z frame are

$$\begin{aligned} &- e^{-s_1} \int_{C(s_1)} \frac{dz}{2\pi i}\,(z - a_0)\, b(z)\, c(e^{s_1} + a_0) - e^{-s_1} c(e^{s_1} + a_0) \int_{C(s_1)} \frac{dz}{2\pi i}\,(z - a_0 - e^{s_1})\, b(z) \\ &= e^{-s_1} \oint \frac{dz}{2\pi i}\,(z - a_0)\, b(z)\, c(e^{s_1} + a_0) + c(e^{s_1} + a_0)\, \mathcal{B}_R^+ \\ &= 1 + c(e^{s_1} + a_0)\, \mathcal{B}_R^+ = -\mathcal{B}_R^+\, c(e^{s_1} + a_0)\,, \end{aligned} \tag{5.6.8}$$

where the first line corresponds to (5.5.19), the second line corresponds to (5.5.20), and we used the anticommutation relation $\{\mathcal{B}_R^+, c(t)\} = -1$ in the last step. From the identification $z_+ = e^s z_-$ in the natural z frame, we find

$$\int \frac{dz_+}{2\pi i}\, b(z_+) = e^{-s} \int \frac{dz_-}{2\pi i}\, b(z_-) \tag{5.6.9}$$

and therefore

$$\int_{C(t+s)} \frac{dz_+}{2\pi i}\, b(z_+) - \int_{C(t)} \frac{dz_-}{2\pi i}\, b(z_-) = (e^{-s} - 1) \int_{C(t)} \frac{dz_-}{2\pi i}\, b(z_-)\,. \tag{5.6.10}$$

We thus obtain the following formula:[13]

$$\mathcal{B}_R^+ [\ldots] = -\frac{e^s}{e^s - 1} \oint \frac{dz}{2\pi i}\, b(z)\, [\ldots]\,, \tag{5.6.11}$$

where the dots $[\ldots]$ represent arbitrary insertions of local operators and the contour encircles all these operators counterclockwise. Using this formula, the operator insertions (5.6.8) in the natural z frame can be calculated as

$$-\mathcal{B}_R^+\, c(e^{s_1} + a_0) = \frac{e^s}{e^s - 1} \oint \frac{dz}{2\pi i}\, b(z)\, c(e^{s_1} + a_0) = \frac{e^s}{e^s - 1}\,. \tag{5.6.12}$$

For (5.6.6) we thus obtain

$$\begin{aligned} |B_*^{(1)}(\psi_0)\rangle &= -e^{\frac{\pi^2}{s}(L_0 + \tilde{L}_0)} \oint_s \int_0^s ds_1\, \mathcal{P}(0, s_1)\, \{\mathcal{B}_R(s_1), \psi_0\}\, \mathcal{P}(s_1, s) \\ &= \int_0^s ds_1 \frac{e^s}{e^s - 1}\, |B\rangle = \frac{s\, e^s}{e^s - 1}\, |B\rangle\,. \end{aligned} \tag{5.6.13}$$

Let us now generalize this calculation to closed string states of the following form:

$$\begin{aligned} &|\Phi\,(n_1, \ldots, n_k)\rangle \\ &\equiv (-1)^k\, e^{\frac{\pi^2}{s}(L_0 + \tilde{L}_0)} \oint_s \mathcal{P}(0, s_1)\, \{\mathcal{B}_R(s_1), \psi_{n_1 - 1}\}\, \mathcal{P}(s_1, s_2)\, \{\mathcal{B}_R(s_2), \psi_{n_2 - 1}\} \\ &\qquad \times \mathcal{P}(s_2, s_3)\, \{\mathcal{B}_R(s_3), \psi_{n_3 - 1}\}\, \ldots \mathcal{P}(s_{k-1}, s_k)\, \{\mathcal{B}_R(s_k), \psi_{n_k - 1}\}\, \mathcal{P}(s_k, s)\,, \end{aligned} \tag{5.6.14}$$

[13] One might worry that the $\mathcal{B}_R^+$ integral cannot be closed without taking into account a contribution from the hidden boundary similar to the contribution $\widehat{\mathcal{B}}$ in (5.2 13) for $\mathcal{B}_R$. Fortunately, this is not the case because the integrand of $\mathcal{B}_R^+$ *vanishes* along the closed string boundary in the Schnabl limit, as we discussed in section 5.5.

where $n_i \geq 1$. Note that $|B_*^{(k)}(\Psi_S)\rangle$ with Ψ_S given in (5.6.3) can be expressed in terms of states of the form $|\Phi(n_1,\ldots,n_k)\rangle$. For example,

$$|B_*^{(2)}(\Psi_S)\rangle = \lim_{N_1,N_2\to\infty}\int_0^s ds_1\int_{s_1}^s ds_2\Bigg[\sum_{n_1=1}^{N_1}\sum_{n_2=1}^{N_2}\frac{\partial}{\partial n_1}\frac{\partial}{\partial n_2}|\Phi(n_1,n_2)\rangle - \sum_{n_1=1}^{N_1}\frac{\partial}{\partial n_1}|\Phi(n_1,N_2)\rangle - \sum_{n_2=1}^{N_2}\frac{\partial}{\partial n_2}|\Phi(N_1,n_2)\rangle + |\Phi(N_1,N_2)\rangle\Bigg]. \tag{5.6.15}$$

In the calculation of $|\Phi(n_1,\ldots,n_k)\rangle$, the operators we insert for ψ_{n_i-1} in the natural z frame are

$$-e^{-s_i}\,c(e^{s_i}+\ell_i)\,\mathcal{B}_R^+\,c(n_i\,e^{s_i}+\ell_i)\,, \tag{5.6.16}$$

where

$$\ell_i = \sum_{j=1}^{i-1} n_j\,e^{s_j} + a_0\,,\quad \ell_1 = a_0\,. \tag{5.6.17}$$

All the operators for the state $|\Phi(n_1,\ldots,n_k)\rangle$ can be written using the formula (5.5.20) as

$$\begin{aligned}
&\prod_{i=1}^{k}\Big[-e^{-s_i}\oint\frac{dz}{2\pi i}(z-\ell_i)\,b(z)\,c(e^{s_i}+\ell_i)\,\mathcal{B}_R^+\,c(n_i\,e^{s_i}+\ell_i) - n_i\,c(e^{s_i}+\ell_i)\,\mathcal{B}_R^+\,c(n_i\,e^{s_i}+\ell_i)\,\mathcal{B}_R^+\Big]\\
&=\prod_{i=1}^{k}\Big[-\mathcal{B}_R^+\,c(n_i\,e^{s_i}+\ell_i) - n_i\,c(e^{s_i}+\ell_i)\,\mathcal{B}_R^+ + n_i\,c(e^{s_i}+\ell_i)\,\mathcal{B}_R^+\Big]\\
&=\prod_{i=1}^{k}\Big[-\mathcal{B}_R^+\,c(n_i\,e^{s_i}+\ell_i)\Big].
\end{aligned} \tag{5.6.18}$$

Using the anticommutation relation $\{\mathcal{B}_R^+, c(t)\} = -1$ and $(\mathcal{B}_R^+)^2 = 0$ repeatedly, we find

$$\mathcal{B}_R^+\,c(t_1)\,\mathcal{B}_R^+\,c(t_2)\,\ldots\mathcal{B}_R^+\,c(t_k) = (-1)^{k-1}\,\mathcal{B}_R^+\,c(t_k) = \frac{(-1)^k\,e^s}{e^s-1}\,, \tag{5.6.19}$$

where we used (5.6.11) in the last step. Therefore we have

$$\prod_{i=1}^{k}\Big[-\mathcal{B}_R^+\,c(n_i\,e^{s_i}+\ell_i)\Big] = \frac{e^s}{e^s-1} \tag{5.6.20}$$

and thus

$$|\Phi(n_1,\ldots,n_k)\rangle = \frac{e^s}{e^s-1}\,|B\rangle\,. \tag{5.6.21}$$

Note that this is independent of n_i. This means that the ψ_n' piece of the solution does not contribute to $|B_*(\Psi_S)\rangle$ because all derivatives of $|\Phi(n_1,\ldots,n_k)\rangle$ with respect to n_i vanish. In particular, mixed terms that involve ψ_n' and ψ_N do not contribute to $|B_*(\Psi_S)\rangle$. Therefore the

whole contribution to $|B_*(\Psi_S)\rangle$ comes entirely from the 'phantom' term $-\psi_N$ of the solution, namely,

$$|B_*^{(k)}(\Psi_S)\rangle = (-1)^k \lim_{N_1,\ldots,N_k\to\infty} \int_0^s ds_1 \int_{s_1}^s ds_2 \ldots \int_{s_{k-1}}^s ds_k \, |\Phi\,(N_1, N_2, \ldots, N_k)\rangle. \tag{5.6.22}$$

Since $|\Phi\,(N_1,\ldots,N_k)\rangle$ is independent of N_i, the limit $N_1,\ldots,N_k \to \infty$ is trivial.[14] The result (5.6.21) is also independent of s_i. Thus the integrals over s_i in (5.6.22) simply gives the following factor:

$$\int_0^s ds_1 \int_{s_1}^s ds_2 \int_{s_2}^s ds_3 \ldots \int_{s_{k-1}}^s ds_k = \frac{s^k}{k!}\,. \tag{5.6.23}$$

We therefore conclude that

$$|B_*(\Psi_S)\rangle = \left[1 + \sum_{k=1}^{\infty} \frac{s^k}{k!}(-1)^k \frac{e^s}{e^s-1}\right]|B\rangle = \left[1 + (e^{-s}-1)\frac{e^s}{e^s-1}\right]|B\rangle = 0\,. \tag{5.6.24}$$

In [30,93] it was shown that the gauge-invariant observables $W(\mathcal{V},\Psi)$ vanish for the tachyon vacuum solution Ψ_S. Their result can be reproduced by calculating the on-shell part of the $k=1$ term $|B_*^{(1)}(\Psi_S)\rangle$ and taking the limit $s\to 0$. The result (5.6.24) can thus be viewed as the generalization of the calculation in [30] to the off-shell part and to finite s. Indeed, the terms with $k\geq 2$ in (5.6.24) are suppressed for small s. In the limit $s\to 0$ the $k=1$ term by itself cancels the original boundary state $|B\rangle$. In summary, we conclude that $|B_*(\Psi_S)\rangle$ for Schnabl's tachyon vacuum solution Ψ_S vanishes for any finite s:

$$\boxed{|B_*(\Psi_S)\rangle \;=\; 0 \qquad \text{for } \mathcal{B}=B \text{ and any finite } s.} \tag{5.6.25}$$

This is consistent with Sen's conjecture that the D-brane disappears at the tachyon vacuum.

5.6.2 Factorization of $|B_*(\Psi)\rangle$ into matter and ghost sectors

We have seen that $|B_*^{(k)}(\Psi_S)\rangle$ is proportional to $|B\rangle$ for any k. In particular, this means that the ghost sector of $|B_*^{(k)}(\Psi_S)\rangle$ is the same as the ghost sector of $|B\rangle$, namely, the boundary state $|B^{(bc)}\rangle$ of the bc CFT. This boundary state satisfies the relations

$$(\,b_n - \tilde{b}_{-n}\,)\,|B^{(bc)}\rangle = 0\,, \qquad (\,c_n + \tilde{c}_{-n}\,)\,|B^{(bc)}\rangle = 0 \tag{5.6.26}$$

for all $n\in\mathbb{Z}$. If the state $|B_*(\Psi)\rangle$ factorizes into matter and ghost sectors as

$$|B_*(\Psi)\rangle = |B_*^{(\text{matter})}(\Psi)\rangle \otimes |B^{(bc)}\rangle\,, \tag{5.6.27}$$

it follows from $Q\,|B_*(\Psi)\rangle = 0$ and (5.6.26) that the matter part $|B_*^{(\text{matter})}(\Psi)\rangle$ satisfies the relation for conformal boundary conditions

$$(\,L_n^{(\text{matter})} - \tilde{L}_{-n}^{(\text{matter})}\,)\,|B_*^{(\text{matter})}(\Psi)\rangle = 0\,. \tag{5.6.28}$$

[14] In particular, the limit $N_1,\ldots,N_k\to\infty$ is independent of the order in which we take $N_i\to\infty$.

While our claim is that the state $|B_*(\Psi)\rangle$ coincides with the BCFT boundary state $|B_*\rangle$ up to a possible BRST-exact term, the state $|B_*(\Psi)\rangle$ factorized as (5.6.27) can be a consistent BCFT boundary state without any BRST-exact term. It is therefore important to examine for what solutions the ghost part of $|B_*(\Psi)\rangle$ becomes the boundary state $|B^{(bc)}\rangle$ of the bc CFT.

We now claim that the ghost part of a closed string state of the form

$$e^{\frac{\pi^2}{s}(L_0+\tilde{L}_0)} \oint_s \mathcal{P}(0,s_1)\,\{\mathcal{B}_R(s_1),A_1\}\,\mathcal{P}(s_1,s_2)\;\{\mathcal{B}_R(s_2),A_2\}\,\mathcal{P}(s_2,s_3)\;\{\mathcal{B}_R(s_3),A_3\}\;\cdots \\ \times\,\mathcal{P}(s_{k-1},s_k)\,\{\mathcal{B}_R(s_k),A_k\}\,\mathcal{P}(s_k,s) \tag{5.6.29}$$

coincides with the boundary state of the bc CFT if open string fields $A_1, A_2, \ldots, A_k$ of ghost number one are made of wedge states with

- local operator insertions of the c ghost and its derivatives,
- b-ghost line integrals $\mathcal{B}_R^+$,
- arbitrary insertions of matter operators, and
- line integrals $\mathcal{L}_R^+ = \{Q, \mathcal{B}_R^+\}$ of the energy-momentum tensor. We demand that there are no other operators on the contour of each $\mathcal{L}_R^+$.

This can be shown in the following way. First consider the case where there are no line integrals of $\mathcal{L}_R^+$. The b-ghost integral $\mathcal{B}_R(s_i)$ in $\{\mathcal{B}_R(s_i), A_i\}$ can be written in the form (5.5.20):

$$\{\mathcal{B}_R(s_i), A_{\alpha_i}\} \;\to\; -\oint \frac{dz}{2\pi i}\,(z-\ell_i)\,b(z)\,[\ldots] - e^{s_i}\alpha_i\,[\ldots]\,\mathcal{B}_R^+\,, \tag{5.6.30}$$

where α_i is the length of the wedge state associated with A_i and ℓ_i is defined in (5.5.18). Nonvanishing contributions to the first term come only from local operator insertions of the c ghost and its derivatives in $[\ldots]$. Therefore, after performing the integrals of the form (5.6.30), remaining operator insertions in the ghost sector are insertions of $\mathcal{B}_R^+$ and insertions of the c ghost and its derivatives. It then follows from $(\mathcal{B}_R^+)^2 = 0$ and the transformation property (5.6.9) that there must be at least one insertion of the c ghost or its derivatives between two insertions of $\mathcal{B}_R^+$ for the result to be nonvanishing. However, since the total ghost number vanishes, there must be only one insertion of the c ghost or its derivatives between two insertions of $\mathcal{B}_R^+$. Then such contributions can be calculated using the formula (5.6.19). In fact, terms which contain derivatives of the c ghost vanish because the right-hand side of (5.6.19) is independent of t_i's. Nonvanishing contributions are of the form (5.6.19) and no ghost operators remain in the end. We have thus shown that the ghost part of (5.6.29) coincides with $|B^{(bc)}\rangle$.

Let us next consider the case where there is one line integral of $\mathcal{L}_R^+$. The insertion of $\mathcal{L}_R^+$ in the definition of a state A_i appears in the form

$$\langle \phi\,,\, A_i\rangle = \langle\, f\circ\phi(0)\;[\ldots]_1\,\mathcal{L}_R^+\,[\ldots]_2\rangle_{\mathcal{W}_{\alpha_i}}\,, \tag{5.6.31}$$

where we denoted all the operator insertions to the left of the $\mathcal{L}_R^+$ line integral by $[\ldots]_1$ and those to the right by $[\ldots]_2$. Such separation is possible because of our assumption that there are no operators on the contour of $\mathcal{L}_R^+$. The state $A_\imath$ can be written as

$$A_\imath = -\partial_t A_\imath(t)\Big|_{t=0}\,, \tag{5.6.32}$$

where the state $A_\imath(t)$ for $t > 0$ is defined by[15]

$$\langle\, \phi\,,\, A_\imath(t)\,\rangle = \langle\, f\circ\phi(0)\;[\ldots]_1\; g\circ[\ldots]_2\,\rangle_{\mathcal{W}_{\alpha_\imath+t}} \quad \text{with} \quad g(z) = z + t\,. \tag{5.6.33}$$

Since $A_\imath(t)$ belongs to the class of states considered before, the ghost part of (5.6.29) with $A_\imath$ replaced by $A_\imath(t)$ for any positive t coincides with $|B^{(bc)}\rangle$. Therefore, the ghost part of (5.6.29) with $A_\imath$ replaced by $\partial_t A_\imath(t)$ also coincides with $|B^{(bc)}\rangle$. It thus follows that the ghost part of (5.6.29) with $A_\imath$ given by (5.6.32) also coincides with $|B^{(bc)}\rangle$. It is straightforward to generalize the proof to the case with an arbitrary number of insertions of $\mathcal{L}_R^+$. We conclude that the state $|B_*(\Psi)\rangle$ takes the form (5.6.27) if the solution Ψ consists of wedge states with local operator insertions of the c ghost and its derivatives, line integrals $\mathcal{B}_R^+$ and $\mathcal{L}_R^+$, and arbitrary insertions of matter operators.[16]

This condition on the solution for which $|B_*(\Psi)\rangle$ satisfies (5.6.27) is a sufficient condition and is not a necessary condition. However, this class of states covers all known wedge-based analytic solutions such as Schnabl's tachyon vacuum solution [43] as analyzed in section 5.6.1 and the solutions associated with marginal deformations for both regular and singular operator products constructed in [12, 13, 16, 21].

In the case of marginal deformations with regular operator products, the solutions in Schnabl gauge constructed in [12, 13] and those in [21] are expected to be gauge-equivalent. We just argued that these different solutions give the same state $|B_*(\Psi)\rangle$ in the form (5.6.27). We thus expect that the form (5.6.27) is preserved for a certain class of gauge transformations. We have shown in section 5.3.4 that the state $|B_*(\Psi)\rangle$ changes under a gauge transformation $\delta_\chi\Psi = Q\chi + [\,\Psi, \chi\,]$ by the following BRST-exact term:

$$\delta_\chi|B_*(\Psi)\rangle = Q\left[\, e^{\frac{\pi^2}{s}(L_0+\tilde{L}_0)} \oint_s \int_0^s dt\, \mathcal{P}_*(0,t)\,[\,\mathcal{B}_R(t), \chi\,]\,\mathcal{P}_*(t,s)\right]. \tag{5.6.34}$$

Consider a closed string state of the form

$$\begin{aligned} e^{\frac{\pi^2}{s}(L_0+\tilde{L}_0)} \oint_s \mathcal{P}(0,s_1)\,\{\mathcal{B}_R(s_1), A_1\}\,\mathcal{P}(s_1,s_2)\;\{\mathcal{B}_R(s_2), A_2\}\,\mathcal{P}(s_2,s_3)\;\{\mathcal{B}_R(s_3), A_3\}\;\ldots \\ \times\,\mathcal{P}(s_{\imath-1},s_\imath)\;[\,\mathcal{B}_R(s_\imath), A_\imath\,]\,\mathcal{P}(s_\imath,s_{i+1})\;\ldots\mathcal{P}(s_{k-1},s_k)\,\{\mathcal{B}_R(s_k), A_k\}\,\mathcal{P}(s_k,s)\,, \end{aligned} \tag{5.6.35}$$

[15]The definition of $A_\imath(t)$ can be extended to $t < 0$ until operator insertions in $[\;..]_1$ and $g\circ[\ldots]_2$ collide. The derivative of $A_\imath(t)$ at $t = 0$ is therefore well defined.

[16]In general, if we have a one-parameter family of closed string states of the form (5.6.29) with their ghost sectors being $|B^{(bc)}\rangle$, ghost sectors of closed string states obtained by taking derivatives with respect to the parameter are also given by $|B^{(bc)}\rangle$. We considered the case with line integrals of $\mathcal{L}_R^+$ as a particular example of this generalization because ψ_n' in the tachyon vacuum solution contains a line integral of $\mathcal{L}_R^+$, but various other generalizations will be possible. Derivatives of the c ghost can also be treated in this way.

where A_i carries ghost number zero and all other states $A_1, A_2, \ldots, A_k$ carry ghost number one. They are made of wedge states with local operator insertions of the c ghost and its derivatives, line integrals $\mathcal{B}_R^+$ and $\mathcal{L}_R^+$, and arbitrary insertions of matter operators. The b-ghost integral $\mathcal{B}_R(s_i)$ in $[\mathcal{B}_R(s_i), A_i]$ for the Grassmann-even state A_i can be written as

$$[\mathcal{B}_R(s_i), A_{\alpha_i}] \;\to\; -\oint \frac{dz}{2\pi i}\,(z-\ell_i)\,b(z)\,[\ldots] + e^{s_i}\alpha_i\,[\ldots]\,\mathcal{B}_R^+\,, \tag{5.6.36}$$

which follows from the same manipulations that led to (5.5.20) for Grassmann-odd states. Line integrals of $\mathcal{L}_R^+$ can be treated in the same way as before so that it is sufficient to consider the case when they are absent. After performing the integrals of the form (5.6.30) and (5.6.36), remaining operator insertions in the ghost sector are again insertions of $\mathcal{B}_R^+$ and insertions of the c ghost and its derivatives. In this case, however, the total ghost number is -1 and thus we have one more insertions of $\mathcal{B}_R^+$ than insertions of the c ghost and its derivatives. Any term with more than one insertion of $\mathcal{B}_R^+$ immediately vanishes because of $(\mathcal{B}_R^+)^2 = 0$ and the transformation property (5.6.9). In the case of one insertion of $\mathcal{B}_R^+$, we do not have any other insertions of ghost operators, and it follows from the formula (5.6.11) that the contribution vanishes. We thus conclude that $\delta_\chi|B_*(\Psi)\rangle$ vanishes if the solution Ψ and the gauge parameter χ consist of wedge states with local operator insertions of the c ghost and its derivatives, line integrals $\mathcal{B}_R^+$ and $\mathcal{L}_R^+$, and arbitrary insertions of matter operators. In particular, gauge transformations generated by gauge parameters made of wedge states with only matter operator insertions do not change the state $|B_*(\Psi)\rangle$.

5.6.3 Marginal deformations with regular operator products

Deformations of BCFT generated by a matter primary field V of weight one are exactly marginal when operator products $V(t_1)\,V(t_2)\,\ldots\,V(t_n)$ are regular. In this case we expect to have a one-parameter family of solutions to the equation of motion of open string field theory. In fact, we presented analytic solutions for such marginal deformations with regular operator products in chapters 2 and 3. In [30, 37], the gauge-invariant observables $W(\mathcal{V}, \Psi)$ were calculated for these solutions, and the results confirmed the relation (5.1.2). These calculations essentially extracted the on-shell part of $|B_*^{(1)}(\Psi)\rangle$ in the limit $s \to 0$. In this section we calculate the full state $|B_*(\Psi)\rangle$ constructed using the Schnabl propagator strips for these analytic solutions to see if it coincides with the BCFT boundary state

$$|B_*\rangle = \exp\left[\lambda \int_0^{2\pi} d\theta\, V(\theta)\right] |B\rangle\,, \tag{5.6.37}$$

where θ with $0 \le \theta \le 2\pi$ parameterizes the boundary of the disk.

The leading term

The leading term $\Psi^{(1)}$ defined by

$$\langle\, \phi, \Psi^{(1)} \,\rangle = \langle\, f \circ \phi(0)\, cV(1) \,\rangle_{\mathcal{W}_1} \tag{5.6.38}$$

is identical for all solutions [12,13,21] associated with a marginal operator V. Let us calculate

$$|B_*^{(1)}(\Psi^{(1)})\rangle = -e^{\frac{\pi^2}{s}(L_0+\tilde{L}_0)} \oint_s \int_0^s ds_1 \, \mathcal{P}(0,s_1) \, \{\mathcal{B}_R(s_1), \Psi^{(1)}\} \, \mathcal{P}(s_1,s) \, . \tag{5.6.39}$$

The required shift a_0 from (5.5.15) is given by

$$a_0 = \frac{e^{s_1}}{e^s - 1} \, . \tag{5.6.40}$$

Using (5.5.20), the operator insertions in the natural z frame are

$$\begin{aligned} &\oint \frac{dz}{2\pi i} \, (z - a_0) \, b(z) \, cV(e^{s_1} + a_0) + e^{s_1} \, cV(e^{s_1} + a_0) \, \mathcal{B}_R^+ \\ &= e^{s_1} \, V(e^{s_1} + a_0) + e^{s_1} \, cV(e^{s_1} + a_0) \, \mathcal{B}_R^+ \\ &= -e^{s_1} \, \mathcal{B}_R^+ \, cV(e^{s_1} + a_0) \, . \end{aligned} \tag{5.6.41}$$

The ghost sector of these operator insertions is identical to the one calculated in (5.6.12) for the tachyon vacuum solution. We obtain

$$-e^{s_1} \, \mathcal{B}_R^+ \, cV(e^{s_1} + a_0) = \frac{e^s \, e^{s_1}}{e^s - 1} \, V(e^{s_1} + a_0) \, . \tag{5.6.42}$$

If we define

$$u_1 = e^{s_1} + a_0 = \frac{e^s \, e^{s_1}}{e^s - 1} \, , \tag{5.6.43}$$

we observe that

$$\int_0^s ds_1 \, \frac{e^s \, e^{s_1}}{e^s - 1} \, V(e^{s_1} + a_0) = \int_{\frac{e^s}{e^s-1}}^{\frac{e^{2s}}{e^s-1}} du_1 \, V(u_1) \, . \tag{5.6.44}$$

Namely, the measure factor

$$\frac{\partial u_1}{\partial s_1} = \frac{e^s \, e^{s_1}}{e^s - 1} \tag{5.6.45}$$

has been correctly provided through the calculation. Since the point $\frac{e^s}{e^s-1}$ and the point $\frac{e^{2s}}{e^s-1}$ are identified in the natural z frame, the operator corresponds to

$$\int_0^{2\pi} d\theta \, V(\theta) \tag{5.6.46}$$

in the ζ frame, where θ parameterizes the boundary $|\zeta| = 1$ as $\zeta = e^{i\theta}$. Therefore we find

$$|B_*^{(1)}(\Psi^{(1)})\rangle = -e^{\frac{\pi^2}{s}(L_0+\tilde{L}_0)} \oint_s \int_0^s ds_1 \, \mathcal{P}(0,s_1) \, \{\mathcal{B}_R(s_1), \Psi^{(1)}\} \, \mathcal{P}(s_1,s) = \int_0^{2\pi} d\theta \, V(\theta) \, |B\rangle \, . \tag{5.6.47}$$

This is indeed the $\mathcal{O}(\lambda)$ term in the path-ordered exponential (5.6.37) that we expected.

Regular marginal deformations in Schnabl gauge

Let us next calculate $|B_*(\Psi)\rangle$ with Ψ being the Schnabl-gauge solutions for marginal deformations constructed in chapter 2. Recall, that this solution is given by

$$\Psi = \sum_{n=1}^{\infty} \lambda^n \, \Psi^{(n)} \,, \tag{5.6.48}$$

where[17]

$$\begin{aligned} \langle \, \phi, \Psi^{(n)} \, \rangle = - \int_0^1 dt_1 \int_0^1 dt_2 \ldots \int_0^1 dt_{n-1} \, \langle \, f \circ \phi(0) \, cV(1) \\ \times V(1+t_1) \, V(1+t_1+t_2) \, \ldots V(1+t_1+t_2+\ldots+t_{n-2}) \\ \times \mathcal{B}_R^+ \, cV(1+t_1+t_2+\ldots+t_{n-1}) \, \rangle_{\mathcal{W}_{1+t_1+t_2+\ \ +t_{n-1}}} \,. \end{aligned} \tag{5.6.49}$$

The calculation of the ghost sector has been done in section 5.6.1 so that we only need to calculate the matter sector.[18]

There are two terms which contribute to $|B_*(\Psi)\rangle$ at $\mathcal{O}(\lambda^2)$. The first one is

$$\begin{aligned} |B_*^{(2)}(\Psi^{(1)})\rangle = e^{\frac{\pi^2}{s}(L_0+\tilde{L}_0)} \oint_s \int_0^s ds_1 \int_{s_1}^s ds_2 \, \mathcal{P}(0,s_1) \, \{\mathcal{B}_R(s_1), \Psi^{(1)}\} \\ \times \mathcal{P}(s_1,s_2) \, \{\mathcal{B}_R(s_2), \Psi^{(1)}\} \, \mathcal{P}(s_1,s) \,. \end{aligned} \tag{5.6.50}$$

The operator insertion in the natural z frame is given by

$$\frac{e^s}{e^s-1} \int_0^s ds_1 \int_{s_1}^s ds_2 \, e^{s_1} \, V\Big(\frac{e^s e^{s_1} + e^{s_2}}{e^s-1} \Big) \, e^{s_2} \, V\Big(\frac{e^s e^{s_1} + e^s e^{s_2}}{e^s-1} \Big) \,, \tag{5.6.51}$$

where we used (5.6.20) to calculate the ghost sector. The second one is

$$|B_*^{(1)}(\Psi^{(2)})\rangle = - e^{\frac{\pi^2}{s}(L_0+\tilde{L}_0)} \oint_s \int_0^s ds_1 \, \mathcal{P}(0,s_1) \, \{\mathcal{B}_R(s_1), \Psi^{(2)}\} \, \mathcal{P}(s_1,s) \,. \tag{5.6.52}$$

The operator insertion in the natural z frame is given by

$$\frac{e^s}{e^s-1} \int_0^s ds_1 \int_0^1 dt_1 \, e^{s_1} \, V\Big(\frac{e^s e^{s_1} + t_1 \, e^{s_1}}{e^s-1} \Big) \, e^{s_1} \, V\Big(\frac{e^s e^{s_1} + e^s \, t_1 \, e^{s_1}}{e^s-1} \Big) \,. \tag{5.6.53}$$

If we define

$$s_1' = s_1 \,, \quad s_2' = s_1 + \ln t_1 \,, \tag{5.6.54}$$

this can be written as follows:

$$\frac{e^s}{e^s-1} \int_0^s ds_1' \int_{-\infty}^{s_1'} ds_2' \, e^{s_1'} \, V\Big(\frac{e^s e^{s_1'} + e^{s_2'}}{e^s-1} \Big) \, e^{s_2'} \, V\Big(\frac{e^s e^{s_1'} + e^s e^{s_2'}}{e^s-1} \Big) \,. \tag{5.6.55}$$

[17] Note that the operator $\mathcal{B}$ in chapter 2 corresponds to $-\mathcal{B}_R^+$ in this chapter. This expression can thus be derived from (2.3.3) by replacing $\mathcal{B}$ with $-\mathcal{B}_R^+$ and by using $\{ \mathcal{B}_R^+, c(t) \} = -1$ and $(\mathcal{B}_R^+)^2 = 0$ recursively.

[18] The separation of matter and ghost sectors depends on a frame. We separate them in the sliver frame used in (5.6.49). For example, the operator cV in the sliver frame $z^{(i)}$ is divided into $e^{-s_i} c$ and $e^{s_i} V$ in the natural z frame via the conformal transformation (5.5.17).

Note that the second factor of e^{s_1} in (5.6.53) has been changed to $e^{s_2'}$ because of the Jacobian

$$\frac{\partial(s_1', s_2')}{\partial(s_1, t_1)} = \frac{1}{t_1}\,. \tag{5.6.56}$$

The two expressions (5.6.51) and (5.6.55) are combined to give

$$\frac{e^s}{e^s-1}\int_0^s ds_1 \int_{-\infty}^s ds_2\, e^{s_1}\, V\Big(\frac{e^s e^{s_1}+e^{s_2}}{e^s-1}\Big)\, e^{s_2}\, V\Big(\frac{e^s e^{s_1}+e^s e^{s_2}}{e^s-1}\Big)\,. \tag{5.6.57}$$

If we define

$$u_1 = \frac{e^s e^{s_1}+e^{s_2}}{e^s-1}\,, \quad u_2 = \frac{e^s e^{s_1}+e^s e^{s_2}}{e^s-1}\,, \tag{5.6.58}$$

this expression can be written in the following form:

$$\int_{\Gamma^{(2)'}} du_1 du_2\, V(u_1)\, V(u_2)\,, \tag{5.6.59}$$

where we have used

$$\frac{\partial(u_1,u_2)}{\partial(s_1,s_2)} = \frac{e^s}{e^s-1}\, e^{s_1}\, e^{s_2}\,. \tag{5.6.60}$$

Since

$$e^{s_1} = u_1 - e^{-s}u_2\,, \quad e^{s_2} = u_2 - u_1\,, \tag{5.6.61}$$

the integration region $\Gamma^{(2)'}$ can be characterized by

$$1 \le u_1 - e^{-s}u_2 \le e^s\,, \quad 0 \le u_2 - u_1 \le e^s\,. \tag{5.6.62}$$

Using the identification $z \sim e^s z$ in the natural z frame, this integral can also be written as

$$\int_{\Gamma^{(2)}} du_1 du_2\, V(u_1)\, V(u_2) \tag{5.6.63}$$

with $\Gamma^{(2)}$ given by

$$1 \le e^s u_1 - u_2 \le e^s\,, \quad 0 \le u_2 - u_1 \le 1\,. \tag{5.6.64}$$

It is straightforward to generalize the calculations to the case of $\mathcal{O}(\lambda^n)$. The details are presented in appendix A.1 of [38]. The matter sector of the boundary state $|B_*(\Psi)\rangle$ can be written in the z frame with the identification $z \sim e^s z$ as follows:

$$\sum_{n=0}^{\infty} \lambda^n \int_{\Gamma^{(n)}} du_1 du_2 \ldots du_n\, V(u_1)\, V(u_2)\, \ldots V(u_n)\,, \tag{5.6.65}$$

where the region $\Gamma^{(n)}$ is given by

$$0 \le u_2 - u_1 \le 1\,, \quad 0 \le u_3 - u_2 \le 1\,, \quad \ldots \quad 0 \le u_n - u_{n-1} \le 1\,, \quad 1 \le e^s u_1 - u_n \le e^s\,. \tag{5.6.66}$$

In appendix A.2 of [38] we use the identification $z \sim e^s z$ in the z frame repeatedly to show that

$$\int_{\Gamma^{(n)}} du_1 du_2 \ldots du_n\, V(u_1)\, V(u_2) \ldots V(u_n) = \int_1^{e^s} du_1 \int_{u_1}^{e^s} du_2 \ldots \int_{u_{n-1}}^{e^s} du_n\, V(u_1)\, V(u_2) \ldots V(u_n)\,. \tag{5.6.67}$$

It follows that

$$\sum_{n=0}^{\infty} \lambda^n \int_{\Gamma^{(n)}} du_1 du_2 \dots du_n \, V(u_1)\, V(u_2) \, \dots V(u_n) = \exp\left[\lambda \int_1^{e^s} du \, V(u) \right] . \tag{5.6.68}$$

Therefore we conclude that

$$\boxed{ |B_*(\Psi)\rangle = \exp\left[\lambda \int_0^{2\pi} d\theta \, V(\theta) \right] |B\rangle \, . } \tag{5.6.69}$$

Other solutions for regular marginal deformations

We have so far considered solutions in Schnabl gauge, and thus the choice of the propagator strip $\mathcal{B} = B$ and the gauge condition on the solution $B\Psi = 0$ are correlated. However, neither the explicit calculability of $|B_*(\Psi)\rangle$ nor the factorizability (5.6.27) depend on the Schnabl-gauge condition $B\Psi = 0$. We next consider the analytic solutions for regular marginal deformations presented in section 3.2, which do not satisfy $B\Psi = 0$. While there is an obstruction in the construction of solutions in Schnabl gauge for marginal deformations with singular operator products, the regular solutions of section 3.2 were generalized to such singular cases in section 3.3 and they still belong to the class of solutions discussed in section 5.6.2.

Recall, that the regular solution Ψ_L constructed in chapter 3 is given by

$$\Psi_L = \sum_{n=1}^{\infty} \Psi_L^{(n)} , \tag{5.6.70}$$

where[19]

$$\langle \phi, \Psi_L^{(n)} \rangle = \lambda^n \int_1^2 dt_2 \int_{t_2}^3 dt_3 \int_{t_3}^4 dt_4 \, \dots \int_{t_{n-1}}^n dt_n \, \langle f \circ \phi(0) \; cV(1)\, V(t_2)\, V(t_3) \, \dots \, V(t_n) \rangle_{\mathcal{W}_n} . \tag{5.6.71}$$

While Ψ_L solves the equation of motion, it does not satisfy the reality condition

$$\Psi = \mathrm{hc}^{-1}(\Psi^\star) \tag{5.6.72}$$

on the string field, where hc denotes hermitian conjugation. In section 3.2.2, a real solution Ψ_{real} that satisfies (5.6.72) was constructed from Ψ_L using a gauge transformation. As the gauge parameter χ of the required gauge transformation is of the type described in section 5.6.2,[20] we conclude from the discussion in that section that

$$|B_*(\Psi_L)\rangle = |B_*(\Psi_{\text{real}})\rangle \, . \tag{5.6.73}$$

It is thus sufficient to calculate $|B_*(\Psi_L)\rangle$.

[19] For future convenience, we have slightly shifted notation compared to (3.2.23): $t_i^{\text{there}} = t_{i+1}^{\text{here}}$.

[20] The infinitesimal gauge parameter χ for this transformation is proportional to $\ln\sqrt{U}$. As U is a wedge-based state with only matter operator insertions and $U = 1 + \mathcal{O}(\lambda)$, we conclude that χ is well defined perturbatively in λ and of the form described in section 5.6.2.

Consider the term with k insertions $\Psi_L^{(n_1)}, \ldots, \Psi_L^{(n_k)}$ in $|B_*(\Psi_L)\rangle$:

$$\begin{aligned}(-1)^k\, e^{\frac{\pi^2}{s}(L_0+\tilde{L}_0)} \oint_s \int_0^s ds_1 \int_{s_1}^s ds_2 \ldots \int_{s_{k-1}}^s ds_k\, \mathcal{P}(0,s_1)\, \{\mathcal{B}_R(s_1), \Psi_L^{(n_1)}\} \\ \times \mathcal{P}(s_1,s_2)\, \{\mathcal{B}_R(s_2), \Psi_L^{(n_2)}\}\, \mathcal{P}(s_2,s_3)\, \{\mathcal{B}_R(s_3), \Psi_L^{(n_3)}\} \ldots \\ \times \mathcal{P}(s_{k-1},s_k)\, \{\mathcal{B}_R(s_k), \Psi_L^{(n_k)}\}\, \mathcal{P}(s_k,s)\,.\end{aligned} \tag{5.6.74}$$

At $\mathcal{O}(\lambda^n)$, all partitions $\vec{n} = \{n_1, \ldots, n_k\}$ with

$$\sum_{i=1}^k n_i = n \tag{5.6.75}$$

contribute. The solution Ψ_L has the structure discussed in section 5.6.2 and we can thus eliminate all ghost-sector operators in the natural z frame as described in that section. It is shown in appendix B.1 of [38] that the numerical factor which remains after this manipulation is given by

$$\Delta_k \prod_{i=1}^k e^{s_i} \quad \text{with} \quad \Delta_k = 1 + \frac{1}{e^s-1} - \frac{1}{e^s-1} \prod_{i=1}^k (1-n_i)\,. \tag{5.6.76}$$

Let us denote the marginal operators from the insertion $\Psi_L^{(n_i)}$ in the natural z-frame picture as $V(t_1^{(i)}), V(t_2^{(i)}), \ldots, V(t_{n_i}^{(i)})$ with $t_1^{(i)} \leq t_2^{(i)} \leq \ldots \leq t_{n_i}^{(i)}$. Note that $cV(t_1^{(i)})$ is the only unintegrated vertex operator from $\Psi_L^{(n_i)}$ and the others $V(t_2^{(i)}), \ldots, V(t_{n_i}^{(i)})$ are integrated vertex operators. After the calculation of the ghost sector in the natural z frame, we expect the factor (5.6.76) to provide the correct measure for the integration over positions of the operators $V(t_1^{(i)})$ with $i = 1 \ldots k$. This is indeed the case:

$$\frac{\partial(t_1^{(1)}, t_1^{(2)}, \ldots, t_1^{(k)})}{\partial(s_1, s_2, \ldots, s_k)} = \Delta_k \prod_{i=1}^k e^{s_i}\,. \tag{5.6.77}$$

This was shown in appendix B.2 of [38].

The operator insertions in the natural z frame of any term (5.6.74) with partition $\vec{n}$ thus take the form

$$\int_{\Gamma(\vec{n})} dt_1^{(1)} dt_2^{(1)} \ldots dt_{n_k-1}^{(k)} dt_{n_k}^{(k)}\; V(t_1^{(1)}) V(t_2^{(1)}) \ldots V(t_{n_k-1}^{(k)}) V(t_{n_k}^{(k)}) \tag{5.6.78}$$

for some integration region $\Gamma(\vec{n})$ associated with the particular partition $\vec{n}$. The integration regions are complicated, and we were not able to explicitly combine the regions $\Gamma(\vec{n})$ of all partitions into the expected form. We instead choose a different approach to show that the BCFT boundary state is indeed recovered. Consider any point in the integration region $\Gamma(\vec{n})$ of any partition $\vec{n}$ which contributes to $|B_*(\Psi)\rangle$ at $\mathcal{O}(\lambda^n)$. The associated positions $\{t_1^{(1)}, \ldots, t_{n_k}^{(k)}\}$ in the z frame are mapped to a set of angles $\{\theta_1, \ldots, \theta_n\}$ on the unit circle in the ζ frame:

$$\{t_1^{(1)}, \ldots, t_{n_k}^{(k)}\} \;\to\; \{e^{i\theta_1}, \ldots, e^{i\theta_n}\} \qquad \text{with} \quad 0 \leq \theta_1 \leq \cdots \leq \theta_q \leq \cdots \leq \theta_n \leq 2\pi\,. \tag{5.6.79}$$

Note that this is a map between sets, and the order of insertion points $t_j^{(i)}$ in the z-frame will in general be a cyclic permutation of the ordering of the angles θ_q. In particular, we do not expect that $t_1^{(1)}$ is necessarily mapped to θ_1.

We pick any one of the angles in the set $\{\theta_1, \ldots, \theta_n\}$, and denote its index by $\tilde{q}$. We now vary this angle, keeping all other angles fixed to their original values. In appendix B.3 of [38] it is shown that for any $\theta_{\tilde{q}-1} \leq \tilde{\theta} \leq \theta_{\tilde{q}+1}$, one can find a partition $\tilde{\vec{n}}$ such that some point in its integration region $\Gamma(\tilde{\vec{n}})$ maps to the positions

$$\{e^{\imath\theta_1}, \ldots, e^{\imath\theta_{\tilde{q}-1}}, e^{\imath\tilde{\theta}}, e^{\imath\theta_{\tilde{q}+1}}, \ldots, e^{\imath\theta_n}\} \tag{5.6.80}$$

in the ζ frame. As $\tilde{\theta}$ is varied, one generically reaches the boundary of the integration region $\Gamma(\vec{n})$ of the current partition $\vec{n}$. We show that such points can always be smoothly matched to the boundary of the integration region $\Gamma(\tilde{\vec{n}})$ of a different partition $\tilde{\vec{n}}$. The variation of $\tilde{\theta}$ can thus continue until it either coincides with $\theta_{\tilde{q}-1}$ or $\theta_{\tilde{q}+1}$.[21] Denoting the image of the region $\Gamma(\vec{n})$ in the ζ frame by $\zeta\big(\Gamma(\vec{n})\big)$, we conclude that

$$\{e^{\imath\theta_1}, \ldots, e^{\imath\theta_{\tilde{q}-1}}, e^{\imath\tilde{\theta}}, e^{\imath\theta_{\tilde{q}+1}}, \ldots, e^{\imath\theta_n}\} \subset \bigcup_{\vec{n}} \zeta\big(\Gamma(\vec{n})\big) \quad \text{for all } \theta_{\tilde{q}-1} \leq \tilde{\theta} \leq \theta_{\tilde{q}+1}\,. \tag{5.6.81}$$

Note that the angles θ_q with $q \neq \tilde{q}$ are not arbitrary because they are determined by the point in the integration $\vec{n}$ that we picked originally as the starting point for the argument. It is obvious, however, that we can use the above argument iteratively for all $1 \leq \tilde{q} \leq n$ and complete the integration region to all $\{\theta_1, \ldots, \theta_n\}$ satisfying

$$0 \leq \theta_1 \leq \ldots \leq \theta_n \leq 2\pi\,. \tag{5.6.82}$$

This is the integration region expected from (5.6.37) at $\mathcal{O}(\lambda^n)$. As the above argument requires a choice of a starting point, it does not rule out multiple covering and we conclude that

$$|B_*(\Psi_L)\rangle = \sum_{n=0}^{\infty} \frac{C_n}{n!}\Big[\lambda \int_0^{2\pi} d\theta\, V(\theta)\Big]^n |B\rangle \quad \text{for some } C_n \in \mathbb{N}\,. \tag{5.6.83}$$

It now remains to show that $C_n = 1$ for all n. Consider any partition $\vec{n} = \{n_1, \ldots, n_k\}$ with $k \geq 2$. In the natural z frame, the last operator insertion of $\Psi^{(n_1)}$ and the first operator insertion of $\Psi^{(n_2)}$ are located at

$$t_{n_1}^{(1)} \leq e^{s_1} n_1 + a_0\,, \qquad t_1^{(2)} = e^{s_1} n_1 + e^{s_2} + a_0 \tag{5.6.84}$$

with

$$a_0 = \frac{1}{e^s - 1} \sum_{i=1}^{k} n_i\, e^{s_i} \leq \frac{e^s n}{e^s - 1}\,. \tag{5.6.85}$$

In the ζ frame, their angular separation $\Delta\theta$ is thus bounded from below:

$$\Delta\theta \geq \Delta\theta_{\min} \quad \text{with} \quad \Delta\theta_{\min} = \frac{2\pi}{s} \log\Big[\frac{e^s n + (e^s - 1)(n_1 + 1)}{e^s n + (e^s - 1) n_1}\Big]\,. \tag{5.6.86}$$

[21] For the special case of $\tilde{q} = 1$, the lower boundary of the variation is $\theta_1 = 0$. Similarly, the upper boundary of the variation for $\tilde{q} = n$ is $\theta_n = 2\pi$.

The lower bound $\Delta\theta_{\text{min}} > 0$ is independent of the Schwinger parameters s_i. Using cyclicity, we similarly conclude that

$$\Delta\theta \leq 2\pi - \Delta\theta_{\text{min}} \,. \tag{5.6.87}$$

Now consider the subset of the integration region (5.6.82) where all operator insertions are separated by less than the angle $\Delta\theta_{\text{min}}$, namely,

$$|\theta_i - \theta_j| < \Delta\theta_{\text{min}} \quad \text{for all } 1 \leq i, j \leq n \,. \tag{5.6.88}$$

This is a finite region for finite s which can only be covered by $\zeta\big(\Gamma(\vec{n})\big)$ with the partition $\vec{n} = \{n\}$ of $k = 1$. On the other hand, we have shown in (5.4.26) that the region from $|B_*^{(1)}(\Psi_L^{(n)})\rangle$ covers the rotational modulus exactly once, so the subset (5.6.88) of the integration region is covered precisely once. Therefore, there cannot be multiple coverings of the integration region (5.6.82) and we obtain

$$C_n = 1 \quad \text{for all } \; n \,. \tag{5.6.89}$$

Recalling the relation (5.6.73), we conclude that

$$\boxed{|B_*(\Psi_L)\rangle = |B_*(\Psi_{\text{real}})\rangle = \exp\left[\lambda \int_0^{2\pi} d\theta\, V(\theta)\right] |B\rangle \,.} \tag{5.6.90}$$

5.7 Discussion

In this chapter we have constructed a class of BRST-invariant closed string states $|B_*(\Psi)\rangle$ for any open string field theory solution Ψ. The construction depends on a choice of a propagator strip. Modifying the propagator strip or performing a gauge transformation on the classical solution generically changes $|B_*(\Psi)\rangle$ by a BRST-exact term. We calculated $|B_*(\Psi)\rangle$ for various known analytic solutions choosing the Schnabl propagator strip and found that $|B_*(\Psi)\rangle$ precisely coincides with the BCFT boundary state $|B_*\rangle$ of the background that the solutions are expected to describe. This is the first construction of the full BCFT boundary state from solutions of open string field theory.

While we claim that the state $|B_*(\Psi)\rangle$ in general coincides with the BCFT boundary state $|B_*\rangle$ up to a possible BRST-exact term, such a term can be absent if the state $|B_*(\Psi)\rangle$ factorizes into the matter and ghost sectors as (5.6.27). We presented a sufficient condition on the solution Ψ such that $|B_*(\Psi)\rangle$, constructed with the choice of the Schnabl propagator strip, factorizes in this way. It would be useful to understand better when the factorization (5.6.27) holds. Our analysis indicates that the remarkable simplifications associated with the choice of Schnabl propagator strip play an important role for the factorization (5.6.27). It follows from the analysis in chapter 4 that all Riemann surfaces associated with closed string states of the form $\oint_s \Sigma(0, s)$ coincide in the Schnabl limit when A_i in the definition (5.2.20) of $\Sigma(0, s)$ are wedge-based states. In fact, the resulting Riemann surface is an annulus whose modulus only depends on s. This outstanding feature was crucially important in this chapter. We expect from the analysis in [9] that the simplifications associated with Schnabl's propagator carry over into other projector-based propagators.

Because the boundary state is a basic object in BCFT, we believe that our construction of $|B_*\rangle$ from a solution Ψ provides an important step towards establishing the map from classical solutions of open string field theory to BCFT's. Partial success in the reverse map from BCFT's to classical solutions was achieved in [16,21,23] for backgrounds connected by arbitrary marginal deformations. A systematic procedure to construct solutions from the BCFT operator that implements a change of boundary conditions along a segment on the boundary was presented for the bosonic string in chapter 3 and for the superstring in [23]. Our ambitious goal is a complete understanding of the relation between BCFT's and classical solutions of open sting field theory.

The construction of the closed string state $|B_*(\Psi)\rangle$ is based on the representation (5.3.4) of the original BCFT boundary state $|B\rangle$ in terms of the half-propagator strip $\mathcal{P}(0,s)$. The state $|B_*(\Psi)\rangle$ is obtained by replacing $\mathcal{P}(0,s)$ in (5.3.4) with the half-propagator strip $\mathcal{P}_*(0,s)$ associated with the background Ψ. This construction of $|B_*(\Psi)\rangle$ is the primary reason for our claim that the state $|B_*(\Psi)\rangle$ coincides with the BCFT boundary state $|B_*\rangle$ up to a possible BRST-exact term.

It would be interesting to study the generalization of our construction to open superstring field theory in the WZW formulation by Berkovits [94, 95]. We can construct BRST-invariant closed string states in the superstring by replacing Ψ in $|B_*(\Psi)\rangle$ with $e^{-\Phi}Q\,e^{\Phi}$, where Φ is the open superstring field and Q is the BRST operator in the superstring. We expect that the resulting states $|B_*(e^{-\Phi}Q\,e^{\Phi})\rangle$ are related to the BCFT boundary state. It would be interesting to study such closed string states extending the discussion in [30] on gauge-invariant observables [96] for the superstring. The construction of the BCFT boundary state in the superstring from open superstring fields can then be used for consistency checks on solutions of open superstring field theory. For example, a solution for the tachyon vacuum in this theory has been proposed in [34], and it would be useful to examine if the state $|B_*(e^{-\Phi}Q\,e^{\Phi})\rangle$ vanishes for this solution.

We hope that our construction of $|B_*(\Psi)\rangle$ will pave the way to the study of closed string physics within string field theory. It may lead us to a novel formulation of open-closed string field theory. In fact, in chapter 5 of [38] it was found that $|B_*(\Psi)\rangle$ encodes a set of consistent open-closed vertices, which constitutes a first step in this direction. If we choose a propagator strip associated with a non-BPZ-even gauge condition, we obtain complex open-closed vertices. To obtain real vertices suitable for open-closed string field theory, it may be useful to examine if our construction of $|B_*(\Psi)\rangle$ can be generalized to the full propagator surface of regular linear b-gauges [46].

Since gravity is contained in the closed string sector, a consistent coupling of open strings to an off-shell closed string in the framework of string field theory can be thought of as a string theory generalization of the energy-momentum tensor. Apart from the reality issue we mentioned earlier, the state $|B_*(\Psi)\rangle$ can thus be regarded as giving such a generalized energy-momentum tensor. Its expression in terms of the path-ordered exponential (5.3.14) is reminiscent of the energy-momentum tensor of noncommutative gauge theory in terms of open Wilson lines derived in [97]. While the on-shell part of $|B_*(\Psi)\rangle$ is gauge-invariant, the off-shell part is not. We believe that information contained in its off-shell part, especially when $|B_*(\Psi)\rangle$ coincides with the BCFT boundary state $|B_*\rangle$, is useful in understanding the map from solutions to BCFT's, but it is an important open

problem whether physical observables are contained in the off-shell part in the context of string theory or of string field theory. For example, off-shell information in the BCFT boundary state was used in the study of the rolling tachyon by Sen [50]. Finally, the coupling of open string fields to closed string modes plays an important role in the AdS/CFT correspondence. The study of open string field theory with such open-closed vertices was reviewed in section 5 of [38]. It indicates that a large amount of the closed string physics can in principle be reproduced, and the results in this chapter further provide a prospect that they might actually be calculable. We hope that exciting developments await us in this direction.

Bibliography

[1] E. Witten, "Noncommutative Geometry and String Field Theory," *Nucl. Phys.* **B268** (1986) 253.

[2] B. Zwiebach, "Closed string field theory: Quantum action and the B-V master equation," *Nucl. Phys.* **B390** (1993) 33–152, arXiv:hep-th/9206084.

[3] Y. Okawa, "Comments on Schnabl's analytic solution for tachyon condensation in Witten's open string field theory," *JHEP* **04** (2006) 055, arXiv:hep-th/0603159.

[4] E. Fuchs and M. Kroyter, "On the validity of the solution of string field theory," *JHEP* **05** (2006) 006, arXiv:hep-th/0603195.

[5] E. Fuchs and M. Kroyter, "Schnabl's L(0) operator in the continuous basis," *JHEP* **10** (2006) 067, arXiv:hep-th/0605254.

[6] L. Rastelli and B. Zwiebach, "Solving open string field theory with special projectors," *JHEP* **01** (2008) 020, arXiv:hep-th/0606131.

[7] I. Ellwood and M. Schnabl, "Proof of vanishing cohomology at the tachyon vacuum," *JHEP* **02** (2007) 096, arXiv:hep-th/0606142.

[8] E. Fuchs and M. Kroyter, "Universal regularization for string field theory," *JHEP* **02** (2007) 038, arXiv:hep-th/0610298.

[9] Y. Okawa, L. Rastelli, and B. Zwiebach, "Analytic solutions for tachyon condensation with general projectors," arXiv:hep-th/0611110.

[10] T. Erler, "Split string formalism and the closed string vacuum," *JHEP* **05** (2007) 083, arXiv:hep-th/0611200.

[11] T. Erler, "Split string formalism and the closed string vacuum. II," *JHEP* **05** (2007) 084, arXiv:hep-th/0612050.

[12] M. Schnabl, "Comments on marginal deformations in open string field theory," *Phys. Lett.* **B654** (2007) 194–199, arXiv:hep-th/0701248.

[13] M. Kiermaier, Y. Okawa, L. Rastelli, and B. Zwiebach, "Analytic solutions for marginal deformations in open string field theory," *JHEP* **01** (2008) 028, arXiv:hep-th/0701249.

[14] T. Erler, "Marginal Solutions for the Superstring," *JHEP* **07** (2007) 050, arXiv:0704.0930 [hep-th].

[15] Y. Okawa, "Analytic solutions for marginal deformations in open superstring field theory," *JHEP* **09** (2007) 084, arXiv:0704.0936 [hep-th].

[16] E. Fuchs, M. Kroyter, and R. Potting, "Marginal deformations in string field theory," *JHEP* **09** (2007) 101, arXiv:0704.2222 [hep-th].

[17] Y. Okawa, "Real analytic solutions for marginal deformations in open superstring field theory," *JHEP* **09** (2007) 082, arXiv:0704.3612 [hep-th].

[18] I. Ellwood, "Rolling to the tachyon vacuum in string field theory," *JHEP* **12** (2007) 028, arXiv:0705.0013 [hep-th].

[19] I. Kishimoto and Y. Michishita, "Comments on Solutions for Nonsingular Currents in Open String Field Theories," *Prog. Theor. Phys.* **118** (2007) 347–369, arXiv:0706.0409 [hep-th].

[20] E. Fuchs and M. Kroyter, "Marginal deformation for the photon in superstring field theory," *JHEP* **11** (2007) 005, arXiv:0706.0717 [hep-th].

[21] M. Kiermaier and Y. Okawa, "Exact marginality in open string field theory: a general framework," arXiv:0707.4472 [hep-th].

[22] T. Erler, "Tachyon Vacuum in Cubic Superstring Field Theory," *JHEP* **01** (2008) 013, arXiv:0707.4591 [hep-th].

[23] M. Kiermaier and Y. Okawa, "General marginal deformations in open superstring field theory," arXiv:0708.3394 [hep-th].

[24] O.-K. Kwon, B.-H. Lee, C. Park, and S.-J. Sin, "Fluctuations around the Tachyon Vacuum in Open String Field Theory," *JHEP* **12** (2007) 038, arXiv:0709.2888 [hep-th].

[25] B.-H. Lee, C. Park, and D. D. Tolla, "Marginal Deformations as Lower Dimensional D-brane Solutions in Open String Field theory," arXiv:0710.1342 [hep-th].

[26] T. Takahashi, "Level truncation analysis of exact solutions in open string field theory," *JHEP* **01** (2008) 001, arXiv:0710.5358 [hep-th].

[27] O.-K. Kwon, "Marginally Deformed Rolling Tachyon around the Tachyon Vacuum in Open String Field Theory," *Nucl. Phys.* **B804** (2008) 1–18, arXiv:0801.0573 [hep-th].

[28] S. Hellerman and M. Schnabl, "Light-like tachyon condensation in Open String Field Theory," arXiv:0803.1184 [hep-th].

[29] L. Joukovskaya, "Rolling Solution for Tachyon Condensation in Open String Field Theory," arXiv:0803.3484 [hep-th].

[30] I. Ellwood, "The closed string tadpole in open string field theory," *JHEP* **08** (2008) 063, arXiv:0804.1131 [hep-th].

[31] A. Ishida, C. Kim, Y. Kim, O.-K. Kwon, and D. D. Tolla, "Tachyon Vacuum Solution in Open String Field Theory with Constant B Field," arXiv:0804.4380 [hep-th].

[32] T. Kawano, I. Kishimoto, and T. Takahashi, "Schnabl's Solution and Boundary States in Open String Field Theory," *Phys. Lett.* **B669** (2008) 357–358, arXiv:0804.4414 [hep-th].

[33] M. Kiermaier and B. Zwiebach, "One-Loop Riemann Surfaces in Schnabl Gauge," *JHEP* **07** (2008) 063, arXiv:0805.3701 [hep-th].

[34] E. Fuchs and M. Kroyter, "On the classical equivalence of superstring field theories," *JHEP* **10** (2008) 054, arXiv:0805.4386 [hep-th].

[35] E. Fuchs and M. Kroyter, "Analytical Solutions of Open String Field Theory," arXiv:0807.4722 [hep-th].

[36] M. Asano and M. Kato, "General Linear Gauges and Amplitudes in Open String Field Theory," *Nucl. Phys.* **B807** (2009) 348–372, arXiv:0807.5010 [hep-th].

[37] I. Kishimoto, "Comments on gauge invariant overlaps for marginal solutions in open string field theory," *Prog. Theor. Phys.* **120** (2008) 875–886, arXiv:0808.0355 [hep-th].

[38] M. Kiermaier, Y. Okawa, and B. Zwiebach, "The boundary state from open string fields," arXiv:0810.1737 [hep-th].

[39] I. Kishimoto and T. Takahashi, "Numerical Evaluation of Gauge Invariants for a-gauge Solutions in Open String Field Theory," arXiv:0902.0445 [hep-th].

[40] I. Ellwood, "Singular gauge transformations in string field theory," arXiv:0903.0390 [hep-th].

[41] I. Y. Aref'eva, R. V. Gorbachev, and P. B. Medvedev, "Pure Gauge Configurations and Solutions to Fermionic Superstring Field Theories Equations of Motion," arXiv:0903.1273 [hep-th].

[42] A. Sen, "Universality of the tachyon potential," *JHEP* **12** (1999) 027, arXiv:hep-th/9911116.

[43] M. Schnabl, "Analytic solution for tachyon condensation in open string field theory," *Adv. Theor. Math. Phys.* **10** (2006) 433–501, arXiv:hep-th/0511286.

[44] L. Rastelli and B. Zwiebach, "Tachyon potentials, star products and universality," *JHEP* **09** (2001) 038, arXiv:hep-th/0006240.

[45] L. Rastelli and B. Zwiebach, "The off-shell Veneziano amplitude in Schnabl gauge," *JHEP* **01** (2008) 018, arXiv:0708.2591 [hep-th].

[46] M. Kiermaier, A. Sen, and B. Zwiebach, "Linear b-Gauges for Open String Fields," *JHEP* **03** (2008) 050–050, arXiv:0712.0627 [hep-th].

[47] A. Sen and B. Zwiebach, "Large marginal deformations in string field theory," *JHEP* **10** (2000) 009, arXiv:hep-th/0007153.

[48] L. Rastelli, A. Sen, and B. Zwiebach, "Boundary CFT construction of D-branes in vacuum string field theory," *JHEP* **11** (2001) 045, arXiv:hep-th/0105168.

[49] M. Schnabl, "Wedge states in string field theory," *JHEP* **01** (2003) 004, arXiv:hep-th/0201095.

[50] A. Sen, "Rolling Tachyon," *JHEP* **04** (2002) 048, arXiv:hep-th/0203211.

[51] A. Sen, "Time evolution in open string theory," *JHEP* **10** (2002) 003, arXiv:hep-th/0207105.

[52] N. Moeller and B. Zwiebach, "Dynamics with infinitely many time derivatives and rolling tachyons," *JHEP* **10** (2002) 034, arXiv:hep-th/0207107.

[53] N. D. Lambert, H. Liu, and J. M. Maldacena, "Closed strings from decaying D-branes," *JHEP* **03** (2007) 014, arXiv:hep-th/0303139.

[54] D. Gaiotto, N. Itzhaki, and L. Rastelli, "Closed strings as imaginary D-branes," *Nucl. Phys.* **B688** (2004) 70–100, arXiv:hep-th/0304192.

[55] T. Erler, "Level truncation and rolling the tachyon in the lightcone basis for open string field theory," arXiv:hep-th/0409179.

[56] E. Coletti, I. Sigalov, and W. Taylor, "Taming the tachyon in cubic string field theory," *JHEP* **08** (2005) 104, arXiv:hep-th/0505031.

[57] A. Sen, "Tachyon matter," *JHEP* **07** (2002) 065, arXiv:hep-th/0203265.

[58] A. Sen, "Tachyon dynamics in open string theory," *Int. J. Mod. Phys.* **A20** (2005) 5513–5656, arXiv:hep-th/0410103.

[59] M. R. Gaberdiel and B. Zwiebach, "Tensor constructions of open string theories I: Foundations," *Nucl. Phys.* **B505** (1997) 569–624, arXiv:hep-th/9705038.

[60] C. G. Callan, I. R. Klebanov, A. W. W. Ludwig, and J. M. Maldacena, "Exact solution of a boundary conformal field theory," *Nucl. Phys.* **B422** (1994) 417–448, arXiv:hep-th/9402113.

[61] J. Polchinski and L. Thorlacius, "Free fermion representation of a boundary conformal field theory," *Phys. Rev.* **D50** (1994) 622–626, arXiv:hep-th/9404008.

[62] A. Recknagel and V. Schomerus, "Boundary deformation theory and moduli spaces of D-branes," *Nucl. Phys.* **B545** (1999) 233–282, arXiv:hep-th/9811237.

[63] A. Sen, "Descent relations among bosonic D-branes," *Int. J. Mod. Phys.* **A14** (1999) 4061–4078, arXiv:hep-th/9902105.

[64] I. Ellwood and W. Taylor, "Gauge invariance and tachyon condensation in open string field theory," arXiv:hep-th/0105156.

[65] M. Asano and M. Kato, "New covariant gauges in string field theory," *Prog. Theor. Phys.* **117** (2007) 569–587, arXiv:hep-th/0611189.

[66] M. Asano and M. Kato, "Level truncated tachyon potential in various gauges," *JHEP* **01** (2007) 028, arXiv:hep-th/0611190.

[67] A. Sen, "On the background independence of string field theory," *Nucl. Phys.* **B345** (1990) 551–583.

[68] A. Sen, "On the background independence of string field theory 2. Analysis of on-shell S matrix elements.," *Nucl. Phys.* **B347** (1990) 270–318.

[69] A. Sen, "On the background independence of string field theory. 3. Explicit Field redefinitions," *Nucl. Phys.* **B391** (1993) 550–590, arXiv:hep-th/9201041.

[70] A. Sen and B. Zwiebach, "A Proof of local background independence of classical closed string field theory," *Nucl. Phys.* **B414** (1994) 649–714, arXiv:hep-th/9307088.

[71] A. Sen and B. Zwiebach, "Quantum background independence of closed string field theory," *Nucl. Phys.* **B423** (1994) 580–630, arXiv:hep-th/9311009.

[72] N. Berkovits, "SuperPoincare invariant superstring field theory," *Nucl. Phys.* **B450** (1995) 90–102, arXiv:hep-th/9503099.

[73] W. Siegel, "Covariantly second quantized string," *Phys. Lett.* **B142** (1984) 276.

[74] H. Fuji, S. Nakayama, and H. Suzuki, "Open string amplitudes in various gauges," *JHEP* **01** (2007) 011, arXiv:hep-th/0609047.

[75] S. B. Giddings, "The Veneziano Amplitude from Interacting String Field Theory," *Nucl. Phys.* **B278** (1986) 242.

[76] G. Zemba and B. Zwiebach, "Tadpole graph in covariant closed string field theory," *J. Math. Phys.* **30** (1989) 2388.

[77] C. B. Thorn, "Perturbation Theory for Quantized String Fields," *Nucl. Phys.* **B287** (1987) 61.

[78] M. Bochicchio, "Gauge fixing for the field theory of the bosonic string," *Phys. Lett.* **B193** (1987) 31.

[79] C. B. Thorn, "String field theory," *Phys. Rept.* **175** (1989) 1–101.

[80] C. R. Preitschopf, C. B. Thorn, and S. A. Yost, "Superstring field theory," *Nucl. Phys.* **B337** (1990) 363–433.

[81] L. V. Ahlfors, *Conformal Invariants: Topics in Geometric Function Theory.* McGraw-Hill, 1973.

[82] F. P. Gardiner., *Teichmüller theory and quadratic differentials.* John Wiley and Sons, New York, 1987.

[83] D. J. Gross and W. Taylor, "Split string field theory. II," *JHEP* **08** (2001) 010, arXiv:hep-th/0106036.

[84] E. Witten, "Some remarks about string field theory," *Phys. Scripta* **T15** (1987) 70.

[85] A. Hashimoto and N. Itzhaki, "Observables of string field theory," *JHEP* **01** (2002) 028, arXiv:hep-th/0111092.

[86] D. Gaiotto, L. Rastelli, A. Sen, and B. Zwiebach, "Ghost structure and closed strings in vacuum string field theory," *Adv. Theor. Math. Phys.* **6** (2003) 403–456, arXiv:hep-th/0111129.

[87] W. Taylor and B. Zwiebach, "D-branes, tachyons, and string field theory," arXiv:hep-th/0311017.

[88] L. Rastelli, "String field theory," arXiv:hep-th/0509129.

[89] W. Taylor, "String field theory." arXiv:hep-th/0605202.

[90] F. Larsen, A. Naqvi, and S. Terashima, "Rolling tachyons and decaying branes," *JHEP* **02** (2003) 039, arXiv:hep-th/0212248.

[91] A. Bagchi and A. Sen, "Tachyon Condensation on Separated Brane-Antibrane System," *JHEP* **05** (2008) 010, arXiv:0801.3498 [hep-th].

[92] M. Fujita and H. Hata, "Time dependent solution in cubic string field theory," *JHEP* **05** (2003) 043, arXiv:hep-th/0304163.

[93] T. Kawano, I. Kishimoto, and T. Takahashi, "Gauge Invariant Overlaps for Classical Solutions in Open String Field Theory," *Nucl. Phys.* **B803** (2008) 135–165, arXiv:0804.1541 [hep-th].

[94] N. Berkovits, "A new approach to superstring field theory," *Fortsch. Phys.* **48** (2000) 31–36, arXiv:hep-th/9912121.

[95] N. Berkovits, "Super-Poincare covariant quantization of the superstring," *JHEP* **04** (2000) 018, arXiv:hep-th/0001035.

[96] Y. Michishita, "On-shell gauge invariants and field strengths in open superstring field theory," *Nucl. Phys.* **B698** (2004) 111–131, arXiv:hep-th/0406242.

[97] Y. Okawa and H. Ooguri, "How noncommutative gauge theories couple to gravity," *Nucl. Phys.* **B599** (2001) 55–82, arXiv:hep-th/0012218.